JOURNAL OF THE AERONAUTICAL SCIENCES

ST. LOUIS
SEP 20 1955
PUBLIC LIBRARY

VOLUME 22 SEPTEMBER, 1955 NUMBER 9

CONTENTS

On the Laminar Compressible Boundary Layer over a Flat Plate with Suction or Injection.....H. G. LEW AND J. B. FANUCCI 589

Spanwise Variation in the Pitching-Moment Coefficient and the Center of Pressure Due to Various Basic Twist Distributions on Triangular Wings Having Supersonic Leading and Trailing Edges.....JULIAN H. KAINER 598

Similar Solutions of Compressible Boundary-Layer Equations.....TING-YI LI AND HENRY T. NAGAMATSU 607

Quasi-Steady Nonlinear Pitching Oscillations in Transonic Flight.....L. TRILLING AND E. E. COVERT 617

The Dynamic Motion of a Missile Descending Through the Atmosphere.....HANS R. FRIEDRICH AND FRANK J. DORE 628

Some General Comparisons Between the Vibratory and Conventional Rate Gyro.....JOHN B. CHATTERTON 633

Criteria for Longitudinal Stability Requirements.....JAMES L. DECKER 639

The Effect of a Finite Hub on the Optimum Propeller.....B. W. MCCORMICK 645

Readers' Forum: "Simple Shear Flow Past a Flat Plate in an Incompressible Fluid of Small Viscosity," by Ting-Yi Li; "Relative Size of Turbojet Engine Components," by D. Willens; "Application of Kelly's Theory to Cone-Cylinder-Frustum Bodies of Revolution," by Robert E. Lavender; "Estimation of the Lift and Moment Parameters of Leading-Edge Flaps," by Malcolm J. Abzug; "Remarks on 'An Exact Solution for Two-Dimensional Linear Panel Flutter at Supersonic Speeds,'" by S. F. Shen; "On the Flow Behind an Attached Curved Shock," by S. I. Pai; "Free Streamline Analysis for Slotted Two-Dimensional Supersonic Minimum-Length Nozzles," by Robert Wesley Truitt; "Buckling Efficiencies of Plate Materials at Elevated Temperatures," by J. W. Clark; "Errata—Nonlinear Lift and Vortex Separation," by H. K. Cheng; "A Note on 'A Study of Surge in Compressors and Jet Engines,'" by W. C. Randels.....651–660

Published by
INSTITUTE OF THE AERONAUTICAL SCIENCES, INC.

JOURNAL OF THE AERONAUTICAL SCIENCES

Editor: HUGH L. DRYDEN, *Director, NACA*
Associate Editor: ROBERT R. DEXTER
Managing Editor: RITA J. TURINO
Editorial Assistant: CAROLINE TAYLOR

Editorial Committee

Aerodynamics

Dean R. Chapman
Francis H. Clauser
Antonio Ferri
Alexander Flax
R. Paul Harrington
R. T. Jones
Carl Kaplan
H. W. Liepmann
C. C. Lin
H. F. Ludloff
Harold Luskin
John R. Markham
Clark B. Millikan
Shatswell Ober
W. Bailey Oswald
C. D. Perkins
Elliott G. Reid
H. J. E. Reid
Russell Robinson
George S. Schairer
G. B. Schubauer
W. R. Sears
John Stack
Theodore Theodorsen
Th. von Kármán

Air Transport

Charles Froesch
J. A. Herlihy
R. D. Kelly
Otto E. Kirchner
Jerome Lederer
John C. Leslie
R. Dixon Speas

Flight Testing

R. R. Gilruth
Melvin N. Gough
W. L. Howland
W. F. Milliken, Jr.
E. G. Stout

Structures and Materials

W. B. Bleakney
E. W. Conlon
John E. Duberg
E. C. Hartmann
N. J. Hoff
Samuel Levy
J. F. McBrearty
Alfred S. Niles
W. Ramberg
F. R. Shanley
C. R. Strang
S. Timoshenko
H. S. Tsien

Rotating Wing Aircraft

F. B. Gustafson
K. H. Hohenemser
Bartram Kelley
R. B. Maloy
Ralph McClarren
R. H. Miller
R. H. Prewitt
Igor I. Sikorsky

Vibration and Flutter

Lee Arnold
M. A. Biot
R. L. Bisplinghoff
William Bollay
Chieh-Chien Chang
J. P. Den Hartog
I. E. Garrick
Martin Goland
Theodore Theodorsen

Aircraft Design

W. E. Beall
E. H. Heinemann
Hall L. Hibbard
Richard Hutton
C. L. Johnson
A. A. Kartveli
E. G. Stout
F. K. Teichmann
Robert J. Woods

Electronics in Aviation

Welcome W. Bender
K. C. Black
M. V. Kiebert, Jr.
David S. Little
S. B. Rogers
Paul Rosenberg
L. M. Sherer

Physiologic Problems

H. G. Armstrong
Louis H. Bauer
Robert J. Benford
W. Randolph Lovelace, II
Ross A. MacFarland

Fuels and Oils

D. P. Barnard
J. H. Doolittle
Graham Edgar
R. T. Goodwin
A. M. Rothrock

Flight Propulsion

George W. Brady
Frank W. Caldwell
L. S. Hobbs
E. E. Johnson
Joseph Keenan
R. P. Kroon
Hans Reissner
Abe Silverstein
C. Fayette Taylor
E. S. Taylor
P. B. Taylor
E. S. Thompson
H. S. Tsien

Instruments

Allan G. Binnie
Charles H. Colvin
Frank R. Cook
C. S. Draper
S. G. Eskin
O. E. Esval
C. F. Savage
R. C. Sylvander

Meteorology

C. F. Brooks
D. M. Little
F. W. Reichelderfer
K. C. Spengler

SUBSCRIPTION RATES

JOURNAL OF THE AERONAUTICAL SCIENCES, Published Monthly.—United States and Possessions: 1 Year, $12.00; Single Copies, $1.50. Foreign Countries Including Canada (American Currency Rates): 1 Year, $13.00; Single Copies, $1.50.

AERONAUTICAL ENGINEERING REVIEW, Published Monthly.—United States and Possessions: 1 Year, $3.00; Single Copies, $0.50. Foreign Countries Including Canada (American Currency Rates): 1 Year, $3.50; Single Copies, $0.50.

Notices of change of address should be sent to the Institute at least 30 days prior to actual change of address.

Manuscripts for publication, proofs, and all correspondence should be addressed to the Editorial Office of the JOURNAL.

Correspondence regarding subscriptions may be addressed to Publication Office, 20th and Northampton Sts., Easton, Pa., or to the Editorial Office of the JOURNAL OF THE AERONAUTICAL SCIENCES, 2 East 64th Street, New York 21, N.Y.

Copyright, 1955, by the Institute of the Aeronautical Sciences, Inc.

Entered as Second Class Matter at the Post Office, Easton, Pa., May 1, 1937. Acceptance for mailing at a special rate of Postage provided for in the Act of August 24, 1912. Authorized April 29, 1937.

JOURNAL OF THE AERONAUTICAL SCIENCES

VOLUME 22 SEPTEMBER, 1955 NUMBER 9

On the Laminar Compressible Boundary Layer over a Flat Plate with Suction or Injection*

H. G. LEW† AND J. B. FANUCCI‡

The Pennsylvania State University, School of Engineering

ABSTRACT

Exact solutions for the flow of a compressible laminar boundary layer over a flat plate with homogeneous suction or injection are considered in this report. Characteristics of these flows are given in detail, and it is shown that the solutions by the momentum method given in references 1, 2, and 9 compare favorably with these results.

Asymptotic solutions are also developed which are valid for the flow far downstream from the leading edge of the plate or for flows over arbitrary bodies with large suction. It is shown that the exact solutions for the flow over a flat plate with homogeneous suction approach the asymptotic solution downstream of the leading edge. Moreover, for practical purposes, this occurs at a rather short distance from the leading edge. The asymptotic solutions are given in closed form for several cases; they may also be used as a first approximation for the above flows. It is also shown that the method of Lighthill[12] for the approximate calculation of heat transfer at the wall is exact for the asymptotic solution.

SYMBOLS AND NOTATION

$A = T_0/T_1$
$A_1 = \rho_0 v_0/C\mu_1$
$B = 1 - T_0/T_1 + \frac{\gamma - 1}{2} M_1^2$
$B_1 = \rho_1/(C\mu_1)\sqrt{1 + [(\rho_0^2/\rho_1^2)v_0^2]}$
C = constant defined by $\mu^* = CT^*$
c_p = specific heat at constant pressure
$H = c_pT + (u^2/2)$
$i = c_pT$
k = coefficient of thermal conductivity
M = Mach Number
$N = [(\gamma - 1)/2]M_1^2$
S = Sutherland constant
T = absolute temperature
$T^* = T/T_1$
U = free-stream velocity in x direction
u, v = velocity components in x and y directions, respectively
x, y = coordinates parallel and perpendicular to surface, respectively
N_u = Nusselt Number
P_r = Prandtl Number, $(\mu c_p/k)$
y^* = distance parameter, $[-(v_0 y)/(C\nu_1)]$
σ = distance parameter, $[-(\rho_0 v_0)/(C\mu_1)\sqrt{2C\nu_1 x/U}]$
ξ = distance parameter, $(-v_0/U)^2(Ux/\nu_1)$
γ = ratio of specific heat at constant pressure to specific heat at constant volume
ν = kinematic viscosity (μ/ρ)
ρ = mass density of fluid
μ = coefficient of viscosity
τ = shear stress, also dependent variable in Eq. (15)
ψ = stream function
$\rho^* = \rho/\rho_1$
$\mu^* = \mu/\mu_1$

Subscripts

1, ∞ = conditions outside of the boundary layer
0 = conditions at the wall or surface of the body

Superscript

n = exponent occurring in $\mu^* = CT^{*n}$

Received November 4, 1954.

* This research was supported by the United States Air Force, through the Office of Scientific Research of the Air Research and Development Command, and their sponsorship is gratefully acknowledged.

† Associate Professor.

‡ Instructor in Aeronautical Engineering.

INTRODUCTION

A STUDY OF THE FLOW of a compressible boundary layer over a flat plate with a small uniform normal velocity at the plate is presented in this report. This solution might be found useful in several applications. On the one hand, the use of suction to control the boundary layer at high speeds requires the accurate knowledge of the velocity and temperature profiles. On the other hand, the possibility of the use of injection at the wall to cool a body in a high-temperature gas demands a knowledge of the heat-transfer properties in such a combination. Several reports have dealt

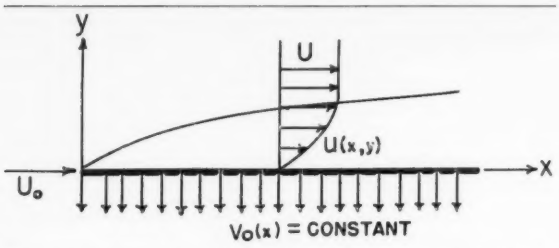

FIG. 1. Explanatory sketch for flat plate in longitudinal flow with constant suction.

with solutions of the above problems. For the case of suction, which this report will deal with for the most part, Lew[1] has solved the flow of a compressible boundary layer over a flat plate with homogeneous suction by a modified Kármán momentum method. In the case of homogeneous injection, the problem has been solved by Lew[2] utilizing the modified Kármán momentum method while Yuan[3] solved the same problem by applying the Kármán-Polhausen method directly as in the incompressible flow. In this report, the problem is explored and exact solutions are calculated for the cases of homogeneous suction and injection. Asymptotic solutions for the suction case are derived in closed form for the case of arbitrary heat transfer at the boundary. These asymptotic solutions represent the flow at an infinite distance from the leading edge in the case of homogeneous suction and the flows for extremely large suction which are compatible with the boundary-layer assumptions. Moreover, they showed the effects of the various parameters easily due to their simplicity of solution. The asymptotic solutions also indicate the validity of an approximate method for the calculation of heat transfer at the boundary.

This work was done with the thought that an exact solution might be found useful for comparison with the approximate solutions and especially for stability calculations. Extensions to the cases of an arbitrary pressure gradient and arbitrary suction or injection distribution could be made.

EQUATIONS OF MOTION

An x-y-Cartesian coordinate system with the origin at the leading edge of a semi-infinite plate is utilized here (see Fig. 1). The equations of the compressible boundary layer are the momentum, mass, and energy conservation laws, and the equation of state of a perfect gas. They are, respectively:

$$\rho\{[u(\partial u/\partial x)] + [v(\partial u/\partial y)]\} = (\partial/\partial y)\,[\mu(\partial u/\partial y)] \quad (1)$$

$$[\partial(\rho u)/\partial x] + [\partial(\rho v)/\partial y] = 0 \quad (2)$$

$$\rho c_p\left(u\frac{\partial T}{\partial x} + v\frac{\partial T}{\partial y}\right) = \frac{\partial}{\partial y}\left(k\frac{\partial T}{\partial y}\right) + \mu\left(\frac{\partial u}{\partial y}\right)^2 \quad (3)$$

$$p = \rho RT \quad (4)$$

A linear viscosity temperature relation is utilized here of the form

$$\mu/\mu_1 = C(T/T_1) \quad (5)$$

as given in reference 4. The constant C is determined by the more accurate Sutherland relation for the temperature dependence of viscosity. The use of this relation [Eq. (5)] has been discussed in reference 4. In addition, the Prandtl Number is taken as unity in the numerical calculations so that some former results can be used. However, this assumption is not necessary in the analysis. The extension to arbitrary Prandtl Number is given in Appendix II of reference 13. For a Prandtl Number of unity, the familiar Crocco integral of the energy equation could be used as shown in reference 6. The momentum and energy equations are satisfied by a polynomial relation between the temperature and the velocity of the form

$$\frac{T}{T_1} = \frac{T_0}{T_1} - \frac{\gamma-1}{2}M_1^2\left(\frac{u}{U}\right)^2 - \left[\frac{T_0}{T_1} - 1 - \left(\frac{\gamma-1}{2}\right)M_1^2\right]\left(\frac{u}{U}\right) \quad (6)$$

In addition, if there is zero heat transfer at the wall, then $(\partial T/\partial y)_0 = 0$, and since the free-stream total temperature ratio is given by

$$T_0/T_1 = 1 + [(\gamma-1)/2]M_1^2$$

Eq. (6) reduces to

$$T/T_1 = (T_0/T_1) - [(\gamma-1)/2]M_1^2(u/U)^2 \quad (7)$$

The boundary conditions for this problem are

$$\left.\begin{aligned} u(x,0) &= 0 \\ u(x,\infty) &= U \\ u(0,y) &= U \\ v(x,0) &= v_0(x) \\ T(x,0) &= T_0 = \text{constant} \\ T(x,\infty) &= T_1 = \text{constant} \end{aligned}\right\} \quad (8)$$

The above equations can be more conveniently used in the (x, ψ) coordinates. Thus, the momentum equation [Eq. (1)] becomes

$$\partial u/\partial x = (1/\rho_1^2)\,(\partial/\partial\psi)\,[\mu\rho u(\partial u/\partial\psi)] \quad (9)$$

where the stream function ψ is defined by

$$\left.\begin{aligned} u &= (\rho_1/\rho)\,(\partial\psi/\partial y) \\ v &= -(\rho_1/\rho)\,(\partial\psi/\partial x) \end{aligned}\right\} \quad (10)$$

The boundary conditions on the velocity components become

$$\left.\begin{aligned} u[x, f(x)] &= 0 \\ u(x,\infty) &= U \\ u(0,\psi) &= U \end{aligned}\right\} \quad (11)$$

and

$$f(x) = -\int_0^x \frac{\rho_0}{\rho_1} v_0(x)dx \qquad \text{at } y = 0$$

The boundaries of integration are curvilinear as can be seen from Eqs. (11), and the following transformation leads to straight line boundaries that are more amenable to analysis. Let

$$\left.\begin{aligned}\phi &= \psi - f(x)\\ \eta &= \int_0^x \sqrt{1 + \frac{f'(x)^2}{U^2}}\,dx\end{aligned}\right\} \tag{12}$$

where $f(x)$ is as defined by eqs. (11) and the prime denotes differentiation. Thus, Eq. (9) becomes

$$-f'(x)\frac{\partial u}{\partial \phi} + \sqrt{1 + \frac{f'(x)^2}{U^2}}\frac{\partial u}{\partial \eta} = \frac{1}{\rho_1^2}\frac{\partial}{\partial \phi}\left(\mu\rho u\frac{\partial u}{\partial \phi}\right) \tag{13}$$

with the boundary conditions

$$\left.\begin{aligned}u(\eta, 0) &= 0\\ u(\eta, \infty) &= U\\ u(0, \phi) &= U\end{aligned}\right\} \tag{14}$$

For the case of constant $v_0(x)$, Eq. (13) and boundary conditions [Eqs. (14)] can be further transformed to the more convenient forms of

$$\sqrt{V}(\partial^2 V/\partial\tau^2) + (\partial V/\partial\tau)\left[+2\tau\sigma + \tau^3 - (\sqrt{V}/\tau)\right] = 2\tau^2\sigma(\partial V/\partial\sigma) \tag{15}$$

and

$$\left.\begin{aligned}V(\sigma, 0) &= 0\\ V(\sigma, \infty) &= 4\end{aligned}\right\} \tag{16}$$

The new variables are defined by

$$\left.\begin{aligned}V(\sigma, \tau) &= (4/U^2)u^2\\ \tau^2 &= \left(\frac{2}{U}\psi + 2\frac{\rho_0 v_0}{\rho_1 U}x\right)\Big/\sqrt{\frac{2C\nu_1 x}{U}}\\ \sigma &= -(\rho_0 v_0)/(C\mu_1)\sqrt{2C\nu_1 x/U}\end{aligned}\right\} \tag{17}$$

The relations of ϕ and η variables to τ and σ are

$$\left.\begin{aligned}\tau &= \sqrt{-A_1\phi}/\sqrt{(A_1^2/B_1)\eta}\\ \sigma &= \sqrt{(A_1^2/B_1)\eta}\end{aligned}\right\} \tag{18}$$

where

$$A_1 = (\rho_0 v_0)/(C\mu_1)$$

$$B_1 = \rho_1/(C\mu_1)\sqrt{1 + (\rho_0^2/\rho_1^2)v_0^2/U^2}$$

Eq. (15) and the boundary conditions [Eqs. (16)] are valid for the flow over a flat plate with uniform suction or injection. It is noted that if suction is considered the constant A_1 is negative and σ is positive. Correspondingly, σ takes on negative values if injection is considered. In these relations the viscosity relation as given by Eq. (5) has been used. In this form, Eqs. (15) and (16) are independent of the magnitude of the suction or injection velocities at the wall and of the physical properties of the fluid. Moreover, the equations have the same form as in the incompressible case so that all results of the incompressible case can be used.

The conversion to the physical plane can be easily accomplished by the relation

$$\xi = (C\sigma^2/2)(T_0/T_1)^2$$

$$-\frac{v_0 y}{C\nu_1} = \left(\frac{T_0}{T_1}\right)2\sigma\int_0^\tau \frac{(T/T_1)\tau d\tau}{\sqrt{V}} \quad \text{for constant } \sigma \tag{19}$$

where $\xi \equiv (-v_0/U)^2(Ux/\nu_1)$. The second of Eqs. (19) is found from Eq. (10) by integration in the y direction for constant x.

At the point $\sigma = 0$ for either suction or injection there is a singularity of the differential equation Eq. (15). However, it can be shown that the velocity profile at this point is a Blasius profile. If an expansion of $V(\sigma, \tau)$ in a series in the neighborhood of $\sigma = 0$ is made of the form

$$V(\sigma, \tau) = V_0(\tau) + \sigma V_1(\tau) + \sigma^2 V_2(\tau) + \dots \tag{20}$$

then Eq. (15) leads to

$$\sqrt{V_0}V_0'' + V_0'[\tau^3 - (\sqrt{V_0}/\tau)] = 0 \tag{21}$$

with the insertion of the expansion, Eq. (20). The boundary conditions for $V_0(\tau)$ are

$$V_0(0) = 0, \quad V_0(\infty) = 4 \tag{22}$$

It is seen that Eqs. (21) and (22) are the Blasius system in the σ, τ coordinates, so it follows that the Blasius profile exists at $\sigma = 0$ for both suction and injection. Iglisch has shown this for the suction case[5] for incompressible flow.

It may be noted that the solutions of the compressible boundary-layer equations with suction and zero pressure gradient can be deduced from the incompressible one when μ is proportional to T by using the transformation given by the senior author in references 1 and 9 as a generalization of Dorodnitzyn's work for zero heat transfer. This transformation is a special case of Illingworth and Stewartson's results given in reference 14 and 15 on the equivalence of compressible and incompressible boundary layer for the cases with non-zero pressure gradient.

Evaluation of the Characteristics of the Flow

The characteristics of the boundary layer are conveniently given in terms of the variable y in the form of

$$y^* = -(v_0 y)/(C\nu_1) \tag{23}$$

The first and second derivatives of the velocity component u are then given by (a)

$$\frac{1}{U}\frac{\partial u}{\partial y^*} = \frac{T_1}{8T_0}\frac{T_1}{T\sigma\tau}\frac{\partial V}{\partial \tau} \tag{24}$$

and (b)

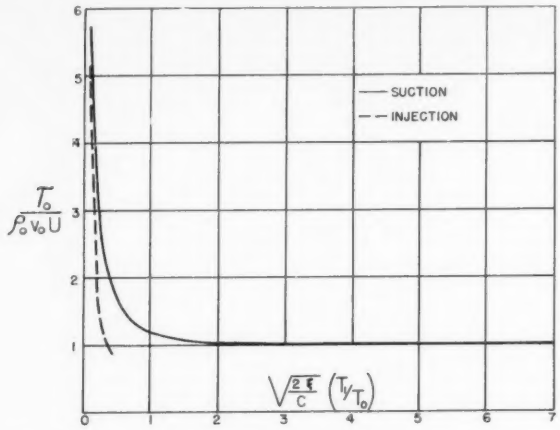

FIG. 2. Skin friction vs. distance parameter ξ for suction and injection.

$$\frac{1}{U}\frac{\partial^2 u}{\partial y^{*2}} = \frac{\sqrt{V}}{16\sigma^2\tau}\left(\frac{T_1}{T_0}\right)^2\left(\frac{T_1}{T}\right)\left[\frac{1}{\tau}\frac{\partial V}{\partial \tau}\frac{\partial}{\partial \tau}\left(\frac{T_1}{T}\right) + \frac{1}{\tau^2}\left(\frac{T_1}{T}\right)\left(\tau\frac{\partial^2 V}{\partial \tau^2} - \frac{\partial V}{\partial \tau}\right)\right]$$

Thus the skin friction at the wall given by the expression

$$\tau_0 = \mu_0(\partial u/\partial y)_0 \tag{25}$$

is

$$\tau_0 = -\rho_0 v_0 U(d_2/4\sigma) \tag{26}$$

where $d_2 = (1/2)\ (\partial^2 V/\partial \tau^2)_{\tau=0}$ and σ is related to ξ by the first of Eqs. (19). Eq. (26) is shown in Fig. 2. (Cf. Table 1.) The displacement thickness defined by

$$\delta^* = \int_0^\infty \left(1 - \frac{\rho}{\rho_1}\frac{u}{U}\right) dy \tag{27}$$

becomes a function of σ in the form of

$$-\frac{v_0\delta^*}{C\nu_1} = 2\frac{T_0}{T_1}\sigma\int_0^\infty \left[\left(\frac{T}{T_1}\right)_\tau - \frac{\sqrt{V(\sigma,\tau)}}{2}\right]\times \frac{\tau d\tau}{\sqrt{V(\sigma,\tau)}} \tag{28}$$

The integration with respect to τ is performed with σ held constant. Lastly, the momentum thickness defined by

$$\theta = \int_0^\infty \frac{\rho}{\rho_1}\frac{u}{U}\left(1 - \frac{u}{U}\right) dy \tag{29}$$

is given in the form of

$$-\frac{v_0\theta}{C\nu_1} = \frac{T_0}{T_1}\sigma\int_0^\infty \left(1 - \frac{\sqrt{V(\sigma,\tau)}}{2}\right)\tau d\tau \tag{30}$$

CASE OF HOMOGENEOUS SUCTION

The solution of Eq. (15) with the boundary conditions [Eqs. (16)] for the suction case (positive σ) has been calculated in detail by Iglisch[5] for incompressible flow by a method of profile continuation using Adam's method of numerical integration for a fixed value of σ. The integration involves replacing the differential term in the σ direction by a finite difference approximation and linearizing the equation by replacing all terms of $\sqrt{V}$ by values at the previous value of σ. The resulting ordinary differential equation is then integrated by Adam's method. From Iglisch's results the values of $V(\sigma, \tau)$ for the case of suction have been calculated. The suction case, of course, corresponds to $\sigma > 0$. These values are tabulated in reference 13. From these values of $V(\sigma, \tau)$, the various characteristics in the compressible case can be calculated by one integration for y^* in the form of the first-order differential equation

$$dy^*/d\tau = Q(\tau) \tag{31}$$

with the initial condition of $y^* = 0$ at $\tau = 0$. Here $Q(\tau)$ is given by the second of Eqs. (19) in the form

$$Q(\tau) = (2T_0/T_1^2)\ \sigma[(T\tau)/\sqrt{V(\sigma,\tau)}]$$

where σ is held constant. The temperature T is related to V by Eqs. (6) or (7) and the first of Eqs. (17).

The velocity profiles at $M_1 = 4$ for several values of ξ have been calculated for zero heat transfer at the wall and are given in Fig. 3. For the purpose of comparison with reference 9, which uses a modified momentum method, one velocity profile was calculated for $M_1 = 2$, $T_0/T_1 = 2$ at $\xi = 0.5$ for $C = 1$. This calculation is shown in Fig. 4 where the result of the momentum method (reference 9, for $n = 1$) is also shown. The comparison is extremely good indicating that the momentum method is accurate as far as the velocity profiles are concerned. A comparison of the first derivatives of the velocity profiles is given in Fig. 5, and again the agreement between the exact method and momentum method is excellent. As to be expected, the second derivatives of the profiles using the momentum method do not agree well with the exact method given here. Values of the second derivatives for the momentum method differ by about 20 per cent at the

TABLE 1
d_2 Coefficients for Various σ

σ	d_2
−0.2	1.412
−0.1	1.633
0	1.878
0.1	2.129
0.2	2.389
0.3	2.659
0.4	2.936
0.5	3.224
0.6	3.521
0.7	3.825
0.8	4.134
0.9	4.453
1.0	4.776
1.2	5.448
1.4	6.126
1.6	6.835
2.0	8.288
2.4	9.782
3.2	12.915
4.0	16.000

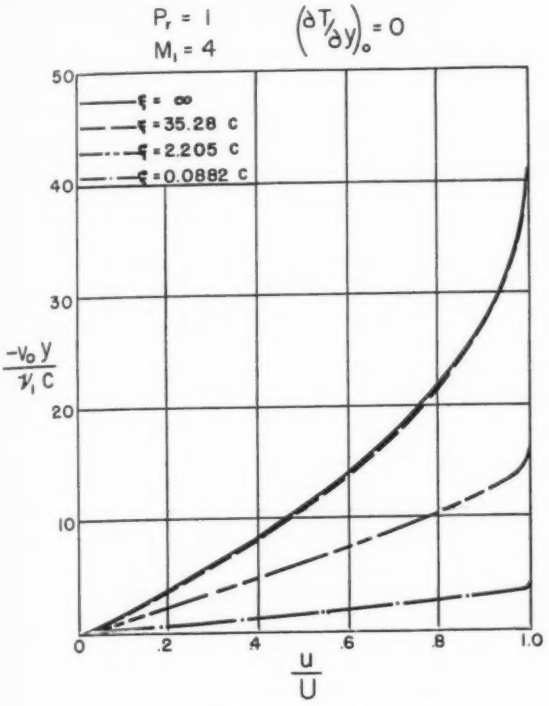

FIG. 3. Suction velocity profile development.

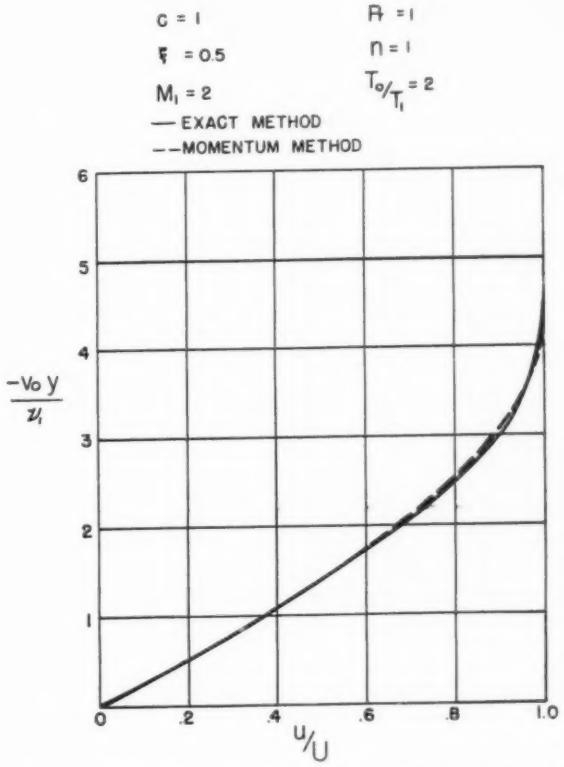

FIG. 4. Comparison of suction velocity profile with reference 9.

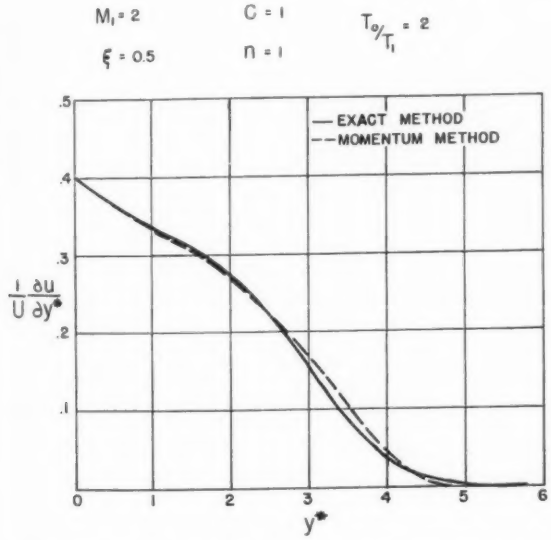

FIG. 5. Comparison of first derivative for suction profile with reference 9.

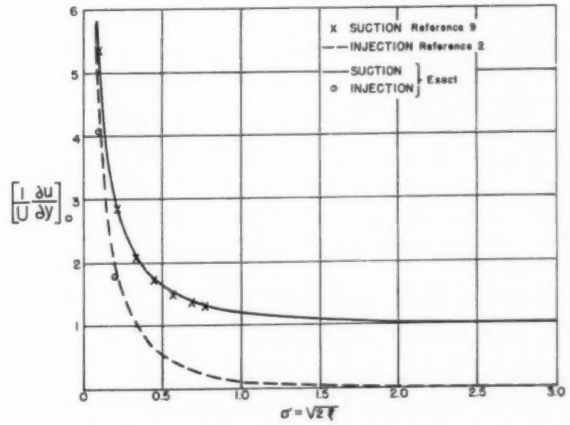

FIG. 6. Comparison of first derivative at the wall for $M_1 = 0$.

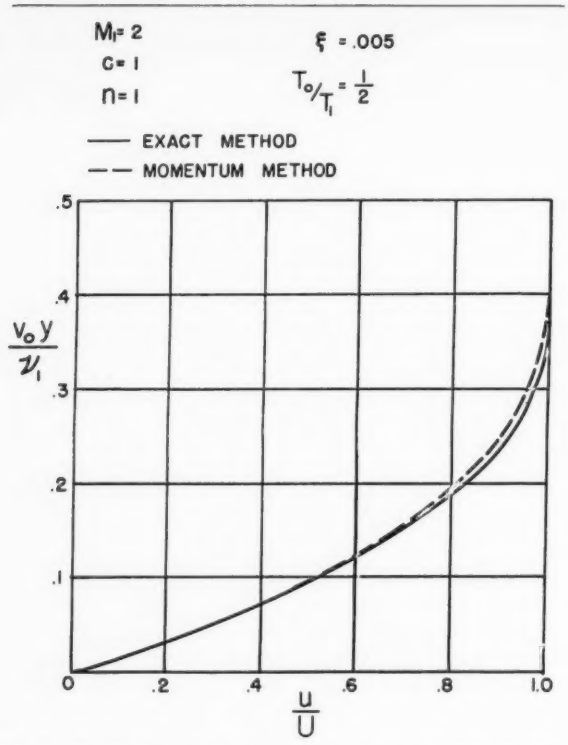

FIG. 7. Comparison of injection velocity profile with reference 2.

wall. A comparison with reference 9 of the first derivative at the wall as a function of σ for $M_1 = 0$ is shown in Fig. 6.

CASE OF HOMOGENEOUS INJECTION

For the case of homogeneous injection, Eq. (15) with boundary conditions [Eqs. (16)] is integrated for negative σ from $\sigma = 0$. The same method as described under the suction section is used. Detailed calculations are presented from $\sigma = 0$ to $\sigma = -0.2$ in reference 13. The comparisons of the characteristics of the flow with the momentum method[2] are shown in Figs. 7 and 8. Again the velocity profiles and its first derivatives are in good agreement even though the comparison is made at a point extremely close to the leading edge of the plate where characteristics of the flow vary rapidly. The second derivatives do not compare well; for example, they differ from each other by about 17 per cent at the wall. The Nusselt Number characterizing the heat transfer at the wall defined by

$$N_u = -(\partial T/\partial y)_0 \, [x/(T_1 - T_0)]$$

appropriate to this analysis is

$$N_u = \frac{-\{1 - (T_0/T_1) + [(\gamma - 1)/2]M_1^2\}\xi d_2\left(\frac{U}{v_0}\right)}{4\sigma C(T_0/T_1)^2 \, [1 - (T_0/T_1)]} \quad (32)$$

At $\xi = 0.005$, $T_0/T_1 = 1/2$, $M_1 = 2$, $C = 1$, Eq. (32) gives a value of

$$N_u = -0.09177(U/v_0)$$

as compared to the momentum method[2] value of $N_u = -0.10048(U/v_0)$. The difference is 8.7 per cent for this value of ξ, which is very near the leading edge. The skin-friction intensity is also shown in Fig. 2, indicating a smaller value than the suction case, as is to be expected. Moreover, this skin-friction intensity will approach zero, indicating a possible separation of the flow. Details of the calculations are given in Appendix I of reference 13.

ASYMPTOTIC SOLUTIONS

The asymptotic characteristics of the flow in the case of suction will be considered in this section. These asymptotic properties will hold for large values of x or large values of the suction velocity at the boundary compatible with the boundary-layer assumptions. The asymptotic results are important since the flow for suction will rapidly approach this state a short length from the leading edge of the plate. Moreover, these equations are some of the relatively few in the theory of compressible laminar boundary layer which can be integrated in closed form. The following case is first considered with the Prandtl Number equal to unity. If the conditions far downstream from the leading edge of the plate are considered, then all properties of the flow are independent of x. Hence Eqs. (1), (2), and (3) become

$$\rho v(du/dy) = (d/dy)\,[\mu(du/dy)] \quad (33)$$

$$\rho v = \text{constant} \quad (34)$$

$$\rho v(dT/dy) = (1/P_r)\,(d/dy)\,[\mu(dT/dy)] + (\mu/c_p)\,(du/dy)^2 \quad (35)$$

for P_r = constant. The boundary conditions are

$$\left.\begin{aligned} y = 0: &\quad u = 0,\ T = T_0 = \text{constant} \\ y \to \infty: &\quad u = U,\ T = T_1 \end{aligned}\right\} \quad (36)$$

When the Prandtl Number is unity the temperature is related to the velocity by Eq. (6). In this analysis, the viscosity can be taken as a function of the temperature in the form

$$\mu^* = CT^{*n} \quad (37)$$

Thus for $n = 1$, Eq. (37) coincides with Eq. (5). For $c = 1$ the usual power relation is obtained for which n is taken usually at 0.7 to 0.8 for air.

Eqs. (33) to (37) can be integrated to the form

$$y = \frac{\mu_1 C}{\rho v}\int_0^{u/U} \frac{(A + Bt + Nt^2)^n}{(t - 1)}\,dt \quad (38)$$

where

$$A = T_0/T_1$$

$$B = \{1 - (T_0/T_1) + [(\gamma - 1)/2]M_1^2\}$$

$$N = -[(\gamma - 1)/2]M_1^2$$

Here t is a dummy variable of integration. For $n = 1$, Eq. (38) integrates to

$$(v_0/\nu_1 C) = (T_0/T_1)\left\{(N/2)\,(u/U)^2 + (B + N)\,(u/U) + \log[1 - (u/U)]\right\} \quad (39)$$

The boundary conditions [Eqs. (36)] have been satisfied in Eqs. (38) and (39). It is noted that Eq. (38) can be simply integrated numerically for nonintegral values of n. Equation (39) reduces to the incompressible asymptotic profile of Griffith[10] if $A = C = 1$ and $M_1 = N = 0$.

For Prandtl Number not equal to unity, an extension of the solution by Young,[11] who considered the problem with zero heat transfer at the wall, to the case of nonzero heat transfer at the wall is possible. Equations (33) to (35) are first transformed from the (y) coordinate to the (u) coordinate; they become

$$\mu(du/dy) = -\rho_1 v_1 (U - u) \quad (40)$$

$$(1 - P_r)\,(di/du) - (U - u) \times \left\{[(d^2 i)/(du^2)] + P_r\right\} = 0 \quad (41)$$

with the boundary conditions of

$$\left.\begin{aligned} u = 0, \quad i = i_0 \quad & \text{at } y = 0 \\ u = U, \quad i = i_1 \quad & \text{as } y \to \infty \end{aligned}\right\} \quad (42)$$

It can be shown that the solution to Eq. (41) and satisfying conditions (42) for arbitrary Prandtl Number is

$$i_1 - i = \left(1 - \frac{u}{U}\right)^{P_r}\left(i_1 - i_0 + \frac{U^2}{2}\right) + \frac{P_r U^2}{2(2 - P_r)}\left[\left(1 - \frac{u}{U}\right)^2 - \frac{2}{P_r}\left(1 - \frac{u}{U}\right)^{P_r}\right] \quad (43)$$

The velocity u is related to y by

$$u/U = 1 - \exp(\zeta) \quad (44)$$

and

$$\zeta = -\int_0^\eta \left(\frac{i_1}{i}\right)^n \frac{d\eta}{C} \quad (45)$$

where $\eta = -(v_1 y)/\nu_1$. The viscosity relation (37) is used here. Substitution of Eq. (44) into Eq. (43) leads to

$$(1 - T^*)/N = (B/N)\exp(P_r\zeta) + [P_r/(2 - P_r)]F(\zeta) \quad (46)$$

where

$$F(\zeta) = (2/P_r)\exp(P_r\zeta) - \exp(2\zeta)$$

For the case where the viscosity varies linearly with the temperature so that $n = 1$, Eq. (45) can be integrated in closed form and is

$$-\frac{\eta}{C} = \zeta - N\frac{P_r}{(2 - P_r)}\left(\frac{2}{P_r^2}e^{P_r\zeta} - \frac{1}{2}e^{2\zeta} - \frac{2}{P_r^2} + \frac{1}{2}\right) - \left(1 - \frac{i_0}{i_1} - N\right)\left(\frac{e^{P_r\zeta} - 1}{P_r}\right) \quad (47)$$

In fact, Eq. (45) can be integrated in closed form for n equal to an integer. Equation (47) reduces to Eq. (39) for the case of $P_r = 1$. The gradient of the temperature gives an indication of the heat transfer at the wall; thus,

$$(dT^*/dy)_0 = -[(v_0 B)/(\nu_1 C)]\,(T_1/T_0)^{n+1} P_r \quad (48)$$

using Eqs. (45) and (46). The skin-friction intensity is particularly simple and has the same form as in the incompressible case of

$$\tau_0 = -\rho_0 U v_0 \quad (49)$$

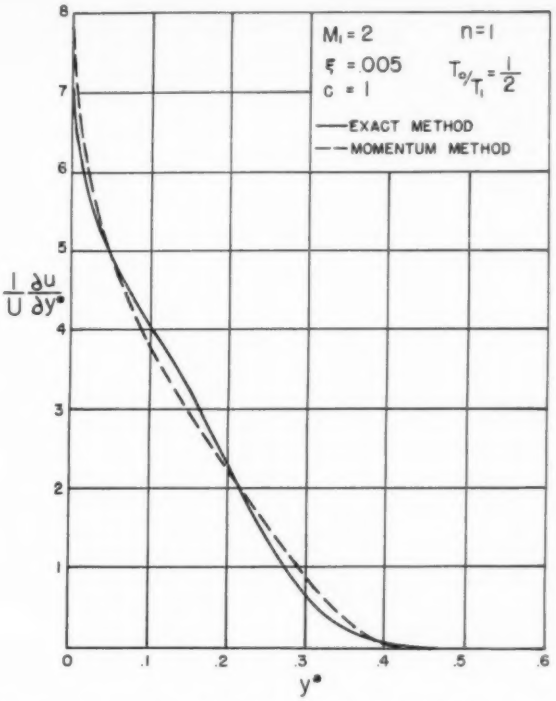

FIG. 8. Comparison of first derivative for injection profile with reference 2.

The temperature profiles for various conditions with $n = 1$ are shown in Fig. 9. The effect of Prandtl Number on the temperature profiles is pronounced, as seen from these curves that were calculated for $P_r = 1$ and $P_r = 0.72$. In fact, the temperature gradient [Eq. (48)] at the wall is directly proportional to the value of the Prandtl Number. Its value for $P_r = 1$ is 40 per cent in error if $P_r = 0.72$ is assumed to be correct. This is another indication that the heat-transfer characteristics should be based on correct values of P_r.

The effect of Prandtl Number on the velocity profiles is negligible as can be readily seen from Fig. 10. The change of the suction velocity profiles from the leading edge to the asymptotic profile occurs rapidly (Fig. 3). For example, at a value of $\xi = (-v_0/U)^2 \times (Ux/\nu_1)$ of the order of 35 to 40, $M_1 = 4$, $P_r = 1$, and $\left(\frac{\partial T}{\partial y}\right)_0 = 0$, the asymptotic profile is already approached for practical purposes.

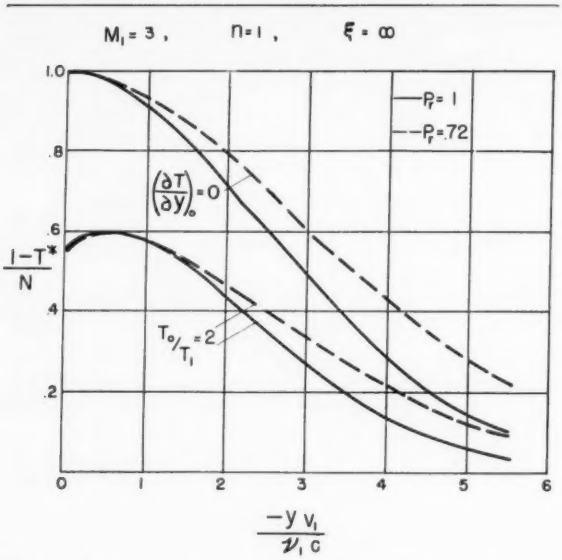

FIG. 9. Asymptotic temperature profile. (Effect of Prandtl Number.)

APPROXIMATE CALCULATION OF HEAT TRANSFER

A method of approximation for the heat transfer at the wall based on Lighthill[12] is easily formulated and examined here. First, define a scalar function $\lambda(y)$ such that

$$\lambda = \int_0^y \frac{\rho u}{\rho_1}\, dy \tag{50}$$

which transforms Eqs. (33), (34), and (35) to

$$(\rho v)\,\frac{dH}{d\lambda} = \frac{1}{P_r}\frac{d}{d\lambda}\left[\mu\,\frac{\rho u}{\rho_1}\frac{dH}{d\lambda} + \mu\frac{\rho u}{\rho_1}\,(P_r - 1)\,\frac{d(u^2/2)}{d\lambda}\right] \tag{51}$$

where

$$H = c_p T + (u^2/2)$$

If the assumption that the second term on the right side of Eq. (51) is small for P_r number close to one, then this term can be neglected. Thus one obtains,

$$(\rho v)\,(dH/d\lambda) = (1/P_r)\,(d/d\lambda)[(\mu\rho u/\rho_1)\,(dH/d\lambda)] \tag{52}$$

If Eqs.(5) and (33) are used, Eq.(52) can be integrated to

$$(1 - T^*)/N = (B/N)\,[1 - (u/U)]^{P_r} + 1 - (u/U)^2 \tag{53}$$

which is the complementary solution of Eq. (41). The temperature gradient at the wall, from Eq. (53), is exactly that given by Eq. (48) with $n = 1$.

If, in addition, the approximation that the velocity u is expanded in a series in λ and only the first term is retained of the form

$$u/U = a\lambda^{1/3} \tag{54}$$

where $a = \sqrt{[(-\rho_1 v_1)2\rho_1]/[(\rho_0\mu_0)U]}$, Eq. (52) becomes

$$(\rho v)\,(dH/d\lambda) = [(\mu\rho U a)/(P_r\rho_1)]\,(d/d\lambda) \times [\lambda^{1/3}(dH/d\lambda)] \tag{55}$$

which has a solution of

$$(1 - T^*)/N = (B/N)e^{(2/F)\lambda^{1/3}} + 1 - (u/U)^2 \tag{56}$$

where $F = [(\mu\rho)Ua]/[P_r\rho_1(\rho v)]$ = constant. The temperature gradient according to Eq. (56) is

$$[dT^*/dy]_0 = -BP_r[v_0/(\nu_1 C)]\,(T_1/T_0)^2 \tag{57}$$

which is again exactly Eq. (48) for $n = 1$. The two approximations made for the asymptotic solution resulted in temperature gradients at the wall which are exact. Thus it appears that if heat transfer at the boundary for a more general problem is required, the approximations as given by Eqs. (52) and (54) would lead to values that should be close to the exact values obtained by more complicated methods.

CONCLUSIONS

An exact solution of the compressible laminar boundary layer over a flat plate with homogeneous suction or injection has been given for $P_r = 1$ and an effective linear viscosity relation with temperature. The details for the suction case are worked out and are in excellent agreement with the results of the modified momentum method[1,9] except for the second derivatives of the velocity profiles which differ by about 20 per cent at the wall. A comparison of the first derivative at the wall is given in Fig. 6, which indicates good agreement in the suction case. This shows that the momentum method as given by references 1 and 9 are sufficiently accurate for any practical purposes. However, any stability calculations should be based on the more exact values as calculated in this report and tabulated in reference 13. The characteristics of the injection case were calculated to a value of $\sigma = -0.2$, and results are in good agreement with the momentum method of reference 2, although the results

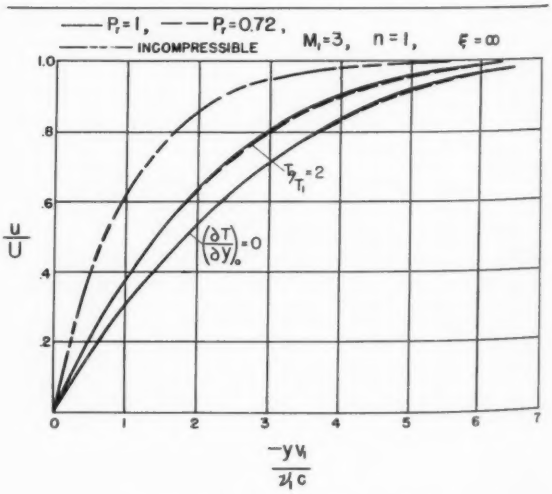

FIG. 10. Asymptotic velocity profile.

of the suction case were in better agreement with the momentum method as indicated by a comparison of Figs. 5 and 8 for the first derivatives of the velocity. However, it is expected that the results of the momentum method differ considerably more from the exact calculations further downstream of the leading edge as separation of the flow is approached. Some further calculations are now being made, and results indicate a possible separation at $\sigma = -1.1$. These results will be presented in a forthcoming report.

The asymptotic solutions for the compressilbe boundary layer over a flat plate with homogeneous suction are completely derived for arbitrary heat transfer at the wall, arbitrary Prandtl Number, and a power law for the viscosity-temperature relation. Since the asymptotic solution can be easily obtained in closed form or by a simple quadrature, they are especially useful in determining the effect of the various parameters. Closed form solutions are given for a linear viscosity-temperature law, and these results show that the effect of Prandtl Number on the velocity profiles is negligible and that the effect on the heat-transfer characteristics is large.

The agreement of the exact solutions for suction in the first part of this report at large distances along the plate with the asymptotic solutions is excellent. It is noted that the asymptotic solutions are also valid for large values of the suction velocity at the wall, even with pressure gradient, compatible with the boundary-layer approximations. Therefore, these results can be used as first approximations in the practical calculation of the characteristics of such flows.

References

[1] Lew, H. G., *On the Compressible Boundary Layer Over a Flat Plate with Uniform Suction*, Contributions to Applied Mechanics, Reissner Anniversary Volume, pp. 43–60, J. W. Edwards, Ann Arbor, Mich., 1949.

[2] Lew, H. G., *The Cooling of a Flat Plate in a Laminar Compressible Flow by Uniform Fluid Injection*, P.I.B.A.L. Report No. 131, Polytechnic Institute of Brooklyn, September, 1948.

[3] Yuan, S. W., *Heat Transfer in Laminar Compressible Boundary Layer on a Porous Flat Plate with Fluid Injection*, Journal of the Aeronautical Sciences, Vol. 16, No. 12, pp. 741–748, December, 1949.

[4] Chapman, D., and Rubesin, M., *Temperature and Velocity Profiles in the Compressible Laminar Boundary Layer with Arbitrary Distribution of Surface Temperature*, Journal of the Aeronautical Sciences, Vol. 16, No. 9, pp. 547–565, September, 1949.

[5] Iglisch, R., *Exact Calculation of Laminar Boundary Layer in Longitudinal Flow Over a Flat Plate with Homogeneous Suction*, NACA TM No. 1205, 1949.

[6] Crocco, L., *Transmission of Heat From a Flat Plate to a Fluid Flowing at a High Velocity*, NACA TM No. 690, 1932.

[7] Salvadori, M. G., *The Mathematical Solution of Engineering Problems*, First Edition, McGraw-Hill Book Company, Inc., New York, 1948.

[8] Van Driest, E. R., *Investigation of Laminar Boundary Layer in Compressible Fluids Using the Crocco Method*, NACA TN No. 2597, 1952.

[9] Lew, H. G., and Romano, F., *The Compressible Laminar Boundary Layer Over a Flat Plate with Uniform Suction and Heat Transfer at the Wall*, P.I.B.A.L. Report No. 132, September, 1948.

[10] Griffith, A. A., and Meredith, F. W., *The Possible Improvement in Aircraft Performance Due to the Use of Boundary Layer Suction*, R.A.E. Report No. E 3501 (A.R.C. 2315).

[11] Young, A. B., *Note on the Velocity and Temperature Distributions Attained with Suction on a Flat Plate of Infinite Extent in Compressible Flow*, Quarterly Journal of Mech. and Applied Math., Vol. 1, Part 1, March, 1948.

[12] Lighthill, M. J., *Contributions to the Theory of Heat Transfer Through a Laminar Boundary Layer*, Proc. of Roy. Soc. (London), Series A, Vol. 202, No. 1070, pp. 359–377, August, 1950.

[13] Lew, H. G., and Fanucci, J. B., *On the Laminar Compressible Boundary Layer Over a Flat Plate with Suction or Injection*, Technical Report No. 4, Dept. of Aeronautical Engineering, Pennsylvania State University, O.S.R.T.N. 54–255, July, 1954.

[14] Illingworth, C. R., *Steady Flow in the Laminar Boundary Layer of a Gas*, Proc. of Roy. Soc. (London), Series A, Vol. 199, pp. 533–557, 1949.

[15] Stewartson, K. *Correlated Incompressible and Compressible Boundary Layers*, Proc. of Roy Soc. (London), Series A, Vol. 200, pp. 84–99, 1949.

Notice to Contributors

Manuscripts submitted for publication *must* be double- or triple-spaced originals. There should be wide margins on both sides of the sheets and triple spacing around formulas to allow for the marking of directions for the printer.

Original drawings (jet black India ink on white paper or tracing cloth) should accompany the manuscript. *(Blueprints are not acceptable.)* Photographs *must* be on glossy white paper. The smallest lettering on 8- by 10-in. figures should be no less than 1/4 in. high.

Only the simplest formulas should be typewritten; all others should be carefully written in pen and ink. The difference between capital and lower-case letters and Greek symbols should be clearly distinguished.

See Inside Back Cover of this issue for further details

Spanwise Variation in the Pitching-Moment Coefficient and the Center of Pressure Due to Various Basic Twist Distributions on Triangular Wings Having Supersonic Leading and Trailing Edges

JULIAN H. KAINER*

Ryan Aeronautical Company

Summary

The linearized supersonic flow theory has been applied to determine the spanwise variation in the pitching-moment coefficients and the centers of pressure due to various basic twist distributions on triangular wings having supersonic leading and trailing edges.

The effects of the flow nonuniformity on the section properties produced by body upwash[1] and by geometric twist may be obtained directly from the span loadings previously presented[2] and the results herein since the spanwise variation in incidence is known everywhere. To account for the effects of aeroelasticity where the spanwise variation in incidence is unknown, the span loadings[2] and the present results are applied to the superposition procedure reported on by Brown, Holtby, and Martin.[3]

Design charts and generalized equations in closed form are presented for the section pitching-moment coefficients and the section centers of pressure corresponding to constant, linear, parabolic, and cubic twist distributions. Graphical procedures are indicated to determine the section bending-moment coefficients, the wing bending-moment coefficients, the wing pitching-moment coefficients, and the corresponding wing centers of pressure due to the aerodynamic loads caused by the variation of angle of attack.

It was found that the effect of washout on the section characteristics decreased with increasing degree of washout and with increased angle of sweep, and increased with Mach Number and the amount of washout at a given angle of attack. For example, at the root chord of a 45° delta wing at $M = 1.6$ with a 5° washout at 10° angle of attack the following results were noted: (1) a forward shift of about $1^1/_2$ per cent in the center of pressure, (2) a decrease of about 7 per cent in the section lift-curve slope, and (3) a decrease of about 11 per cent in the section pitching-moment slope over the wing with zero washout. The net effect of this twist distribution resulted in: (1) a decrease of about 15 per cent in the wing lift-curve slope, (2) a decrease of about 19 per cent in the wing pitching-moment slope, (3) a decrease of about 25 per cent in the wing bending-moment slope, and, (4) an inboard and forward shift of about 2 per cent in the lateral and longitudinal centers of pressure, respectively.

Symbols

Free-Stream Conditions

V = velocity
M = Mach Number
β = $\sqrt{M^2 - 1}$
μ = Mach angle, arcsin $(1/M)$
ρ = mass density of air
q = dynamic pressure, $(1/2)\rho V^2$

Wing Geometry

$b/2$ = half-span
c_0 = root chord
c_{a_w} = average chord
ϵ = half apex angle
δ = angle between trailing edge and plane of symmetry
m = $\beta \tan \epsilon$
m_0 = $\beta \tan \delta$
S = wing area
x, y = Cartesian coordinate of system of axes with origin at leading edge of root chord

Analysis Parameters

ϕ = velocity potential
ϕ_x = horizontal perturbation velocity
θ_1 = arc cos $(1 - mt)/(m - t)$
θ_2 = arc cos $(1 + mt)/(m + t)$
x' = x/c_0 evaluated at the trailing edge
$x_{c.p.}$ = section center of pressure
$x_{c.p.}{}'$ = $x_{c.p.}/c_0$
$\bar{x}_{c.p.}$ = wing longitudinal center of pressure
$\bar{x}_{c.p.}{}'$ = $\bar{x}_{c.p.}/c_0$
$\bar{y}_{cp}$ = wing lateral center of pressure
$\bar{y}_{cp}{}'$ = $[(y_{cp})/(b/2)]$
a_i = coefficients of power series expansion for the angle of attack
C_n = section normal-force coefficient per radian
C_m = section pitching-moment coefficient per radian
C_{m_b} = section bending-moment coefficient per radian
C_L = wing lift coefficient per radian
C_M = wing pitching-moment coefficient per radian (based on mean aerodynamic chord)
C_{m_b} = wing bending-moment coefficient per radian
$A_i(t)$ = conical functions from which the potential and normal-force coefficients are determined
$B_i(t)$ = conical function from which the horizontal perturbation velocities are determined
$\epsilon_i(t)$ = conical functions from which the section centers of pressure are determined
$\bar{\epsilon}_i(t)$ = conical functions obtained for $M = \infty$
γ = an arbitrary characteristic dimension
Subscript i = index representing degree of twist
Superscript $*$ = represents multiplication by β

Received July 20, 1954.

* Aerodynamics Engineer.

Introduction

THE LOADING AND STABILITY of many classes of rigid wings in uniform supersonic streams have been widely investigated both theoretically and experimentally. The increased interest in high-speed performance has created a demand for more reliable design information; hence, a proportionate amount of re-

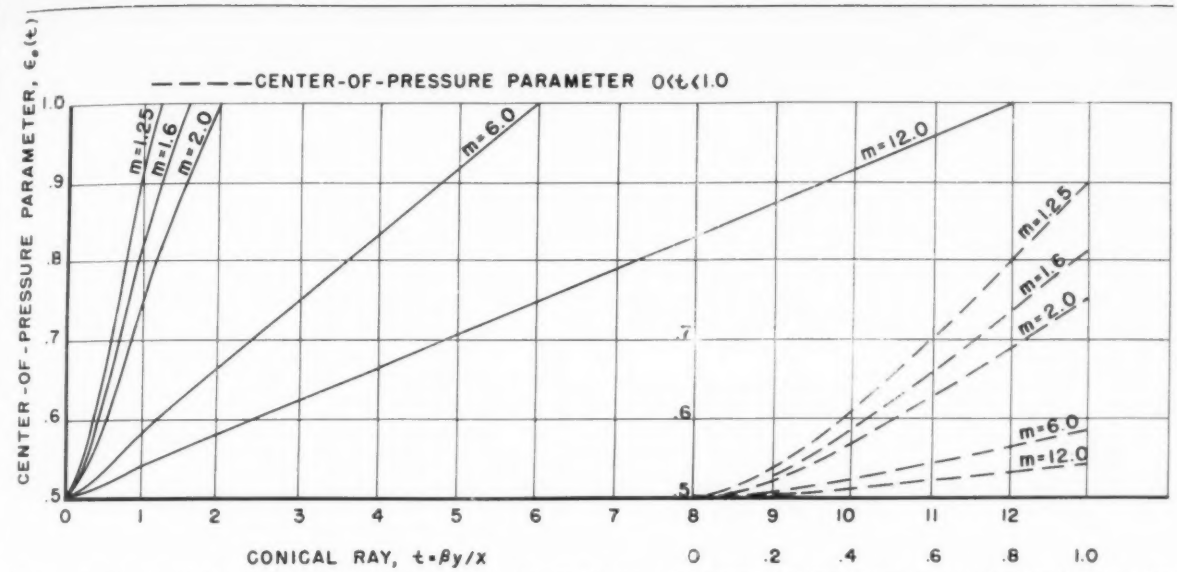

FIG. 1. Section center of pressure coefficient parameter $\epsilon_0(t)$ vs. conical ray, t, for several families of β tan ϵ and all families of β tan δ for constant angle of attack.

search has been directed toward some means of correlating available data with linearized theory and, particularly, improving the present theory to account for such important effects as wing-body interference,[4] the consequences of boundary-layer propagation, and aeroelasticity.[2, 5, 6]

Empirical correlation* by the author of the span-load distributions on delta wings based on linearized theory with some supersonic wind-tunnel data has been sufficiently encouraging to warrant further theoretical study to improve the calculated distributions.

* This classified information is available to properly cleared persons on request.

As pointed out by Beskin,[1] the presence of the body creates an upwash which varies along the span (and, in practice, along the chord of the wing). It seems plausible that the effects of this nonuniform stream on the aerodynamic loading and stability may be determined upon consideration of a uniform stream in which is placed a wing warped to fit the stream lines of the nonuniform stream. The solution to this problem is, uniquely, that corresponding to a twisted and cambered wing in a uniform flow. Furthermore, the effects of aeroelasticity on the structural requirements may be determined by applying such an analysis to the superposition procedure described by Brown, Holtby and Martin.[3] The noniterative procedure described therein

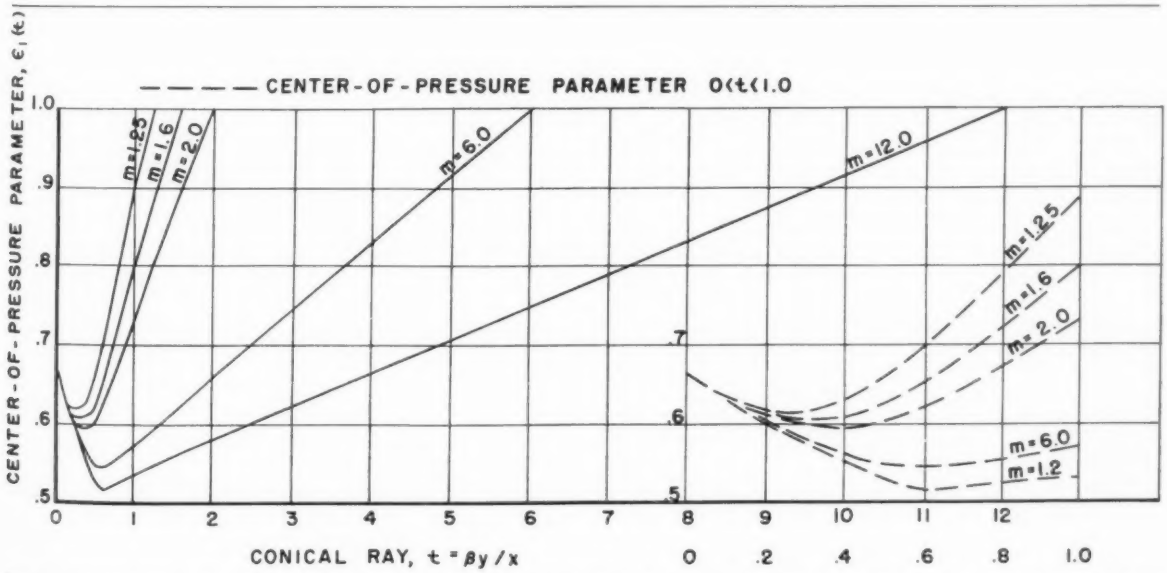

FIG. 2. Section center of pressure coefficient parameter $\epsilon_1(t)$ vs. conical ray, t, for several families of β tan ϵ and all families of β tan δ for linear symmetric twist distribution.

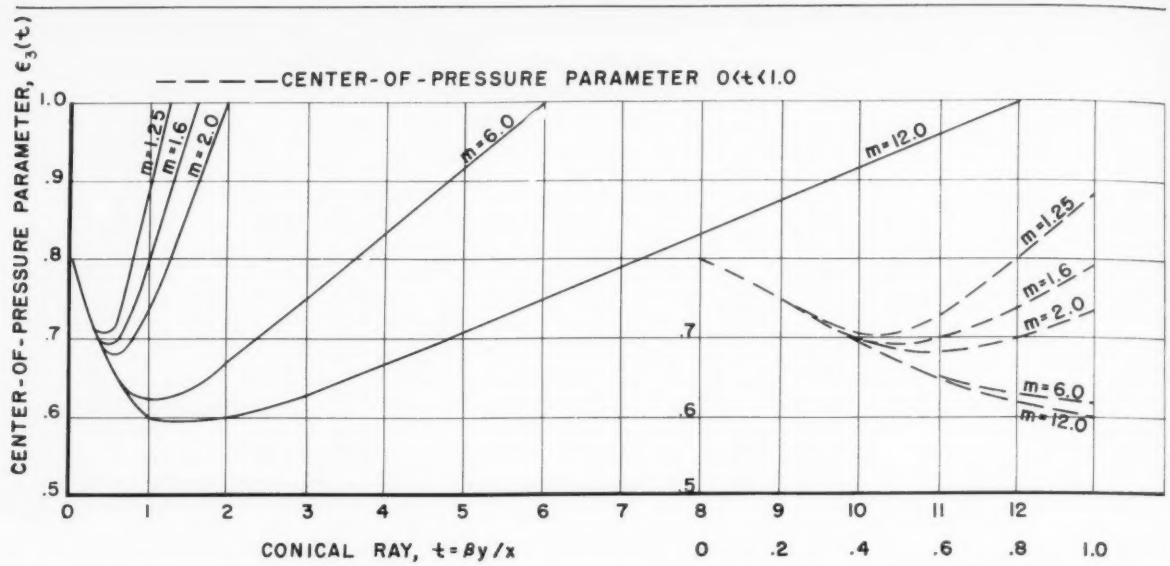

FIG. 3. Section center of pressure coefficient parameter $\epsilon_3(t)$ vs. conical ray, t, for several families of β tan ϵ and all families of β tan δ for parabolic symmetric twist distribution.

requires knowledge of the wing structural matrix and the aerodynamic loading properties[2] of the wing for various known basic angle of attack distributions.

A systematic study[2, 5, 6] is underway to provide the necessary aerodynamic data with which the solution[3] may proceed. The loading distribution for triangular wings having supersonic leading and trailing edges due to various basic twist distributions has been previously presented.[2] The purpose of the current paper is to provide a means of proportioning these loadings to the control points of the structural matrix. The spanwise distributions of the centers of pressure and the pitching-moment coefficients are presented here corresponding to the load distributions[2] due to known basic twist distributions for triangular wings having supersonic leading and trailing edges. From these results it is possible to determine graphically the section and wing bending-moments, wing lift and pitching-moments, and the wing longitudinal and lateral centers of pressure. Derivations have been initiated for the total lift, moments, and centers of pressure corresponding to the configurations considered here. Calculations are underway for similar configurations having various basic camber distributions and will subsequently be extended to include the class of triangular wings having subsonic leading edges and supersonic trailing edges.

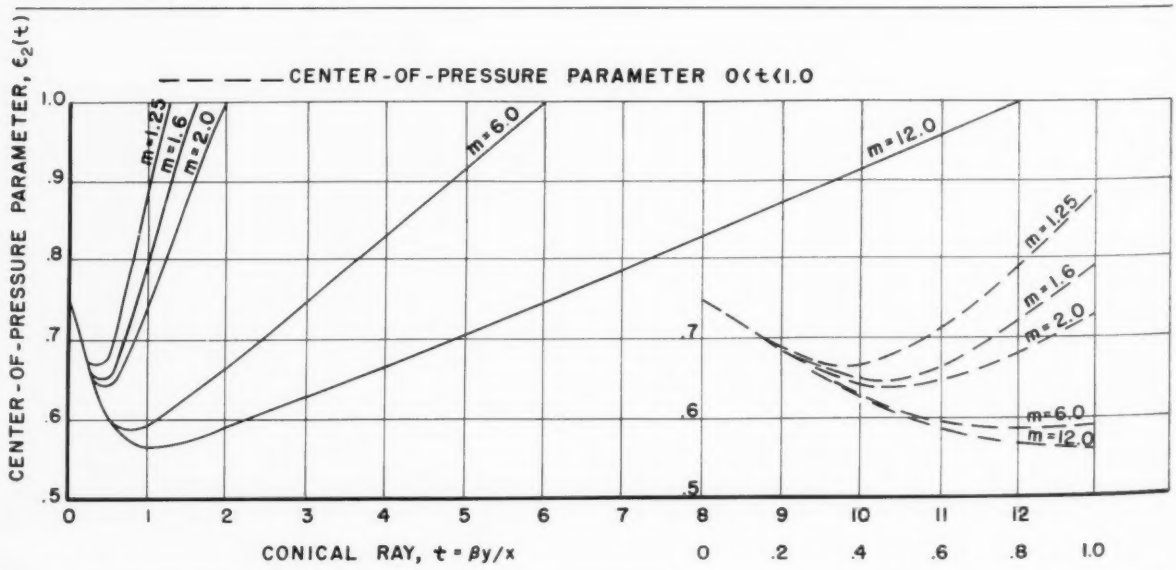

FIG. 4. Section center of pressure coefficient parameter $\epsilon_2(t)$ vs. conical ray, t, for several families of β tan ϵ and all families of β tan δ for cubic symmetric twist distribution.

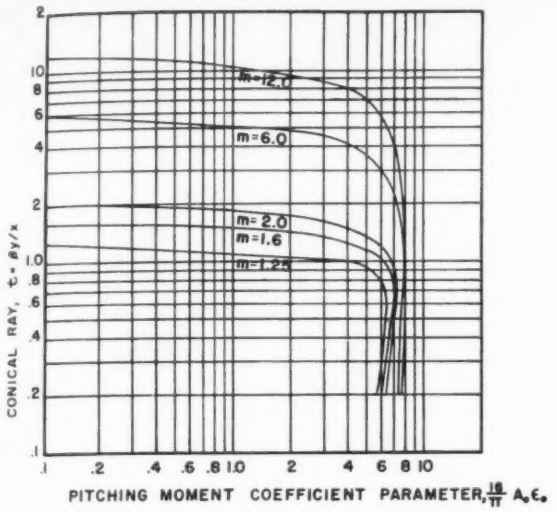

FIG. 5. Section pitching-moment coefficient parameter $(16/\pi)A_{0\epsilon_0}$ vs. conical ray, t, for several families of β tan ϵ and all families of β and δ for constant angle of attack.

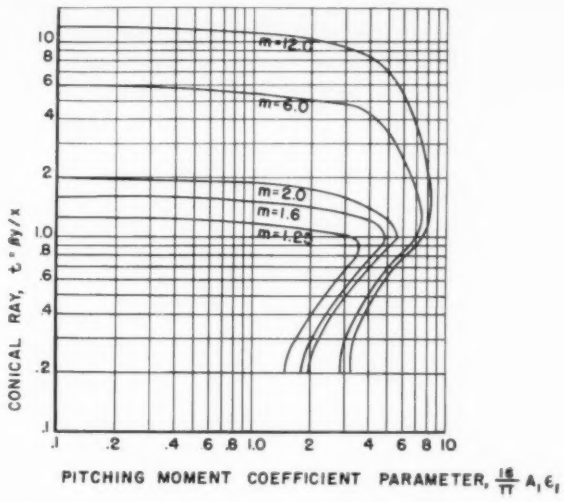

FIG. 6. Section pitching-moment coefficient parameter $(16/\pi)A_{1\epsilon_1}$ vs. conical ray, t, for several families of β tan ϵ and all families of β tan δ for linear symmetric twist distribution.

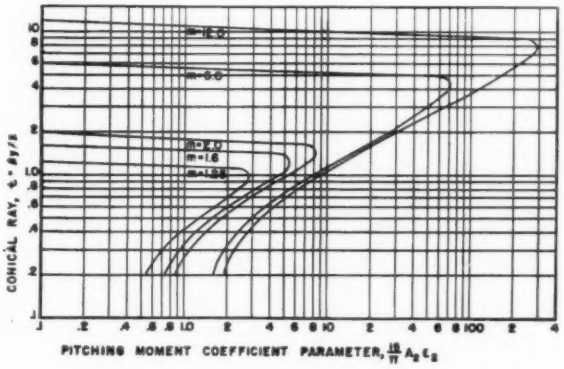

FIG. 7. Section pitching-moment coefficient parameter $(16/\pi)A_{2\epsilon_2}$ vs. conical ray, t, for several families of β tan ϵ and all families of β tan δ for parabolic symmetric twist distribution.

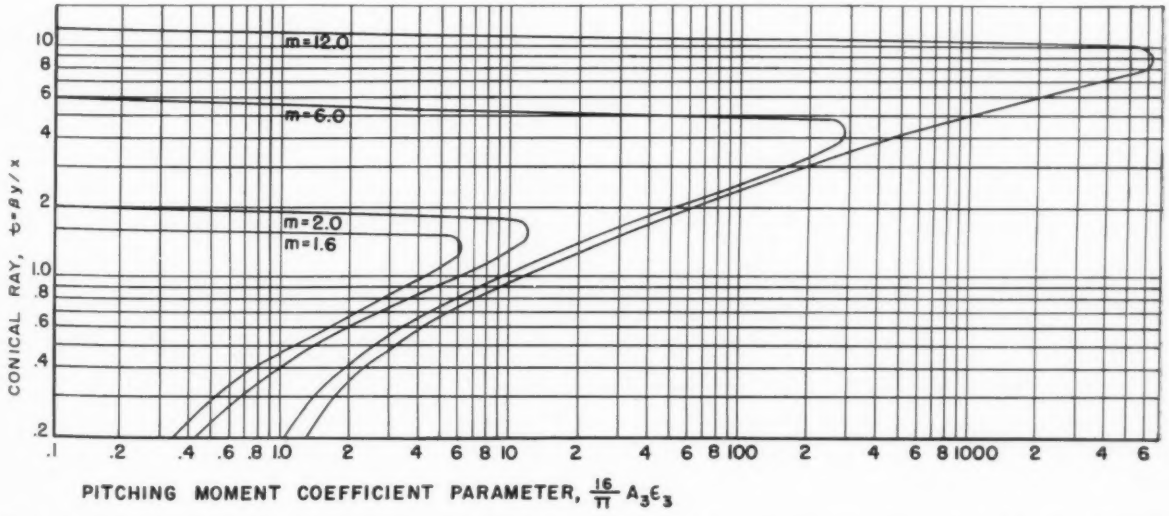

FIG. 8. Section pitching-moment coefficient parameter $(16/\pi)A_{3\epsilon_3}$ vs. conical ray, t, for several families of β tan ϵ and all families of β tan δ for cubic symmetric twist distribution.

Analysis

General Background

The velocity potentials, the horizontal perturbation velocities, and the span-load distributions due to various basic twist distributions on triangular wings having supersonic leading and trailing edges were derived by means of linear theory.[2] The results may be concisely written, respectively, as

$$(\pi/V)\ [(\beta^i\gamma^i)/x^{1+i}]\ (\phi/a)_i^* = A_i(t) \tag{1}$$

$$(\pi/V)\ (\beta/x')^i\ (\phi_x/a)_i^* = B_i(t) \tag{2}$$

$$(\pi/8)\ [(mm_0)/(m_0 - m)]^i\ (1/x')^{1+i} \times (C_n/a)_i^* = A_i(t) \tag{3}$$

where $A_i(t)$ and $B_i(t)$ are the conical functions presented in the Appendix of the original report.[2]

Section Pitching-Moment Coefficient

By definition the section pitching-moment coefficient about the leading edge of the root chord is

$$C_m c^2 = \int_{x_{\text{leading edge}}}^{x_{\text{trailing edge}}} x\,\frac{\Delta p}{q}\,dx \tag{4a}$$

$$= x_{c.p.}C_n c \tag{4b}$$

Hence

$$C_m(c/c_{\text{av.}})^2 = 2x_{c.p.}{}'C_n(c/c_{\text{av.}}) \tag{5}$$

Substituting Eq. (3) into Eqs. (4) and (5)

$$(\pi/16)\ [(mm_0)/(m_0 - m)]^i\ (1/x')^{2+i} \times (C_m/a)_i^*(c/c_{\text{av.}})^2 = A_i(t)\epsilon_i(t) \tag{6}$$

where

$$x_{c.p.}{}' \equiv x'\epsilon_i(t) \tag{7}$$

such that

$$0 < \epsilon_i(t) \leq 1.0$$

From Eq. (6) the resultant section pitching-moment coefficient parameter is, by superposition,

$$C_m{}^*(c/c_{\text{av.}})^2 = \sum_{i=0}^{\infty} (C_m/a)_i^*\,(c/c_{\text{av.}})^2 a_i \tag{8a}$$

$$= 2x' \sum_{i=0}^{\infty} (C_n/a)_i^* a_i \epsilon_i(t) \tag{8b}$$

Section Center of Pressure

By definition:

$$x_{c.p.}{}' = \frac{1}{c_0}\,\frac{\text{section pitching-moment}}{\text{section normal force}} \tag{9a}$$

$$x_{c.p.}{}' = \frac{1}{c_0}\int_{x_{\text{leading edge}}}^{x_{\text{trailing edge}}} x\,\frac{\Delta p}{q}\,dx \Big/ \int_{x_{\text{leading edge}}}^{x_{\text{trailing edge}}} \frac{\Delta p}{q}\,dx \tag{9b}$$

$$= \frac{1}{c_0}\,\frac{x_{TE}\phi_{TE} - \int^{x_{TE}} \phi\,dx}{\phi_{TE}} \tag{9c}$$

(lower limit need not be considered since potential vanishes at a supersonic leading edge).

Substituting Eq. (3) into Eq. (9c):

$$x_{c.p.}{}'/x' = 1 - \frac{\int^{x_{TE}} x^{1+i}A_i(t)\,dx}{x_{TE}{}^{2+i}\,A_i(t)} \tag{10a}$$

$$\equiv \epsilon_i(t) \tag{10b}$$

The results of Eq. (10b) are presented in the Appendix for values of $i = 0, 1, 2, 3$.

From Eqs. (5) and (8), the resultant center of pressure is

$$x_{c.p.}{}'/x' = \frac{\sum_{i=0}^{\infty} (C_n/a)_i^*\,a_i\epsilon_i(t)}{\sum_{i=0}^{\infty} (C_n/a)_i^*\,a_i} \tag{11}$$

Wing Center of Pressure

Derivations are currently being completed for the total wing lift coefficients, pitching-moment coefficients, bending-moment coefficients, and the centers of pressure corresponding to the various basic twist distributions. Until these equations are published the centers of pressure may be graphically determined as follows:

$$\bar{x}_{c.p.} = \int_0^1 C_m c^2\,dy' \Big/ \int_0^1 C_n c\,dy' \tag{12}$$

Upon substitution of Eqs. (3) and (6) into Eq. (12),

$$\bar{x}_{c.p.}{}' = \frac{\int_0^1 (x')^{2+i}A_i(t)\epsilon_i(t)\,dy'}{\int_0^1 (x')^{1+i}A_i(t)\,dy'} \tag{13}$$

but $(x'y')$ may be related to the conical ray, t, at the

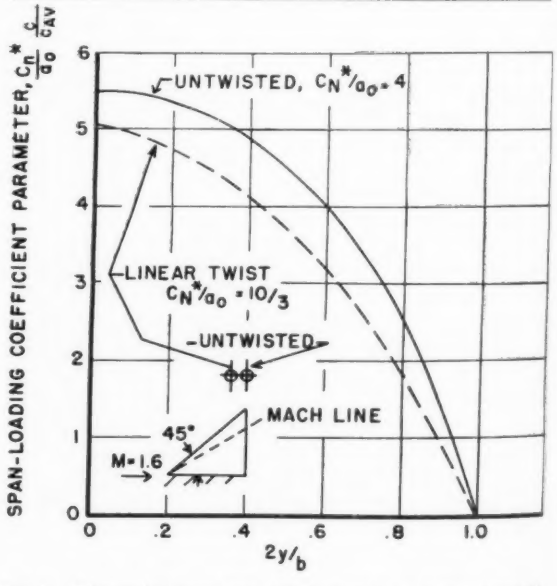

FIG. 9. Theoretical span-load distributions for a delta wing with and without twist. $\Lambda = 45°$, $M = 1.6$, $a_1/a_0 = -0.5$, $a_0 = 10°$.

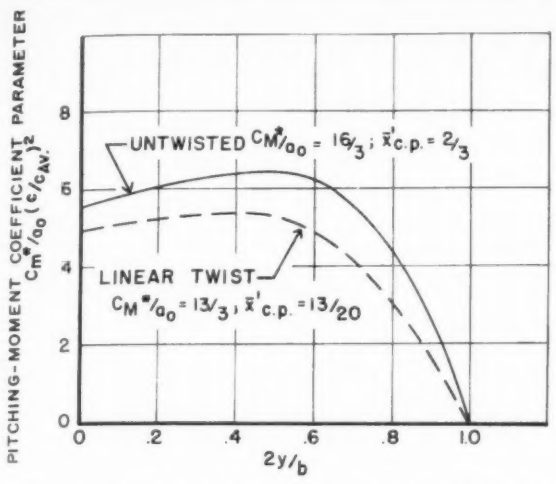

FIG. 10. Theoretical pitching-moment coefficient distributions for a delta wing with and without twist $\epsilon = 45°$, $M = 1.6$, $a_1/a_0 = -0.5$, $a_0 = 10°$.

trailing edge by[2]

$$x' = m_0/(m_0 - t) \tag{14}$$

$$y' = (m_0 - m)t/m(m_0 - t) \tag{15}$$

and Eq. (13) becomes, finally,

$$\bar{x}_{c.p.}' = \frac{m_0 \int_0^m (m_0 - t)^{-4-i} A_i(t)\epsilon_i(t)\, dt}{\int_0^m (m_0 - t)^{-3-i} A_i(t)\, dt} \tag{16}$$

In a similar fashion the lateral position of the center of pressure may be determined for bending-moment investigations by

$$\bar{y}_{c.p.} = \frac{\int_0^1 y' C_n c\, dy'}{\int_0^1 C_N c\, dy'} \tag{17}$$

which becomes

$$\bar{y}_{c.p.}' = [(m_0/m) - 1] \frac{\int_0^m t(m_0 - t)^{-4-i} A_i(t)\, dt}{\int_0^m (m_0 - t)^{-3-i} A_i(t)\, dt} \tag{18}$$

Unswept Wings

The results presented herein are also applicable within the root chord Mach cone of swept wings, hence the limiting case of an unswept wing may be determined by considering $m = \infty$. These limiting cases are presented in the Appendix and are denoted by the barred quantity $\bar{\epsilon}_i(t)$.

DISCUSSION

The results of the analysis for the section pitching-moment coefficients and the section centers of pressure is presented in the form of generalized equations in closed form in addition to the design charts which are presented in parametric form and a numerical example for illustrative purposes.

The section center of pressure parameters, $\epsilon_i(t)$ are presented in Figs. 1 to 4 for basic degrees of twist corresponding to $i = 0, 1, 2, 3$, respectively, and the section pitching-moment coefficient parameters, $(16/\pi)A_i(t)\epsilon_i(t)$, are presented in a similar fashion in Figs. 5 to 8. The results are plotted for several values of the leading edge Mach Number parameter, $\beta \tan \epsilon$, against the conical ray, t, evaluated at the trailing edge. The solutions are valid for all supersonic values of the trailing edge Mach Number parameter, $\beta \tan \delta$.

The numerical results are illustrated in Figs. 9 to 12 for a 45° delta wing at $M = 1.6$ with a linear washout of 5° at an angle of attack of 10°. Table I is presented to illustrate the manner in which the published results[2] are applied with the present results to obtain the section loading characteristics against semispan position. The span-load coefficient parameter corresponding to the twisted wing is compared to an untwisted wing of the same plan form in Fig. 9. At the root chord a decrease of about 7 per cent in the section lift slope multiplied by β is noted. The net effect of this twist ratio reduces the overall lift curve slope by about 15 per cent and produces an inboard shift of about 2 per cent in the lateral center of pressure. The spanwise variation in the pitching-moment coefficient parameter is similarly compared in Fig. 10. At the root chord a decrease of about 11 per cent is noted. The resultant decrease in the wing pitching-moment slope parameter is about 19 per cent with about a 2 per cent forward shift in the longitudinal center of pressure. These overall effects are predicted by some preliminary unpublished* results for triangular wings at supersonic

* To be presented when numerical results are complete.

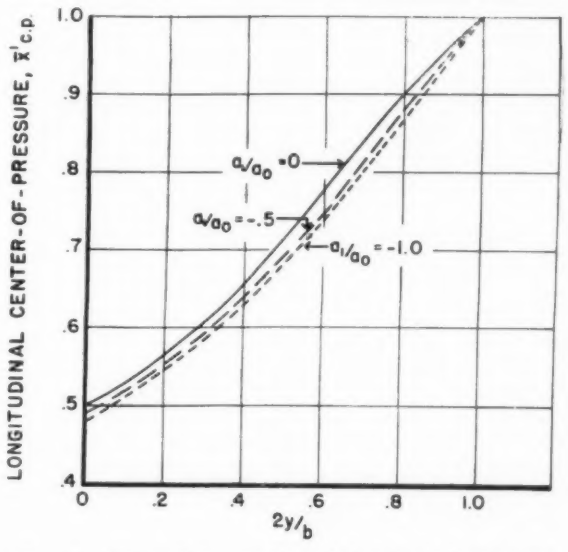

FIG. 11. Theoretical spanwise variation in the longitudinal center of pressure for a delta wing with and without twist $\epsilon = 45°$, $M = 1.6$, $a_0 = 10°$, $a_1/a_0 = 0, -0.5, -1.0$.

speeds which for a delta wing reduce to

$$C_L^*/a_0 = 4 + (4/3)(a_1/a_0) + (2/3)(a_2/a_0) + (2/5)(a_3/a_0) + \ldots \quad (19)$$

$$(\bar{x}_{c.p.}'/x')_t = 2/3, 3/4, 4/5, 5/6, \ldots \quad (20)$$

$$C_M^*/a_0 = 4 + (3/2)(a_1/a_0) + (4/5)(a_2/a_0) + (1/2)(a_3/a_0) + \ldots \quad (21)$$

The comparisons for the effects of twist on the longitudinal centers of pressure are presented in Fig. 11 for the linear twist ratios $a_1/a_0 = 0, -0.5, -1.0$.

The spanwise variation in the bending-moment coefficient parameter for a twisted delta wing is compared to the results for the corresponding untwisted wing. The effect of this washout is to reduce the root bending-moment coefficient parameter by about 25 per cent.

Conclusions

The results of this analysis indicated that the effects of twist—i.e., body upwash—produced wing forces and moments which were greatly reduced in magnitude from those calculated for a wing having a constant angle of attack equal to the geometric angle of attack. Furthermore, small amounts of built-in twist may be used to reduce root chord bending-moments by a considerable magnitude. In general the effect of washout on the section characteristics decreased with increasing degree of washout and leading edge sweep, and increased with Mach Number and with the amount of washout at a given angle of attack. The results for a 45° delta wing at $M = 1.6$ with a 5° washout at 10° angle of attack indicated the following: (1) a forward shift of about $1^1/_2$ per cent in the root chord center of pressure and an overall forward shift of about 2 per cent in the longitudinal center of pressure, (2) a decrease of about 7 per cent in the root chord lift-curve slope and a net loss of about 15 per cent in the wing lift curve slope, (3) a decrease of about 11 per cent in the root chord pitching-moment slope with a net loss of about 19 per cent in the corresponding wing value, and (4) a decrease of about 25 per cent in the root chord bending-moment slope with an inboard shift of about 2 per cent in lateral center of pressure.

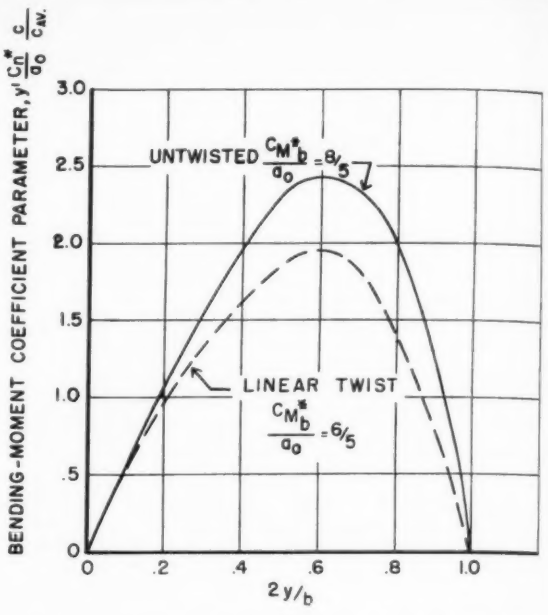

Fig. 12. Theoretical bending-moment coefficient distribution for a delta wing with and without twist $\epsilon = 45°$, $M = 1.6$, $a_1/a_0 = -0.5$, $a_0 = 10°$.

References

[1] Beskin, L., *Determination of Upwash Around a Body of Revolution at Supersonic Velocities*, Convair, CVAC-DEVF Memo BB-6, May 27, 1946.

[2] Kainer, Julian H., *Equations for the Loading on Triangular Wings Having Supersonic Leading and Trailing Edges Due to Various Basic Twist Distributions* (see Bibliography), Journal of the Aeronautical Sciences, Vol. 20, No. 7, pp. 469–476, July, 1953.

[3] Brown, R. B., Holtby, K. F., and Martin, H. C., *A Superposition Method for Calculating the Aeroelastic Behaviour of Swept Wings*, Journal of the Aeronautical Sciences, Vol. 18, No. 8, pp. 531–542, August, 1951.

[4] Flax, A. H., *Integral Relations in the Linearized Theory of Wing-Body Interference* (see References), Journal of the Aeronautical Sciences, Vol. 20, No. 7, pp. 483–490, July, 1953.

[5] Kainer, Julian H., *A Simplified Method to Obtain the Load Distribution Corresponding to the Ackeret Region for Wings Having Arbitrary Source Distribution at Supersonic Speeds*, Ryan Aeronautical Company Report No. G-20-93, April, 1953; Journal of the Aeronautical Sciences, Vol. 20, No. 11, pp. 749–750, November, 1953.

[6] Kainer, Julian H., and Kazan, Elliott, *Equations for the Potential Pressure and Span-Load Distributions on Swept Wings Having Supersonic Leading Edges Due to Various Basic Twist Distributions*, Proposed Republic Aviation Corp., Report No. EAR-280.

Appendix

General Triangular Wings

$$\epsilon_0(t) = \left[1 - \frac{1}{2m}\left\{\frac{(m^2 - t^2)(\theta_1 + \theta_2) - 2t(m - t)\theta_1 + 2t(m + t)\theta_2 - 2\sqrt{m^2 - 1}\, t^2 \cosh^{-1} 1/t}{(m - t)\theta_1 + (m + t)\theta_2}\right\}\right]$$

①	②	③	④	⑤	⑥	⑦	⑧	⑨				⑩			
								$\frac{8}{\pi} A_i(t)$, REF. 2				$\left(\frac{C_n}{a}\right)_i^* \frac{c}{c_{A_V}} = \left(\frac{1-m/m_0}{m}\right)^i (x')^{1+i} \frac{8}{\pi} A_i(t)$			
								a) $i=0$	b) $i=1$	c) $i=2$	d) $i=3$	a) $i=0$	b) $i=1$	c) $i=2$	d) $i=3$
y'	m①	1+①	$\frac{m}{m_0}$③	④-1	②/⑤ = t	⑥/m_0	$\frac{1}{1-⑦} = x'$	FIG. 6 × $\frac{8}{\pi}$	FIG. 7 × $\frac{8}{\pi}$	FIG. 8 × $\frac{8}{\pi}$	FIG. 9 × $\frac{8}{\pi}$	⑧ ⑨a	$\left(\frac{1-m/m_0}{m}\right)$ × ⑧² ⑨b	$\left(\frac{1-m/m_0}{m}\right)^2$ × ⑧³ ⑨c	$\left(\frac{1-m/m_0}{m}\right)^3$ × ⑧⁴ ⑨d
0															
.2															
.4															
.6															
.8															
1.0															

⑪				⑫	⑬				⑭				⑮	⑯
$\left(\frac{C_n}{a}\right)_i^* \frac{c}{c_{A_V}} \frac{a_i}{a_0} = \frac{C_n}{a_0}{}_i^* \frac{c}{c_{A_V}}$				$\frac{C_n}{a_0}^* \frac{c}{c_{A_V}} =$	$\frac{16}{\pi} A_i(t)\epsilon_i(t)$, PRESENT REP.				$\frac{C_{m_i}}{a_0}^* \left(\frac{c}{c_{A_V}}\right)^2 = \left(\frac{C_m}{a}\right)_i^* \frac{a_i}{a_0} \left(\frac{c}{c_{A_V}}\right)^2 = \frac{32}{\pi} A_i \epsilon_i \frac{a_i}{a_0}$				$\frac{C_m}{a_0}^* \left(\frac{c}{c_{A_V}}\right)^2 =$	$\frac{x'_{c.p.}}{x'} = \frac{1}{2} ⑮/⑫$
a) $i=0$	b) $i=1$	c) $i=2$	d) $i=3$		a) $i=0$	b) $i=1$	c) $i=2$	d) $i=3$	a) $i=0$	b) $i=1$	c) $i=2$	d) $i=3$		
⑩a	$\frac{a_1}{a_0}$ ⑩b	$\frac{a_2}{a_0}$ ⑩c	$\frac{a_3}{a_0}$ ⑩d	⑪a + the desired combination of ⑪ b,c,d,	FIG. 5	FIG. 6	FIG. 7	FIG 8	2 × ⑧ × ⑬a	2 × ⑧ × $\frac{a_1}{a_0}$ × ⑬b	2 × ⑧ × $\frac{a_2}{a_0}$ × ⑬c	2 × ⑧ × $\frac{a_3}{a_0}$ × ⑬d	⑬a + the desired combination of ⑬ b,c,d,	

$$t = \frac{my'}{\frac{m}{m_0}(1+y') - 1}, \quad x' = \frac{1}{1 - t/m_0}$$

$$C_{m_b}\left(\frac{b}{2}c\right) = \int_0^1 y' C_n c \, dy'$$

$$\frac{\pi}{8}\left(1/x'\right)^{1+i}\left(\frac{m\,m_0}{m_0-m}\right)^i \left(\frac{C_n}{a}\right)_i^* \frac{c}{c_{A_V}} = A_i(t)$$

$$\frac{\pi}{16}\left(1/x'\right)^{2+i}\left(\frac{m\,m_0}{m_0-m}\right)^i \left(\frac{C_m}{a}\right)_i^* \left(\frac{c}{c_{A_V}}\right)^2 = A_i(t)\epsilon_i(t)$$

TABLE 1

Computational procedure for converting parametric conical functions for the basic twist distributions into span-loading coefficient, pitching-moment coefficient, and center of pressure distributions as functions of $2y/b$.

$$\epsilon_1(t) = \left[1 - \frac{1}{3m}\left\{\frac{3(m^2-1)t(m^2-t^2)(\theta_1-\theta_2) - (m-t)^3\theta_1 - (m+t)^3\theta_2 + \dots}{2m^2\sqrt{m^2-1}\sqrt{1-t^2} + 2(m^2-1)^{3/2}t^2\cosh^{-1}1/t + \dots} \right.\right.$$
$$\frac{-6(m^2-1)t^2[(m-t)\theta_1 + (m+t)\theta_2] + 6m(m^2-1)^{3/2}t^2\cosh^{-1}1/t + \dots}{-(m-t)^2\theta_1 - (m+t)^2\theta_2 + \dots}$$
$$\left.\left.\frac{+ 2m^3\sqrt{m^2-1}(1-t^2)^{3/2} + 4m\sqrt{m^2-1}\,t^2\sqrt{1-t^2}}{2(m^2-1)t[(m-t)\theta_1 - (m+t)\theta_2]}\right\}\right]$$

$$\epsilon_2(t) = \left[1 - \frac{1}{4m}\left\{\frac{6m^4\sqrt{m^2-1}(1-t^2)^{3/2} + 2m^2(17m^2-5)\sqrt{m^2-1}\,t^2\sqrt{1-t^2} + \dots}{2m\sqrt{m^2-1}\,[3m^2+(5m^2-2)t^2]\sqrt{1-t^2} + \dots}\right.\right.$$
$$\frac{+ 12(m^2-1)^{5/2}t^4\cosh^{-1}1/t - (m^2-t^2)\,[m^2(m^2+2) + (12m^4+7m^2+2)t^2]\,(\theta_1+\theta_2) + \dots}{-(m^2+2)\,(m-t)^3\theta_1 - (m^2+2)\,(m+t)^3\theta_2 + \dots}$$
$$\left.\left.\frac{+ 12m^2t[(m^3-t^3)\theta_1 - (m^3+t^3)\theta_2] + 4(6m^4-5m^2+2)t^2[(m-t)\theta_1 - (m+t)\theta_2]}{+ 6m(m^2-1)t[(1-mt)\,(m-t)\theta_1 - (1+mt)\,(m+t)\theta_2]}\right\}\right]$$

$$\epsilon_3(t) = \left[1 - \frac{1}{5m}\left\{\frac{2m^5(4m^2+11)\sqrt{m^2-1}(1-t^2)^{5/2} + \dots}{2m^4(4m^2+11)\sqrt{m^2-1}(1-t^2)^{3/2} + \dots}\right.\right.$$
$$\frac{+ m^3(95m^4+93m^2-8)\sqrt{m^2-1}\,t^2(1-t^2)^{3/2} + 3m^3(5m^4+17m^2-2)\sqrt{m^2-1}\,t^2\sqrt{1-t^2} + \dots}{- 6m^2(1-11m^2-10m^4)\sqrt{m^2-1}\,t^2\sqrt{1-t^2} + \dots}$$
$$\frac{+ 3m(25m^6+67m^4-48m^2+16)\sqrt{m^2-1}\,t^4\sqrt{1-t^2} + 60m(m^2-1)^{7/2}t^4\cosh^{-1}1/t + \dots}{+ 12(m^2-1)^{7/2}t^4\cosh^{-1}1/t + \dots}$$
$$\frac{-3[m^5(2+3m^2) - 5(4+m^2)m^6t + 10(1+4m^2)m^5t^2 - 10(3+2m^2)m^6t^3 + \dots}{-3[(2+3m^2)m^4 - 4(4+m^2)m^5t + 6(1+4m^2)m^4t^2 + \dots}$$
$$\frac{-5m(2-7m^2+8m^4-8m^6)t^4 - (20m^6-35m^4+28m^2-8)t^5]\theta_1 + \dots}{-4(3+2m^2)m^5t^3 - (2-7m^2+8m^4-8m^6)t^4]\theta_1 + \dots}$$
$$\frac{-3[m^5(2+3m^2) + 5(4+m^2)m^6t + 10(1+4m^2)m^5t^2 + 10(3+2m^2)m^6t^3 + \dots}{-3[(2+3m^2)m^4 + 4(4+m^2)m^5t + 6(1+4m^2)m^4t^2 + 4(3+2m^2)m^5t^3 + \dots}$$
$$\left.\left.\frac{-5m(2-7m^2+8m^4-8m^6)t^4 + (20m^6-35m^4+28m^2-8)t^5]\theta_2}{-(2-7m^2+8m^4-8m^6)t^4]\theta_2}\right\}\right]$$

Unswept Wings

$$\bar{\epsilon}_0(t) = 1/2$$

$$\bar{\epsilon}_1(t) = \left\{1 - \frac{1}{3}\left[\frac{(1-t^2)^{3/2} + 3t^2\cosh^{-1}1/t + 3t\sin^{-1}t}{\sqrt{1-t^2} + t^2\cosh^{-1}1/t + 2t\sin^{-1}t}\right]\right\}$$

$$\bar{\epsilon}_2(t) = \left\{1 - \frac{1}{4}\left[\frac{1+12t^2}{1+6t^2}\right]\right\}$$

$$\bar{\epsilon}_3(t) = \left\{1 - \frac{1}{20}\left[\frac{8(1-t^2)^{5/2} + 95t^2(1-t^2)^{3/2} + 15t^2(1+5t^2)\sqrt{1-t^2} + \dots}{2(1-t^2)^{3/2} + 15t^2\sqrt{1-t^2} + \dots}\right.\right.$$
$$\left.\left.\frac{+ 60\,t^4\cosh^{-1}1/t + 30t(1+4t^2)\sin^{-1}t}{+ 3t^4\cosh^{-1}1/t + 6t(1+2t^2)\sin^{-1}t}\right]\right\}$$

JOURNAL EXPANSION PLANS

Beginning with the January, 1956, issue, the contents of the JOURNAL OF THE AERONAUTICAL SCIENCES will be expanded approximately 25 per cent. Subscription rates will be:

IAS Members—$5.00 per year
Nonmember Subscriptions—$15.00 per year
($1.00 additional for foreign subscriptions)

Similar Solutions of Compressible Boundary-Layer Equations*

TING-YI LI† AND HENRY T. NAGAMATSU‡
California Institute of Technology

ABSTRACT

In this investigation, it is disclosed that the partial differential equations for the compressible laminar boundary layer can be transformed into a system of ordinary differential equations by a direct procedure. This new procedure yields explicitly a differential equation for the free-stream velocity distribution, u_1, which allows similar solutions. On integrating this differential equation, the special forms of u_1 are found, and these results are correlated with Stewartson's results. As an example of the similar solutions, the hypersonic viscous flow over a flat plate is discussed. From the analysis of the numerical solutions, obtained on the Reeves Electronic Analogue Computer, the characteristics of the laminar boundary-layer flow with pressure gradient and heat transfer are discussed. It is shown (1) that on a heated surface, the local velocity inside the boundary layer can exceed the free-stream value when a certain favorable pressure gradient exists, (2) that the variation of $C_{h_1}/(1/2)C_{f_1}$, for various surface temperatures with different free-stream pressure gradients can be accurately predicted, and (3) that the effects of heat transfer on the laminar separation phenomenon can be quantitatively studied.

SYMBOLS

x, y	= coordinate axes
u, v	= velocity components in the x, y directions, respectively
ρ	= density
p	= pressure
μ	= viscosity coefficient
k	= coefficient of heat conductivity
R	= gas constant
η	= "similar" variable
σ	= Prandtl Number
$H = C_pT + \frac{1}{2}u^2$	= total energy
T	= temperature
ψ	= stream function
N, K, F, G	= defined in Eqs. (20), (21), and (22), respectively
M	= Mach Number
γ	= ratio of specific heats
C_p	= specific heat at constant pressure
a	= speed of sound
Z	= defined in Eq. (45)
$\beta = \frac{1}{m} = \frac{2m'}{m'+1}$	= the constant parameter in Eqs. (30) and (30a), see also Fig. 7
C_{h_1}	= local heat-transfer coefficient
C_{f_1}	= local skin-friction coefficient

Subscripts 0, 1, and w refer, respectively, to the stagnation conditions, the free-stream conditions, and the surface conditions.

Received May 10, 1954.

* This work was sponsored by the U.S. Army Ordnance and Air Force under Contract No. DA-04-495-Ord-19.

† Senior Research Engineer, Guggenheim Aeronautical Laboratory.

‡ Senior Research Fellow, Guggenheim Aeronautical Laboratory.

(I) INTRODUCTION

THE SEARCH FOR "SIMILAR" SOLUTIONS of the compressible boundary-layer equations can be dated from 1946 when Illingworth[1] examined the question of what forms of the variation of u_1 with x would yield solutions with similar velocity and temperature distributions for different values of x. His investigation demonstrated that such solutions exist only if the external velocity u_1 is constant, and then, as in incompressible flow, the similarity variable is of the form $y/\sqrt{x}$. Later, Howarth,[2] assuming that $\sigma = 1$ and $\mu = (\mu_0/T_0)T$, developed a theory of compressible laminar boundary-layer flow in which he again came to Illingworth's early conclusion that no "similar" solutions other than the one corresponding to $u_1 =$ constant exist. In 1949, Stewartson[3] and Illingworth[4] independently demonstrated that the boundary-layer equations arising from a given main-stream velocity u_1 of a compressible fluid could, by a transformation of coordinates, be converted into the equation for an incompressible fluid with a different mainstream velocity, V_1. The relation between V_1 and u_1 is (1 : 1), thus, solutions known to yield "similar" velocity profiles in incompressible flow readily lead to solutions in compressible flow which are designated by Stewartson as "similar" solutions. The present authors, following Stewartson's approach, have discussed the ordinary differential equations pertaining to these "similar" solutions; a preliminary report was published recently.[5]

Strictly speaking, the "similar" solutions discussed in references 3 and 5 are solutions with similar velocity (u) and total energy (H) distributions for different values of x. They are, therefore, not similar as far as temperature distribution is concerned. In the case $u_1 =$ constant, Illingworth[1] has shown that the momentum equation, the energy equation, and the continuity equation can *all* be reduced to ordinary differential equations involving three unknowns, u, v, and T, which are functions of the independent variable $y/\sqrt{x}$. In Stewartson's approach, the variable v is eliminated by the introduction of the stream function ψ, which satisfies the continuity equation identically, and then the momentum equation and the energy equation are shown to be reducible to ordinary differential equations. Therefore, the introduction of ψ and H and the assumption of $\sigma = 1$ and $\mu = (\mu_0/T_0)T$ are largely responsible

for the success of Stewartson's theory.* In the present paper, it will be shown that, admitting these features into Illingworth's initial work, the "similar" solutions can be deduced by quite a direct procedure without the need of introducing V_1 and transforming coordinates. This new procedure yields explicitly a differential equation for u_1 which allows "similar" solutions. On integrating this differential equation, the special forms of u_1 can be found, and these results are correlated with Stewartson's results. Also, some new "similar" solutions will be presented. As an example of the "similar" solutions, the hypersonic viscous flow over a flat plate is briefly discussed. Also, from the analysis of a number of numerical solutions, the behavior of a laminar boundary-layer flow with pressure gradient and heat transfer is discussed.

(II) Compressible Boundary-Layer Equations

The steady, two-dimensional flow of a compressible viscous fluid along a fixed boundary will be considered. With the coordinate axes of x and y along and at right angles, respectively, to the wall, the usual boundary-layer approximation yields the following equations:

$$\rho\left(u\frac{\partial u}{\partial x}+v\frac{\partial u}{\partial y}\right)=-\frac{\partial p}{\partial x}+\frac{\partial}{\partial y}\left(\mu\frac{\partial u}{\partial y}\right) \tag{1}$$

$$0=\partial p/\partial y \tag{2}$$

$$\rho\left(u\frac{\partial}{\partial x}C_pT+v\frac{\partial}{\partial y}C_pT\right)=u\frac{\partial p}{\partial x}+\mu\left(\frac{\partial u}{\partial y}\right)^2+\frac{\partial}{\partial y}\left(k\frac{\partial T}{\partial y}\right) \tag{3}$$

The equation of continuity is

$$(\partial/\partial x)\,(\rho u)+(\partial/\partial y)\,(\rho v)=0 \tag{4}$$

It is assumed that the fluid is a perfect gas so that the following relation holds:

$$p=R\rho T \tag{5}$$

In the main stream, where the effects of viscosity and heat conduction are neglected, the pressure, density, temperature, and velocity are functions of x only. They satisfy the following equations:

$$\rho_1 u_1(du_1/dx)=-(dp_1/dx) \tag{1a}$$

$$\rho_1\frac{d}{dx}C_pT_1=\frac{dp_1}{dx}\quad\text{or}\quad\frac{C_p}{RT_1}\frac{dT_1}{dx}=\frac{1}{p_1}\frac{dp_1}{dx} \tag{3a}$$

$$p_1=R\rho_1T_1 \tag{5a}$$

The subscript "1" refers to the main-stream quantities. Eqs. (1a) and (3a) imply that

$$C_pT_1+(1/2)u_1^2=\text{constant}=C_pT_0 \tag{6}$$

and thus,

$$a_1^2+[(\gamma-1)/2]u_1^2=\text{constant}=a_0^2 \tag{6a}$$

where T_0 and a_0 are, respectively, the stagnation temperature and the stagnation velocity of sound in the free stream.

By Eq. (2) the pressure is constant, for a given value of x, throughout the boundary layer; consequently, for all values of y,

$$\rho(x,y)T(x,y)=\rho_1(x)T_1(x) \tag{7}$$

It is further assumed that

$$\mu=(\mu_0/T_0)T \tag{8}$$

$$\sigma=1\quad\text{i.e.,}\quad k=\mu C_p=C_p(\mu_0/T_0)T \tag{9}$$

and with the introduction of

$$H=C_pT+(1/2)u^2 \tag{10}$$

Eqs. (1), (3), and (4) can be rewritten as follows:

$$\frac{u}{T}\frac{\partial u}{\partial x}+\frac{v}{T}\frac{\partial u}{\partial y}=-\frac{C_p}{T_1}\frac{dT_1}{dx}+R\frac{\mu_0}{T_0}\frac{1}{p_1}\frac{\partial}{\partial y}\left(T\frac{\partial u}{\partial y}\right) \tag{11}$$

$$\frac{u}{T}\frac{\partial H}{\partial x}+\frac{v}{T}\frac{\partial H}{\partial y}=R\frac{\mu_0}{T_0}\frac{1}{p_1}\frac{\partial}{\partial y}\left(T\frac{\partial H}{\partial y}\right) \tag{12}$$

$$\frac{\partial}{\partial x}\left(\frac{u}{T}\right)+\frac{\partial}{\partial y}\left(\frac{v}{T}\right)=-\frac{C_p}{RT_1}\frac{dT_1}{dx}\left(\frac{u}{T}\right) \tag{13}$$

The boundary conditions are

$$y=0\qquad u=v=0\qquad H=H_w=C_pT_w \tag{14}$$

$$y\to\infty\qquad u=u_1\qquad H=H_1=C_pT_0 \tag{15}$$

(III) Reducibility to Ordinary Differential Equations

When the main-stream velocity is uniform, the terms involving $(1/T_1)\,(dT_1/dx)$ drop out from the boundary-layer equations. Then Eqs. (11), (12), and (13) can be reduced to three ordinary differential equations involving the three unknowns, u, v, and T, which are functions of the independent variable $y/\sqrt{x}$. The possibility of obtaining a reduction from partial to ordinary differential equations when the main-stream velocity is nonuniform will now be examined. Let

$$\psi(x,y)=\int_0^y\frac{u}{T}\,dy \tag{16}$$

Eq. (13) can, then, be rewritten as

$$v/T=-(C_p/RT_1)\,(dT_1/dx)\psi-(\partial\psi/\partial x) \tag{17}$$

and Eqs. (11) and (12) become

$$\frac{\partial\psi}{\partial y}\frac{\partial u}{\partial x}-\frac{\partial u}{\partial y}\left(\frac{C_p}{RT_1}\frac{dT_1}{dx}\psi+\frac{\partial\psi}{\partial x}\right)=-\frac{C_p}{T_1}\frac{dT_1}{dx}+R\frac{\mu_0}{T_0}\frac{1}{p_1}\frac{\partial}{\partial y}\left(T\frac{\partial u}{\partial y}\right) \tag{18}$$

$$\frac{\partial\psi}{\partial y}\frac{\partial H}{\partial x}-\frac{\partial H}{\partial y}\left(\frac{C_p}{RT_1}\frac{dT_1}{dx}\psi+\frac{\partial\psi}{\partial x}\right)=R\frac{\mu_0}{T_0}\frac{1}{p_1}\frac{\partial}{\partial y}\left(T\frac{\partial H}{\partial y}\right) \tag{19}$$

* Of course, Howarth's theory also contained these features.

Suppose that

$$\psi(x, y) = N(x)K(\eta) \tag{20}$$

$$u(x, y) = u_1(x)F(\eta) \tag{21}$$

$$H(x, y) = H_1G(\eta) \tag{22}$$

where η is the similarity variable. By definition,

$$u = T(\partial\psi/\partial y) \tag{23}$$

Therefore, it is implied that

$$T(\partial\eta/\partial y) = (u_1/N)\,(F/K') \tag{24}$$

where the prime denotes $d/d\eta$. After simple reductions, Eqs. (18) and (19) can be expressed as follows:

$$u_1\frac{du_1}{dx}F^2 - \left(\frac{C_p}{RT_1}\frac{dT_1}{dx} + \frac{1}{N}\frac{dN}{dx}\right)u_1^2\frac{KF'F}{K'} = -\frac{C_p}{T_1}\frac{dT_1}{dx}T + R\frac{\mu_0}{T_0}\frac{u_1^3}{p_1N^2}\frac{F}{K'}\left(\frac{F}{K'}F'\right)' \tag{18a}$$

$$-\left(\frac{C_p}{RT_1}\frac{dT_1}{dx} + \frac{1}{N}\frac{dN}{dx}\right)KG' = R\frac{\mu_0}{T_0}\frac{u_1}{N^2p_1}\left(\frac{F}{K'}G'\right)' \tag{19a}$$

but

$$C_pT = H - (1/2)u^2 = H_1G - (1/2)u_1^2F^2 \tag{25}$$

therefore, Eq. (18a) can be rewritten as

$$\frac{1}{u_1}\frac{du_1}{dx}F^2 - \left(\frac{c_p}{RT_1}\frac{dT_1}{dx} + \frac{1}{N}\frac{dN}{dx}\right)\times\frac{KFF'}{K'} = \frac{1}{T_1}\frac{dT_1}{dx}\left(\frac{1}{2}F^2 - \frac{H_1}{u_1^2}G\right) + R\frac{\mu_0}{T_0}\frac{u_1}{p_1N^2}\left(\frac{F}{K'}\right)\left(\frac{F}{K'}F'\right)' \tag{18b}$$

By rearranging the terms in Eq. (18b), it can be reduced to

$$\left(1 + \frac{\gamma - 1}{2}M_1^2\right)(F^2 - G) = \left(\frac{1}{u_1}\frac{du_1}{dx}\right)^{-1}\times\left(\frac{C_p}{RT_1}\frac{dT_1}{dx} + \frac{1}{N}\frac{dN}{dx}\right)\frac{KFF'}{K'} + R\frac{\mu_0}{T_0}\frac{u_1^2}{p_1N^2(du_1/dx)}\frac{F}{K'}\left(\frac{F}{K'}F'\right)' \tag{18c}$$

In Eq. (18c), let

$$\frac{C_p}{RT_1}\frac{dT_1}{dx} + \frac{1}{N}\frac{dN}{dx} = \frac{m}{u_1}\frac{du_1}{dx}\left(1 + \frac{\gamma - 1}{2}M_1^2\right) \tag{26}$$

Whence, it is found that

$$\frac{1}{N}\frac{dN}{dx} = \frac{m}{u_1}\frac{du_1}{dx} - \frac{(m + 2)\gamma - m}{\gamma - 1}\frac{1}{a_1}\frac{da_1}{dx} \tag{27}$$

The integration of Eq. (27) yields

$$N = N_0u_1^m\,(a_1)^{\frac{m-(m+2)\gamma}{\gamma-1}} \tag{28}$$

where N_0 is an integration constant. Therefore, Eq. (18c) becomes an ordinary differential equation provided that

$$u_1^{2m-2}(a_1^2)^{\frac{m-(m+2)\gamma}{\gamma-1}}p_1\frac{du_1}{dx} = 1\Big/\left[m\left(1 + \frac{\gamma - 1}{2}M_1^2\right)\right] \tag{29}$$

where it has been assumed that $N_0^2 = R(\mu_0/T_0)$. Evidently, this same condition is sufficient to reduce Eq. (19a) to an ordinary differential equation. The momentum equation and the energy equation are, therefore, reducible to ordinary differential equations; they are, by letting $F = K'$, the following equations.

$$KK'' + K''' = (1/m)\,(K'^2 - G) \tag{30}$$

$$G'' + KG' = 0 \tag{31}$$

The boundary conditions are

$$\eta = 0 \qquad K = K' = 0 \qquad G = G_w = T_w/T_0 \tag{32}$$

$$\eta \to \infty \qquad K' = 1 \qquad G = 1 \tag{33}$$

Here it is assumed that $\eta = 0$ or ∞ according to $y = 0$ or ∞. That this is the case can be seen from the equation for η as follows:

$$\eta(x, y) = \frac{1}{N_0}\int_0^y (a_1)^{\frac{\gamma(m+2)-m}{\gamma-1}}u_1^{1-m}\frac{dy}{T(x, y)} \tag{34}$$

(IV) Sufficient Condition of Reducibility to Ordinary Differential Equations

It has been shown that if the main stream variables $u_1(x)$, $p_1(x)$, $a_1(x)$ satisfy Eq. (29), the reduction from partial to ordinary differential equations is possible. Therefore, Eq. (29) can be regarded as a sufficient condition for reducibility to ordinary differential equations. Eq. (29) can be rewritten as

$$(a_0^2 - a_1^2)^{m-s/2}(a_1^2)^{\frac{(m+1)-(m+2)\gamma}{\gamma-1}}\frac{da_1^2}{dx} = -\frac{\gamma - 1}{mp_0}\left(\frac{2}{\gamma - 1}\right)^{s/2-m}(a_0^2)^{\frac{1}{\gamma-1}} \tag{35}$$

This differential equation must be integrated to yield $a_1(x)$, which then can be substituted into Eq. (6a) to find $u_1(x)$. Such $u_1(x)$ functions would yield solutions with "similar" velocity (u) and total energy (H) distributions for different values of x.

Let

$$(a_1/a_0)^2 = \xi \tag{36}$$

then Eq. (35) can be rewritten as

$$(1 - \xi)^{m-s/2}\xi^{\frac{(m+1)-(m+2)\gamma}{\gamma-1}}\frac{d\xi}{dx} = -\frac{\gamma - 1}{mp_0}a_0^{\frac{5\gamma-1}{\gamma-1}}\left(\frac{2}{\gamma - 1}\right)^{s/2-m} \tag{37}$$

The integration of Eq. (37) yields

$$\int_0^\xi (1-\xi)^{m-3/2}\,\xi^{\frac{(m+1)-(m+2)\gamma}{\gamma-1}}\,d\xi = A - \frac{\gamma-1}{mp_0}\,a_0^{\frac{5\gamma-1}{\gamma-1}}\left(\frac{2}{\gamma-1}\right)^{3/2-m} x \quad (38)$$

where A is the integration constant. The integral on the left-hand side is an incomplete Beta integral which can also be expressed as follows:

$$\int_0^\xi (1-\xi)^{m-3/2}\,\xi^{\frac{(m+1)-(m+2)\gamma}{\gamma-1}}\,d\xi = \left[\frac{\gamma-1}{m-(m+1)\gamma}\right]\xi^{\frac{m-(m+1)\gamma}{\gamma-1}}\,F\left(\frac{m-(m+1)\gamma}{\gamma-1},\ \frac{3}{2}-m;\ \frac{m-1-m\gamma}{\gamma-1};\ \xi\right) \quad (39)$$

where F is the hypergeometric series, convergent for

$$|\xi| \leq 1 \text{ and } m > 1/2.$$

A combination of Eqs. (38) and (39) yields[6]

$$\left[\frac{\gamma-1}{m-(m+1)\gamma}\right]\left(\frac{a_1}{a_0}\right)^{\frac{2m-(m+1)2\gamma}{\gamma-1}} \times \sum_{n=0}^{\infty} \frac{\left(\frac{m-(m+1)\gamma}{\gamma-1}\right)_n \left(\frac{3}{2}-m\right)_n}{\left(\frac{(m-1)-m\gamma}{\gamma-1}\right)_n n!}\left(\frac{a_1}{a_0}\right)^n = A - \frac{\gamma-1}{mp_0}\,a_0^{\frac{5\gamma-1}{\gamma-1}}\left(\frac{2}{\gamma-1}\right)^{3/2-m} x \quad (40)$$

where

$$(s)_0 = 1$$
$$(s)_n = s(s+1)\ldots(s+n-1) = [\Gamma(s+n)]/[\Gamma(s)] \qquad n = 1, 2, 3, \ldots$$

To find $a_1(x)$, it is necessary to invert the series given in Eq. (40); the computations are, therefore, in general, rather complicated. A question of more immediate interest is that of correlating the present results with Stewartson's "similar" solutions.

(V) Correlation with Stewartson's Theory

If $m = 3/2$, Eq. (35) becomes simply

$$a_1^{\frac{4-6\gamma}{\gamma-1}}\,(da_1/dx) = -[(\gamma-1)/3p_0]\,a_0^{\frac{2}{\gamma-1}} \quad (41)$$

which can be integrated easily to yield

$$\frac{a_1}{a_0} = \left(1 - \frac{3-5\gamma}{3p_0}\,a_0^{\frac{5\gamma-1}{\gamma-1}}\,x\right)^{\frac{\gamma-1}{3-5\gamma}} \quad (42)$$

Therefore, by Eq. (6a), it is found that

$$u_1^2 = \frac{2}{\gamma-1}\,a_0^2\left[1 - \left(1 + \frac{5\gamma-3}{3p_0}\,a_0^{\frac{5\gamma-1}{\gamma-1}}\,x\right)^{\frac{2\gamma-2}{3-5\gamma}}\right] \quad (43)$$

The value of $m = 3/2$ corresponds to Stewartson's $\beta = 2/3 = (2m'/m'+1)$ or $m' = 1/2$; for such a case, Stewartson's theory gives [Eq. (4.7), reference 3]

$$u_1^2 = \frac{2}{\gamma-1}\,a_0^2\left[1 - \left(1 + \frac{5\gamma-3}{4}\,\frac{Bx}{a_0^2}\right)^{\frac{2\gamma-2}{3-5\gamma}}\right] \quad (43a)$$

By letting $B = (4/3p_0)a_0^{\frac{7\gamma-3}{\gamma-1}}$, Eqs. (43) and (43a) become identical. In reference 5, it was pointed out that, for "similar" solutions, the main-stream conditions must satisfy an integral equation of the following kind [see Eq. (34), reference 5]:

$$m' = -\left(\frac{a_0}{a_1}\right)^{\frac{3\gamma-1}{\gamma-1}}\left(1 + \frac{\gamma-1}{2}\,M_1^2\right) \times \frac{1}{\rho_1 u_1^2}\,\frac{dp_1}{dx}\int_0^x \left(\frac{a_1}{a_0}\right)^{\frac{3\gamma-1}{\gamma-1}} dx \quad (44)$$

This last relation can also be written as

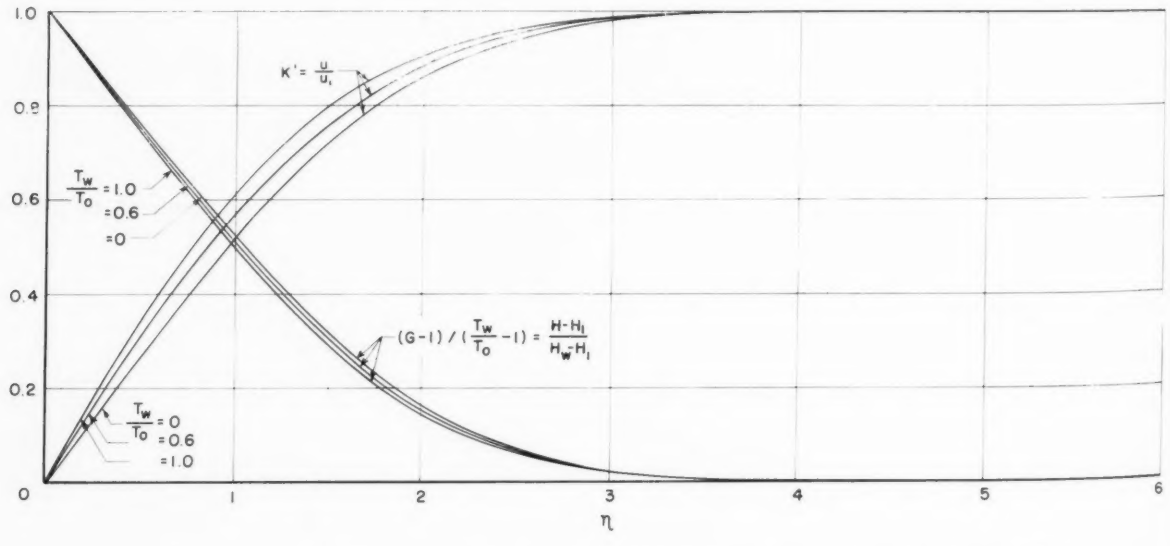

FIG. 1 – NUMERICAL SOLUTIONS OF K' AND G (EQS. 55 AND 56) FOR $\beta = 0.286$ AND VARIOUS $\frac{T_w}{T_0}$'S

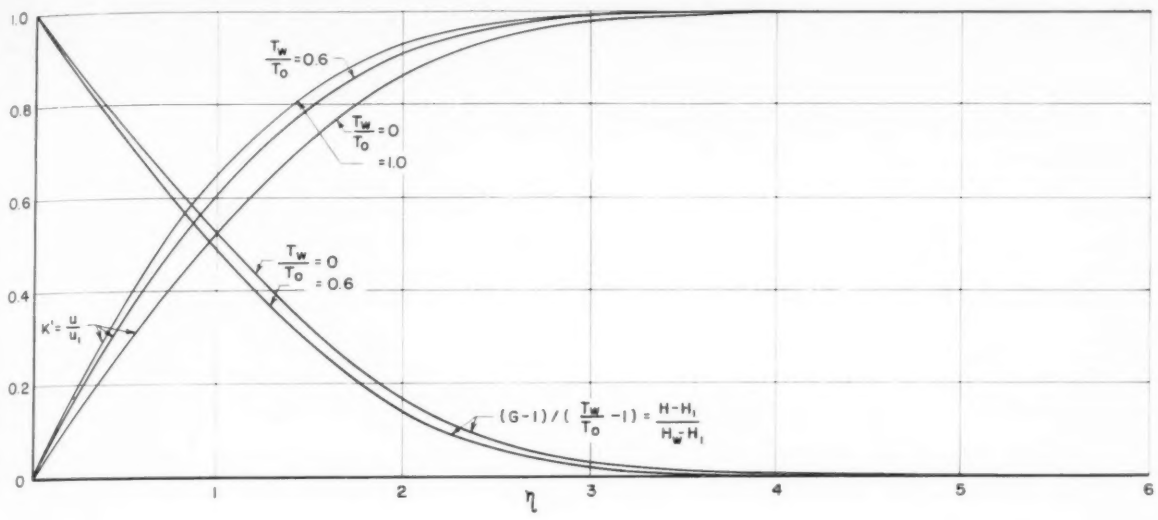

FIG. 2 - NUMERICAL SOLUTIONS OF K' AND G (EQS. 55 AND 56) FOR β = 0.4 AND VARIOUS $\frac{T_w}{T_0}$'S

$$m' = \frac{1}{2}\left(\frac{a_0}{a_1}\right)^{\frac{5\gamma-3}{\gamma-1}} \frac{1}{u_1^2}\frac{d}{dx}(u_1^2)\int_0^x \left(\frac{a_1}{a_0}\right)^{\frac{3\gamma-1}{\gamma-1}} dx \qquad (44a)$$

It can be verified that for $m' = 1/2$, Eq. (43) actually satisfies this last integral equation. It is perhaps interesting to point out that the integral equation, Eq. (44a), actually constitutes the condition of reducibility to ordinary differential equations. Its position in Stewartson's theory corresponds somewhat to Eq. (35) in the present theory.

If, now, a transformation of coordinates, $Z = Z(x)$, is introduced so that

$$Z = \int_0^x (a_1^2)^{\frac{(m+2)\gamma-(m+1)}{\gamma-1}} dx \qquad (45)$$

then Eq. (35) may be written as

$$u_1^{2m-2}(du_1/dZ) = (1/mp_0)a_0^{2/(\gamma-1)} \qquad (46)$$

Integrating Eq. (46) gives

$$u_1 = \left(\frac{2m-1}{mp_0}a_0^{2/(\gamma-1)}Z\right)^{1/(2m-1)} + \text{constant} \qquad (47)$$

For $m = 1/2$, Eq. (46) can be integrated to yield

$$u_1 = (\text{constant})\exp[(2/p_0)a_0^{2/(\gamma-1)}Z] \qquad (48)$$

The Z-transformation in Eq. (45) is analogous to Stewartson's transformation [Eq. (2.21), reference 3]. The special forms of u_1 in Eqs. (47) and (48) are analogous to those previously found by the present authors. [See Eqs. (26) and (27) in reference 5.]

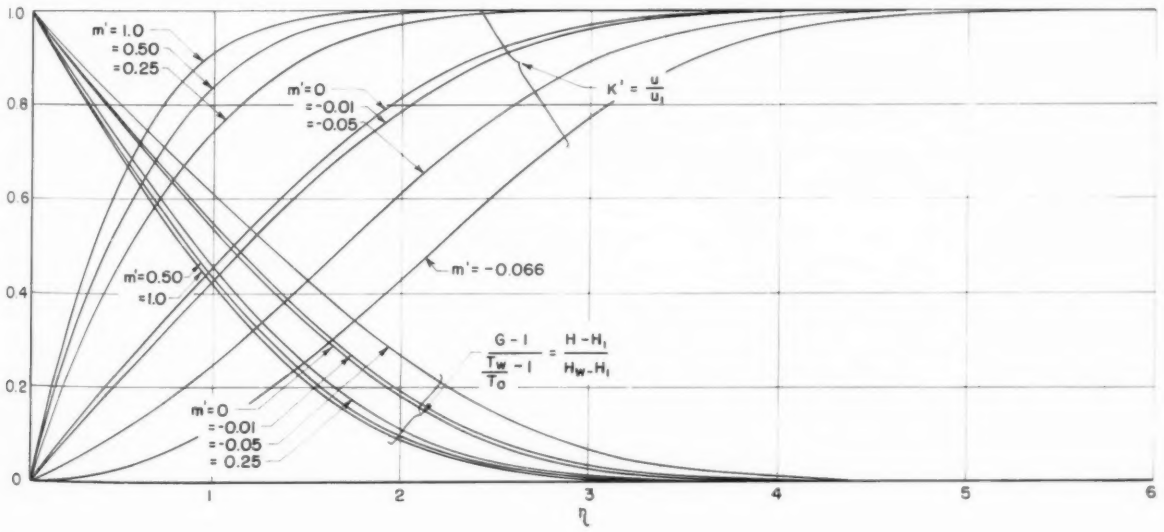

FIG. 3 - NUMERICAL SOLUTIONS OF K' AND G (EQS. 30a AND 31) FOR $\frac{T_w}{T_0}$=2 AND VARIOUS (m') 'S

(VI) Derivation of Simple $u_1(x)$'s for Special Values of γ

For $m = -[(2\gamma - 1)/(\gamma - 1)]$, Eq. (35) can be rewritten as follows:

$$\left(1 - \frac{a_1^2}{a_0^2}\right)^{-\frac{2\gamma-1}{\gamma-1}-\frac{3}{2}} \frac{d}{dx}\left(\frac{a_1^2}{a_0^2}\right) = \frac{(\gamma-1)^2}{(2\gamma-1)p_0} a_0^{\frac{5\gamma-1}{\gamma-1}} \left(\frac{2}{\gamma-1}\right)^{\frac{3}{2}+\frac{2\gamma-1}{\gamma-1}} \quad (49)$$

which can be easily integrated to yield

$$\frac{1}{5\gamma-3}\left[\frac{2}{\gamma-1} a_0^2 \left(1 - \frac{a_1^2}{a_0^2}\right)\right]^{-\frac{5\gamma-3}{2(\gamma-1)}} = \frac{1}{(2\gamma-1)p_0} a_0^{\frac{2}{\gamma-1}} (x + x_0) \quad (50)$$

Therefore, the special form of $u_1(x)$ becomes

$$u_1 = \left(\frac{2\gamma-1}{5\gamma-3} p_0\right)^{\frac{\gamma-1}{5\gamma-3}} a_0^{\frac{2}{3-5\gamma}} (x + x_0)^{\frac{\gamma-1}{3-5\gamma}} \quad (51)$$

That is, the main stream represents a decelerating flow, at $x = -x_0$, $u_1 \to \infty$, while as $x \to \infty$, $u_1 \to u_0 = 0$. For triatomic gases, such as CO_2, $\gamma = 9/7$, Eq. (51) becomes

$$u_1 = \left(\frac{11}{24} p_0\right)^{1/12} a_0^{-(7/12)} (x + x_0)^{-(1/12)} \quad (51a)$$

In the case of diatomic gases, such as N_2, O_2, or air, $\gamma = 7/5$, Eq. (51) becomes

$$u_1 = \left(\frac{9}{20} p_0\right)^{1/10} a_0^{-(1/2)} (x + x_0)^{-(1/10)} \quad (51b)$$

For monatomic gases, such as He, $\gamma = 5/3$, Eq. (51) becomes

$$u_1 = [(7/16)p_0]^{1/8} a_0^{-(3/8)} (x + x_0)^{-(1/8)} \quad (51c)$$

The values of m corresponding to $\gamma = 9/7, 7/5, 5/3$ are, respectively, $m = -11/2, -9/2, -7/2$. For the case of an insulated surface, $G = 1$, Eq. (30) reduces to

$$KK'' + K''' = \beta(K'^2 - 1) \qquad \beta = 1/m \quad (30a)$$

This last equation has been studied by Hartree.[9] The solution was found numerically for a range of values of β. When $\beta = -.1988$, K'' vanishes at $\eta = 0$, so that $\partial u/\partial y$ vanishes when $y = 0$ for all values of x. Therefore, the values of $m = -9/2, -7/2$ may not be used because separation could already have taken place; however, in the case of a noninsulated surface, Eqs. (30) and (31) must be solved together; then separation does not always occur for these m's (cf. later discussions of the effects of heat transfer on separation).

(VII) Hypersonic Viscous Flow on a Flat Plate

The problem of the "strong" interaction between the leading edge shock and the viscous layer over a flat plate has been discussed recently by several authors.[7, 8] In reference 7, the present authors first deduced, by the momentum integral method, that the pressure on an insulated surface behaves like $x^{-1/2}$; this prediction is in qualitative agreement with recent experimental findings. On the edge of the boundary layer it can easily be deduced from Eqs. (1a), (3a), and (5a) that

$$p_1 \rho_1^{-\gamma} = \text{constant} \quad (52)^*$$

The fact that this particular relation holds along the edge of the boundary layer makes it plausible to treat the problem of hypersonic viscous flow on a flat plate as a particular example of the "similar" solutions. Thus, Eq. (44) can be rewritten as follows for $M_1^2 \gg 1$:

$$m' = -\left(\frac{p_0}{p_1}\right)^{\frac{3\gamma-1}{2\gamma}} \left(\frac{\gamma-1}{2\gamma}\right)\left[\frac{x}{p_1/p_0}\frac{d}{dx}\left(\frac{p_1}{p_0}\right)\right] \times \frac{1}{x}\int_0^x \left(\frac{p_1}{p_0}\right)^{\frac{3\gamma-1}{2\gamma}} dx \quad (53)$$

Since

$$[x/(p_1/p_0)]\,(d/dx)\,(p_1/p_0) = -(1/2)$$

it is deduced that

$$m' = \frac{\gamma-1}{\gamma+1} \qquad \beta = \frac{1}{m} = \frac{2m'}{m'+1} = \frac{\gamma-1}{\gamma} \quad (54)$$

Therefore, for this particular case, the ordinary differential equations are

$$K''' + KK'' = [(\gamma-1)/\gamma]\,(K'^2 - G) \quad (55)$$

$$G'' + KG' = 0 \quad (56)$$

These equations were first obtained by Lees.[8] Eqs. (55) and (56) with the boundary conditions of Eqs. (32) and (33) have been integrated on a REAC machine with $\gamma = 1.4$ and $\gamma = 1.67$ for a range of values of $T_w/T_0 \leq 1$.† These solutions are presented in Figs. 1 and 2. It is perhaps interesting to note that Lees in reference 8 treated only the cases of $T_w/T_0 = 1$ and $T_w \div T_0 = 0$; for the latter case, an approximate equation instead of Eq. (55) was solved.

(VIII) Laminar Boundary-Layer Flow with Pressure Gradient and Heat Transfer

The "similar" solutions are interesting because they are "exact" solutions of the boundary-layer flow with pressure gradient and heat transfer. A study of the "similar" solutions can provide some understanding of the effects of pressure gradient and heat transfer. In Figs. 1 and 2, some effects of cooling the surface are exhibited. For a fixed $\beta > 0$—i.e., a fixed favorable pressure gradient—these figures show that the skin friction, $\tau_w = \mu_w(\partial u/\partial y)_w$, is lower when the surface is cooled. This is because both $\mu_w \sim T_w$ and $(\partial u/\partial y)_w \sim K''(0)$ are smaller on a cooled surface. To study the

* At the outer edge of the boundary layer, strictly speaking, one should use the equations of inviscid rotational flow instead of Eqs. (1a), (3a), and (5a). Therefore, this condition is correct only as a first approximation.

† The authors wish to acknowledge their sincere thanks to Dr. C. Gazley, Jr., of the RAND Corporation for his kind help in obtaining these solutions.

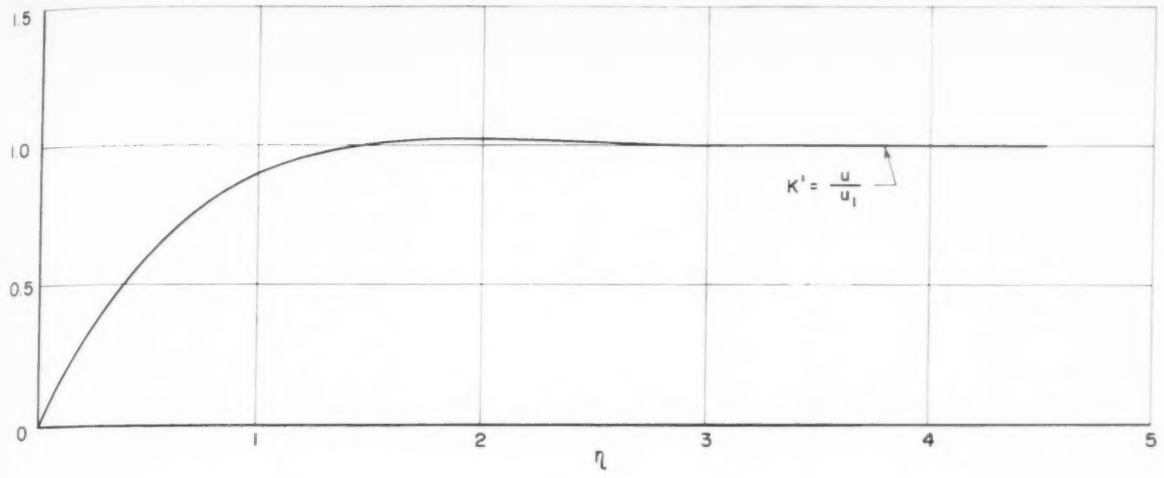

FIG. 4 - NUMERICAL SOLUTION OF K' (EQ. 55) FOR $\beta = 0.4$, $\frac{T_w}{T_0} = 4.0$

effects of surface heating, a numerical integration of the ordinary differential equations, Eqs. (30) and (31), with the proper boundary conditions, Eqs. (32) and (33), has been carried out for a range of values of $T_w/T_0 \geq 1$ and for $\beta > 0$ or $\beta < 0$.* A typical set of data is shown in Fig. 3. This figure is particularly interesting because it shows the effects of pressure gradient on the boundary-layer flow over a heated surface ($T_w/T_0 = 2$). It is observed that the effect of a favorable pressure gradient is to increase the value of $(\partial u/\partial y)_w \sim K''(0)$, consequently, the skin friction increases with a favorable pressure gradient; the effect of an adverse pressure gradient is just the opposite. It is also interesting to mention that when the surface is excessively heated, the local velocity in the boundary layer under a favorable pressure gradient may become faster than the free stream—for instance, when $T_w/T_0 = 4.0$, $\beta = 0.40$, a velocity profile ($u/u_1 = K'$) of the form as in Fig. 4 is actually obtained. In Fig. 5 a curve showing the "critical" values of T_w/T_0 and m' is given; for values of $(T_w/T_0 - 1)$ and m' inside the shaded region under the curve, the velocity ratio ($u/u_1 = K'$) will not have values exceeding unity. Analysis of the numerical results of the "similar" solutions also provides values of $C_{h_1}/(1/2)C_{f_1}$ for various surface temperatures with different free-stream pressure gradients (Fig. 6). These data are obtained by using the following formula:

$$(2C_{h_1})/C_{f_1} = -[1/(G_w - 1)]\,[G'(0)/K''(0)] \quad (57)$$

where

$$C_{h_1} = \frac{k_w(\partial T/\partial y)_w}{\rho_1 u_1 H_1(G_w - 1)} \qquad C_{f_1} = \frac{\mu_w(\partial u/\partial y)_w}{(1/2)\,\rho_1 u_1^2} \quad (58)$$

are respectively the local coefficients of heat transfer and skin friction. As expected, $2C_{h_1}/C_{f_1} = 1$ on a flat surface with zero pressure gradient ($m' = 0$, Fig. 6). For a flat surface with a favorable pressure gradient, $dp_1/dx < 0$, $m' > 0$, it is found that $2C_{h_1}/C_{f_1} < 1$; the curves in Fig. 6 become steeper as T_w/T_0 increases. For a flat surface with an adverse pressure gradient, $dp_1/dx > 0$, $m' < 0$, it is found that $2C_{h_1}/C_{f_1} > 1$; the negative m' branch of the curve given in Fig. 6 is com-

* These results were previously discussed in reference 5. The authors are indebted to A. Presson of the Jet Propulsion Laboratory for his close cooperation in obtaining these numerical solutions on a REAC.

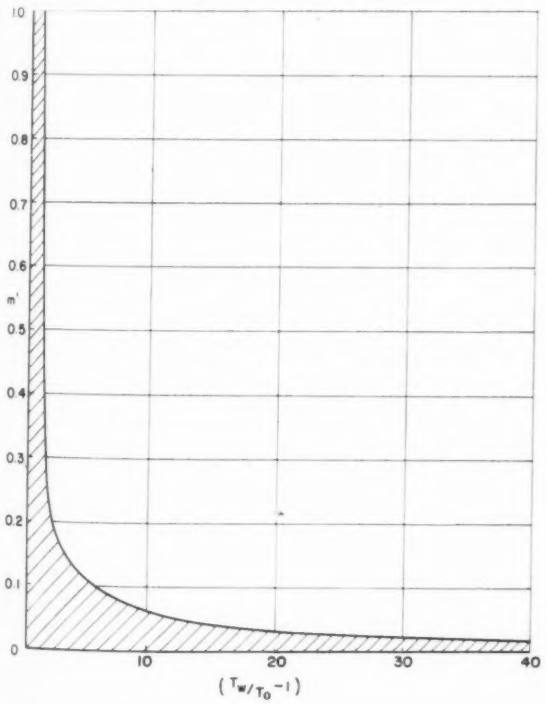

FIG. 5 - "CRITICAL" VALUES OF T_w/T_0 vs. THE PARAMETER m'

TABLE 1

Solutions of $KK'' + K''' = \beta(K'^2 - G)$, $G'' + KG' = 0$ With Boundary Conditions: $K = K' = 0$, $G = T_w/T_0$ for $\eta = 0$; $K' = 1$, $G = 1$ for $\eta \to \infty$

β	0.286		0.286		0.286		0.40		0.40		0.40	
$m' = \beta/(2-\beta)$	0.1667		0.1667		0.1667		0.25		0.25		0.25	
$K''(0)$	0.540		0.670		0.765		0.561		0.741		0.855	
$G'(0)$	−0.409		−0.505		−0.520		−0.488		−0.517		−0.526	
$(T_w/T_0) - 1$												
$C_{h_1}/[(1/2)C_{f_1}]$	0.907		0.754		0.680		0.870		0.698		0.615	
T_w/T_0	0		0.6		1.0		0		0.6		1.0	
η	K'	$\frac{G-1}{(T_w/T_0)-1}$	K'	$\frac{G-1}{(T_w/T_0)-1}$	K'	$\frac{G-1^*}{(T_w/T_0)-1}$	K'	$\frac{G-1}{(T_w/T_0)-1}$	K'	$\frac{G-1}{(T_w/T_0)-1}$	K'	$\frac{G-1^*}{(T_w/T_0)-1}$
0.0	0	1.0	0	1.0	0	1.0	0	1.000	0	1.000	0	1.00
0.1	0.05	0.95	0.06	0.95	0.065	0.950	0.053	0.948	0.069	0.944	0.077	0.945
0.2	0.105	0.90	0.125	0.90	0.150	0.895	0.108	0.899	0.138	0.892	0.157	0.890
0.3	0.160	0.855	0.190	0.85	0.215	0.850	0.165	0.850	0.205	0.841	0.234	0.838
0.4	0.210	0.805	0.250	0.80	0.280	0.795	0.219	0.801	0.272	0.790	0.320	0.788
0.5	0.265	0.760	0.310	0.75	0.345	0.740	0.274	0.754	0.335	0.740	0.369	0.738
0.6	0.315	0.705	0.365	0.70	0.405	0.690	0.325	0.708	0.396	0.690	0.432	0.686
0.7	0.370	0.660	0.415	0.65	0.465	0.640	0.378	0.659	0.452	0.640	0.495	0.633
0.8	0.420	0.615	0.475	0.60	0.515	0.595	0.428	0.612	0.506	0.590	0.556	0.583
0.9	0.470	0.565	0.525	0.55	0.565	0.545	0.480	0.568	0.558	0.542	0.606	0.533
1.0	0.515	0.520	0.570	0.505	0.610	0.500	0.525	0.522	0.605	0.496	0.649	0.490
1.2	0.600	0.435	0.660	0.420	0.695	0.410	0.612	0.437	0.689	0.408	0.729	0.401
1.4	0.650	0.350	0.730	0.340	0.770	0.325	0.690	0.355	0.761	0.323	0.796	0.319
1.6	0.750	0.280	0.795	0.265	0.830	0.250	0.759	0.282	0.822	0.252	0.855	0.247
1.8	0.810	0.220	0.845	0.205	0.875	0.190	0.817	0.219	0.872	0.191	0.899	0.185
2.0	0.860	0.160	0.890	0.150	0.910	0.145	0.863	0.163	0.909	0.140	0.932	0.138
2.2	0.900	0.115	0.920	0.110	0.940	0.100	0.902	0.121	0.938	0.100	0.953	0.097
2.4	0.930	0.080	0.945	0.075	0.960	0.070	0.932	0.088	0.959	0.068	0.969	0.065
2.6	0.955	0.050	0.960	0.050	0.970	0.040	0.953	0.060	0.973	0.043	0.981	0.045
2.8	0.970	0.030	0.970	0.030	0.980	0.025	0.969	0.040	0.983	0.027	0.989	0.030
3.0	0.980	0.020	0.980	0.020	0.990	0.015	0.980	0.027	0.991	0.015	0.993	0.022
3.2	0.990	0.010	0.985	0.010	0.990	0.010	0.986	0.018	0.994	0.009	0.996	0.013
3.4	0.995	0	0.990	0.005	0.995	0.005	0.991	0.011	0.998	0.003	0.997	0.009
3.6	0.995		0.995	0.005	0.995	0	0.993	0.006	1.00	0	0.997	0.004
3.8	1.00		1.000	0	1.000		0.996	0.004			0.999	0.002
4.0							0.997	0.003			1.0	0.000
4.2							1.000	0				

* Insulated surface, $G = 1$ is the solution.

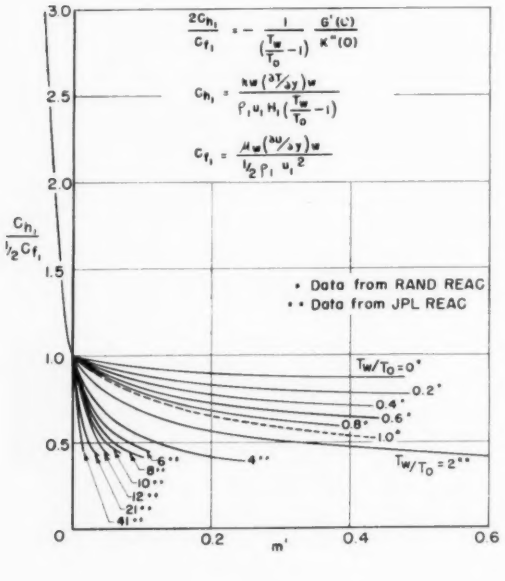

FIG. 6 – VALUES OF $\frac{2C_{h_1}}{C_{f_1}}$ FOR VARIOUS SURFACE TEMPERATURES WITH DIFFERENT FREE STREAM PRESSURE GRADIENTS

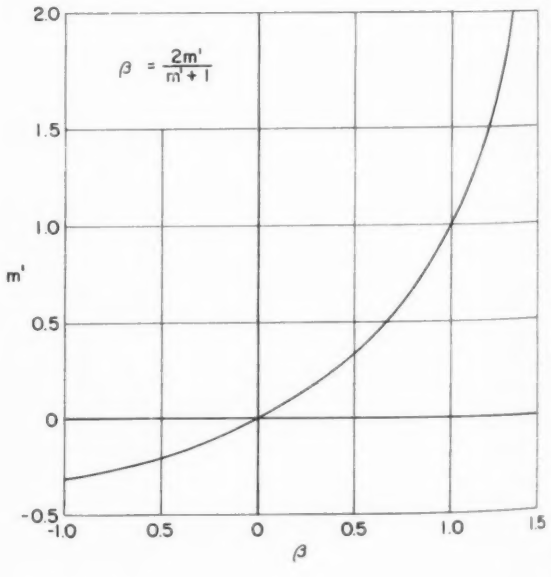

FIG. 7 - VARIATION OF m' WITH β

puted for the case of a heated surface ($T_w/T_0 = 2$). The rapid rise of the value of $2C_{h_1}/C_{f_1}$ for $m' < 0$, in this case, seems to indicate that C_{f_1} rapidly approaches zero and the boundary layer tends to separate under an adverse pressure gradient of a certain magnitude.

It is rather difficult to discuss the effects of heat transfer on separation since there are not yet a sufficient number of solutions with varying T_w/T_0's for $dp_1/dx > 0$. Nevertheless, it is interesting to discuss qualitatively the separation of a compressible boundary layer as follows:

(1) Insulated surface: Eq. (30a) is the equation studied by Hartree.[9] When $\beta = -0.1988$, $K''(0) = 0$. Thus, for $\beta < -0.1988 < 0$, the boundary layer will separate.

(2) Noninsulated surface: Eq. (30) can be rewritten as

$$K'' = (1/K)\,[\beta(K'^2 - G) - K'''] \tag{59}$$

In discussing the effect of heat transfer on separation, it is interesting to consider the following:

$$G = 1 + \Delta G \qquad \text{where} \qquad \Delta G \ll 1 \tag{60}$$

This is the case of a surface with a very small amount of heat transfer. If for $G = 1$, $K''(0)$ vanishes when $\beta = \beta_0 < 0$, it is expected that for $G = 1 + \Delta G$, $K''(0)$ would vanish when $\beta = \beta_0 + \Delta\beta$, where $\Delta G \ll 1$, and $\Delta\beta \ll \beta_0 = 0(1)$. As $\eta \to 0$, from Eq. (59), it is found that

$$\lim_{\eta\to 0} K'' - \lim_{\eta\to 0} \frac{\beta_0(K'^2 - 1) - K'''}{K} = \lim_{\eta\to 0}\left[-\frac{\beta_0\Delta G - \Delta\beta(K'^2 - 1)}{K}\right] \tag{61}$$

This can be interpreted as follows:

$$K''(0) - [K''(0)]_{\Delta G\to 0} = \lim_{\eta\to 0}\left[-\frac{\beta_0\Delta G - \Delta\beta(K'^2 - 1)}{K}\right] \tag{62}$$

Hence, it is easy to see that

$$\lim_{\Delta G\to 0} \frac{\{K''(0) - [K''(0)]_{\Delta G\to 0}\}}{\Delta G} = \lim_{\substack{\eta\to 0\\ \Delta G\to 0}}\left(-\frac{\beta_0}{K} + \frac{\Delta\beta}{\Delta G}\,\frac{K'^2 - 1}{K}\right) \tag{63}$$

The boundary conditions are such that $K = K' = 0$ at $\eta = 0$; therefore, from the right hand side of Eq. (63), it can be seen that the limit exists only when

$$\Delta\beta = -\beta_0\Delta G \tag{64}$$

That is, the condition in Eq. (64) is necessary if $K''(0)$ changes continuously with G. Therefore, for a heated

TABLE 2

Solutions of $KK'' + K''' = \beta(K'^2 - G)$, $G'' + KG' = 0$ With Boundary Conditions: $K = K' = 0$, $G = T_w/T_0$ for $\eta = 0$; $K' = 1$, $G = 1$, for $\eta \to \infty$

β	1.0	.667	0.40	0	−0.0202	−0.1053
$m' = \beta/(2 - \beta)$	1.0	.50	0.25	0	−0.01	−0.05
T_w/T_0	2.0	2.0	2.0	2.0	2.0	2.0
$K''(0)$	1.7386	1.4226	1.1154	0.480	0.415	0.120
$G'(0)$	−0.612	−0.588	−0.560	−0.480	−0.460	−0.393
$\frac{G'(0)}{(T_w/T_0) - 1}$						
$C_{h_1}/[(1/2)C_{f_1}]$	0.3520	0.4133	0.5021	1.000	1.110	3.28

η	K'	$\frac{G-1}{(T_w/T_0)-1}$	K'	$\frac{G-1}{(T_w/T_0)-1}$	K'	$\frac{G-1}{(T_w/T_0)-1}$	K'	$\frac{G-1}{(T_w/T_0)-1}$	K'	$\frac{G-1}{(T_w/T_0)-1}$	K'	$\frac{G-1}{(T_w/T_0)-1}$
0	0	1.000	0	1.000	0	1.000	0	1.000	0	1.0	0	1.00
0.1	0.161	0.941	0.134	0.943	0.107	0.946	0.046	0.955	0.042	0.958	0.015	0.966
0.2	0.306	0.880	0.260	0.884	0.210	0.890	0.094	0.908	0.085	0.911	0.033	0.927
0.3	0.433	0.818	0.368	0.825	0.302	0.833	0.140	0.861	0.128	0.865	0.054	0.887
0.4	0.541	0.756	0.465	0.765	0.386	0.777	0.187	0.814	0.171	0.818	0.076	0.847
0.5	0.634	0.696	0.551	0.707	0.463	0.721	0.235	0.767	0.215	0.773	0.100	0.807
0.6	0.712	0.637	0.627	0.649	0.533	0.666	0.280	0.719	0.258	0.727	0.127	0.768
0.7	0.777	0.579	0.693	0.593	0.597	0.613	0.327	0.673	0.302	0.681	0.155	0.728
0.8	0.831	0.524	0.750	0.538	0.654	0.560	0.371	0.628	0.345	0.637	0.184	0.690
0.9	0.875	0.469	0.799	0.485	0.705	0.508	0.417	0.582	0.389	0.592	0.216	0.650
1.0	0.910	0.417	0.840	0.435	0.751	0.459	0.461	0.538	0.431	0.548	0.249	0.611
1.2	0.959	0.326	0.903	0.342	0.826	0.368	0.545	0.453	0.514	0.466	0.317	0.536
1.4	0.985	0.246	0.945	0.262	0.882	0.286	0.624	0.374	0.593	0.386	0.390	0.463
1.6	0.997	0.180	0.972	0.194	0.924	0.216	0.696	0.302	0.667	0.314	0.464	0.394
1.8	1.000	0.127	0.987	0.139	0.952	0.158	0.760	0.237	0.734	0.249	0.538	0.328
2.0		0.088	0.995	0.097	0.972	0.112	0.816	0.182	0.792	0.193	0.611	0.269
2.2		0.058	0.998	0.064	0.984	0.077	0.863	0.135	0.843	0.145	0.680	0.215
2.4		0.037	1.000	0.041	0.992	0.050	0.901	0.097	0.885	0.107	0.743	0.168
2.6		0.023		0.025	0.996	0.032	0.930	0.068	0.918	0.075	0.801	0.128
2.8		0.014		0.014	0.999	0.019	0.953	0.046	0.944	0.052	0.849	0.095
3.0		0.008		0.008	1.000	0.010	0.969	0.029	0.963	0.034	0.890	0.068
3.2		0.005		0.004		0.005	0.980	0.018	0.976	0.022	0.922	0.048
3.4		0.003		0.001		0.002	0.988	0.010	0.986	0.013	0.947	0.032
3.6		0.002		0.000		0.000	0.993	0.005	0.992	0.008	0.966	0.022
3.8		0.001					0.996	0.002	0.995	0.004	0.979	0.014
4.0		0.000					0.998	0.000	0.998	0.002	0.988	0.009
4.2							1.000		0.999	0.001	0.993	0.006
4.4									1.000	0.000	0.997	0.004
4.6											0.999	0.003
4.8											1.000	0.002
5.0												0.000

surface, $\Delta G > 0$, $-\beta_0 \times (\Delta G) > 0$; that is, $\beta = \beta_0 + \Delta\beta > \beta_0$; this means that the boundary layer on a heated surface will separate under a comparatively weaker adverse pressure gradient than in the case of an insulated surface. This prediction is in qualitative agreement with the results obtained on the REAC for the case $m' < 0$, $T_w/T_0 = 2$ (see Fig. 6). Thus, the boundary layer on a heated surface may separate for a value of β in the range $0 > \beta > -0.1988$. The effect of cooling is opposite to that of heating—i.e., the boundary layer on a cooled surface can sustain a stronger adverse pressure gradient. From a physical standpoint, the effect of heating the surface is to decrease the density of the gas layer immediately adjacent to the surface; this seems to decrease proportionately the kinetic energy of such a gas layer so that it can sustain only a very weak adverse pressure gradient.

(IX) Conclusions

(1) A direct procedure has been used whereby the reducibility of the partial to ordinary differential equations can be shown without the need of introducing V_1 and transforming coordinates.[3, 5] The reducibility condition gives the special form of $u_1(x)$ for which "similar" solutions are permitted. Correlation of the present results with Stewartson's result is discussed. For $m = 3/2$, $u_1(x)$ as given in Eq. (43) can be shown to be identical to Stewartson's answer.

(2) The forms of the $u_1(x)$'s for "similar" solutions are, in general, very complicated. Nevertheless in some special cases, simple forms of $u_1(x)$'s are obtained in the present paper.

(3) The hypersonic viscous flow past a flat plate can be formulated as a special case of the "similar" solutions. The pertinent value of β is $(\gamma - 1)/\gamma$. Numerical solutions for this case are given in Figs. 1 and 2. The data are also tabulated in Table 1.

(4) Figure 3 shows the distribution of u/u_1 and H/H_1 inside a laminar boundary layer on a heated surface ($T_w/T_0 = 2$) for various pressure gradients in the free stream. The data are also tabulated in Table 2. The variation of the boundary-layer thickness under various pressure gradients is clearly seen here.

(5) On an excessively heated surface, the boundary layer under a favorable pressure gradient can be so greatly energized that the local velocity in the boundary layer may be faster than the free stream (see Fig. 4). The data are tabulated in Table 3.

(6) The variation of $2C_{h_1}/C_{f_1}$ for various surface temperatures with different free-stream pressure gradients is shown in Fig. 6.

(7) The effects of heat transfer on separation are qualitatively discussed. The effect of surface heating is to cause the boundary-layer flow to separate at a value of β in the range $0 > \beta > -0.1988$; the effect of surface cooling is to delay the separation of boundary layer to values of $\beta < -0.1988$.

(8) In Fig. 7, the values of m' [from the equation $\beta = (2m')/(m' + 1)$] are plotted against β.

Table 3

Solution of $KK'' + K''' = \beta(K'^2 - G)$ With Boundary Conditions: $G'' + KG' = 0$ $K = K' = 0, G = T_w/T_0$ for $\eta = 0$; $K' = 1, G = 1,$ for $\eta \to \infty$

$\beta = 0.4$ $\quad \dfrac{G'(0)}{T_w/T_0 - 1} = -0.605$

$T_w/T_0 = 4.0$ $\quad \dfrac{C_{h_1}}{(1/2)C_{f_1}} = 0.383$

$K''(0) = 1.580$

η	K'	$\dfrac{G - 1}{(T_w/T_0) - 1}$
0.0	0	1.00
0.1	0.140	0.960
0.2	0.275	0.880
0.3	0.400	0.820
0.4	0.510	0.760
0.5	0.600	0.700
0.6	0.685	0.640
0.7	0.755	0.580
0.8	0.815	0.530
0.9	0.860	0.480
1.0	0.900	0.425
1.2	0.960	0.330
1.4	0.995	0.180
1.6	1.010	0.130
1.8	1.020	0.090
2.0	1.020	0.060
2.2	1.020	0.040
2.4	1.010	0.025
2.6	1.005	0.015
2.8	1.00	0.010
3.0		0.005
3.2		0.005
3.4		0

References

[1] Illingworth, C. R., Rep. Memor. Aero. Res. Coun., No. 2590, 1946.

[2] Howarth, L., Proc. Roy. Soc., Series A, Vol. 194, p. 16, 1948.

[3] Stewartson, K., Proc. Roy. Soc., Series A, Vol. 200, p. 84, 1949.

[4] Illingworth, C. R., Proc. Roy. Soc., Series A, Vol. 199, p. 533, 1949.

[5] Li, T. Y., and Nagamatsu, H. T., *Similar Solutions of Compressible Boundary-Layer Equations*, Journal of the Aeronautical Sciences, Readers' Forum, Vol. 20, No. 9, p. 653, September, 1953.

[6] Erdelyi, A., Magnus, W., Oberhettinger, F., and Tricomi, F. G., *Higher Transcendental Functions*, McGraw-Hill Book Company, Inc., 1953.

[7] Li, T. Y., and Nagamatsu, H. T., *Shock-Wave Effects on the Laminar Skin Friction of an Insulated Flat Plate at Hypersonic Speeds*, Journal of the Aeronautical Sciences, Vol. 20, No. 5, pp. 345–355, May, 1953.

[8] Lees, L., *On the Boundary-Layer Equations in Hypersonic Flow and Their Approximate Solutions*, Journal of the Aeronautical Sciences, Readers' Forum, Vol. 20, No. 2, p. 143, February, 1953.

[9] Hartree, D. R., Proc. Cambridge Philos. Soc., Vol. 33, p. 237, 1937.

Quasi-Steady Nonlinear Pitching Oscillations in Transonic Flight*

L. TRILLING† AND E. E. COVERT‡

Massachusetts Institute of Technology

List of Symbols

A_0 = constant [see Eqs. (41a), (41b)]
A = wing area
a = $(3/2)(1 + \bar{\alpha})$ [see Section (4)]
$\bar{a}_n$ = critical point [see Section (3)]
B = (dC_M/dC_L) $[C_{L\alpha}/(3\alpha_1\alpha_2)]$ (—for stable air frame)
b = $3\bar{\alpha}_1$ [see Section (4)]
b_n = critical point [see Section (3)]
$b_0(\bar{\alpha})$ = initial polynomial in sequence solution [Eq. (14)]
$b_n(\bar{\alpha})$ = nth correction to $b_0(\bar{\alpha})$ [Eq. (23a)]
$C(\bar{\alpha})$ = normalized damping function [see Eqs. (11b), (11c)]
$C_{L\alpha}(\alpha)$ = slope of lift coefficient curve
$C_M(\alpha)$ = pitching-moment coefficient curve (+ nose up)
C_{Mq} = damping due to pitching coefficient
$C_{M\dot{\alpha}}$ = damping due to vertical velocity coefficient
$\bar{c}$ = mean aerodynamic chord
c = $-\bar{\alpha}_0(\bar{\alpha}_0^2 - a + b)$ in normalized equations [see Section (4)]
$\bar{c}_n$ = critical point [see Section (3)]
D_n = coefficient in reciprocal series [see Eq. (27b)]
d_n = critical point [see Section (3)]
$f(\bar{\alpha})$ = $d\bar{\alpha}/d\tau$
$f_n(\bar{\alpha})$ = nth approximation to f
g = acceleration due to gravity
K = balancing tail moment for trim
k = radius of gyration in pitch plane
$M(\bar{\alpha})$ = normalized moment curve [see Eq. (11a)]
R = wing aspect ratio
R_1, R_2, R_3 = regions in phase plane (see Fig. 3)
r_1, r_2, r_3, r_4 = roots of b^2 [Eq. (17)]
S_1, S_2, S_3 = points of possible trim [see Eq. (4)]
S_1 = stable focal point
S_2 = saddle point
S_3 = center point
t = time, sec.
T_1, T_3 = semitrajectories through S_2 from $t = -\infty$
T_2, T_4 = Semitrajectories through S_2 to $t = \infty$
T_{10}, T_{20} = undamped trajectories through S_2
U = constant forward velocity
W = aircraft weight
α = angle of attack ($\alpha = \theta - \gamma$)
α_0 = trim angle of attack
α_1, α_2 = values of α where pitching moment is extremals
α_L = angle of attack at which $C_{L\alpha}$ ceases to be constant
$\bar{\alpha} = \alpha/\alpha_2$ = normalized angle of attack
$\bar{\alpha}_0$ = normalized initial trim value
$\bar{\alpha}_i$ = normalized initial displacement
α_I, α_{II} = intercepts of undamped velocity function [see Section (3)]
β_S = $\bar{\alpha} - S_2$
β = $\bar{\alpha} - \bar{\alpha}_0$
ϵ = dimensionless measure of flight-path curvature [see Eq. (11c)]
γ = flight-path angle with respect to horizon + nose up
γ_1 = a damping constant [see Eq. (49)]
λ_1, λ_2 = numerical parameter [see Eq. (19b)]
ϕ = phase angle [see Eqs. (41a), (41b)]
ρ = air density slugs
θ = airplane pitch angle with respect to horizon + nose up
$\tau = t\sqrt{(ag)/(3k^2\alpha_0\alpha_1)}$ = dimensionless time
μ = dimensionless measure of damping [see Eq. (11c)]
ω_n = undamped natural frequency for a linear system
ζ = critical damping ratio for a linear system
ζ = $\mu/2\omega_n$
prime = denotes $d/d\tau$

Received August 13, 1954. Revised and received March 1, 1955.

* This work was sponsored in part by the Transonic Aircraft Control project under Air Force Contract AF 33(038)-22184 and in part as a portion of the internally sponsored research program of the Naval Supersonic Laboratory.

† Assistant Professor, Department of Aeronautical Engineering.

‡ Research Engineer, Naval Supersonic Laboratory.

(1) Introduction

This paper discusses the nonlinear pitching of a swept-wing aircraft with two degrees of freedom in transonic flight. The problem arises because beyond a critical angle of attack which depends on the Mach Number and aircraft geometry the lift and moment are no longer proportional to the angle of attack. The spanwise pressure gradient apparently induces a strong outflow of the low-speed air within the upper wing surface boundary layer,[1] and the resulting thickening of the boundary layer near the wing tips causes local stalling and moves the center of pressure of the lifting system forward. Meanwhile if the wing is thin enough,[2] a suction region develops near the leading edge of the upper wing surface and this also contributes to the forward motion of the center of pressure. At higher angles of attack, the stall moves inboard and the suction region extends toward the trailing edge, so that the center of pressure moves back. When the aircraft reaches the full stall point, the pressure distribution and the center of pressure reach another extremum.

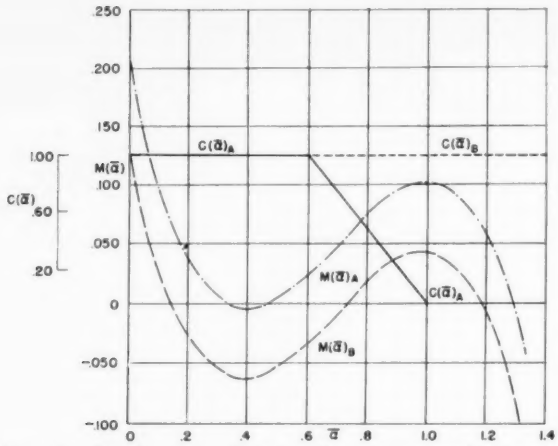

FIG. 1. Aerodynamic characteristics of assumed aircraft (A) and (B).

In the following pages, the quasi-steady nonl near longitudinal oscillation of an aircraft with such lift and moment characteristics is examined in some detail. The moment curve $C_M(\alpha)$ has extrema at angles of attack α_1 and α_2 and is represented as a cubic in α. The lift curve slope $C_{L_\alpha}(\alpha)$ is constant up to an angle of attack α_L; it then decreases linearly until it vanishes at the stall point α_2 and remains zero thereafter.

The equations for the longitudinal oscillation of this aircraft are derived and expressed in terms of suitable dimensionless parameters. Two approximate methods are worked out to solve the initial displacement problem: The exact solution of the undamped motion equation is used as the first step of an iteration procedure when the damping is small. The exact solution of the equation with critical damping and a special nonlinearity serves as the basis for calculations when the damping is appreciable. Numerical examples are given to illustrate both methods.

(2) Equations of Motion

The moment curve postulated in this investigation is a cubic with extrema at α_1, α_2. It has the form:

$$C_M = B[\alpha^3 - (3/2)\,(\alpha_1 + \alpha_2)\alpha^2 + 3\alpha_1\alpha_2\alpha - K] \quad (1)$$

where B, K are constants that will now be evaluated. The constant B is related to the static margin a/c, since by definition:

$$dC_M/dC_L(0) = (1/C_{L_{\alpha_0}})\,(dC_M/d\alpha)\,(0) = (3B\alpha_1\alpha_2)/C_{L_{\alpha_0}} = -a/c \quad (2)$$

The aircraft is trimmed at an angle of attack α_0 by application of a tail moment just sufficient to cancel the wing moment. If one examines a fixed control maneuver, that tail moment remains essentially constant throughout the maneuver, and K gives its contribution to the total moment at any time; K is therefore selected to make $C_M(\alpha)$ vanish when $\alpha = \alpha_0$. The complete moment curve is then:

$$C_M = -[(aC_{L_{\alpha_0}})/(3c\alpha_1\alpha_2)]\,(\alpha - \alpha_0) \times \{\alpha^2 + [\alpha_0 - (3/2)\,(\alpha_1 + \alpha_2)]\alpha + [\alpha_0^2 - (3/2)\,(\alpha_1 + \alpha_2) + 3\alpha_1\alpha_2]\} \quad (3)$$

$$K = \alpha_0^3 - (3/2)\,(\alpha_1 + \alpha_2)\alpha_0^2 + 3\alpha_1\alpha_2\alpha_0 \quad (3a)$$

This moment vanishes at the following values $S(\alpha)$:

$$\left.\begin{aligned} S &= \alpha_0 \\ S &= 1/2\{(3/2)\,(\alpha_1 + \alpha_2) - \alpha_0 \pm \sqrt{[\alpha_0 - (3/2)\,(\alpha_1 + \alpha_2)]^2 - 4[\alpha_0^2 - (3/2)\,(\alpha_1 + \alpha_2)\alpha_0 + 3\alpha_1\alpha_2]}\} \end{aligned}\right\} \quad (4)$$

The first root represents trimmed equilibrium flight. The other roots are real if:

$$(3\alpha_1 - \alpha_2)/2 \le \alpha_0 \le (3\alpha_2 - \alpha_1)/2 \quad (5)$$

When these last roots exist, it is necessary to investigate which initial displacements (α_i) from equilibrium lead to oscillations about α_0 and under what conditions the motion ends at another value of S.

The lift slope curve assumed in this study is:

$$\left.\begin{aligned} C_{L_\alpha}/C_{L_{\alpha_0}} &= 1 && 0 < \alpha < \alpha_L \\ &= (\alpha_2 - \alpha)/(\alpha_2 - \alpha_L) && \alpha_L < \alpha < \alpha_2 \\ &= 0 && \alpha_2 < \alpha \end{aligned}\right\} \quad (6)$$

Typical normalized lift slope and moment curves are shown on Fig. 1.

If an aircraft flies at constant velocity U along a course inclined to the horizontal by an angle $\gamma(t)$, its equations of motion are

$$(W/g)U\dot{\gamma} = (1/2)\rho U^2 A C_L - W\cos\gamma \quad (7)$$

$$(W/g)k^2(\ddot{\gamma} + \ddot{\alpha}) = (1/2)\rho U^2 Ac\{C_M(\alpha) + [c/(2U)]\,[(C_{M_q} + C_{M_{\dot\alpha}})\dot{\alpha} + C_{M_q}\dot{\gamma}]\} \quad (8)$$

where W is the aircraft weight, k is the longitudinal radius of gyration, g is the acceleration of gravity, ρ is the air density, A is the wing area, C_{M_q} is the damping in pitch,* $C_{M_{\dot\alpha}}$ is the damping in lift,* and c is the mean aerodynamic chord.

The following dimensionless parameters are introduced:

$$\left.\begin{aligned} \tau &= t\sqrt{(ag)/(3k^2\alpha_0\alpha_1)} \\ \bar{\alpha} &= \alpha/\alpha_2 \end{aligned}\right\} \quad (9)$$

Then, after some manipulation and under the two assumptions that $\alpha \sin\gamma \ll 1$ and $(C_{M_{\dot\alpha}} + C_{M_q})_{\text{wing}}$ is proportional to C_{L_α}, the equations of motion yield:

$$\bar{\alpha}'' + \mu C(\bar{\alpha})\bar{\alpha}' + M(\bar{\alpha}) = \mu^2\epsilon\int_{\bar{\alpha}_0}^{\bar{\alpha}} C(\bar{\alpha})\,d\bar{\alpha} \quad (10)$$

where

$$M(\bar{\alpha}) = (\bar{\alpha} - \bar{\alpha}_0)\{\bar{\alpha}^2 + [\bar{\alpha}_0 - (3/2)\,(1 + \bar{\alpha}_1)]\bar{\alpha} + [\bar{\alpha}_0^2 - (3/2)\,(1 + \bar{\alpha}_1)\bar{\alpha}_0 + 3\bar{\alpha}_1]\} \quad (11a)$$

* These coefficients include contributions from both wing and tail. The wing contribution is assumed proportional to lift curve slope while the tail contribution is approximately constant.

$$\left.\begin{aligned} C(\bar{\alpha}) &= 1 && 0 < \bar{\alpha} < \bar{\alpha}_L \\ &= (1 - \bar{\alpha})/(1 - \bar{\alpha}_L) && \bar{\alpha}_L < \bar{\alpha} < 1 \\ & && \text{(delta aircraft)} \\ &= 0 && 1 < \bar{\alpha} \\ C(\bar{\alpha}) &= 1 && \text{(aircraft with tail)} \end{aligned}\right\} \tag{11b}$$

$$\mu = \left(1 - \frac{c^2}{2k^2}\frac{C_{M\dot{\alpha}} + C_{Mq}}{c_{L\alpha_0}}\right)\sqrt{\frac{3k^2 g\alpha_1}{a l'^2 \alpha_0}} \tag{11c}$$

$$\epsilon = \left\{[c^2/(2k^2)]\,(C_{Mq}/C_{L\alpha_0})\right\} \div \left\{1 - [c^2/(2k^2)]\,[(C_{M\dot{\alpha}} + C_{Mq})/C_{L\alpha_0}]\right\}^2$$

The important dimensionless numerical coefficients are therefore the damping coefficient μ and the coefficient ϵ, which measures the effect of flight path curvature. In general, at high speed and high altitude, μ is small, and $\epsilon\mu^2$ is small in most cases. Two typical aircraft are illustrated below, and μ, ϵ are computed for them:

	(A)	(B)
Weight	30,000 lbs.	30,000 lbs.
Wing area	200 sq.ft.	300 sq.ft.
AR & Shape	2.31 (60° delta)	4.00 (45° swept)
Mean chord	9.2 ft.	12.7 ft.
Radius of gyration	3.9 ft.	6.2 ft.
Lift curve slope $C_{L\alpha}$	3.0 radians^{-1}	4.0 radians^{-1}
Static margin	1.8 ft.	0.4 ft.
Damping coefficients		
C_{Mq}	−0.75	−2.5
$C_{M\dot{\alpha}}$	−0.60	−2.0
Flight altitude	35,000 ft.	Sea level
Air speed	600 knots	400 knots

For both of these aircraft, the stall angle is selected to be 0.40 radian and the first extremum of the moment curve is at 0.16 radian. It is then found that

$(\alpha_0)_A = 0.136$ radian	$(\alpha_0)_B = 0.0079$ radian
$\mu_A = 0.107$	$\mu_B = 1.04$
$\epsilon_A = -0.132$	$\epsilon_B = -0.074$

In example (A) where μ, $\epsilon\mu^2 \ll 1$ the solution is expanded in powers of μ and only the first term is retained; the neglected terms being of order μ^2 introduce negligible errors. While a scheme for finding higher order terms is shown, the calculations involved rapidly become so cumbersome that if the first term is not sufficient, the problem may be better handled by numerical or analog methods. In example (B), the term in $\epsilon\mu^2$ is neglected, and the equation is solved by relating it to a special critically damped nonlinear motion.

Both solutions are conveniently examined in the phase plane whose coordinates are $\bar{\alpha}$ and f. If $\bar{\alpha}' = f(\bar{\alpha})$ is introduced into the fundamental Eq. (10) with the term $\epsilon\mu^2$ neglected, it becomes

$$ff' + \mu C(\bar{\alpha}) + M(\bar{\alpha}) = 0 \tag{12a}$$

where

$$\tau = \int_{\bar{\alpha}_i}^{\bar{\alpha}} \frac{d\bar{\alpha}}{f} \tag{12b}$$

with the boundary condition $f(\bar{\alpha}_i) = 0$. The point $\bar{\alpha}_i$ represents an initial disturbance from trimmed conditions of flight, which may be due either to entry into a sharp gust or to a displacement of the control surfaces. The problem is then to trace the history of the motion as a function of trimmed angle of attack $\bar{\alpha}_0$ and initial displacement $\bar{\alpha}_i$.

(3) Slightly Damped Nonlinear Oscillations

If μ is sufficiently small, Eq. (12a) can be solved formally by expanding $f(\alpha)$ into a power series in μ, substituting this series into the equation and equating coefficients of like powers of μ. The first term of such a series is the solution of the undamped problem $f_0(\alpha)$ which is now discussed in some detail. It satisfies the equation:

$$f_0 f_0' + M(\bar{\alpha}) = 0 \tag{13a}$$

$$\tau_0 = \int_{\bar{\alpha}_i}^{\bar{\alpha}} \frac{d\bar{\alpha}}{f_0}; \qquad f_0(\bar{\alpha}_i) = 0 \tag{13b}$$

which is integrated as follows:

$$\left.\begin{aligned} f_0^2(\bar{\alpha}, \bar{\alpha}_i) &= -2\int_{\bar{\alpha}_i}^{\bar{\alpha}} M(\bar{\alpha})_d\bar{\alpha} = b_0 \\ &= -(1/2)\,(\bar{\alpha} - \bar{\alpha}_i)\,\{\bar{\alpha}^3 + \\ &\qquad [\bar{\alpha}_i - 2(\bar{\alpha}_1 + 1)]\bar{\alpha}^2 + \\ &\qquad [\bar{\alpha}_i^2 - 2\bar{\alpha}_i(\bar{\alpha}_1 + 1) + 6\bar{\alpha}_1]\bar{\alpha} + \\ &\qquad [\bar{\alpha}_i^3 - 2(\bar{\alpha}_1 + 1)\bar{\alpha}_i^2 + 6\bar{\alpha}_1\bar{\alpha}_2 - 4K(\bar{\alpha}_0)]\} \end{aligned}\right\} \tag{14}$$

The direction of integration must be so chosen that the integral is negative. If at $\bar{\alpha}_i$, $M(\bar{\alpha})$ is positive, the direction of integration is negative and vice versa. This requirement is equivalent to the physical condition that motion proceeds in the direction of the spring force.

Since the moment curve $M(\bar{\alpha})$ in general has two stable focal points S_1, S_3, and a saddle point S_2,[2] the trajectory field is divided into three regions R_1, R_2, R_3 by the double trajectory through the saddle point S_2. That loop is given by

$$\left.\begin{aligned} f_{s_0}^2 &= -2\int_{S_2}^{\bar{\alpha}} M(\bar{\alpha})\,d\bar{\alpha} \\ &= -(1/2)\beta_s^2\{\beta_s^2 + 4\{S_2 - \\ &\qquad [(\bar{\alpha}_1 + 7)/2]\} + 6(S_2 - \bar{\alpha}_1)\,(S_2 - 1))\} \end{aligned}\right\} \tag{15}$$

where $\beta_S = \bar{\alpha} - S_2$, the distance from the saddle point S_2. It follows from the geometry of $M(\bar{\alpha})$ that $\bar{\alpha}_1 < S_2 < 1$ so that $(S_2 - \bar{\alpha}_1)\,(S_2 - 1) < 0$, and f_S^2 exists when

$$\begin{aligned} &(1 + \bar{\alpha}_1 - S_2) - \sqrt{(1 + \bar{\alpha}_1 - 2S_2)^2 - 6(S_2 - \bar{\alpha}_1)\,(S_2 - 1)} \leq \\ &\qquad \bar{\alpha} \leq (1 + \bar{\alpha}_1 - S_2) + \sqrt{(1 + \bar{\alpha}_1 - 2S_2)^2 - 6(S_2 - \bar{\alpha}_1)\,(S_2 - 1)} \end{aligned} \tag{16}$$

In particular f_{S0} vanishes at the two extreme points $\bar{\alpha}_I$, $\bar{\alpha}_{II}$ defined by (16). If $\bar{\alpha}_I < \bar{\alpha}_i < S_2$, the trajectory $f(\bar{\alpha}_i)$ is a closed loop in region R_1, and the motion is a

periodic oscillation about the focus S_1. If $S_2 < \bar{\alpha}_i < \bar{\alpha}_{II}$, the trajectory is a periodic oscillation about S_3 in R_3. If either $\bar{\alpha}_i < \bar{\alpha}_I$ or $\bar{\alpha}_i > \bar{\alpha}_{II}$, the motion is a large amplitude oscillation about S_2 in R_2 which is exterior to R_1, R_3. The polynomial $b_0(\bar{\alpha}_1\bar{\alpha}_i)$ has four real roots—two each in R_1, R_3, if inequality (16) holds for $\bar{\alpha}_i$, and two real roots in R_2 if (16) does not hold.

If $M(\bar{\alpha})$ has only one root, it is a focus and the motion is not essentially different from linear motion. That case is not treated here; it has been discussed by Oswald.[8]

If the four roots of the equation $b_0(\bar{\alpha}_i, \bar{\alpha}) = 0$ are denoted by $r_i(\bar{\alpha}_i, \bar{\alpha}_0)$, one writes:

$$f_0^2 = -(1/2)\,[\bar{\alpha}^2 - (r_1 + r_2)\bar{\alpha} + r_1r_2] \times [\bar{\alpha}^2 - (r_3 + r_4)\bar{\alpha} + r_3r_4] \quad (17)$$

The negative sign is due to the fact that either $r_1 < \bar{\alpha} < r_2$ in R_1 or $r_3 < \bar{\alpha} < r_4$ in R_3 if all r_i are real and $r_i < r_2 < r_3 < r_4$; or $r_1 < \bar{\alpha} < r_2$ in R_2 with r_1, r_2 real and r_3, r_4 complex conjugates, so that in all cases the product b_0 is negative.

Substitution of Eq. (17) into Eq. (13a) gives the solution as follows:

$$\tau_0 = \int_{\bar{\alpha}_i}^{\bar{\alpha}} \frac{d\bar{\alpha}}{\sqrt{-(1/2)\,[\bar{\alpha}^2 - (r_1 + r_2)\bar{\alpha} + r_1r_2] \times [\bar{\alpha}^2 - (r_3 + r_4)\bar{\alpha} + r_3r_4]}} \quad (18)$$

where one of the roots r_i is the initial value $\bar{\alpha}_i$ and $\bar{\alpha}$ varies between $\bar{\alpha}_i$ and its associated root. This integral equation may be inverted in terms of Jacobian elliptic functions to give:

$$\bar{\alpha}(\tau_0) = \left\{a - b\sqrt{\frac{1-\lambda_2}{1-\lambda_1}}\,\mathrm{cn}\left[\frac{a-b}{\lambda_2-\lambda_1}\sqrt{\frac{1-\lambda_2}{2\lambda_1(\lambda_1-1)}}\,\tau;\ \sqrt{1-\left(\frac{\lambda_2}{\lambda_1}\right)^2}\right]\right\} \Big/ \left\{1 - \sqrt{\frac{1-\lambda_2}{1-\lambda_1}} \times \mathrm{cn}\left[\frac{a-b}{\lambda_2-\lambda_1}\sqrt{\frac{1-\lambda_2}{2\lambda_1(\lambda_1-1)}}\,\tau;\ \sqrt{1-\left(\frac{\lambda_2}{\lambda_1}\right)^2}\right]\right\} \quad (19a)$$

where

$$\lambda_1, \lambda_2 = \frac{[(r_1 + r_2)(r_3 + r_4) - 2(r_1r_2 + r_3r_4) \mp 2\sqrt{(r_1 - r_3)(r_4 - r_2)(r_1 - r_4)(r_3 - r_2)}]}{(r_3 - r_4)^2} \quad (19b)$$

$$a, b = \sqrt{(r_1r_2 - \lambda_{1,2}r_3r_4)/(1 - \lambda_{1,2})} \quad (19c)$$

and $\mathrm{cn}(\sigma\tau, k)$ is a Jacobian elliptic cosine function of modulus k. If the roots are positive, it can be shown that λ_1, λ_2 are both real negative numbers; if two roots are complex conjugates, λ_1, λ_2 are of opposite sign. The period of the motion is

$$\tau_0 = [(\lambda_2 - \lambda_1)/(a - b)]\sqrt{[2\lambda_1(\lambda_1 - 1)]/(1 - \lambda_2)} \times K(|\lambda_2/\lambda_1|) \quad (20)$$

The period has three singularities at $\bar{\alpha}_I$, $\bar{\alpha}_{II}$ (the displacement $\bar{\alpha}_i$ is chosen so that the trajectory is the singular one through S_2), and S_2, the nodal point. At S_1 and S_3, τ_0 takes the values predicted by a linear perturbation of the moment curve about those points. For a given value of $\bar{\alpha}$ [aircraft (A)], $\tau_0(\bar{\alpha}_i)$ is plotted on Fig. 2.

Returning now to the differential Eq. (12) which becomes after one integration:

$$f^2 = b_0(\bar{\alpha}) - 2\mu\int_{\bar{\alpha}_i}^{\bar{\alpha}} fC\,d\bar{\alpha} \quad (21)$$

one defines a sequence of functions f_n as follows:

$$f_n^2 = b_0(\bar{\alpha}) - 2\mu\int_{\bar{\alpha}_i}^{\bar{\alpha}} f_{n-1}C\,d\bar{\alpha} \quad (22)$$

If the sequence f_n converges, it converges to the required solution. Now, one has

$$f_1 = \sqrt{b_0(\bar{\alpha})}\left[1 - \frac{2\mu}{b_0(\bar{\alpha})}\int_{\bar{\alpha}_i}^{\bar{\alpha}} C\sqrt{b_0(\bar{\alpha})}\,d\bar{\alpha}\right]^{1/2} = \sqrt{b_0}[1 - (2\mu b_1/b_0)]^{1/2} \quad (23a)$$

and taking the first term of the binomial expansion:

$$f_1 = \sqrt{b_0}\,[1 - \mu(b_1/b_0)] \quad (23b)$$

Similarly for f_2, f_3, after integrating by parts and expanding up to μ^2, μ^3 one finds:

$$\begin{aligned} f_2 &= \left[b_0 - 2\mu\int_{\bar{\alpha}_i}^{\bar{\alpha}} C\sqrt{b_0}\left(1 - \mu\frac{b_1}{b_0}\right)d\bar{\alpha}\right]^{1/2} \\ &= \sqrt{b_0}\left[1 - \mu\frac{b_1}{b_0} + \frac{\mu^2}{b_0}\left(\frac{b_1^2}{2b_0} + \int_{\bar{\alpha}_i}^{\bar{\alpha}}\frac{b_1b_1'}{b_0}\,d\bar{\alpha}\right)\right] \\ &= \sqrt{b_0}\,[1 - \mu(b_1/b_0) + \mu^2(b_2/b_0)] \end{aligned} \quad (24a)$$

$$\begin{aligned} f_3 &= \left\{b_0 - 2\mu\int_{\bar{\alpha}_i}^{\bar{\alpha}}\left[1 - \frac{\mu b_1}{b_0} + \frac{\mu^2}{b_0}\left(\frac{b_1^2}{2b_0} + \int_{\bar{\alpha}_i}^{\bar{\alpha}}\frac{b_1b_1'}{b_0}\,d\bar{\alpha}\right)b_1'\right]d\bar{\alpha}\right\}^{1/2} \\ &= \sqrt{b_0}\left[1 - \mu\frac{b_1}{b_0} + \mu^2\frac{b_2}{b_0} - \frac{\mu^3}{b_0}\left(\frac{b_1b_2}{2b_0} + \int_{\bar{\alpha}_i}^{\bar{\alpha}}\frac{b_2b_1'}{b_0}\,d\bar{\alpha}\right)\right] \\ &= \sqrt{b_0}\,[1 - \mu(b_1/b_0) + \mu^2(b_2/b_0) - \mu^3(b_3/b_0)] \end{aligned} \quad (24b)$$

and generally

$$f = \sqrt{b_0}\sum_{n=1}^{\infty}(-\mu)^n\frac{b_n}{b_0}$$

$$b_n = \int_{\bar{\alpha}_i}^{\bar{\alpha}}\frac{b_1'b_{n-1}}{b_0}\,d\bar{\alpha} + \frac{b_1b_{n-1}}{b_0} + \frac{b_2b_{n-2}}{b_0} + \ldots + \epsilon_n\frac{b^2_{n/2}}{2b_0} \quad (25a)$$

where

$$b_0 = 2\int_{\bar{\alpha}_i}^{\bar{\alpha}} M\,d\bar{\alpha},\ b_1 = \int_{\bar{\alpha}_i}^{\bar{\alpha}} c\sqrt{b_0}\,d\bar{\alpha},\ \epsilon_n = \begin{matrix}1 (n \text{ even}) \\ 0 (n \text{ odd})\end{matrix} \quad (25b)$$

This sequence converges nonuniformly if μ is sufficiently small since b_n/b_0 is of order n. Special care must be exercised in the region where $b_0 < \mu$ (near $\bar{\alpha}_I$ and $\bar{\alpha}_{II}$) where the expansion process breaks down, and one must iterate on Eq. (12) directly.

The time history of the motion in terms of the initial conditions is calculated by carrying out the integration (13b) with $f(\bar{\alpha})$ given by Eqs. (25a) and (25b).

$$\tau = \int_{\bar{\alpha}_i}^{\bar{\alpha}} \frac{d\bar{\alpha}}{f(\bar{\alpha})} = \int_{\bar{\alpha}_i}^{\bar{\alpha}} \frac{d\bar{\alpha}}{\sqrt{b_0 \sum [(-\mu)^n b_n/b_0]}} \tag{26}$$

It is convenient to take the reciprocal of the series in Eq. (26) as follows:

$$\tau = \int_{\bar{\alpha}_i}^{\bar{\alpha}} \sum_0^\infty \mu^n D_n(\bar{\alpha}) \frac{d\bar{\alpha}}{\sqrt{b_0}} \tag{27a}$$

$$\begin{aligned}
D_0 &= 1 \\
D_1 &= b_1/b_0 \\
D_2 &= \frac{1}{2b_0^2} \int_{\bar{\alpha}_i}^{\bar{\alpha}} \frac{b_1^2 b_1'}{b_0^2}\, d\bar{\alpha} \\
D_3 &= \frac{b_1}{2b_0^3} \int_{\bar{\alpha}_i}^{\bar{\alpha}} \frac{b_1^2 b_1'}{b_0^2}\, d\alpha + \frac{1}{b_0^2} \int_{\bar{\alpha}_i}^{\bar{\alpha}} \frac{b_2 b_1'}{b_0}\, d\bar{\alpha} \\
D_4 &= \frac{b_2^2}{2b_0^3} - \frac{2b_1^2}{b_0^4} \int_{\bar{\alpha}_i}^{\bar{\alpha}} \frac{b_1^2 b_1'}{b_0^2}\, d\bar{\alpha} - \frac{1}{b_0^2} \int_{\bar{\alpha}_i}^{\bar{\alpha}} \frac{b_3 b_1'}{b_0}\, d\bar{\alpha}
\end{aligned} \tag{27b}$$

etc., and the integral (27a) is evaluated term by term. The first term is given by the preceding analysis of undamped motion and the other terms are corrections to it so that

$$\tau = \tau_0 + \sum_{n=1}^{\infty} \mu^n \tau_n \tag{27c}$$

$$\tau_n = \int_{\bar{\alpha}_i}^{\bar{\alpha}} D_n \frac{d\bar{\alpha}}{\sqrt{b_0}} \tag{27d}$$

and since the parameters D_n are rational algebraic expressions, the corrections τ_n are expressible in terms of elliptic functions.

The general structure of the trajectory field in the phase plane (Fig. 3) is best studied by considering the four critical semitrajectories through the saddle point S_2. The trajectories T_1, T_3, which start from S_2 at $\tau = -\infty$ toward S_1 and S_3 with positive slope $f' = -MC/2 + \sqrt{\mu^2C^2/4 + M'}$, always lie between the $\bar{\alpha}$ axis and the undamped trajectories $T_{10}T_{30}$ through S_2. They must therefore converge to S_1 and S_3 or a closed loop surrounding S_3.

The trajectories T_2, T_4, which reach S_2 at $\tau \to +\infty$ with negative slope $f' = -\mu C/2 - \sqrt{\mu^2C^2/4 + M'}$ coming from outside, divide the phase plane into two spiral-shaped noncommunicating domains R_1 and R_3, which contain the stable focal points S_1 and S_3, respectively. Since the damping function $C(\bar{\alpha})$ is everywhere nonnegative, the trajectory through any point of R_1 converges to S_1 in a finite period of time, and the trajectory through any point of R_3 similarly converges to S_3 or to a closed loop including S_3.

Because of their spiral-like nature, the trajectories T_2, T_4 intersect the $\bar{\alpha}$ axis at a doubly infinite sequence of points. T_2 intersects the $\bar{\alpha}$ axis at points $\bar{\alpha} =$

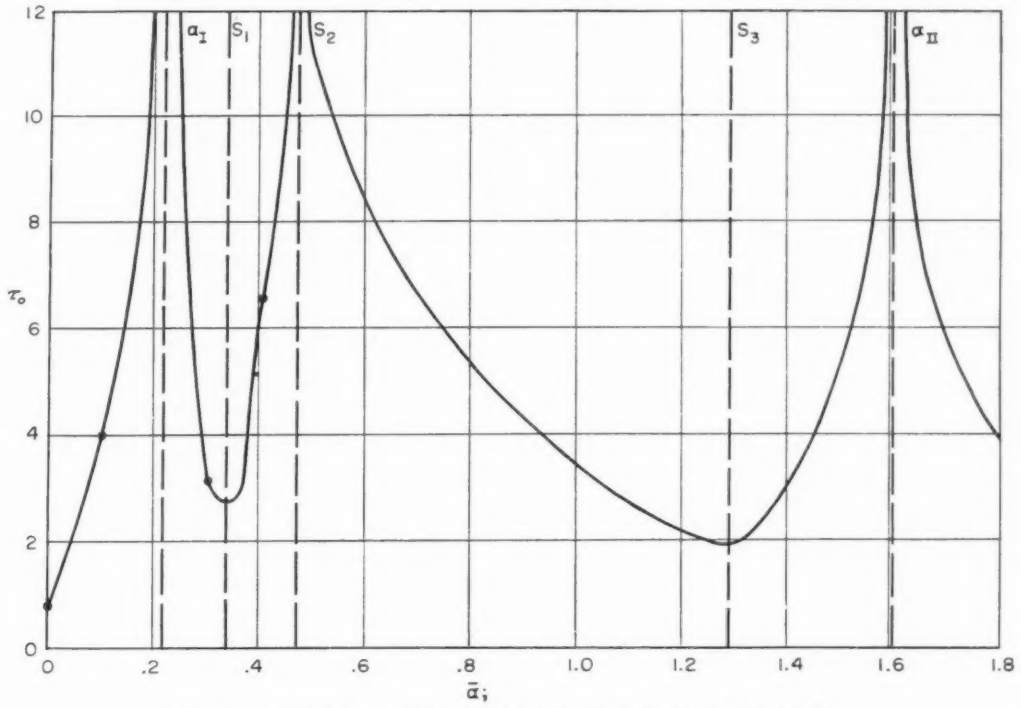

FIG. 2. Variation of period with initial displacement for pitch of aircraft (A).

$\bar{a}_1, \bar{a}_2, \bar{a}_3 \ldots$ to the left of S_1 and at points $\bar{\alpha} = \bar{b}_1, \bar{b}_2, \bar{b}_3 \ldots$ to the right of S_3. T_4 intersects the $\bar{\alpha}$ axis at points $\bar{\alpha} = \bar{c}_1, \bar{c}_2, \bar{c}_3 \ldots$ to the left of S_1 and at points $\bar{\alpha} = \bar{d}_1, \bar{d}_2, \bar{d}_3 \ldots$ to the right of S_3. These sets of points are related by the inequalities:

$$\left.\begin{aligned} &\bar{a}_1 > \bar{c}_1 > \bar{a}_2 > \bar{c}_2 > \bar{a}_3 > \bar{c}_3 \ldots \\ &\bar{d}_1 < \bar{b}_1 < \bar{d}_2 < \bar{b}_2 < \bar{d}_3 < \bar{b}_3 \ldots \end{aligned}\right\} \tag{28}$$

Any trajectory with initial value $\bar{\alpha}_i$ defined by

$$\left.\begin{aligned} &\bar{a}_n > \bar{\alpha}_i > \bar{c}_n \\ &\bar{b}_n < \bar{\alpha}_i < \bar{d}_{n+1} \end{aligned}\right\} \tag{29a}$$

converges to S_3; any trajectory with initial value $\bar{\alpha}_i$ defined by

$$\left.\begin{aligned} &\bar{a}_n > \bar{\alpha}_i > \bar{c}_{n-1} \\ &\bar{d}_n < \bar{\alpha}_i < \bar{b}_n \end{aligned}\right\} \tag{29b}$$

converges to S_1. The number of large amplitude oscillations of such a trajectory is n. Note that a trajectory does not always converge to the nearest stable singular point. The case (29a) in particular, corresponds to the observed pitch-up phenomenon observed in transonic flight.

In view of this discussion, it is interesting to estimate the location of the critical points $\bar{a}_n, \bar{b}_n, \bar{c}_n, \bar{d}_n$ which are defined by:

$$f(\lambda_n) = 0 \quad \lambda_n = \bar{a}_n, \bar{b}_n, \bar{c}_n, \bar{d}_n \tag{30}$$

From Eq. (21), one obtains, for $\bar{a}_1$:

$$b_0(\bar{a}_1) - 2\mu \int_{S_2}^{\bar{a}_1} fC \, d\bar{\alpha} = 0 \tag{31}$$

If μ is sufficiently small, the integral in Eq. (31) is small and one may write approximately

$$\left.\begin{aligned} b_0(\bar{a}_1) &= b_0(\bar{\alpha}_I) + (\bar{a}_1 - \bar{\alpha}_I) \times \\ &\quad (db_0/d\bar{\alpha}) = 2M(\bar{\alpha}_I)\,(\bar{a}_1 - \bar{\alpha}_I) \\ &= 2\mu \int_{S_1}^{\bar{\alpha}I} fC \, d\bar{\alpha} \end{aligned}\right\} \tag{32}$$

so that up to the first power of μ

$$\bar{a}_1 - \bar{\alpha}_I = \frac{\mu}{2M(\bar{\alpha}_I)} \int_{S_2}^{\bar{\alpha}I} f_0 \, C \, d\bar{\alpha} \tag{33}$$

Similarly

$$\bar{d} - \bar{\alpha}_{II} = \frac{\mu}{2M(\bar{\alpha}_{II})} \int_{S_2}^{\bar{\alpha}II} f_0 C \, d\bar{\alpha} \tag{34}$$

since $\bar{a}_1$ is outside $\bar{\alpha}_I$ while $\bar{d}_1$ is outside $\bar{\alpha}_{II}$. The other points are defined by

$$\left.\begin{aligned} \bar{a}_1 - \bar{c}_1 &= \frac{\mu}{2M(\bar{a}_1)} \int_{\bar{a}_1}^{\bar{d}_1} f_0 C \, d\bar{\alpha} \\ \bar{b}_1 - \bar{d}_1 &= \frac{\mu}{2M(\bar{d}_1)} \int_{\bar{d}_1}^{\bar{c}_1} f_0 C \, d\bar{\alpha} \\ \bar{c}_1 - \bar{a}_2 &= \frac{\mu}{2M(\bar{c}_1)} \int_{\bar{c}_1}^{\bar{b}_1} f_0 C \, d\bar{\alpha} \\ \bar{d}_2 - \bar{b}_1 &= \frac{\mu}{2M(\bar{b}_1)} \int_{\bar{b}_1}^{\bar{a}_2} fC \, d\bar{\alpha} \\ &\text{etc.} \ldots \end{aligned}\right\} \tag{35}$$

From Eqs. (34) and (35) the entire pattern of critical points $\bar{a}_n, \bar{b}_n, \bar{c}_n, \bar{d}_n$ is determined approximately in terms of $S_2(\bar{\alpha}_0)$, and the final outcome of any motion characterized by an initial trim $\bar{\alpha}_0$ and an initial displacement $\bar{\alpha}_i$ is determined from inequalities (29a, 29b). This is illustrated on Fig. 4 where the abscissa is $\bar{\alpha}_0$ and the ordinate is $\bar{\alpha}_i$. Every point of the $(\bar{\alpha}_i, \bar{\alpha}_0)$ plane specifies a trimmed attitude and an initial displacement and therefore defines an oscillation. The curves $a_n(\bar{\alpha}_0)$, $\bar{b}_n(\bar{\alpha}_0)$, etc., give the intersections of the trajectories T_i with the $\bar{\alpha}$ axis for all values of $\bar{\alpha}_0$ and, consequently, the ranges of $\bar{\alpha}_i$ for any value of $\bar{\alpha}_0$ which lead to motions in R_1 and in R_3. Therefore, by plotting the critical points $a_n, \bar{b}_n, \bar{c}_n, \bar{d}_n$ as functions of $\bar{\alpha}_0$ and cross hatching the regions where (29b) holds, one can predict the outcome of any motion. If the specified initial point $(\bar{\alpha}_i, \bar{\alpha}_0)$ is in a cross-hatched region, the motion converges to S_1; if it is in a blank region, the motion converges to S_3. Furthermore, the number of stripes to be crossed in going from $\bar{\alpha}_i$ to the equilibrium point along a vertical line is the number of large-scale oscillations.

A numerical example of slightly damped nonlinear pitch-up is shown on Fig. 5. The trimmed angle of attack is $\bar{\alpha}_0 = 0.34$ [aircraft (A)], and the initial disturbance is defined by $\bar{\alpha}_i = 0.15$, which corresponds to a sudden normal acceleration of 0.55g. It is seen that although the nearest stable equilibrium point is $S_1 = \bar{\alpha}_0 = 0.34$, a sufficient initial acceleration is imposed to cause pitch-up and an oscillation about the stable point $\bar{\alpha} = S_3 = 1.29$. Since the oscillation eventually takes place completely in the stalled region ($\bar{\alpha} > 1$) in which the damping vanishes, the final state is a half-limit cycle instead of a subsidence in the neighborhood of S_3.

(4) Heavily Damped Nonlinear Oscillations

The method described in Section (3) converges in some range $\mu < \mu_0$. However, it converges more slowly as the damping increases ($\mu \to \mu_0$) and the labor required to get a solution increases. It is therefore worth while to look for a different approximation which retains the characteristics of the nonlinear equation and is based on a known exact solution.

For purposes of convenience the trimmed equilibrium point will now be taken as the origin. The governing differential equation is of the form

$$\bar{\alpha}'' + \mu\bar{\alpha}' + M(\bar{\alpha}) = 0 \tag{36a}$$

or more specifically

$$\bar{\alpha}'' + \mu\bar{\alpha}' + \bar{\alpha}^3 + a\bar{\alpha}^2 + b\bar{\alpha} + c = 0 \tag{36b}$$

where the coefficients a, b, c are given in terms of the airplane characteristics by

$$\begin{aligned} a &= (3/2)\,(1 + \bar{\alpha}_1) \\ b &= 3\bar{\alpha}_1 \\ c &= -\bar{\alpha}_0[\bar{\alpha}_0^2 - (3/2)\,(1 + \bar{\alpha}_1) + 3\bar{\alpha}_1] \end{aligned}$$

Note that in this investigation, one assumes $C(\bar{\alpha}) = 1$.

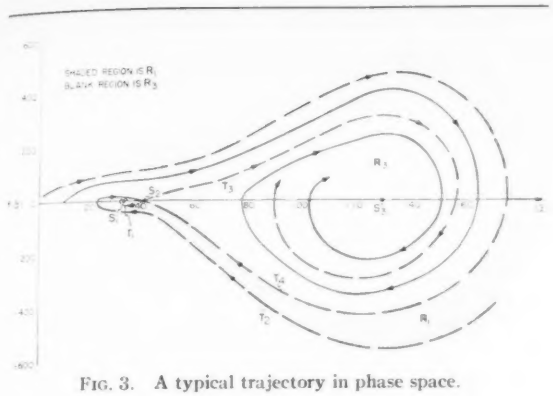

FIG. 3. A typical trajectory in phase space.

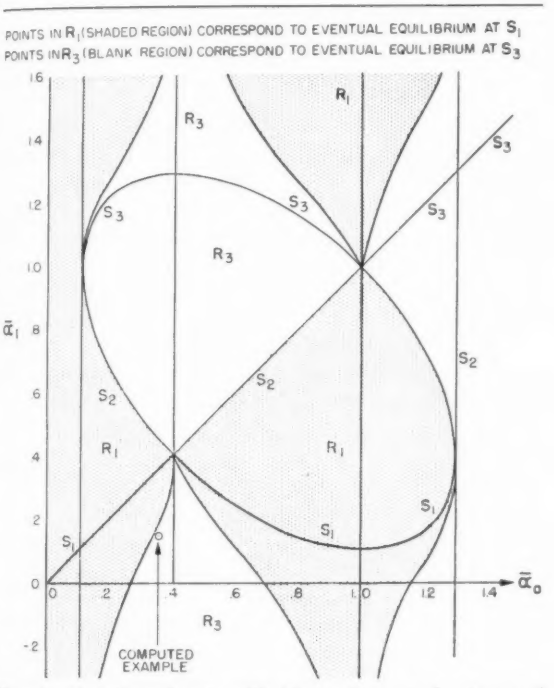

FIG. 4. Variation of roots with trim and eventual outcome of oscillations as function of initial trim and displacement position.

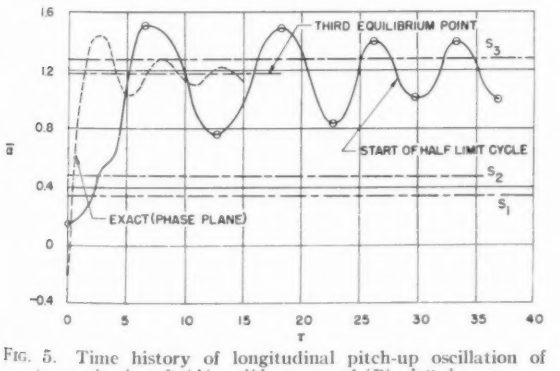

FIG. 5. Time history of longitudinal pitch-up oscillation of transonic aircraft (A), *solid curve*, and (B), *dotted curve*.

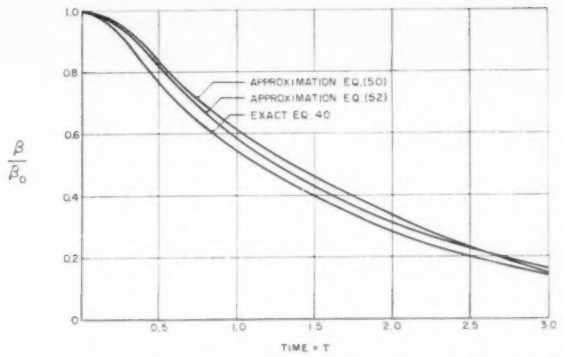

FIG. 6. Comparison of exact and approximate solutions for $\ddot{\beta} + 2\beta + \dot{\beta} + (1/4)\beta^2 = 0$ $\beta_0 = \beta(0) = 1$, and $\dot{\beta}(0) = 0$.

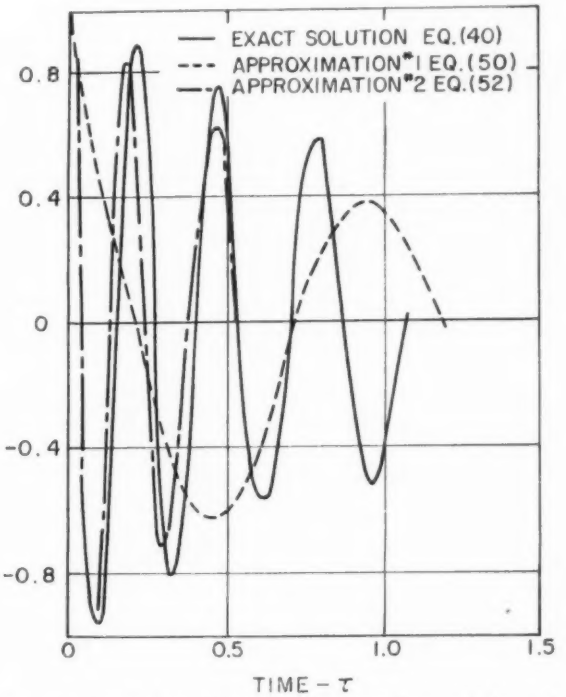

FIG. 7. Comparison of exact and approximate solutions of $\ddot{\beta} + 2\beta + \beta + 100\beta^2 = 0$, $\beta_0 = \beta(0) = 5$, and $\dot{\beta}_0(0) = -5$.

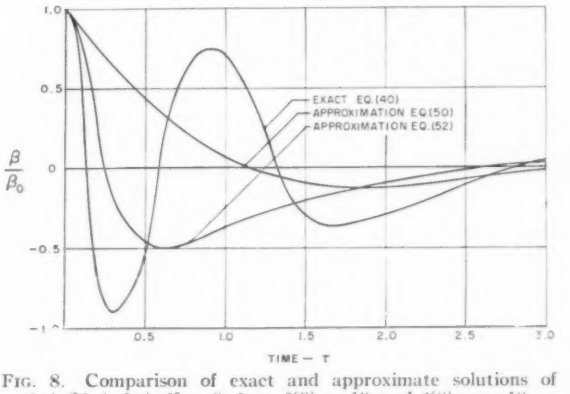

FIG. 8. Comparison of exact and approximate solutions of $\ddot{\beta} + 2\beta + \dot{\beta} + \beta^2 = 0$, $\beta_0 = \beta(0) = 10$, and $\dot{\beta}(0) = -10$.

If $C(\bar{\alpha})$ changes its value, the approximations to be presented can be corrected by replacing $\mu\tau$ by $\mu \int C(\bar{\alpha})d\tau$. In this substitution it is most important that the period and phase of the approximation be as accurate as possible.

If the dependent variable is changed to β where

$$\beta = \bar{\alpha} - \bar{\alpha}_0$$

the governing equation becomes

$$\beta'' + \mu\beta' + \beta^3 + (3\bar{\alpha}_0 + a)\beta^2 + (3\bar{\alpha}_2 + 2a\bar{\alpha}_0 + b)\beta = 0 \quad (36c)$$

This equation can be reduced to the canonical form by the substitution $\beta = ye^{-\mu\tau/2}$, which gives

$$y'' + [3\bar{\alpha}_0^2 + 2a\bar{\alpha}_0 + b - (\mu^2/4)]y + (3\bar{\alpha}_0 + a)y^2e^{-(\mu/2)\tau} + y^3e^{-\mu\tau} = 0 \quad (37)$$

with initial conditions

$$\left.\begin{aligned} y_0 &= y(0) = \bar{\alpha}_i - \bar{\alpha}_0 \\ y_0' &= y'(0) = \beta'(0) + (\mu/2)y_0 = \\ &\qquad \bar{\alpha}'(0) + (\mu/2)\,(\bar{\alpha}_i - \bar{\alpha}_0) \end{aligned}\right\} \quad (38)$$

Equations (36) or (37) can be integrated exactly[4] if the coefficient of y^2 is zero and if the damping coefficient takes the value

$$\mu = (3/\sqrt{2})\,\sqrt{3\bar{\alpha}_0^2 + 2a\bar{\alpha}_0 + b} \quad (39)$$

This value of μ can be related to the critical damping ratio ζ, if ζ is defined as $\zeta = \mu/2\omega_n$ and ω_n^2 is the coefficient of β. Making the substitutions it is seen that $\zeta = 3/2\sqrt{2} = 1.06$

The exact solution is then

$$\beta = A_0e^{-\mu\tau}\,\mathrm{cn}\,(A_0\sqrt{3\bar{\alpha}_0^2 + 2a\bar{\alpha}_0 + b}\times e^{-(\tau/2)\sqrt{3\bar{\alpha}_0^2+2a\bar{\alpha}_0+b}} + \varphi;\, 1/\sqrt{2}) \quad (40)$$

and the constants A_0 and φ can be calculated in terms of the initial conditions from the formulas

$$A_0 = \beta_0\{1 + \{(\beta_0' + \beta_0)/[\beta_0^2(3\bar{\alpha}_0^2 + 2a\bar{\alpha}_0 + b)]\}^2\}^{1/4} \quad (41a)$$

$$\varphi = \mathrm{cn}^{-1}[(\beta_0/A_0),\,(1/\sqrt{2})] - A_0\sqrt{3\bar{\alpha}_0^2 + 2a\bar{\alpha}_0 + b} \quad (41b)$$

If the equations were linear—i.e., if the coefficient of y were extremely large in comparison to unity—Eq. (37) would have the solution

$$y = \beta_0\sqrt{1 + [(\alpha_0'/\beta_0) + (\mu/2)]^2/\omega^2}\times \cos\{\omega\tau - \tan^{-1}[(\alpha_0'/\beta_0) + (\mu/2)]/\omega\} \quad (42)$$

which can be written in terms of β as

$$\beta = \beta_0e^{-\mu\tau/2}\sqrt{1 + [(\alpha_0'/\beta_0) + (\mu/2)]^2/\omega^2}\times \cos\{\omega\tau - \tan^{-1}[(\alpha_0'/\beta_0) + (\mu/2)]/\omega\} \quad (43)$$

where

$$\omega = \sqrt{3\bar{\alpha}_0^2 + 2a\bar{\alpha}_0 + b - (\mu^2/4)}$$

The linear solution [Eq. (43)] is valid for all μ as long as ω is real. The solution to the nonlinear equation [Eq. (40)] as noted before is valid for only one particular value of $\mu(\mu = 2\omega_n\zeta)$, which corresponds to heavily damped motion.

Examination of Eqs. (40) and (43) indicates certain similarities: they both have exponential multipliers and have a phase angle introduced to allow for the effects of damping upon the motion at the initial point. Equation (40) will be useful in verifying the accuracy of the approximations.

The simplest approximation for the solution of Eq. (37) consists in replacing the time dependent exponentials by constants, so that if

$$\gamma_1 = e^{-\mu T/2} \quad (44)$$

where T is the period of the motion or its linear approximation, then Eq. (37) becomes

$$y'' + [3\bar{\alpha}_0^2 + 2a\bar{\alpha}_0 + b - (\mu^2/4)]y + (3\bar{\alpha}_0 + a)\gamma_1y^2 + \gamma_1^2y^3 = 0 \quad (45)$$

This is an undamped equation and its solution may be found by the method of Section (3). Combination of the solution of Eq. (45) with the exponential gives

$$\beta = e^{-\mu\tau/2}y \quad (46)$$

This approximation reduces the effectiveness of the damping in the earlier part of the cycle and increases it in the later part.

It was demonstrated earlier that the nature of the solution depends upon the roots of a polynomial, in this case the quartic

$$b_0 = C_1 - [3\bar{\alpha}_0^2 + 2a\bar{\alpha}_0 + b - (\mu^2/4)]y^2 - (2/3)\gamma_1(3\bar{\alpha}_0 + a)y^3 - (\gamma_1^2/2)y^4 = 0 \quad (47)$$

where

$$C_1 = y_0'^2 + (\gamma_1^2/2)y_0^4 + (2/3)\gamma_1(3\bar{\alpha}_0 + a)y_0^3 + [3\bar{\alpha}_0^2 + 2a\bar{\alpha}_0 + b - (\mu^2/4)]y_0^2$$

It is sufficient to say here that if the quartic has four real roots, $y_1 > y_2 > y_3 > y_4$, the coefficient of τ in the solution is[5,6]

$$[\gamma_1/(2\sqrt{2})]\,\sqrt{(y_1 - y_3)\,(y_2 - y_4)} \quad (48)$$

If the quartic has two real roots $y_1 > y_2$ and a complex pair—the roots of $(y - r)^2 + S^2$; $S > 0$—the coefficient of τ is[5]

$$(\gamma_1/2)\,\sqrt{[s(y_1 - y_2)/k\sqrt{1 - k^2}]} \quad (49)$$

where k is the modulus defined in Section (3).

Note that γ_1 appears above explicitly and will appear in the expression for the roots. For example, if the cubic term in Eq. (47) is zero, the solution can be written as

$$\beta = A_0e^{-(\mu\tau/2)}\,\mathrm{cn}\times \{[\sqrt{(3\bar{\alpha}_0^2 + 2a\bar{\alpha}_0 + b - (\mu^2/4) + \gamma_1^2A_0^2)}\,\tau + \varphi], k\} \quad (50)$$

where A_0 and ϕ are as previously defined and

$$k = A_0\gamma_1/[\sqrt{2}\sqrt{\gamma_1^2A_0^2 + 3\bar{\alpha}_0^2 + 2\bar{\alpha}_0 a + b - (\mu^2/4)}] \quad (51)$$

The objection to the use of a constant γ_1 can be removed by replacing γ_1 by the exponential $e^{-\mu\tau/2}$. The functions $y(\tau)$ no longer satisfy the differential equation, but the approximation to the solution is improved. The approximation approaches the exact solution as μ approaches zero and behaves properly for large time when the exponential term is small. This approximation will be useful if the equation is nearly linear or if the motion decays so slowly that the oscillatory terms have a smaller period than the characteristic time of the exponential. The latter case could be either a moderately damped motion where the linear and nonlinear terms are of the same order or a strongly damped motion with a large nonlinear term.

The exact solution, Eq. (40), the first approximation (γ_1 = constant), Eq. (50), and the suggested approximation

$$\beta = A_0e^{-(\mu/2)\tau}\,\mathrm{cn}\times[\sqrt{3\bar{\alpha}_0^2 + 2a\bar{\alpha}_0 + b - (\mu^2/4) + e^{-\mu\tau}A_0^2\tau + \varphi; k}] \quad (52)$$

have been calculated for a motion whose damping would be approximately critical if the spring force were linear. The results are compared on Figs. 6, 7, and 8. When the nonlinear terms are either small or large compared to the damping and linear spring terms, the relaxation of the restriction to constant γ_1 improves the agreement, which is considered satisfactory. When the nonlinear terms are of the same order as the damping and linear spring terms, the agreement is less satisfactory.

In the general case the roots of the quartic are complicated functions of time. It seems more practical to compute them numerically either by Newton's or Lin's method at several values of time. The variation of the roots with time can be approximated as suggested in the Appendix. Once the roots are known, the required constants can be computed as functions of time and the values of the elliptic functions found from a table.[7] The amount of work seems to be independent of μ, depending only on the time interval selected.

As an application of the methods described above, consider airplane (B) of Section (1). In normalized form the equation of motion is, if the damping is approximately constant,

$$\bar{\alpha}'' + 1.04\bar{\alpha}' + \bar{\alpha}^3 - 2.10\bar{\alpha}^2 + 1.17\bar{\alpha} - 0.115 = 0 \quad (53)$$

with initial conditions

$$\left.\begin{aligned}\bar{\alpha}_0 - \bar{\alpha}_t &= -0.75\bar{\alpha}_0 = -0.06\\ \bar{\alpha}_0' &= 0\end{aligned}\right\} \quad (54)$$

These conditions correspond roughly to a $-0.75g$ gust. The reduced equation about the equilibrium point $\bar{\alpha} = 0.12$ is

$$y'' + 0.438y - 1.74y^2e^{-0.52\tau} + y^3e^{-1.04\tau} = 0 \quad (55)$$

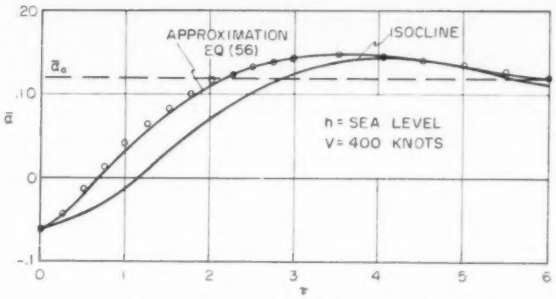

FIG. 9. Response of airplane (B) to $a = 3/4g$ gust.

and

$$y_0 = -0.18$$
$$y_0' = 0.0936$$

The quartic here has four real roots and the solution is of the form

$$y = [\bar{a}\,\mathrm{sn}^2(\omega\tau; k) + \bar{b}]/[\bar{c}\,\mathrm{sn}^2(\omega\tau; k) + \bar{d}] \quad (56)$$

where

$$k^2 = [(y_1 - y_2)(y_3 - y_4)]/[(y_1 - y_3)(y_2 - y_4)] \quad (57a)$$
$$\bar{a} = y_1\bar{c} \quad (57b)$$
$$\bar{b} = y_4\bar{d} \quad (57c)$$
$$\bar{c} = y_3 - y_4 \quad (57d)$$
$$\bar{d} = y_1 - y_2 \quad (57e)$$

and

$$\omega = [e^{-0.52\tau}/(2\sqrt{2})]\sqrt{(y_1 - y_3)(y_2 - y_4)} \quad (57f)$$

This solution (in the $\bar{\alpha}$, τ plane) is plotted in Fig. 9 and is compared with the exact solution from an isoclinic integration of the phase plane. The agreement in the overshoot is not unreasonable, and the frequency and damping agree well as τ increases.

It will be noted that this air frame possesses three trim points, two of which are stable ($\bar{\alpha}_0 = 0.12$, $\bar{\alpha}_0 = 1.12$); the third is unstable ($\bar{\alpha}_0 = 0.76$). The damping is high ($\zeta \sim 0.5$), and the main effect of this damping is to make the air frame much less susceptible to any tendency to seek the second equilibrium point. Thus, in order to encounter pitch-up, much larger inputs are required at sea level than at high altitude. For example, if the same air frame were pulling up at about $5g$ and encountered a $-2.5g$ gust, it would pitch up violently. Here

$$\bar{\alpha}_0 - \bar{\alpha}_t = -0.18$$

and

$$\bar{\alpha}_t' = -1.2$$

The reduced equation is

$$y'' + 0.488y + 1.26e^{-0.52\tau}y^2 + e^{-1.04\tau}y^3 = 0 \quad (58)$$

where

$$y(0) = -1.3$$
$$y'(0) = 1.79$$

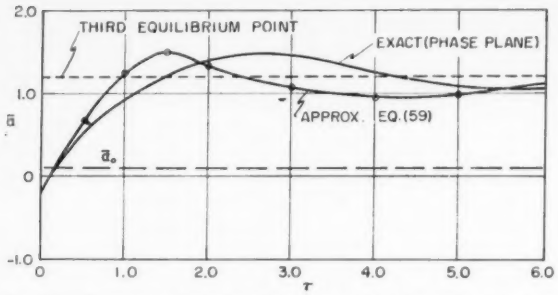

FIG. 10. Response of airplane (B) to $a - 2\,(1/2)g$ gust while in a $5g$ pull-up.

In this case the quartic has two real roots, y_1, y_2, $(y - r)^2 + S^2$ [see Eq. (49)] and in terms of these roots the solution of the reduced equation is

$$y = \{y_2k_1(y_1 - r) + Sy_1 + [y_2k_1(y_1 - r) - y_1S] \times \operatorname{cn}(\omega\tau + \varphi; k)\}/\{(y_1 - r)k_1 + S + [(y_1 - r)k_1 - S] \operatorname{cn}(\omega\tau + \varphi; k)\} \quad (59)$$

where

$$k_1 = A \pm \sqrt{A^2 + 1}$$

and the sign is chosen such that

$$-(1/2)e^{-1.04\tau}k_1 < 0$$

and where

$$A = [s^2 + (y_1 - r)(y_2 - r)]/[s(y_1 - y_2)]$$

$$k^2 = 1/(1 + k_1^2)$$

$$\omega = (e^{0.52\tau}/2)\sqrt{[S(y_1 - y_2)]/(k\sqrt{1 - k^2})}$$

$$\varphi = \operatorname{cn}^{-1}(\{y_2k_1(y_1 - r) + y_1S + 1.3[(y_1 - r) \times k_1 + s]\}/\{1.3[(y_1 - r)k_1 - s] + y_2k_1(y_1 - r) - y_1s\})$$

This solution has also been compared with a phase-plane integration; while the agreement is not as good as the earlier example, the main features of the motion are recognizable and the values found by the approximation are conservative (Fig. 10).

(5) Conclusion

In the preceding pages, approximate methods were developed to estimate the occurrence and severity of of nonlinear pitch-ups in transonic swept-wing aircraft. The cause of such pitch-ups is usually a combination of tip-stall and chordwise center-of-pressure shift due to the appearance of shock-wave patterns on the upper wing surface. These phenomena, which are not discussed in detail here, lead to the appearance of one unstable and two stable equilibrium points on the moment curve. If a sufficiently strong initial disturbance from the first equilibrium point is applied to a trimmed aircraft with such a moment curve, the resulting oscillatory motion may subside about the second equilibrium point. This is far more likely to occur at high altitudes where the damping coefficient is small and where the trimmed angle of attack is so large that the trimmed equilibrium point is close to the unstable equilibrium point.

Approximate techniques that rapidly yield approximate results and define the general nature of the expected motion have been developed to study this problem; while they do not replace analog analyzers or other devices for the construction of numerical solutions, they may serve as complements particularly useful in investigating the variation of flight parameters such as damping, undisturbed attitude, etc., analytically and in suggesting the most effective techniques of carrying out detailed computations. Numerical examples have been worked out to give time histories of nonlinear oscillations under various conditions, both at high and low altitudes.

APPENDIX

A Discussion of the Computations of the Roots of the Quartic

Consider the quartic

$$x^4 + Bx^3 + Cx^2 + Dx + E = 0$$

where B, C, D, and E are known functions of time. If B and C are five to ten times larger than D and E, the quartic has two real roots, largely uninfluenced by D and E, and these roots are governed by the quadratic

$$x^2 + Bx + C = 0$$

The approximation for the small roots is found by writing the quadratic as

$$(x^2 + B'x + C')(x^2 + b'x + c') = 0$$

Expanding the product gives relations between B, B', b', etc., and letting $B' = B$ and $C' = C$, it is found that

$$c' = E/C$$

$$b' = (CD - EB)/C^2$$

These expressions may be used to obtain a better approximation to B' and C'; namely,

$$B' = B - [(CD - EB)/C^2]$$

$$C' = C$$

This approximation is valid whenever

$$(1/C^2)(E + (CD - EB)\{B - [(CD - EB)/C^2]\}) \ll 1$$

and

$$[(CD - EB)/C^2]^2 \ll D$$

or if $D = 0$, the latter condition becomes

$$(EB/C^2) \sim 0$$

If the roots chosen by this approximation are r_1, r_2, r_3, and r_4, then the average error in the roots is about

$$\Delta r \simeq (E + (CD - EB)\{B - [(CD - EB)/C^2]\}) \div \{CB\sqrt{1 + [2(r_1^2 + r_2^2 + r_3^2 + r_4^2)/B^2]}\}$$

In the examples in the text, $B = 0(e^{\mu t/2})$, $C = 0(e^{\mu t})$, and $E = 0(e^{\mu t})$; hence at least two of the roots are of

order $0(e^{\mu t})$. Thus $\Delta r = 0(e^{-\mu t/2})$ so that the approximation improves as the time increases.

In the second example in Section (4) for small t, B, and C are nearly unity, $D = 0$, and E is large and negative compared to unity. This implies that it is reasonable to assume that the roots are nearly symmetric with respect to the origin so that $C' = c' = \pm\sqrt{E}$.

Again splitting the quartic into the quadratic and multiplying,

$$B = b' + B'$$

and

$$B'c' + C'b' = 0$$

Thus

$$b' = B' = B/2$$

This approximation is valid as long as $B^2/4 \sim C$—that is, for $t \leq 2.0$.

Two approximations were required in the second example of Section (4) due to the change in the character of the motion as the trajectory is captured by the outer equilibrium point.

Another approximation useful if B is of the same order as D and both are much larger than C and E is based on the existence of a real root which is approximately

$$x = -B + (C/B)$$

The small real root is

$$x \simeq [-(E/D)]\,[1 - (CE/D^2)]$$

The quadratic that remains is easily found to be

$$x^2 + [(C/B) - (E/D)]x + (D/B) = 0$$

This sort of approximation to the roots has no hard and fast rules governing it, and, in general, once the approximation has been decided upon it is wise to multiply the factors and compare with the original quartic to determine its accuracy.

References

[1] Emslie, E., Hosking, L., and Marshall, W. S. D., *Some Experiments on the Flow in the Boundary Layer of a 45-Degree Sweptback Untapered Wing of Aspect Ratio 4*, Cranfield College of Aeronautics, Report No. 69, February, 1953.

[2] Epstein, M., *The Aerodynamic Coefficients of Thin Lifting Airfoils at High Subsonic Speeds*, WADC Tech. Note WCRR-53-8, March, 1953.

[3] Minorski, N., *An Introduction to Nonlinear Mechanics*, Edwards Brothers, Ann Arbor, Mich., 1947.

[4] Ince, E. L., *Ordinary Differential Equations*, p. 334; Dover, New York, 1944.

[5] Grobner, W., and Hofrieter, N., *Integral Tafel*, Pt. 1, Unbestimmte Intgrale, Springerverlag, Wien und Innsbruck, pp. 84–88, 1949.

[6] Pierce, B. O., *A Short Table of Integrals*, pp. 70, 71.

[7] Spencely, G. W., and Spencely, R. M., *Smithsonian Tables of Elliptic Functions*, Smithsonian Institution, Vol. 109, Smithsonian Miscellaneous Collection, Washington, D.C., November, 1947.

[8] Oswald, T. W., *The Effect of Nonlinear Aerodynamic Characteristics on the Dynamic Response to a Sudden Change in Angle of Attack*. *Journal of the Aeronautical Sciences*, Vol. 19, No. 5, pp. 302–316, May, 1952.

An Authorized Binding for Journal of the Aeronautical Sciences

Arrangements have been made by the Institute of the Aeronautical Sciences for members and subscribers to have their Journals bound into distinctively designed books.

Twelve issues, January through December, bound in best grade blue washable buckram, imprinted with your name on cover, cost but $3.45 per volume.

Ship Journals parcel post insured. Within 30 days after receipt, bound volumes will be shipped prepaid in the U.S.A. Full remittance must accompany order.

Publishers' Authorized Bindery Service
(*Binders of all Journals*)

308 West Randolph St. Chicago 6, Ill.

The Dynamic Motion of a Missile Descending Through the Atmosphere

HANS R. FRIEDRICH* AND FRANK J. DORE†
Convair, A Division of General Dynamics Corporation

ABSTRACT

A method is presented for computing rapidly, yet accurately, the dynamic motion of a ballistic-type missile descending through the atmosphere. The equations of motion are separated into a set of "static" trajectory equations (zero angle of attack) and a set of "rotational" equations describing the oscillatory motion of the missile about its center of gravity. A transformation allows the rotational equations to be written in a manner analogous to the equation for an undamped oscillating spring mass system with the mass equal to unity and a time variable spring constant. For given initial conditions this equation can be solved to obtain the envelope of maximum angle of attack. An additional transformation allows the calculation of the complete oscillatory motion at any time during the trajectory as a function of the maximum angle of attack at that time.

This solution shows that the maximum angle of attack of a missile descending through the atmosphere at relatively constant speed is reduced even when the aerodynamic damping is neglected.

(1) NOMENCLATURE

a_r = acceleration radial to missile flight path
a_t = acceleration tangential to missile flight path
b = reference length
C_1, C_2 = constants defined by Eqs. (37) and (38)
C_D = drag coefficient, drag/qS
C_{Di} = induced drag coefficient due to angle of attack, drag/qS
C_L = lift coefficient, lift/qS
C_m = pitching moment coefficient, moment/qSb
C_{mq} = pitch damping coefficient, $dC_m/d(\dot{\theta}b/V)$
D = defined by Eq. (12)
d = pitch damping parameter defined by Eq. (12)
ω = oscillatory frequency
g = gravitational acceleration
I = pitching moment of inertia about center of gravity
J = Bessel function of first kind
M = defined by Eq. (12)
$\bar{M}$ = defined by Eq. (16)
m = mass
P = period of oscillatory motion
q = dynamic pressure, $(1/2)\rho V^2$
R = radius of earth
S = reference area
t = time
V = velocity tangential to missile flight path
Y = Bessel function of second kind
y = altitude
Z = Bessel function defined by Eq. (33)
α = angle between missile axis and flight path
$\bar{\alpha}$ = defined by Eq. (14)
$\bar{\bar{\alpha}}$ = defined by Eq. (30)
β = defined by Eq. (23)
γ = angle between flight path and horizontal
δ = lift parameter defined by Eq. (12)
θ = angle between missile axis and horizontal
μ = moment parameter defined by Eq. (12)
ξ = integration variable
ρ = density
τ = defined by Eq. (28)

Subscript

0 = value associated with zero-angle-of-attack trajectory

Received August 13, 1954.

* Dynamics Group Engineer, and Lecturer in Engineering, University of California at Los Angeles.
† Senior Aerodynamics Engineer.

(2) INTRODUCTION

THE PURPOSE OF THIS PAPER is to present a simple yet quite accurate method of determining the motion of a ballistic-type missile during its descending flight through the atmosphere, for the case of oscillatory motion about the center of gravity. Knowledge of this motion is required for computation of the maximum loads, surface pressures, and temperatures, and dispersion of the missile from its zero-angle-of-attack flight path. The cause of the oscillatory motion could be an initial angle of attack or rotational velocity at high altitude or could arise from the effect of an atmospheric wind gust at lower altitudes. Irrespective of the cause of the disturbing condition, the designer in the past has been forced to solve the equations of motion in a step-by-step iterative procedure due to the nonlinearity of the aerodynamic coefficients at high angles of attack and the time-altitude dependency of the dynamic pressure due to the change in both missile velocity and air density.

In actual missile flights the pitching motion could occur in any plane, but since it is only desired to obtain the representative motion for design purposes, this paper assumes that pitching motion occurs in the plane of the missile trajectory. The additional assumption of a power-off, fixed controls, rotationally symmetric missile are not deemed restrictive for a ballistic-type missile.

During the development of the German V-2 rocket in World War II, H. Unger at the Technische Hochschule, Darmstadt, Germany, approached the solution of the problem in question in a simple way. The simplicity of Unger's method is based on the fact that for many missile flight conditions the missile oscillatory motion about its center of gravity has negligible influence on the trajectory followed by the missile center of gravity during the descending flight through the atmosphere. When this condition is met, the equations of motion describing the oscillatory motion can be separated from the trajectory equations. The latter equations can be readily solved by the usual tabular

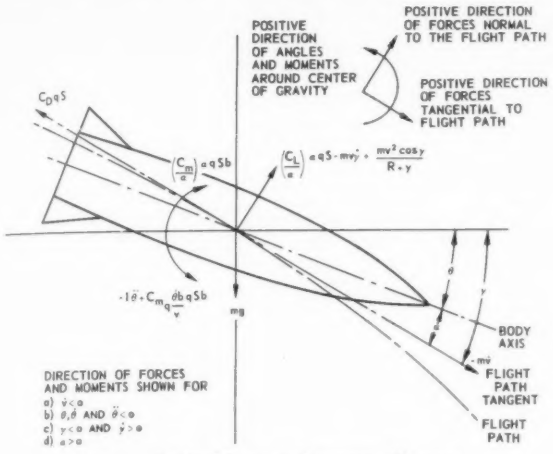

FIG. 1. Typical force and moment diagram.

methods, giving as a result the missile velocity, altitude, and dynamic pressure as a function of time. The equations describing the oscillatory motion about the center of gravity are then solved for the envelope of the maximum angle of attack. At any desired point along the trajectory, the angle of attack oscillation can be computed in detail, utilizing the pre-established maximum angle-of-attack envelope for initial conditions.

(3) Equations of Motion

The complete equations describing the motion of a missile descending through the atmosphere are complicated by the fact that oscillatory motion can occur in planes nonorthogonal to the plane of the missile re-entry trajectory, and with atmospheric winds affecting the motion. In order to reduce the problem to its simplest aspect, and still keep the element of practical application in mind, the motion is restricted to oscillatory motion in the plane of the missile trajectory and with no effect from atmospheric winds.

The angular deflections, forces, and moments acting on the missile are shown in Fig. 1. The forces are the gravitational force, the aerodynamic forces due to lift and drag, and the inertial forces arising from the accelerations radial and tangential to the missile flight path, a_r and a_t, where

$$a_r = -[V^2\cos\gamma/(R+y)] + V\dot{\gamma} \quad (1)$$

$$a_t = \dot{V} \quad (2)$$

The moments about the center of gravity are the inertial moment due to angular acceleration and the aerodynamic moments due to the static stability and the pitch damping. The set of second-order nonlinear differential equations describing the motion of the missile are then:

$$-m\dot{V} - C_D qS - mg\sin\gamma = 0 \quad (3)$$

$$-mV\dot{\gamma} + (C_L/\alpha)\alpha qS + m\{[V^2/(R+y)] - g\}\times\cos\gamma = 0 \quad (4)$$

$$-I\ddot{\theta} + C_{m_q}(\dot{\theta}b/V)qSb + (C_m/\alpha)\alpha qSb = 0 \quad (5)$$

$$\theta = \alpha + \gamma \quad (6)$$

The solution described herein depends on separating these equations into two sets of solutions, one describing the "static" trajectory of the center of gravity and the other set describing the oscillatory motion about the center of gravity. There are two conditions affecting the division of the equations.

First, experience with the type of solutions in this report shows that the angle of attack generally decreases rapidly as the missile descends in altitude while the dynamic pressure increases with decreasing altitude due to the rapid increase in air density. However, in most practical cases, the product αq has a maximum at some altitude before the missile strikes the ground. This fact entails that the induced drag due to the pitch angle of attack will influence the trajectory calculations only for an extremely short period of time and, thus, can be neglected. [This can be seen from the approximation that $C_D qS \cong (C_L/\alpha)\alpha(\alpha q)S$.] This assumption is conservative for computation of the maximum normal acceleration because the dynamic pressure is larger and the duration of time in the atmosphere is shorter than if the actual C_D value were used. However, there are some cases that are not amenable to this simplification. The solution of the equations is then simplified by a procedure described in Section (8).

The second condition affecting the division of the equations concerns Eq. (4). During the time duration of the re-entry trajectory, the missile will generally make many complete oscillations. The angle of attack α, and with it the lift term, $(C_L/\alpha)\alpha qS$, will change sign twice during each cycle. Therefore the overall disturbing influence of the oscillatory motion on the lateral component of the re-entry trajectory will be small. This allows the lift term to be neglected in Eq. (4) for static trajectory calculations. Conversely, the term containing $\cos\gamma$ in Eq. (4) generally has a negligibly small influence on the angular oscillations compared to the lift term.

The system of Eqs. (3) through (6) therefore reduces to

$$-m\dot{V}_0 - C_{D_0}q_0 S - mg\sin\gamma_0 = 0 \quad (7)$$

$$-mV_0\dot{\gamma}_0 + m\{[V_0^2/(R+y)] - g\}\cos\gamma_0 = 0 \quad (8)$$

which describe the static trajectory of the missile, and

$$-mV_0\dot{\gamma} + (C_L/\alpha)\alpha q_0 S = 0 \quad (9)$$

$$-I\ddot{\theta} + C_{m_q}(\dot{\theta}b/V_0)q_0 Sb + (C_m/\alpha)\alpha q_0 Sb = 0 \quad (10)$$

$$\theta = \alpha + \gamma \quad (11)$$

for the angular motion of the missile about its center of gravity.

A tabular solution of the static trajectory equations is relatively simple and straightforward. For the remainder of this paper it will be assumed that the static trajectory solution is available, hence that the time dependency of q_0, V_0, m, and I is known.

(4) Solution for the Envelope of Maximum Angle of Attack

The following definitions* are used throughout the remainder of the paper.

$$\left.\begin{aligned} \delta &= (C_L/\alpha)\ [(q_0 S)/(m V_0)] \\ d &= -C_{mq}[(q_0 S b^2)/(I V_0)] \\ \mu &= -(C_m/\alpha)\ (q_0 S b/I) \\ D &= d + \delta \\ M &= \mu + d\delta + \dot{\delta} \end{aligned}\right\} \qquad (12)$$

Using these definitions allows the combination of Eqs. (9), (10), and (11) to give

$$\ddot{\alpha} + D\dot{\alpha} + M\alpha = 0 \qquad (13)$$

The following deduction is based on a method described in reference 1. Introducing the transformation

$$\alpha(t) = \bar{\alpha}(t) e^{-\frac{1}{2}\int_0^t D(\xi)d\xi} \qquad (14)$$

reduces Eq. (13) to

$$\ddot{\bar{\alpha}} + \bar{M}\bar{\alpha} = 0 \qquad (15)$$

where

$$\bar{M} = M - (1/2)\dot{D} - (1/4)D^2 \qquad (16)$$

Eq. (15) corresponds to the equation for an undamped oscillating spring mass system with the mass equal to unity and a time variable spring constant, $\bar{M}(t)$.

Multiplying Eq. (15) by $\dot{\bar{\alpha}}$ and adding $\bar{M}\bar{\alpha}^2/2$ to both sides of the equation allows it to be written as

$$(d/dt)\ [(\dot{\bar{\alpha}}^2/2) + (\bar{M}\bar{\alpha}^2/2)] = \dot{\bar{M}}\bar{\alpha}^2/2 \qquad (17)$$

This equation says that the time rate of change of the total energy of the "spring mass" system—namely, the sum of the kinetic and potential energy—is equal to $\dot{\bar{M}}\bar{\alpha}^2/2$.

For the maximum and minimum points, $\bar{\alpha}_{max}$, of the $\bar{\alpha}$ curve the kinetic energy is zero because $\dot{\bar{\alpha}} = 0$. The total energy then consists of potential energy only—namely, $\bar{M}\ \bar{\alpha}_{max}^2/2$. By replacing the total energy $(\dot{\bar{\alpha}}^2/2 + \bar{M}\bar{\alpha}^2/2)$ on the left side of Eq. (17) by a fictitious potential energy $\bar{M}\bar{\alpha}_{max}^2/2$ for the same "spring constant" $\bar{M}$, the differential equation of another curve is found which can be considered as the locus for the maximum and minimum points of the $\bar{\alpha}$ curve. This fictitious potential energy represents the true potential energy of the $\bar{\alpha}$ curve at the maximum and minimum points. Eq. (17) can then be represented by

$$(d/dt)\ (\bar{M}\bar{\alpha}_{max}^2/2) = \dot{\bar{M}}\bar{\alpha}^2/2 \qquad (18)$$

or

$$\dot{\bar{\alpha}}_{max}/\bar{\alpha}_{max} = -(1/2)\ (\dot{\bar{M}}/\bar{M})\ [1 - (\bar{\alpha}/\bar{\alpha}_{max})^2] \qquad (19)$$

The curve described by this differential equation still has a big disadvantage. It is not a smooth connection of the maximum and minimum points of the $\bar{\alpha}$ curve. Because of the term $\bar{\alpha}^2/\bar{\alpha}_{max}^2$ in Eq. (19), the locus curve $\bar{\alpha}_{max}$ is slightly oscillatory, displaying double the frequency of the $\bar{\alpha}$ curve.

For ballistic-type missiles, the assumption generally can be made that the functions d, δ, μ and thus $\bar{M}$ do not show extremely rapid changes over the time interval required to complete half a cycle of oscillatory motion. Therefore, by only slightly affecting the location of the maximum and minimum points of the $\bar{\alpha}$ curve it is possible to assume the $\bar{\alpha}$ curve approximated from half wave to half wave by a sine oscillation as

$$\bar{\alpha}/\bar{\alpha}_{max} = \sin \omega t \qquad (20)$$

From Eqs. (19) and (20) then follows

$$\dot{\bar{\alpha}}_{max}/\bar{\alpha}_{max} = -(1/4)\ (\dot{\bar{M}}/\bar{M})\ (1 + \cos 2\omega t) \qquad (21)$$

This last equation clearly shows the wave form of the locus curve and that it makes one full cycle for each half cycle of the $\bar{\alpha}$ curve. It follows that the mean value for each half cycle of the $\bar{\alpha}$ curve is then

$$-\frac{1}{\pi/2}\int_0^{\pi/2} \cos 2\omega t\, d(\omega t) = \frac{1}{\pi/2}\left(\frac{1}{2}\sin 2\omega t\right)_0^{\pi/2} = 0 \qquad (22)$$

The wave curve $\bar{\alpha}_{max}$ can then be smoothed by the following excellent approximation

$$\dot{\bar{\alpha}}_{max}/\bar{\alpha}_{max} = -(1/4)\ (\dot{\bar{M}}/\bar{M}) \qquad (23)$$

From this equation follows the equation for the envelope, at any time $t > 0$, of the maximum and minimum points of the $\bar{\alpha}$ oscillations described by Eq. (15)—namely,

$$\bar{\alpha}_{max}(t) = \bar{\alpha}_{max}(0)\ \sqrt[4]{[\bar{M}(0)]/[\bar{M}(t)]} \qquad (24)$$

In Eq. (24) the time $t = 0$ is defined such that $\bar{\alpha}_{max}(0)$ coincides with the first maximum or minimum of the $\bar{\alpha}$ curve after it has become possible to approximate the $\bar{\alpha}$ curve from half wave to half wave by the sinusoidal motion indicated in Eq. (20). This condition is illustrated in Fig. (2a).

The equation for the envelope of the maximum and minimum points of the angle of attack oscillations is found by combining Eqs. (14) and (24) to get

$$\alpha_{max}(t) = \bar{\alpha}_{max}(0)\ \sqrt[4]{[\bar{M}(0)]/[\bar{M}(t)]}\, e^{-\frac{1}{2}\int_0^t D(\xi)d\xi} \qquad (25)$$

but from Eq. (14) and the above definition of the time $t = 0$ follows $\bar{\alpha}_{max}(0) \equiv [\alpha(0)]_{max} = \alpha(0)$. Therefore, the general equation for $\alpha_{max}(t)$ is

$$\alpha_{max}(t) = \alpha(0)\ \sqrt[4]{[\bar{M}(0)]/[\bar{M}(t)]}\, e^{-\frac{1}{2}\int_0^t D(\xi)d\xi} \qquad (26)$$

(5) Motion During a Cycle

After the envelopes of the angle of attack oscillations have been found according to the method in the preceding section, it is possible to calculate the representative angle of attack oscillations, piecewise, in a closed form at various points of interest.

* The time dependency of the functions is noted in the remainder of this report only when required for clarity.

The solution for the maximum angle of attack envelope of the preceding section is general in that nonlinear aerodynamic coefficients can be handled. In this section the solution for the oscillatory motion during a cycle is more restricted in that it is assumed that the parameter $\bar{M}(t)$ can be approximated with sufficient accuracy over a quarter cycle by the relation

$$\bar{M}(t) = \bar{M}(t_0)\tau \tag{27}$$

where

$$\tau = e^{\beta(t - t_0)} \tag{28}$$

and where t_0 is the time at the start of the quarter cycle. [Eq. (27) is exact for a missile with linear aerodynamic coefficients descending at constant velocity in the isothermal atmosphere.] β is obtained from Eqs. (27) and (28) as

$$\beta = [1/(t - t_0)] \ln_e \bar{M}(t)/\bar{M}(t_0) \tag{29}$$

For the conditions where Eqs. (27) and (28) are applicable, the parameter β is relatively independent of time.

Introducing the transformation

$$\bar{\alpha}(t) = \bar{\alpha}(\tau) \tag{30}$$

allows Eq. (15) to be written as

$$\tau^2[d^2\bar{\alpha}(\tau)/d\tau^2] + \tau[d\bar{\alpha}(\tau)/d\tau] + [\bar{M}(t_0)/\beta^2]\bar{\alpha}(\tau) = 0 \tag{31}$$

which has as the solution[2]

$$\bar{\alpha}(\tau) = Z_0[(2/\beta)\sqrt{\bar{M}(t_0)\tau}] \tag{32}$$

where

$$Z_0(\ ) = C_1 J_0(\ ) + C_2 Y_0(\ ) \tag{33}$$

J_0 is the Bessel function of the first kind of order zero, and Y_0 is the Bessel function of the second kind of order zero, both of argument $[(2/\beta)\sqrt{\bar{M}(t_0)\tau}]$.

Eqs. (14), (27), (28), and (30) are used to transform Eq. (32) into an expression for α giving

$$\alpha(t) = Z_0[(2/\beta)\sqrt{\bar{M}(t)}\,]e^{-\frac{1}{2}\int_0^t D(\xi)d\xi} \tag{34}$$

The values of $\dot{\alpha}$ and $\ddot{\alpha}$ are obtained from Eq. (34) as

$$\dot{\alpha} = \{-(1/2)DZ_0[(2/\beta)\sqrt{\bar{M}}] - \sqrt{\bar{M}}\,Z_1[(2/\beta)\sqrt{\bar{M}}]\}\, e^{-\frac{1}{2}\int_0^t D(\xi)d\xi} \tag{35}$$

$$\ddot{\alpha} = \{[(1/4)D^2 - (1/2)\dot{D} - M]Z_0[(2/\beta)\sqrt{\bar{M}}] + D\sqrt{\bar{M}}\,Z_1[(2/\beta)\sqrt{\bar{M}}]\}\, e^{-\frac{1}{2}\int_0^t D(\xi)d\xi} \tag{36}$$

where Z_1 is the Bessel function (or cylinder function) of order one. The values C_1 and C_2 of Eq. (33) are determined by assuming a time t_0 such that $\dot{\alpha}(t_0) = 0$, therefore $\alpha(t_0) = \alpha_{\max}(t_0)$, where $\alpha_{\max}(t_0)$ is taken from the maximum angle of attack envelope. Substituting these conditions into Eqs. (33), (34), and (35) and solving for C_1 and C_2 gives

$$C_1 = \frac{\alpha_{\max}(t_0)}{\sqrt{\bar{M}(t_0)}} \left(\frac{\sqrt{\bar{M}(t_0)}\,Y_1[(2/\beta)\sqrt{\bar{M}(t_0)}] + (1/2)D(t_0)Y_0[(2/\beta)\sqrt{\bar{M}(t_0)}]}{J_0[(2/\beta)\sqrt{\bar{M}(t_0)}]\,Y_1[(2/\beta)\sqrt{\bar{M}(t_0)}] - J_1[(2/\beta)\sqrt{\bar{M}(t_0)}]\,Y_0[(2/\beta)\sqrt{\bar{M}(t_0)}]} \right) \tag{37}$$

$$C_2 = \frac{\alpha_{\max}(t_0)}{\sqrt{\bar{M}(t_0)}} \left(\frac{\sqrt{\bar{M}(t_0)}\,J_1[(2/\beta)\sqrt{\bar{M}(t_0)}] + (1/2)D(t_0)J_0[(2/\beta)\sqrt{\bar{M}(t_0)}]}{-J_0[(2/\beta)\sqrt{\bar{M}(t_0)}]\,Y_1[(2/\beta)\sqrt{\bar{M}(t_0)}] + J_1[(2/\beta)\sqrt{\bar{M}(t_0)}]\,Y_0[(2/\beta)\sqrt{\bar{M}(t_0)}]} \right) \tag{38}$$

It should be noted that $\alpha_{\max}(t_0)$ appears in both C_1 and C_2, therefore in Z_0 and Z_1. From the form of Eqs. (34), (35), and (36), this means that $\alpha(t)$, $\dot{\alpha}(t)$, and $\ddot{\alpha}(t)$ are proportional to $\alpha_{\max}(t_0)$.

Once the values of α, $\dot{\alpha}$, and $\ddot{\alpha}$ are known, the values of θ, $\dot{\theta}$, and $\ddot{\theta}$ are readily obtained by the application of Eqs. (6) and (12).

(6) Frequency of the Motion

In the preceding section it was shown that the motion during a cycle could be approximated by Bessel functions with the argument $[(2/\beta)\sqrt{\bar{M}(t)}]$. For large values of the argument, the Bessel function can be written in terms of sine and cosine functions with the same argument. This means that the oscillatory portion of the motion can be represented by sinusoidal motion. For example, if the angle of attack is a maximum at $t = t_0$, a quarter of a period later it will be zero, or writing this in terms of the cosine of the argument, at

$$t = t_0;\ \cos[(2/\beta)\sqrt{\bar{M}(t_0)}] = 1 \tag{39}$$

at

$$t = t_0 + P/4;\ \cos[(2/\beta)\sqrt{\bar{M}(t_0 + P/4)}] = 0 \tag{40}$$

But since a quarter period corresponds to $\pi/2$ radians, the argument of Eq. (40) can be written as

$$(2/\beta)\sqrt{\bar{M}(t_0)} + (\pi/2) = (2/\beta)\sqrt{\bar{M}(t_0 + P/4)} \tag{41}$$

But from the approximation for $\bar{M}(t)$ given by Eqs. (27) and (28), the period can be obtained from Eq. (41) as

$$P = (4/\beta)\ln_e\{[\sqrt{\bar{M}(t_0)} + \pi\beta/4]^2/[\bar{M}(t_0)]\} \tag{42}$$

with β given by Eq. (29).

Since the period is time dependent it is desirable to be able to plot the envelope of the period as a function of time, t. The derivation for the period given above is still correct if the parameter β is evaluated as

$$\beta = \lim_{t \to t_0} \left[\frac{1}{(t - t_0)} \ln_e \frac{\bar{M}(t)}{\bar{M}(t_0)} \right] \tag{43}$$

With this definition of β it is then correct to speak of $P(t)$ as the instantaneous value of the period at time t, analogous to $\alpha_{max}(t)$ being the instantaneous value of α_{max} at time t. The oscillatory frequency is given by the usual definition

$$\omega = 2\pi/P \tag{44}$$

(7) Approximate Solutions for the Dynamic Motion

The Bessel solutions for the dynamic motion—$\alpha(t)$, $\dot{\alpha}(t)$, and $\ddot{\alpha}(t)$—are cumbersome to evaluate. This difficulty is overcome by taking advantage of two conditions indicated by the Bessel solution: first, $\alpha(t)$, $\dot{\alpha}(t)$, and $\ddot{\alpha}(t)$ are proportional to $\alpha_{max}(t)$, and second, the oscillations can be approximated by sinusoidal motion with a time dependent frequency, $\omega(t)$. These statements lead to the type of equation

$$\alpha(t) = \alpha_{max}(t) \cos [(\omega(t)t] \tag{45}$$

Differentiating this equation for $\dot{\alpha}(t)$ and $\ddot{\alpha}(t)$ gives

$$\dot{\alpha}(t) = -\alpha_{max}\{\sin [\omega(t)t]\} [\omega(t) + \dot{\omega}(t)t] + \dot{\alpha}_{max}\{\cos[\omega(t)t]\} \tag{46}$$

$$\ddot{\alpha}(t) = -\alpha_{max}\{\cos [\omega(t)t]\} [\omega(t) + \dot{\omega}(t)t]^2 - \alpha_{max}\{\sin [\omega(t)t]\} [2\dot{\omega}(t) + \ddot{\omega}(t)t] - 2\dot{\alpha}_{max}\{\sin [\omega(t)t]\} [\omega(t) + \dot{\omega}(t)t] + \ddot{\alpha}_{max}\{\cos [\omega(t)t]\} \tag{47}$$

where

$$\left.\begin{aligned} \dot{\alpha}_{max} &= [d\alpha_{max}(t)]/dt \\ \ddot{\alpha}_{max} &= [d^2\alpha_{max}(t)]/dt^2 \end{aligned}\right\} \tag{48}$$

The maximum values of $\dot{\alpha}(t)$ and $\ddot{\alpha}(t)$ are usually easier and more useful to work with. These are

$$[\dot{\alpha}(t)]_{max} = \alpha_{max}(t)\omega(t) \tag{49}$$

and

$$[\ddot{\alpha}(t)]_{max} = \alpha_{max}(t)[\omega(t)]^2 + [d^2\alpha_{max}(t)]/dt^2\} \tag{50}$$

It is seen that the equations for $[\dot{\alpha}(t)]_{max}$ and $[\ddot{\alpha}(t)]_{max}$ are similar to the values obtained for simple harmonic motion except for the last term of Eq. (50). In practice this particular term is usually of small magnitude.

(8) Approximate Solutions Neglecting Aerodynamic Damping

One of the original suppositions of this paper was that the solutions are particularly applicable to high-speed missiles in their descending flight through the atmosphere. Now for some types of missiles it is possible that the ratio of the aerodynamic damping term to the static stability term of Eq. (5) is small, in fact, much less than for airplanes or missiles designed to maneuver at transonic or low supersonic speeds. If

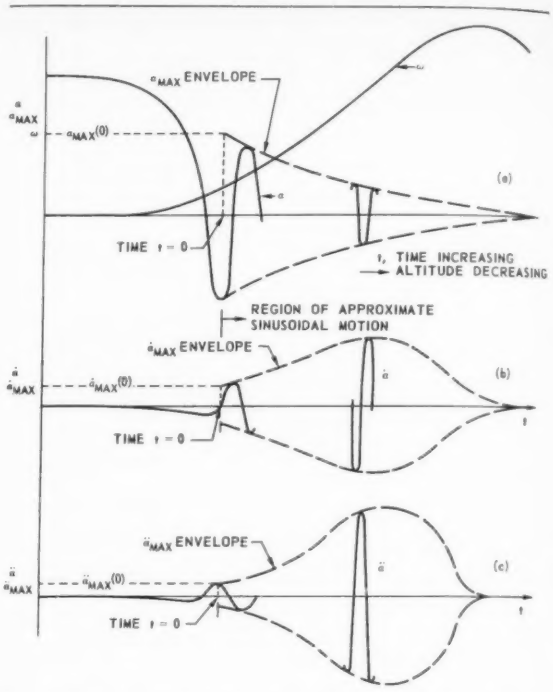

Fig. 2. The dynamic motion of a missile descending through the atmosphere.

the aerodynamic damping term is small, then certain useful approximations can be made to simplify the calculations considerably. Generally speaking, it may be found that

$$\mu \gg \dot{\delta} + d\delta - (1/2)\dot{D} - (1/4)D^2 \tag{51}$$

so that

$$\bar{M} \approx \mu \tag{52}$$

is an extremely good approximation. Furthermore, the aerodynamic damping builds up slowly so that

$$e^{-\frac{1}{2}\int_0^t D(\xi)\, d\xi} \lesssim 1 \tag{53}$$

for a sizable portion of the re-entry trajectory.

With these assumptions Eq. (26) can be approximated by

$$\alpha_{max}(t) \approx \alpha(0) \sqrt[4]{[\mu(0)]/[\mu(t)]} \tag{54}$$

This equation is readily solved by iteration. Eq. (54) is interesting because it clearly shows that the maximum angle of attack is usually reduced even when the aerodynamic damping is neglected. This occurs because the increase in dynamic pressure due to the density change with decreased altitude effectively amounts to an increased "spring constant" in the moment equation, requiring a decrease in angle of attack (i.e., "spring deflection") to maintain the same kinetic energy of the system. Obviously the opposite situation can occur (pitch oscillation divergence) if the reduction in velocity due to a large amount of drag is more than

(*Continued on page 638*)

Some General Comparisons Between the Vibratory and Conventional Rate Gyro

JOHN B. CHATTERTON*

Sperry Gyroscope Company Division of Sperry Rand Corporation

ABSTRACT

The new vibratory rate gyro is compared analytically with the conventional elastically restrained rate gyro. Developed torques, sensitivity bandwidth factors, output transfer functions, and some of the inherent errors are developed simultaneously in a simple unified manner to give a theoretical understanding of the vibratory gyro and its characteristics relative to the familiar conventional rate gyro. The discussion is of a general nature and does not attempt to compare performance data of practical instruments. The conclusion is reached that the vibratory rate gyro has many relative advantages.

INTRODUCTION

RECENT DEVELOPMENTS in the field of gyroscopics have brought forth the vibratory rate gyro (VRG), which has the obvious advantage of no moving wearable parts. Its usual configuration is such that two identical masses, electrically maintained in opposed co-planner vibration, produce an alternating torque about the symmetrical axis in the plane of vibration when angular inertial velocity is applied about the axis.[1, 2] The device is comparable in its measurement function to the conventional elastically restrained (and supported) single degree of freedom gyro or rate gyro (RG).

It is the purpose of this paper to compare some of the more interesting and important characteristics of the two devices. The comparison is held to a very general discussion of inherent properties rather than the examination of characteristics of working models. It is believed that what follows is considerably more significant.

DEVELOPED TORQUES

In the derivation of the torques developed for each type of gyro, the similarities are best shown by starting with the familiar vector equation of motion for a particle in spherical coordinates. The radial and transverse components of velocity of a particle of mass, m, moving in a secondary inertial system, x, y, z, at a distance r from the origin is (see Fig. 1):

$$\bar{v} = \dot{r}\hat{r} + r\dot{\theta}\hat{\theta} + r\dot{\phi}\sin\theta\hat{\phi} \tag{1}$$

where $\hat{r}$ is the unit vector along r, $\hat{\theta}$ is a unit vector at right angles to r and in the direction of increasing θ, and $\hat{\phi}$ is a unit vector at right angles to the $\hat{r}\hat{\theta}$ plane and in the direction of increasing ϕ. The time derivative of this velocity[3] gives the vectorial acceleration of the particle relative to the inertial system

$$\begin{aligned}\bar{a} = {} & [\ddot{r} - r(\dot{\theta})^2 - r(\dot{\phi})^2\sin^2\theta]\hat{r} + \\ & [2\dot{r}\dot{\theta} + r\ddot{\theta} - r(\dot{\phi})^2\sin\theta\cos\theta]\hat{\theta} + \\ & [2\dot{r}\dot{\phi}\sin\theta + 2r\dot{\theta}\dot{\phi}\cos\theta + r\ddot{\phi}\sin\theta]\hat{\phi}\end{aligned} \tag{2}$$

The typical rate gyro configuration consists of a rigid rotor mounted in an instrument frame and oriented with respect to a spin, input, and output axis as shown in Fig. 2. With the instrument frame axes positioned with respect to the inertial system as shown, and rotating in it with velocity Ω, Eq. (2) is valid for each mass particle of the rotor. The reaction torque output of any particle will be due only to the $\hat{\phi}$ component of acceleration, therefore, with r of constant length, this incremental torque amplitude becomes, with the direction of positive output,

$$t = m[2r\dot{\theta}\dot{\phi}\cos\theta + r\ddot{\phi}\sin\theta]r\cos\theta \tag{3}$$

With $\dot{\phi} = \Omega$ the inertial angular velocity input, with $\dot{\theta} = \omega_R$ the rotor velocity, and considering $\ddot{\phi} = 0$ for the moment, Eq. (3) becomes

$$t = 2mr^2\omega_R\Omega\cos^2\theta \tag{4}$$

If the total rotor mass, M, is considered to be distributed along the circle at r,

$$m = (M/2\pi)d\theta \tag{5}$$

and the total output torque becomes

$$T_{RG} = \frac{r^2\omega_R M\Omega}{\pi}\int_0^{2\pi}\cos^2\theta\, d\theta \tag{6}$$

or

$$T_{RG} = r^2\omega_R M\Omega \tag{7}$$

which, of course, is simply $I\omega_R\Omega$, where I is the inertia of the rotor about the spin axis.

The vibratory rate gyro configuration is somewhat similar and is shown in Fig. 3 with rotation in the inertial frame as before. The instrument frame coordinate axes can be designated here as the input, vibration, and transverse axis. The mass vibrates about the vibration axis in the input-transverse plane and symmetrically with respect to the input axis. The output axis could be taken along the input axis. To avoid a double frequency output torque, however, the output axis is taken parallel to the input at a transverse distance R. The output torque will again be due to only the $\hat{\phi}$ component of the acceleration of Eq. (2). The magnitude of the incremental reaction torque output

Received June 3, 1954.

* Senior Engineer, Flight Instrument Engineering Department.

in the direction of negative input becomes, with r constant in length,

$$t = m[2r\dot{\theta}\dot{\phi}\cos\theta + r\ddot{\phi}\sin\theta](R - r\sin\theta) \quad (8)$$

If the motion of m is such that

$$\theta = \Delta\theta\sin\omega_F t \quad (9)$$

representing a mass vibration of peak amplitude $\Delta\theta$ and angular frequency ω_F, and with $\dot{\phi} = \Omega$ and $\ddot{\phi} = 0$ as before, Eq. (8) becomes

$$t = m[2r\Omega\omega_F\Delta\theta\cos\omega_F t\cos(\Delta\theta\sin\omega_F t)] \times [R - r\sin(\Delta\theta\sin\omega_F t)] \quad (10)$$

The total vibration mass M can be lumped at m and assuming $\Delta\theta$ small, the total output torque can be written approximately,

$$T_{VRG} = 2MRr\Delta\theta\omega_F\Omega\cos\omega_F t \quad (11)$$

Since the input angular acceleration $\ddot{\phi}$ was considered to be zero, Eq. (11) will still be valid for Ω applied about the z' or output axis.

Output Motions

It is the usual practice to have these torques produce a torsional motion of a restraining system with respect to the instrument frame and, with some appropriate transducer, produce an output voltage or signal proportional to the motion. Typical configurations are shown in Figs. 4 and 5.

The RG must utilize a differential displacement sensitive transducer in order to detect differential applied rate; hence, the displacement of a spring mass system driven by the torque of Eq. (7) will be calculated. With I_0 the total moment of inertia about the output axis, k, the torsional spring constant of the torsion system, and C the mechanical damping resistance, the displacement, D_{RG}, for the steady state case when $\Omega = V\cos\omega t$, becomes

$$D_{RG} = T_{RG}/\{j\omega[j\omega I_0 + C + (k/j\omega)]\} \quad (12)$$

With the natural angular frequency,

$$\omega_0 = \sqrt{k/I_0} \quad (13)$$

and the Q of the system

$$Q = (\omega_0 I_0/C) = 1/[2(C/C_c)] \quad (14)$$

where C_c is the critical damping resistance, Eq. (12) becomes

$$D_{RG} = \frac{T_{RG}}{k[1 - (\omega/\omega_0)^2 + j(1/Q)(\omega/\omega_0)]} \quad (15)$$

Substituting the torque of Eq. (7) and converting the imaginary expression

$$D_{RG} = (r^2\omega_R MV/kq)\cos(\omega t - \beta) \quad (16)$$

where

$$\beta = \tan^{-1}[\omega\omega_0/Q(\omega_0^2 - \omega^2)] \quad (17)$$

and

$$q = \sqrt{[1 - (\omega/\omega_0)^2]^2 + [(1/Q)(\omega/\omega_0)]^2} \quad (18)$$

For a practical design the Q is usually chosen near 0.62 as a compromise for best response time and transient overshoot. For this value the approximate rate transfer function becomes, from Eq. (15),

$$G_{RG}(j\omega) = T_{RG}/k[1 + j(\omega/\omega_0)]^2 \quad (19)$$

resulting in a maximum phase shift of 180° lagging as would be expected in a second-order system.

The VRG, because of the higher frequency carrier centering of torque, can utilize a velocity sensitive nondifferential transducer and, hence, the velocity of a spring mass system driven by the torque of Eq. (11) will be shown.

With $\Omega = V\cos\omega t$ as before,

$$v_{VRG} = T_{VRG}/[j\omega I_0 + C + (k/j\omega)] \quad (20)$$

Using Eqs. (13) and (14) with $\omega_F = \omega_0$ and assuming arithmetic symmetry of the response near resonance so that

$$[(\omega_0 + \omega)/\omega_0] - [\omega_0/(\omega_0 + \omega)] \approx 2(\omega/\omega_0) \equiv K \quad (21)$$

the solution for Eq. (20), assuming $\omega \ll \omega_0$, can be shown to be

$$v_{VRG} = \frac{MRr\Delta\theta\omega_0 V}{C\sqrt{1 + Q^2K^2}} \times \{\cos[(\omega_0 + \omega)t - \alpha] + \cos[(\omega_0 - \omega)t + \alpha]\} \quad (22)$$

where, $\alpha = \tan^{-1}QK$. Eq. (22) shows the double sideband characteristic of the suppressed-carrier motion, and rewriting,

$$v_{VRG} = \frac{2MRr\Delta\theta\omega_0 V}{C\sqrt{1 + Q^2K^2}}\cos(\omega t - \alpha)\cos\omega_0 t \quad (23)$$

The rate transfer function of interest would be that of the velocity output after a perfect demodulation or phase detection operation has been accomplished. This could be written immediately from Eq. (23) after the $\cos\omega_0 t$ factor is dropped and ω is assumed small to be consistent with the condition on Eq. (22). This condition could then be changed to give an approximate output velocity for large ω, and complete the transfer function approximation. However, a simple and readily visualized method, similar to a.c. servo techniques, can be used to obtain the entire output response. If the torsion system amplitude response characteristic is assumed to be a perfect even function about its natural frequency, ω_0, and the phase, α, a perfect odd function about ω_0, approaching 90° lead to the left of ω_0 for lower frequencies and 90° lag to the right, then for an arbitrary suppressed-carrier input, centered at ω_0,

$$\text{Input} = A\cos\omega t\cos\omega_0 t = (A/2)[\cos(\omega_0 + \omega)t + \cos(\omega_0 - \omega)t] \quad (24)$$

and, with points ΔA on the amplitude curve corresponding to frequencies $\omega_0 + \omega$ and $\omega_0 - \omega$, the output is

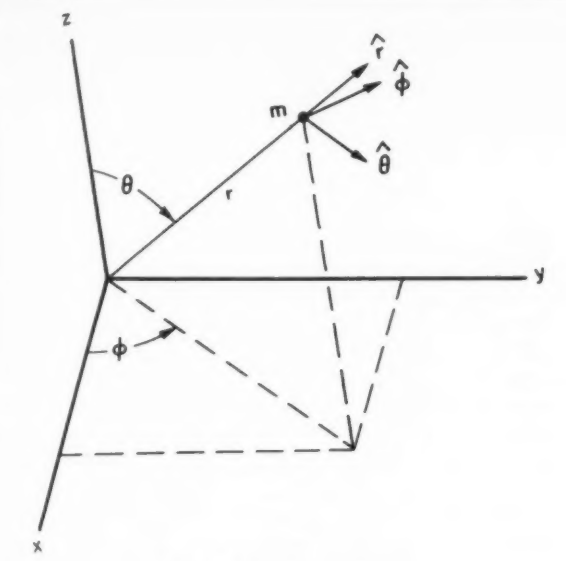

FIG. 1. Spherical coordinates.

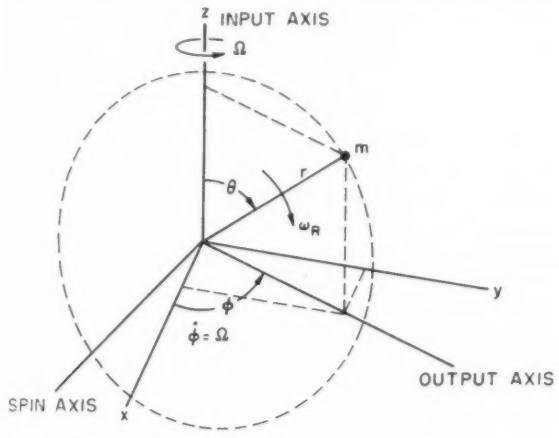

FIG. 2. Conventional rate gyro particle motion.

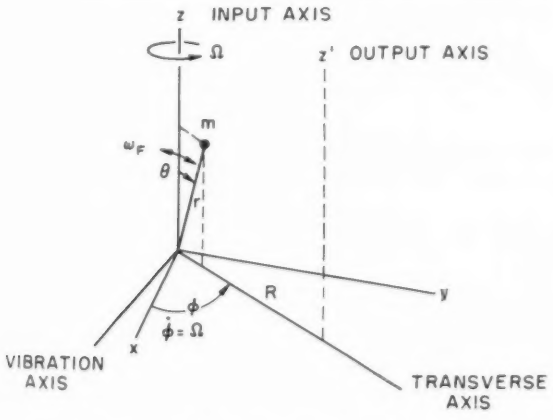

FIG. 3. Vibratory rate gyro particle motion.

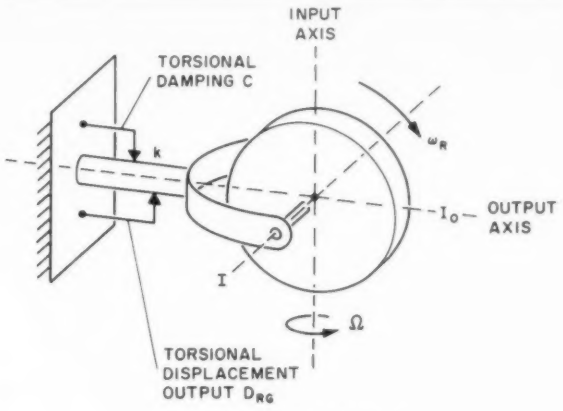

FIG. 4. RG system schematic.

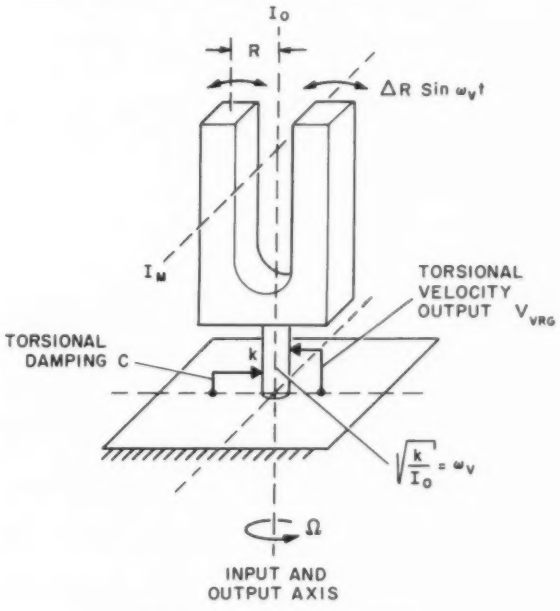

FIG. 5. VRG system schematic.

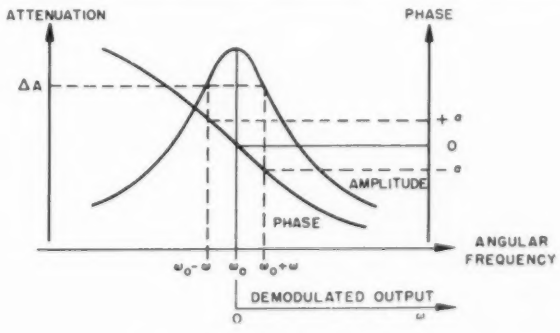

FIG. 6. VRG torsion system response.

$$\text{Output} = (A/2)\Delta A\{\cos[\omega_0 t + (\omega t - \alpha)] + \cos[\omega_0 t - (\omega t - \alpha)]\}$$
$$= A\Delta A \cos(\omega t - \alpha)\cos\omega_0 t \quad (25)$$

Hence, the demodulated output is identical to the right or higher frequency symmetrical half of the torsion response curve with the value of $\omega = 0$ starting now at ω_0. This is clarified in Fig. 6. When these characteristics are redrawn on semilog coordinates, the approximate attenuation asymptotes can be drawn immediately. This is shown in Fig. 7 along with the phase characteristics for each asymptote. The solid lines show the true value and the dashed the approximate. Thus, from Eq. (23), and with the restriction on ω as seen from Fig. 7, the transfer function can be written for the demodulated output

$$G_{VRG}(j\omega) = \frac{T_{VRG}/\cos\omega_0 t}{1 + 2Qj(\omega/\omega_0)} \qquad \text{for } \omega \leq \frac{\omega_0}{2Q} \quad (26)$$

and

$$G_{VRG}(j\omega) = \frac{T_{VRG}/\cos\omega_0 t}{2Q^2 j(\omega/\omega_0)} \qquad \text{for } \omega > \frac{\omega_0}{2Q} \quad (27)$$

Thus, the maximum phase shift possible in the *VRG* is 90° lagging and can be approximated by a first-order rather than second-order system.

Sensitivity Bandwidth Factors

In any transducer it is generally desirable to have as large a sensitivity (using sensitivity as a gain factor) as possible. Furthermore, if the transducer or instrument is required to transmit information, it is desirable to have as wide a frequency response as possible. Therefore, the possibility exists that the product of sensitivity and bandwidth for each gyro could be a useful figure of merit.

The significant bandwidth for the RG is simply

$$BW_{RG} = \omega_0/2\pi \quad (28)$$

and the sensitivity, from Eq. (16), per unit steady rate input,

$$S_{RG} = (r^2\omega_R M)/k \quad (29)$$

or, in terms of the spin and output axis inertias,

$$S_{RG} = (\omega R/\omega_0^2)(I/I_0) \quad (30)$$

The sensitivity-bandwidth product is then

$$SBW_{RG} = (\omega_R/2\pi\omega_0)(I/I_0) \quad (31)$$

For the *VRG*, from Eq. (23), the sensitivity is

$$S_{VRG} = (2MRr\Delta\theta\omega_F)/C \quad (32)$$

which is a function of the damping unlike the *RG*. Setting $\Delta R = r\Delta\theta$, the mass transverse displacement, and, comparable to the spin inertia of the RG, a vibratory axis inertia of $I = MR^2$, the sensitivity becomes, using Eq. (14),

$$S_{VRG} = (2\Delta RQ/R)(I/I_0) \quad (33)$$

The bandwidth, considering the double sideband nature of force, as was seen in Fig. 7,

$$BW_{VRG} = \omega_F/4\pi Q \quad (34)$$

and the sensitivity-bandwidth product becomes

$$SBW_{VRG} = (\Delta R\omega_F/2\pi R)(I/I_0) \quad (35)$$

The result for the *VRG*, unlike that for the *RG*, is seen to be constant for any particular design. The factor for the *RG* depends on the inverse bandwidth (a high price in sensitivity is paid for an increased bandwidth) and is therefore not a particularly useful figure of merit except for this comparison. As an example of the numerical values of these results, take the *VRG* with a vibration amplitude of 0.002 in. at 2,000 cycles per sec., an R of 0.25 in. and an inertia ratio of 0.3; for the RG, take a rotor speed of 12,000 r.p.m. and an inertia ratio of unity. The two *SBW* factors will be equal for an RG bandwidth of 6.6 cycles per sec., the *SBW* factor for the VRG being higher for RG bandwidths larger than this value. For equal pickoff transducer gains (volts per unit angular displacement and volts per unit angular velocity), these figures would represent the relative electrical outputs for the same applied angular velocity inputs.

Subminiaturization

The sensitivity-bandwidth factors can be used as general design equations for possible subminiaturization. As the configuration for either device is scaled down in physical size, the inertia ratios will remain constant. With constant rotor speed for the RG, the sensitivity and *SBW* factor will be independent of physical dimensions if the bandwidth is held constant. The bandwidth is likely to increase with subminiaturization, however, and, depending on the application, might result in too low a sensitivity. The VRG, on the other hand, will have the product $\Delta R\omega_F$ nearly independent of physical size and a decrease in R will in-

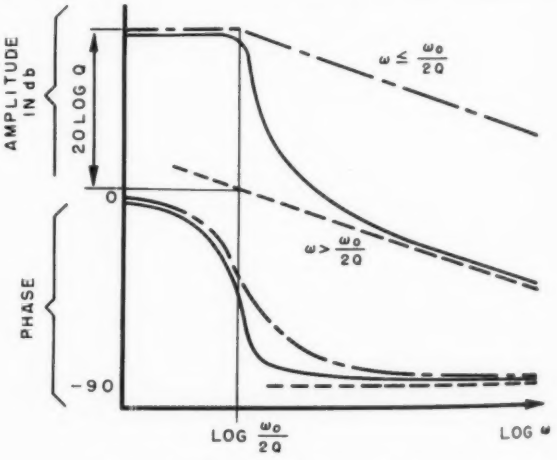

FIG. 7. VRG demodulated output response.

crease the SBW factor. Scaling down the output pickoff will lower the overall sensitivity in each case. Subminiaturization of the pickoff will not affect the performance of the VRG through a resolution loss, however, since it utilizes a nondifferential pickoff. This will not be the case for the RG.

Errors

It is not necessary to point out that the output motions discussed are for the ideal case, where output is linear with applied inertial rate. There is probably an uncountable number of deviations from the ideal, quantities which can be added or superposed on the ideal and quantities which become factors of the ideal. These deviations can perhaps be divided into two groups—uncertainties, those deviations that are difficult to discuss analytically in the general case; and errors, those that more or less may be described quantitatively. In general, the uncertainties limit resolution. In comparing two different types of instruments it is therefore mandatory that a discussion of the largest or most important of these deviations be included.

In developing Eqs. (7) and (11), the applied angular acceleration about the input axis, $\ddot{\phi}$, was assumed to be zero. Considering this component now, for the case of the RG from Eq. (3)

$$t_A = mr^2\ddot{\phi} \sin\theta \cos\theta \tag{36}$$

and the total component becomes

$$T_{RGA} = \frac{Mr^2\ddot{\phi}}{2\pi}\int_0^{2\pi} \sin\theta \cos\theta \, d\theta = 0 \tag{37}$$

For accelerations about the output axis, however, there is obviously

$$T_{RGA} = I_0\ddot{\phi}_{\text{out}} \tag{38}$$

which would be superposed on the developed torque due to an input velocity and represents an acceleration error.

For the VRG, the acceleration component becomes, from Eq. (8)

$$t_A = mr\ddot{\phi} \sin\theta(R - r\sin\theta) \tag{39}$$

and using Eq. (9) with $\Delta\theta$ small, the total torque becomes approximately

$$T_{VRGA} = MRr\Delta\theta\ddot{\phi} \sin\omega_F t \tag{40}$$

In addition to this component, transfering the input axis to the z' or output axis will cause an angular acceleration component of torque, similar to Eq. (38),

$$T_{VRGA} = I_0\ddot{\phi} \tag{41}$$

The two torques of Eqs. (40) and (41) represent an acceleration error for the VRG about its input axis. It is seen, however, that the torque of Eq. (40) is out of time phase with the primary torque of Eq. (11). It is therefore possible to eliminate this quadrature term when the output signal is subjected to a demodulation process. The component of Eq. (41) is not of the carrier frequency and would ordinarily be attenuated by the torsion system response characteristic.

More generally, the acceleration errors discussed above become transient errors when the applied input is not considered to be a steady sinusoidal. For a step function of velocity applied simultaneously about the input and output axes of the RG, the output response will be the response of the output torsion system for torques of step and impulse functions respectively. In fact, the latter output amplitude can be made relatively low by proper design. For the step function of velocity applied to the input axis of the VRG, the forcing function of the torsion system will be a step function of carrier torque and a unit impulse due to Eq. (41). Since the Q of the torsion system is high, an intolerable overshoot would result. It is therefore mandatory that either the Q be lowered or that the instrument frame be isolated from the vehicle and offer low transmissibility to frequencies near ω_F. Since ω_F is usually large compared to the BW, the latter solution is very practical.

Another source of possible error in each device is the effect of output motion on the applied input. For the case of the VRG, the output velocity of Eq. (23), v_{VRG}, is applied to the input like feedback. The corrected output velocity is then

$$v_c = \frac{v_{VRG}}{1 + v_{VRG}/\Omega} = v_{VRG}\left[1 - \frac{v_{VRG}}{\Omega} + \left(\frac{v_{VRG}}{\Omega}\right)^2 - \ldots\right] \tag{42}$$

which reduces approximately to v_{VRG} since the second term in the denominator (although indeterminate at times) is always less than unity. The displacement output D_{RG} of the RG, Eq. (16), causes a displacement between the effective input axis and the prescribed input axis of the frame. The corrected output displacement becomes

$$D_c = D_{RG}\cos D_{RG} = D_{RG}[1 - (D_{RG}^2/2!) + \ldots] \tag{43}$$

which reduces to D_{RG} for small displacements. Comparing the expansions of Eq. (42) and (43), both output motions appear to be nonlinear. The VRG output, however, is seen to be linear if only the carrier frequency term is used. This could be practically accomplished with the use of a full-wave demodulation process on the output. The output motion of the RG will have another effect in that applied rotation about the frame spin axis will cause an additional output displacement proportional to the sine of the total displacement and will result in a cross-coupling error.

Another error of the RG, which has nothing comparable contained in the VRG, is the error due to mechanical hysteresis of the output torsion system. Essentially the same system is used for the VRG but because of the carrier-type of torque, hysteresis produces only a negligibly small phase distortion.

Because of the errors of cross-coupling and hysteresis, an upper limit on allowable output displacements

for the RG is required. Consequently, the VRG, with no upper limit on output motion other than the fatigue endurance limit, has a practical linear amplitude range of perhaps 1,000 times that of the RG.

Uncertainties

Since the inertial rate that is desired to be measured is a differential quantity (clockwise and counterclockwise directions must be distinguished) a device to measure this must be of the differential type. Any practical differential measuring device will have a nonzero or minimum null with zero applied input. Since the cause of these nulls could never remain entirely constant, in order that compensation or bucking could be totally effective, a source of a null will also be a source of variation of the null or an uncertainty.

The RG has essentially three sources of null and uncertainty. These are due to the static unbalance of the output system about the output axis when acted upon by linear accelerations such as gravity, the noise produced by the dynamic unbalance of the rotor, and the displacement pickoff which must be of the differential type.

The VRG has a nondifferential pickoff and a monochromatic mass motion which produces no noise. There are nulls, however, due to the dynamic unbalance of the double-ended vibrating system and to a possible static unbalance when acted upon by linear accelerations. It has been found experimentally, however, that this later null is apparently a function of the first and follows the dynamic unbalance as a second-order effect. Thus it might be said that the VRG contains essentially one source of null and uncertainty.

Conclusions

There is no doubt that the VRG has inherent features relative to the RG which make it outstanding in many areas. In fact, an audit of absolute advantages and disadvantages for each device would certainly favor the VRG. If the audit were weighted according to usefulness for application, especially today's applications, the superiority is not as great. The fact, however, that the VRG is a new device with a lower number of causes of uncertainty should make it relatively more susceptible to future development.

References

[1] Lyman, J., *A New Space Rate Sensing Instrument*, Aeronautical Engineering Review, Vol. 12, No. 11, pp. 24–30, November, 1953.

[2] Barnaby, R. E., Chatterton, J. B., and Gerring, F. H., *General Theory and Operational Characteristics of the Gyrotron® Angular Rate Tachometer*, Aeronautical Engineering Review, Vol. 12, No. 11, pp. 31–36, 106, November, 1953.

[3] Page, L., *Introduction to Theoretical Physics*, 2nd Ed., p. 52, D. Van Nostrand Company, Inc., 1935.

The Dynamic Motion of a Missile . . .

(*Continued from page 632*)

sufficient to offset the increased density at lower altitudes.

Approximate expressions can also be obtained for $[\dot{\alpha}(t)]_{max}$, $[\ddot{\alpha}(t)]_{max}$, and $\omega(t)$ with the same restrictions as for Eq. (54). The resulting equations are

$$[\dot{\alpha}(t)]_{max} \cong [\dot{\alpha}(0)]_{max} \{[\mu(t)]/[\mu(0)]\}^{1/4} \quad (55)$$

$$[\ddot{\alpha}(t)]_{max} \cong [\ddot{\alpha}(0)]_{max} \{[\mu(t)]/[\mu(0)]\}^{3/4} \quad (56)$$

$$\omega(t) \cong \omega(0) \{[\mu(t)]/[\mu(0)]\}^{1/2} \quad (57)$$

The use of Eq. (54) allows a rapid calculation of the maximum possible α_{max} envelope, which can then be used to establish the magnitude of $D(t)$ and $\bar{M}(t)$ required for the exact calculation of α_{max} with the consideration of aerodynamic damping. In addition, the effect on the "static" trajectory of the increased drag coefficient due to angle of attack effects can also be readily computed.

(9) Conclusions

This paper presents a method for computing the dynamic motion of a ballistic-type missile descending through the atmosphere. The equations of motion are separated into a set of "static" trajectory equations (zero angle of attack) and a set of "rotational" equations describing the oscillatory motion of the missile about its center of gravity. These equations are solved separately to obtain the "static" trajectory and the envelope of the maximum angle of attack. At any desired point along the trajectory, the angle of attack oscillations can be computed in detail, utilizing the pre-established maximum angle-of-attack envelope for initial conditions. The type of information resulting from this calculating procedure is shown in Fig. 2.

References

[1] Zech, Th., *The Damping of Non-Linear Vibrations (General Case of Amplitude Modulation)*, Ingenieur-Archiv, Vol. 13, No. 1, pp. 21–33, February, 1942. Translated by L. T. Goodlet, R.T.P. translation No. 2044 issued by the Ministry of Aircraft Production.

[2] Kamke, E., *Differential Gleichungen; Lösungs Methoden und Lösungen*, Vol. I, p. 440; Akademische Verlags Gesellschaft, Leipzig, 1944.

Criteria for Longitudinal Stability Requirements

JAMES L. DECKER*
The Glenn L. Martin Company

Abstract

This paper proposes a new set of requirements for the longitudinal stability characteristics of aircraft. The factors influencing the flying qualities of piloted aircraft have been analyzed, and the proposed requirements are based primarily on stick-free dynamics and control force characteristics. It is shown that the stick-fixed neutral point is not always a valid criterion for longitudinal stability.

The proposed requirements are listed below.

The aft center-of-gravity limit: (1) shall not be behind the c.g. location at which the stick force-per-g is less than a specified value, depending upon airplane type and limit-load factor, and (2) shall be forward of the stick-fixed short-period divergence point.

The short-period dynamic stability characteristics shall be such that: (1) the stick-free short-period airplane oscillation damps to one-half amplitude within one cycle and (2) the stick-free short-period airplane oscillation damps to one-half amplitude within $1^1/_2$ sec.

The latter requirements may also limit the aft center of gravity loading.

The long-period stick-free dynamics may be unstable—except in cruising and climbing flight—but the motion shall not double in amplitude in less than 8 sec. In cruising and climbing flight, positive-force stability must exist so that push and pull forces are required to stabilize at speeds above and below trim, respectively. This force gradient should be of sufficient magnitude to maintain essentially the trim speed after a sharp control displacement and release.

Symbols and Definitions

D = drag, lb.
L = lift, lb.
M = pitching moment, ft.lb.
F = control force, lb.
P = period of oscillatory motion, sec.
S = wing area, sq. ft.
T = thrust, lb.
V = velocity, ft. per sec.
W = airplane gross weight, lb.
$\bar{c}$ = mean aerodynamic chord of wing, ft. (MAC)
g = gravity acceleration, ft. per sec.^{2}
n = load factor in g's
q = dynamic pressure, lbs. per sq.ft.
I_y = pitching moment of inertia, slug-ft.^{2}
α = angle of attack, radians
θ = pitch angle, radians
δ_e = elevator deflection, radians
C_L = lift coefficient, L/Sq
C_D = drag coefficient, D/Sq
C_m = pitching-moment coefficient, $M/S\bar{c}q$
$C_{H\alpha}$ = the slope of the elevator-hinge moment-coefficient curve with tail angle of attack at constant elevator deflection
$C_{H\delta}$ = the slope of the elevator-hinge moment-coefficient curve with elevator deflection at a constant tail angle of attack

Stick-fixed neutral point = center-of-gravity location at which $\partial\delta_e/\partial V = 0$ in steady one-g flight.

Stick-fixed, maneuvering neutral point = center-of-gravity location at which $\partial\delta_e/\partial n = 0$ for a constant-speed maneuver.

Stick-free neutral point = center-of-gravity location at which $\partial(F/q)/\partial V = 0$ in steady one-g flight.

Stick-free, maneuvering neutral point = center-of-gravity location at which $\partial F/\partial n = 0$ for a constant-speed maneuver.

Aerodynamic center = center-of-gravity location at which $\partial C_M/\partial\alpha = 0$, with speed being held constant.

Introduction

The handling characteristics of aircraft were subjects of extensive study even before man's first flight. From the earliest days of aviation, the designer's central problem has been to develop workable controls and to supply stability or, at least, to hold instabilities within controllable limits. As the art of designing and building aircraft progressed, pilots became more discriminating and demanded airplanes with better flying qualities. Eventually, the desirable handling characteristics became well enough defined to warrant writing specifications outlining minimum requirements. Some of the most important of these requirements relate to longitudinal stability. Since static longitudinal stability decreases as the center of gravity is moved aft, it follows that the longitudinal stability requirements can limit the aft c.g. location. However, inappropriate requirements may be detrimental to the utility of an airplane if they impose unnecessarily restricted loading limits.

Before the advent of jet aircraft, the requirements for satisfactory longitudinal flying qualities were well established and generally accepted. These same requirements—couched in terms of static margin, relative to the neutral point-c.g. relationship—are employed today. The curve of elevator-to-trim versus speed-in-flight is presently used to evaluate the stability characteristics. Positive stability is indicated when an increment in down elevator is required to trim at increased speeds. However, compressibility and aeroelastic effects may introduce reversals in the trim curve with speed—just as power effects do with a propeller airplane—even though the airplane is very stable to disturbances in the angle of attack at a fixed speed. Nevertheless, the airplane may be quite acceptable for the pilot to fly under these conditions. Since this is true, it appears timely to reconsider the basis of the

Received August 17, 1954.
* Design Engineer, Stability and Control.

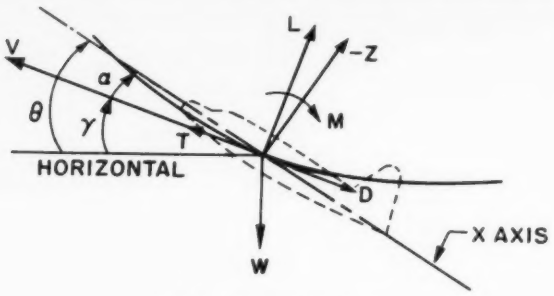

FIG. 1. Coordinate system.

longitudinal stability requirements with an eye toward developing more fitting criteria.

THEORETICAL CONSIDERATIONS

The longitudinal motion considered will be restricted to the plane of symmetry and will allow freedom in the angle of attack, pitch angle, and speed, as shown in Fig. 1. The wind axis system is employed. The elevator will be assumed to be fixed for this part of the analysis.

The stick-fixed equations of motion become:

$$\left.\begin{aligned} &\Delta\alpha(T_\alpha - D_\alpha) + \Delta V(T_V - D_V) - \\ &\qquad (W/qS)\,(\Delta\theta - \Delta\alpha) = (W/g)\,[\dot{V}/(qS)] \\ &\Delta\alpha L_\alpha + \Delta V L_V = (W/g)\,[V/(qS)]\,(\dot{\theta} - \dot{\alpha}) \\ &\Delta\alpha M_\alpha + \dot{\alpha}M_{\dot{\alpha}} + \Delta V M_V + \dot{\theta}M_{\dot{\theta}} = [I_y/(qS_c)]\ddot{\theta} \end{aligned}\right\} \quad (1)$$

where

$$D_\alpha = [1/(qS)]\,(\partial D/\partial\alpha); \quad M_{\dot{\theta}} = [1/(qS_c)]\,(\partial M/\partial\dot{\theta}); \quad \text{etc.}$$

This system of equations may be expanded to yield the characteristic equation of the system:

$$A\lambda^4 + B\lambda^3 + C\lambda^2 + D\lambda + E = 0 \quad (2)$$

where

$$A = (C_L/g)^2 V[I_y/(qS_c)]$$

$$B = -(C_L/g)^2 V(M_\alpha + M_{\dot{\theta}}) + (C_L/g)\,[I_y/(qS_c)]\,[L_\alpha - V(T_V - D_V)]$$

$$C = -[I_y/(qS_c)]\,[(D_\alpha - C_L)L_V + (T_V - D_V)L_\alpha] + (T_V - D_V)C_L(V/g)\,(M_\theta + M_{\dot{\alpha}}) - (C_L/g)\,[L_\alpha M_\theta + C_L(V/g)M_\alpha]$$

$$D = (T_V - D_V)\,[L_\alpha M_\theta + C_L(V/g)M_\alpha] + C_L[M_V C_L(V/g) - L_V M_\alpha] + (D_\alpha - C_L)\,[L_V M_\theta + C_L(V/g)M_V]$$

$$E = C_L(L_\alpha M_V - L_V M_\alpha)$$

Neutral static stability is indicated when $E = 0$. A positive value of E ensures that a pure divergence does not exist, while a negative value of E permits a positive real root, indicative of a pure divergence.

It is evident that the change in moment with speed (M_V), as well as the change in moment with angle of attack (M_α), influences the static stability. A negative value of M_α and a positive value of M_V are in the stable sense. For stable conditions then, increased angle of attack and increased speed result in diving and stalling moments, respectively.

TABLE 1
Airplane Characteristics

Characteristics	Airplane 1 Propeller	Airplane 2 Jet
V	89 knots	528 knots
q	26.6 lbs. per sq.ft.	945
T_V	−0.0020	0
C_D	0.0936	0.0250
D_V	0.00125	0.0000705
D_α	0.634	0
L_V	0.0124	0.000125
C_L	1.13	0.0556
$C_{L\alpha}$	5.73	4.59
M_V	−0.00125	−0.000032
T_e' (Total)	0.30	0.0250
c.g.	31 per cent MAC	44 per cent MAC
M_α	−0.309	−0.115
$M_{\dot{\theta}}$	−0.629	−0.0514
$M_{\dot{\alpha}}$	−0.346	−0.00922
GW	42,200 lbs.	100,000 lbs.
I_Y	500,000 slug-ft.^{2}	1.65×10^6 slug-ft^2
S	1,408 sq.ft.	1,900 sq.ft.
$\bar{c}$	13.08 ft.	20.7 ft.

The quartic equation governing the pitch motion generally yields two oscillatory modes that make up the airplane's response to a disturbance. The short-period motion is generally heavily damped, while the long-period motion—classically called the phugoid motion—is ordinarily lightly damped. In the classical phugoid motion for which $M_V = 0$, the phugoid period is a linear function of speed, theoretically given as $P = 0.138 V_{fps}$. The short-period mode is then primarily a function of M_α and is usually little affected by M_V, *except at center-of-gravity locations which have M_α values near zero.*

If these two motions are stable and adequately damped, the airplane must be considered to have satisfactory stick-fixed longitudinal stability. The stability requirements of reference 3, however, are not expressed in terms of the damping of these motions. The longitudinal stick-fixed stability requirements are expressed therein in terms of the stick-fixed neutral point. The stick-fixed neutral point is defined as the c.g. location at which the elevator position gradient (with changing speed in a steady one-g flight with fixed throttle) is zero.

Mathematically, this condition requires dC_m/dC_L in steady flight to be zero, but

$$dC_m/dC_L = [(\partial C_m/\partial\alpha)/(\partial C_L/\partial\alpha)] + (\partial C_M/\partial V)\,(\partial V/\partial C_L) \quad (3)$$

In steady one-g flight, $\partial V/\partial C_L = -V/(2C_L)$, so at the neutral point,

$$[(\partial C_m/\partial\alpha)/(\partial C_L/\partial\alpha)] - (\partial C_m/\partial V)\,[V/(2C_L)] = 0 \quad (4)$$

It should be noted that in maneuvering flight at constant speed, $\partial V/\partial C_L = 0$, and the effect of a change in pitching moment with speed cannot influence the total value of dC_M/dC_L. It is then possible to have the elevator deflection per g in maneuvering flight

stable at center-of-gravity locations well aft of the neutral point, if $\partial C_M / \partial V$ has a large negative or unstable value.

The dynamic stability with free controls is also of great importance. The stick-free longitudinal motion involves four degrees of freedom with the elevator motion providing the additional degree of freedom above those considered thus far. For a mass balanced control system, the hinge moment equation is given below.

$$\Delta\alpha H_\alpha + \dot{\alpha} H_{\dot{\alpha}} + \theta H_\theta + \Delta\delta H_\delta + \dot{\delta} H_{\dot{\delta}} = [I_e/(qS_e c_e)]\,(\ddot{\theta} + \ddot{\delta}) \quad (5)$$

Equations (1) and (5) will then define the airplane dynamics with the stick-free.

Analysis of Representative Airplanes

To clarify some of the principles involved, two representative airplanes will be considered. The first is a propeller-driven airplane flying at 89 knots in a power-approach condition, the second, a jet airplane flying at Mach 0.8 in the tuck range. The airplane characteristics are tabulated in Table 1.

The stick-fixed, stability quartic $A\lambda^4 + B\lambda^3 + C\lambda^2 + D\lambda + E = 0$ may be factored into two quadratics $(\lambda^2 + A_1\lambda + B_1)$ and $(\lambda^2 + C_1\lambda + D_1)$. These quadratics are representative of the short- and long-period stick-fixed modes. If complex roots denoting an oscillatory mode are assumed—i.e., $\lambda_{1,2} = a \pm ib$—the period and damping of the mode may be determined from the values of a and b.

$$T_{1/2} = 0.693/a$$

and

$$P = 6.28/b$$

It is easily seen that the cycles to one-half amplitude may be determined as

$$C_{1/2} = 0.1104\, b/a$$

The quadratic factors are functions of the center-of-gravity position, and, for certain locations of the c.g., the roots of the quadratic may both be real numbers. The motion is then nonoscillatory in nature and is a pure divergence if one or more roots are positive.

The roots of the quadratic equation defining the stick-fixed short-period motion for both airplanes are plotted on the complex plane in Fig. 2. Inspection of this figure shows that, as the c.g. is moved aft, the imaginary values of the roots disappear, and one real root eventually moves to the right-hand half of the plane where a pure divergent motion is indicated. A pair of lines corresponding to the damping to one-half amplitude in one cycle are also included. It may be seen, as the center of gravity is moved forward, that the roots move farther from the real axis and eventually will cross the $C_{1/2} = 1$ lines. Outside these lines, the damping of the short-period oscillations is poorer, due to excessive static stability. Past experience indicates that the short-period pitch oscillation should damp to

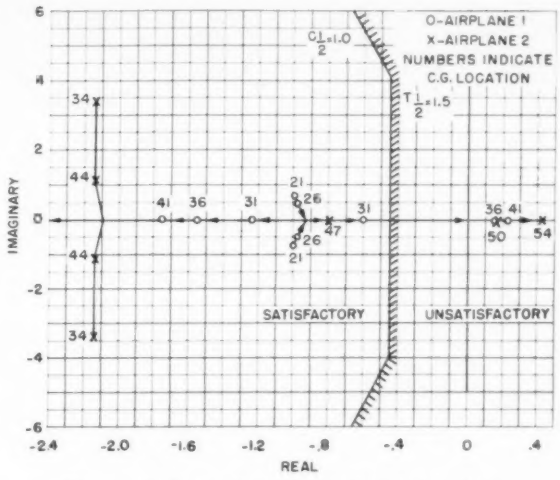

Fig. 2. Roots for stick-fixed short-period motion.

one-half amplitude in one cycle or less. Therefore, certain limits to the roots of the short-period mode are specified.

However, a further stability requirement for the short-period mode is needed. The return to the initial condition after a disturbance should be reasonably rapid. As a tentative value, based on present experience, it is proposed that the time required to damp to one-half amplitude should not exceed 1.5 sec. This requirement will prevent an excessively sluggish airplane response. On the complex plane, this excludes a real root to the right of -0.46.

The two requirements for short-period stick-fixed stability—namely, (1) damping to one-half amplitude in one cycle or less and (2) damping to one-half amplitude in 1.5 sec. or less—will then define an area on the complex plane for satisfactory values of the roots of the stability equations.

It is apparent that these requirements will define the aft limit for the center of gravity of the airplane. For the propeller-driven aircraft under consideration, the aft limit is indicated at 32 per cent MAC. For the jet airplane flying at Mach 0.8 at sea level, the aft limit is at 48.2 per cent MAC.

A comparison of the aft c.g. location with the aerodynamic center, c.g. for divergence, stick-fixed maneuvering neutral point, and the level-flight neutral-point is shown in Table 2.

It is significant to note that, for Airplane 1, this proposed aft c.g. location is 4.4 per cent MAC forward of the aerodynamic center or c.g. at which $\partial C_M/\partial\alpha = 0$, while on Airplane 2, the dynamics criteria aft c.g. is

Table 2
Comparison of Criteria for Aft Center-of-Gravity Location

Airplane	Aerodynamic center $\partial C_M/\partial\alpha = 0$	Stick-fixed maneuvering neutral point	Dynamics criteria aft c.g. stick-fixed	Divergence c.g.	Neutral point
1 (Propeller)	36.4	48.4	32.0	35.0	28.1
2 (Jet)	46.5	55.0	48.2	49.5	20.8

All c.g. locations are per cent MAC.

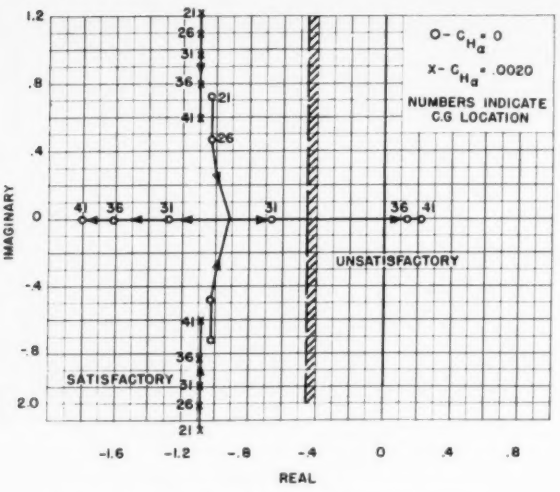

FIG. 3. Roots for stick-free short-period motion.

located at 1.7 per cent aft of the aerodynamic center. Flying at 89 knots, Airplane 1 has a stable dead-beat short-period oscillation over a c.g. range from approximately 28 to 35 per cent MAC but has very sluggish response near 35 per cent MAC. Airplane 2, flying at Mach 0.8, has a stable dead-beat oscillation over a c.g. range from approximately 45.5 per cent MAC to 49.5 per cent MAC. Note also that stick-fixed divergence occurs well forward of the stick-fixed maneuvering neutral point. This is due to the unstable values of $\partial C_M/\partial V$ for the airplanes used as examples.

It is evident that the neutral point has little correlation with the airplane short-period motion for these airplanes with their unstable $\partial C_M/\partial V$ characteristics. At the neutral point, both airplanes have very strong short-period restoring tendencies. Airplane 2, in particular, is extremely stable from a short-period standpoint, the aerodynamic center being 25.7 per cent MAC aft of the neutral point. It is clear that the neutral point is not a reliable means for determining the aft center-of-gravity limit, and a specification that sets the aft c.g. limit as a function of the neutral point may be unnecessarily conservative. Conversely, however, for aircraft with stable values of $\partial C_M/\partial V$, the neutral point could be an unsafe criterion for the aft center-of-gravity limit.

In any discussion of the short-period, longitudinal dynamics, it is, of course, necessary to consider the stick-free case. Calculations of the stick-free dynamics and stick force-per-g have been made for Airplane 1, and the results are shown in Figs. 3 and 4. Two combinations of hinge-moment characteristics were used: $C_{H\alpha} = 0$ and $C_{H\delta} = -0.0040$ per degree; also $C_{H\alpha} = +0.0020$ and $C_{H\delta} = -0.0040$. For the case in which $C_{H\alpha} = 0$, the center-of-gravity location at which $T_{1/2} = 1.5$ sec. is 31.8 per cent MAC; when $C_{H\alpha} = 0.0020$, the comparable c.g. position is approximately 50 per cent MAC. It is seen that for the zero-floating-tendency condition, the stick-fixed and stick-free dynamics are nearly identical. However, from dynamics considerations, a positive $C_{H\alpha}$ can appreciably improve the aft center-of-gravity limit, as shown by the calculations for $C_{H\alpha} = 0.0020$.

Consider the stick force-per-g in a steady pull-up for the two cases with Airplane 1. For this aircraft the minimum acceptable stick force-per-g is 22.5 lbs.-per-g. The aft-most c.g. at which this stick force-per-g requirement is met is 33.1 per cent MAC for $C_{H\alpha} = 0$ and 45.5 per cent MAC for $C_{H\alpha} = 0.0020$. For the case in which $C_{H\alpha} = 0$, the stick-free damping requirements limit the usable aft center-of-gravity location. But, with $C_{H\alpha} = +0.0020$, the stick force-per-g and stick-free dynamics are satisfactory to approximately 45 per cent MAC. This is appreciably aft of the stick-fixed divergence limit of 35 per cent MAC.

In the author's opinion, center-of-gravity positions aft of the stick-fixed divergence point are unsafe, even though the stick-free dynamics and stick force-per-g are satisfactory. An extremely dangerous condition would arise if, with this c.g. position, the aircraft feel is lost somehow, as when there is binding of the controls or failure of the synthetic feel-system. Consequently, the safeguard of a dynamically stable aircraft in the stick-fixed condition is deemed necessary. With this one restriction, however, it is considered that the stick-free dynamics are of more fundamental importance.

The premises upon which the aft center-of-gravity limit is set should be based primarily upon stick-free considerations. It is believed that control force, rather than control position, sensory cues are of overriding importance in the pilot's opinion of aircraft flying qualities. In summary, from consideration of both stick-fixed and stick-free flight, the following requirements for short-period longitudinal stability are proposed. The aft center-of-gravity limit: (1) shall not be behind the c.g. location at which the stick force-per-g is less than a specified value, depending upon airplane type and limit-load factor; and (2) shall be forward of the stick-fixed short-period divergence point. The short-period, dynamic stability characteristics

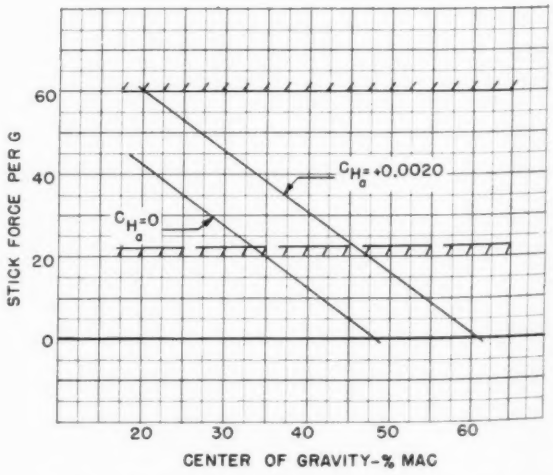

FIG. 4. Characteristics of stick force-per-g, Airplane 1.

shall be such that: (1) the stick-free, short-period, airplane oscillation damps to one-half amplitude within one cycle; and (2) the stick-free, short-period airplane oscillation damps to one-half amplitude within $1^1/_2$ sec.

These latter requirements may also limit the aft loading.

The characteristics of the stick-fixed, long-period motions are not closely related to center-of-gravity location for either of the airplanes considered. Table 3 shows the characteristics of this mode. The main characteristics in common between the two example airplanes are that, as the c.g. is shifted aft to produce an unstable short-period motion, a stable long-period oscillation comes into existence; and the long period mode is most unstable, in both cases, in the area just forward of short-period divergence. It is apparent that the long-period mode cannot be used as a condition to limit the location of the airplane's center of gravity. However, it is believed that some requirement should be specified, relative to the rate of divergence of the long-period mode and in a manner similar to that specified for the rate of divergence of the spiral mode in lateral-directional stability considerations. The analogy between the long-period, longitudinal mode and the spiral mode is strong. Both can be unstable, and yet easily controlled, if the rate of divergence is low.

It is entirely possible that the stick-fixed, long-period longitudinal requirements may be eliminated in favor of stick-free equivalents. The pilot flies almost exclusively by sensations of force with respect to speed changes. To slow an airplane down from any particular trim speed, the stick must first be pulled back to rotate the airplane nose upward, and then repositioned for stabilized trim at the desired speed. In this sequence of operations, the original position reference is lost, and only the force trim reference remains. The same reasoning holds true if a speed build-up is desired; the force reference remains and the position reference is lost.

As previously mentioned, since a mildly divergent, long-period, pitching oscillation can be easily controlled by the pilot, it should be permissible under such conditions as take-off, wave-off, and high-speed runs. However, a limit to the allowable divergence rate should be set. It is recommended that, for the flight conditions under which a stick-free, long-period divergence is tolerable, the motion shall not double in amplitude in less than 8 sec.

In Table 4 are presented the results of the calculations of the long-period, stick-free motion for Airplane 1. Comparing the results for $C_{H_\alpha} = 0$ with the stick-fixed long-period dynamics, it may be seen that the period and damping characteristics are very similar. Aft center-of-gravity movement first results in decreased phugoid stability, and then, as the short-period motion becomes unstable, the long-period motion becomes quite stable. When a value of $C_{H_\alpha} = 0.0020$ is employed, the long-period motion is stable over the c.g. range of the calculations, although it becomes just mildly convergent at a c.g. location of 41 per cent MAC. The very favorable effect of the positive C_{H_α} is apparent. For both cases of $C_{H_\alpha} = 0$ and $C_{H_\alpha} = 0.0020$, the stick-free phugoid divergence-time exceeds the proposed time to double amplitude—of 8 sec. over the c.g. range—which is permissible from short-period considerations. Thus it is satisfactory within the framework of the proposed requirements.

However, in the cruising and climbing conditions, it is necessary that the airplane not require constant attention from the pilot to maintain the desired flight attitude. This requires positive stability under these conditions. Consequently, it is believed that the requirements should demand a pull force to stabilize at a decreased speed and a push force to stabilize at an increased speed in cruising and climbing flight. This force gradient should be of sufficient magnitude to maintain essentially the trim speed after a sharp control displacement and release.

Discussion

In essence, it is proposed that the characteristics of the airplane control forces and short-period motion, rather than the neutral point, be used as the criterion for the determination of the aft loading-limit.

The two airplanes considered have unstable variations of pitching moment with speed, and these exert a large influence on the neutral-point location. In Airplane 1, this is due to power effects; in Airplane 2, the cause is compressibility. Because of the unstable $\partial C_M/\partial V$, the neutral point is very far forward of the center-of-gravity locations where the restoring tendency of the airplane to a pitch disturbance is small.

Table 3
Long-Period Pitching Motion—Stick-Fixed

Airplane	Center of gravity, per cent of MAC	$T_{1/2}$	Period	T_2
1	21	15.4	58.2	..
	26	62.0	..	..
	31	..	..	8.10
	36	2.01	29.3	..
	41	2.52	21.2	..
2	34	34.0	221	..
	44	33.6	225	..
	47	27.3	95.0	..
	50	8.1	41.3	..
	54	29.5	74.7	..

Table 4
Long-Period Pitching Motion—Stick-Free

Airplane	Center of gravity, per cent of MAC	$T_{1/2}$	Period	T_2
		$C_{H_\alpha} = 0$		
1	21	15.9	56.1	...
	26	63	..	...
	31	..	..	8.1
	36	2.06	26.2	...
	41	2.62	20.5	...
		$C_{H_\alpha} = 0.0020$		
	21	18.6	35.8	...
	26	18.0	39.2	...
	31	16.9	45.6	...
	36	15.3	62.5	...
	41	155	..	...

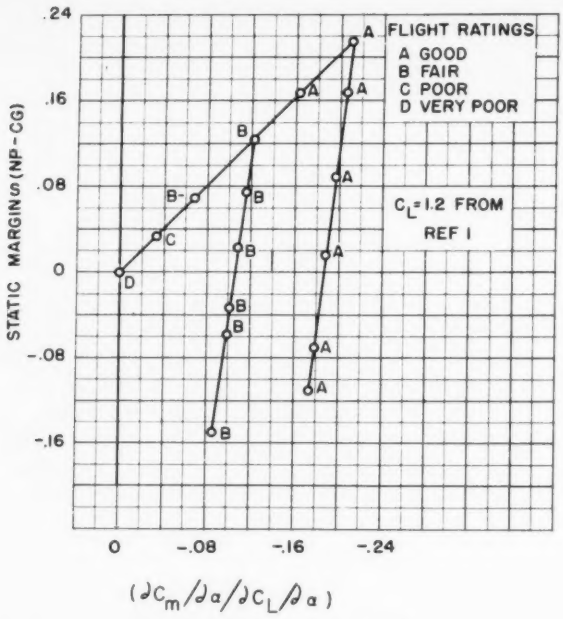

FIG. 5. Longitudinal steadiness.

The long-period mode, which may become unstable due to adverse variations of pitching moment with speed, does not necessarily become more stable as the c.g. is shifted forward. Therefore, it does not appear to be an appropriate criterion for the determination of the aft center-of-gravity limit. However, the motion can be annoying and unacceptable if its rate of divergence is high. Because of this fact, it is considered necessary to put a limit on the rate of divergence of the long-period pitching motion. It is furthermore considered appropriate to require stick-free, long-period, longitudinal stability in cruising and climbing flight.

The fact that the short-period motion is of overriding importance to an airplane's flying qualities has also been demonstrated in the free-flight model tests reported by Schade.[1] In these tests, center-of-gravity shifts, and thrust-line offset were used to obtain various neutral-point locations for particular values of the aerodynamic center. The model flight behavior was then evaluated for numerous combinations. In Fig. 5 the results are re-plotted from reference 1.

It is readily seen that the neutral-point location had negligible effect upon the flight behavior, as rated by the pilots. The important factor was adequate constant-speed stability to produce the strong restoring tendency in the short-period motion. Considerable negative static margin—in terms of neutral point, −11 per cent MAC—still permitted good flying qualitites if enough aerodynamic center margin was present. This aerodynamic center margin is measured by the value of $(\partial C_M/\partial \alpha)/(\partial C_L/\partial \alpha)$.

The requirements that have been advanced are considered to be sufficiently stringent and comprehensive to ensure an aircraft that is safe and one that should be readily accepted by pilots. However, an attempt has been made to formulate the requirements in a manner that stipulates no unnecessarily severe or inappropriate conditions. Although no claim is made that these proposals are inflexible, it is believed that the concept of the specification requirements which has been advanced is important and that an approach of this type will provide better aircraft.

Concluding Remarks

An attempt has been made to improve the longitudinal stability requirements. This problem is considered of importance, since a poorly founded specification requirement can severely limit the utility of an aircraft. Specifically, it has been shown that the steady-flight neutral point has little significance in determining the allowable aft center-of-gravity location. The short-period, dynamic characteristics and the stick force-per-g are considered to be the important factors in determining the allowable aft c.g. location.

The recommended requirements are summarized below. The aft center-of-gravity limit: (1) shall not be behind the c.g. location at which the stick force-per-g is less than a specified value, depending upon airplane type and limit-load factor; and (2) shall be forward of the stick-fixed, short-period divergence point. The short-period dynamic stability characteristics shall be such that: (1) the stick-free, short-period airplane oscillation damps to one-half amplitude within one cycle; and (2) the stick-free, short-period airplane oscillation damps to one-half amplitude within $1^1/_2$ sec.

These latter requirements may also limit the aft loading.

The long-period, stick-free dynamics may be unstable, except in cruising and climbing flight, but the motion shall not double in amplitude in less than 8 sec. In cruising and climbing flight, positive-force stability must exist so that push and pull forces are required to stabilize at speeds above and below trim, respectively. This force gradient should be of sufficient magnitude to maintain essentially the trim speed after a sharp control displacement and release.

Some of the proposed requirements have already been stated in the Air Force and Navy Handling Qualities Specifications[3] and thus conform to generally accepted practice. These specifications, recently unclassified, have provided the basis for flying qualities design of military aircraft from 1948 through 1954. It is clear that the newest concepts introduced in the present pages must be confirmed by specific flight tests.

References

[1] Schade, Robert O., *Free Flight Tunnel Investigation of Dynamic Longitudinal Stability as Influenced by the Static Stability Measured in Wind-Tunnel Force Tests Under Conditions of Constant Thrust and Constant Power*, NACA TN 2075, April, 1950.

[2] Perkins, Courtland D., and Hage, Robert E., *Airplane Performance, Stability and Control*, John Wiley and Sons, 1949.

[3] Anonymous, *Flying Qualities of Piloted Airplanes*, USAF Spec. R-1815B and Navy Spec. SR-119B, June, 1948.

The Effect of a Finite Hub on the Optimum Propeller*

B. W. McCORMICK†
The Pennsylvania State University

ABSTRACT

Goldstein's analysis of a propeller satisfying the Betz condition is extended to the case where the hub radius is appreciable relative to the propeller radius. The solution, which satisfies the boundary conditions of an infinitely long cylinder representing the hub, is expressed as an infinite series of modified Bessel functions. It is shown that to a close approximation the differences between the present case and that with a zero hub radius can be calculated without too much difficulty. Examples are presented which show that for a trailing vortex sheet of given pitch, the insertion of a hub increases the value of the bound circulation of the line vortex generating the sheet. This change is more pronounced the smaller the number of blades.

SYMBOLS

a_m	= coefficients in the Γ-distribution for $r_h \leq r \leq R$
A_m	= coefficients proportional to a_m's
b_m	= coefficients in the Γ-distribution for $r_h \leq r \leq R$
B	= number of blades
C_n	= coefficients in the Γ-distribution for $r > R$
$f_m(\mu)$	= function defined by Eq. (14)
$g_m(\mu)$	= function defined by Eq. (18)
$I_n(x)$	= modified Bessel function of the first kind
$K_n(x)$	= modified Bessel function of the second kind
m	= index
n	= index
r	= radial distance from propeller axis
R	= propeller radius
$S_{1,\nu}(z)$	= Lommel's function
$t_{1,\nu}(\bar{\mu})$	= function defined by Eq. (21)
$T_{1,\nu}(\bar{\mu})$	= function defined by Eq. (22)
v	= advance velocity of the propeller
w	= advance velocity of the helical vortex surfaces
z	= axial distance behind propeller
Γ	= bound circulation
ϵ_m	= small correction to A_m to obtain exact value of a_m
ζ	= independent variable defined by Eq. (4)
θ	= angular coordinate
μ	= independent variable defined by Eq. (4)
ϕ	= velocity potential
ϕ_1	= portion of ϕ as defined by Eq. (11)
ω	= propeller rotational velocity

Subscripts

0	= pertaining to quantities defined at $r = R$
h	= pertaining to quantities defined at the hub radius

Superscript

Note: a bar over an argument indicates that the argument of of the function is given by the product of the unbarred argument with the order of the function.

Received August 26, 1954.

* This work was supported by the Navy Bureau of Ordnance under Contract No. NOrd 7958. The author wishes to acknowledge the assistance of Robert L. Klinedinst and Joseph J. Eisenhuth, members of the Ordnance Research Laboratory, in performing the calculations involved in this study.

† Associate Professor of Engineering Research, Ordnance Research Laboratory.

INTRODUCTION

THE PROBLEM TO BE CONSIDERED is that of calculating the distribution of bound circulation of an optimum propeller, the hub radius of which is relatively large compared to the propeller radius. By optimum propeller is meant a propeller in potential flow which satisfies the Betz condition for minimum energy loss—namely, that the generated trailing vortex sheet, in the steady case, moves as a rigid helicoid. The limiting case of this problem is that of the optimum propeller with a zero hub radius. The classic solution by Goldstein to this problem can be found in reference 1. The present development represents an extension of Goldstein's methods to the more general case of a finite hub. It will be shown that the general case is most easily calculated by considering the difference between it and Goldstein's case. Thus the results which are available for the zero hub case can be applied directly to the more general one as developed here.

Formulation of the Potential Problem

The formulation of the potential problem is nearly identical to Goldstein's case with the exception of the additional boundary condition at the hub surface. If R is the propeller radius, ω the angular velocity, and v the velocity of advance of the propeller, the equations of the trailing vortex sheets are

$$\theta - (\omega z/v) = 0, (2\pi n/B) \qquad n = 1, 2, 3, \ldots \quad (1)$$

for $r_h \leq r \leq R$, where

r, θ, z = polar cylindrical coordinates
B = number of blades
r_h = hub radius

Eq. (1) assumes the propeller to be lightly loaded with the effect of the induced velocities upon the position of the trailing vortex sheets being neglected.

If w is the velocity of advance of the trailing helical vortex surfaces in the z-direction and if ϕ is the velocity potential, then the boundary condition that the velocity normal to the surface of the sheets be zero is

$$\omega r w = \omega r(\partial\phi/\partial z) - (v/r)(\partial\phi/\partial\theta) \qquad (2)$$

for

$$\theta - (\omega z/v) = 0, (2\pi n/B) \qquad r_h \leq r \leq R$$

At the hub surface the condition is imposed that the normal velocity must vanish. If the hub is replaced by an infinitely long circular cylinder of radius r_h,

the imposed boundary condition means that for all θ, it must hold that

$$(\partial\phi/\partial r)_{r=r_h} = 0 \tag{3}$$

In addition to conditions (2) and (3), grad ϕ must vanish as r becomes infinitely large.

From its symmetry, the problem can be reduced to a two-dimensional one with the independent variables being

$$\left.\begin{aligned} \zeta &= \theta - (\omega z/v) \\ \mu &= \omega r/v \end{aligned}\right\} \tag{4}$$

In terms of these new variables, the boundary conditions can be rewritten as

$$(\partial\phi/\partial\zeta)_{\zeta=0,\frac{2\pi n}{B}} = -[\mu^2/(1+\mu^2)] \qquad r_h \leq r \leq R \tag{5}$$

$$(\partial\phi/\partial\mu)_{\mu=\mu_h} = 0 \tag{6}$$

where $\mu_h \equiv \omega r_h/v$.

These boundary conditions take the constant quantity wv/ω temporarily to be unity. The actual ϕ will be given by the product of the ϕ thus obtained and the quantity wv/ω.

The differential equation to be satisfied by ϕ is

$$\nabla^2\phi = 0 \tag{7}$$

which in terms of μ and ζ can be written as

$$[\mu(\partial/\partial\mu)]^2\phi + (1+\mu^2)(\partial^2\phi/\partial\zeta^2) = 0 \tag{8}$$

where the operator

$$[\mu(\partial/\partial\mu)]^2 \equiv \mu(\partial/\partial\mu)\,[\mu(\partial/\partial\mu)]$$

In addition to satisfying Eqs. (5), (6) and (8), the function ϕ must be single valued, have vanishing derivatives as μ becomes infinitely large, and be continuous everywhere except at the vortex sheet.

Solution for $r > R$

For radii larger than the radius of the propeller, the solution of ϕ will take the same form as Goldstein's case—namely,

$$\phi = \sum_{n=1}^{\infty} \frac{2C_n}{B}\,\frac{K_{Bn}(Bn\mu)}{K_{Bn}(Bn\mu_0)}\,\sin Bn\zeta \qquad n = 1, 2, 3, \ldots \tag{9}$$

In the above equation, $K_{Bn}(Bn\mu)$ is the modified Bessel function of the second kind and the C_n's are undetermined constants. The constant μ_0 is defined by

$$\mu_0 \equiv \omega R/v$$

At this time a matter of notation is emphasized. In order to avoid unnecessary writing, a bar notation will be used for the argument of any Bessel function to signify that the argument of the function is given by the product of the term under the bar with the order of the function. For example,

$$I_\nu(\bar{\mu}) \equiv I_\nu(\nu\mu)$$

Using this bar notation, Eq. (9) will become

$$\phi = \sum_{n=1}^{\infty} \frac{2C_n}{B}\,\frac{K_{Bn}(\bar{\mu})}{K_{Bn}(\bar{\mu}_0)}\,\sin Bn\zeta \qquad n = 1, 2, 3, \ldots \tag{10}$$

The constants, C_n, will be determined later from the conditions that ϕ and its derivative be continuous at $\mu = \mu_0$.

Solution for $r_h \leq r \leq R$

In this region the solution for ϕ again follows quite closely the development presented by Goldstein. However the differences between the two are sufficient to warrant a detailed presentation.

Following the lead of reference 1, the velocity potential is assumed to be of the form

$$\phi = -[\mu^2/(1+\mu^2)]\zeta + \phi_1 \tag{11}$$

From Eq. (8), it follows that ϕ_1 must satisfy the following differential equation:

$$[\mu(\partial/\partial\mu)]^2\phi_1 + (1+\mu^2)(\partial^2\phi_1/\partial\zeta^2) = [\mu(\partial/\partial\mu)]^2\,[\mu^2/(1+\mu^2)]\zeta \tag{12}$$

Since ϕ is periodic with ζ only the region for which $0 \leq \zeta \leq (2\pi/B)$ need be considered. In this region, ζ can be expanded in a half-range cosine series

$$\zeta = \frac{\pi}{B} - \frac{8}{\pi B}\sum_{m=0}^{\infty}\frac{\cos[(2m+1)/2]B\zeta}{(2m+1)^2} \tag{13}$$

ϕ_1 is expanded in a semi-infinite cosine series in ζ for this interval

$$\phi_1 = f_0(\mu) + \sum_{m=0}^{\infty} f_m(\mu)\cos\frac{2m+1}{2}B\zeta \tag{14}$$

For Eq. (12) to be satisfied for all values of ζ, it follows that

$$[\mu(\partial/\partial\mu)]^2 f_0(\mu) = (\pi/B)\,[\mu(\partial/\partial\mu)]^2\,[\mu^2/(1+\mu^2)] \tag{15}$$

and

$$\left(\mu\frac{\partial}{\partial\mu}\right)^2 f_m(\mu) - (1+\mu^2)\left[\frac{2m+1}{2}B\right]^2 f_m(\mu) = -\frac{8}{\pi B}\,\frac{1}{(2m+1)^2}\left(\mu\frac{\partial}{\partial\mu}\right)^2\left(\frac{\mu^2}{1+\mu^2}\right) \tag{16}$$

Eq. (15) can be integrated at once to give

$$f_0 = (\pi/B)\,[\mu^2/(1+\mu^2)] + C_0\ln\mu \tag{17}$$

where C_0 is the constant of integration. The second constant of integration was taken to be zero since the level of ϕ is arbitrary.

A new function $g_m(\mu)$ is now defined by

$$f_m(\mu) = -\frac{8}{\pi B}\,\frac{1}{(2m+1)^2}\left[\frac{\mu^2}{1+\mu^2} - g_m(\mu)\right] \tag{18}$$

In terms of $g_m(\mu)$ Eq. (16) becomes

$$\left(z\frac{d}{dz}\right)^2 g_m(z) + \left[z^2 - \left(\frac{2m+1}{2}B\right)^2\right] g_m(z) = z^2 \quad (19)$$

where $z = i[(2m+1)/2]B\mu$.

If ∇_ν is an operator signifying

$$\nabla_\nu \equiv [z(d/dz)]^2 + z^2 - \nu^2$$

then Eq. (19) reads

$$\nabla_{\left(\frac{2m+1}{2}B\right)} g_m(z) = z^2 \quad (20)$$

A particular solution of the above equation is Lommel's function discussed in reference 2. If this particular solution is denoted by $S_{1,\frac{2m+1}{2}B}(z)$ then one form which the solution takes is

$$S_{1,\frac{2m+1}{2}B}(z) = \frac{\frac{2m+1}{2}B\pi}{2\sin\left(\frac{2m+1}{2}\frac{\pi B}{2}\right)} \times I_{\frac{2m+1}{2}B}(\bar{\mu}) - t_{1,\frac{2m+1}{2}B}(\bar{\mu}) + \frac{2m+1}{2}Be^{\left(\frac{2m+1}{2}\frac{\pi B}{2}i\right)} K_{\frac{2m+1}{2}B}(\bar{\mu}) \quad (21)$$

where

$$t_{1,\nu}(x) = \frac{x^2}{2^2-\nu^2} + \frac{x^4}{(2^2-\nu^2)(4^2-\nu^2)} + \frac{x^6}{(2^2-\nu^2)(4^2-\nu^2)(6^2-\nu^2)} + \cdots$$

For two, six, ten . . . bladed propellers the coefficient of the $K_{\frac{2m+1}{2}B}(\bar{\mu})$ is purely imaginary and can be dropped. Goldstein defines Eq. (21) without this term as $T_{1,\frac{2m+1}{2}B}(\bar{\mu})$.

$$T_{1,\frac{2m+1}{2}B}(\bar{\mu}) = S_{1,\frac{2m+1}{2}B}(\bar{\mu}) - \frac{2m+1}{2}Be^{\left(\frac{2m+1}{2}\frac{\pi B}{2}i\right)} K_{\frac{2m+1}{2}B}(\bar{\mu}) = \frac{[(2m+1)/2]B\pi}{2\sin\left(\frac{2m+1}{2}\frac{B\pi}{2}\right)} I_{\frac{2m+1}{2}B}(\bar{\mu}) - t_{1,\frac{2m+1}{2}B}(\bar{\mu}) \quad (22)$$

The function $T_{1,\frac{2m+1}{2}B}(\bar{\mu})$ is also a particular solution of Eq. (20). For four, eight, twelve . . . bladed propellers, the form (21) for $S_{1,\frac{2m+1}{2}B}(\bar{\mu})$ is indeterminate. In this instance the asymptotic solution for $S_{1,\nu}(ix)$ given in reference 2 must be used.

$$T_{1,\nu}(\bar{\mu}) = 1 - \frac{\nu^2}{\bar{\mu}^2} + \frac{\nu^2(\nu^2-2^2)}{\bar{\mu}^4} - \frac{\nu^2(\nu^2-2^2)(\nu^2-4^2)}{\bar{\mu}^6} + \cdots - \nu e^{i\frac{\pi\nu}{2}} K_\nu(\bar{\mu}) \quad (23)$$

The general solution for $g_m(\mu)$ includes the homogeneous solution of Eq. (20) which is a linear combination of the modified Bessel functions of order $[(2m+1)/2]B$ and argument $\bar{\mu}$. Thus $g_m(\mu)$ is given by

$$g_m(\mu) = T_{1,\frac{2m+1}{2}B}(\bar{\mu}) + a_m I_{\frac{2m+1}{2}B}(\bar{\mu}) + b_m K_{\frac{2m+1}{2}B}(\bar{\mu}) \quad (24)$$

Redefining the coefficients a_m, b_m, and C_0 to include the values of the modified Bessel functions for argument of $\bar{\mu}_0$ and the number of blades, expression (11) for ϕ becomes

$$\phi = \sum_{m=0}^{\infty}\left[\frac{8}{\pi B}\frac{T_{1,\frac{2m+1}{2}B}(\bar{\mu})}{(2m+1)^2} + \frac{2a_m}{B}\frac{I_{\frac{2m+1}{2}B}(\bar{\mu})}{I_{\frac{2m+1}{2}B}(\bar{\mu}_0)} + \frac{2b_m}{B}\frac{K_{\frac{2m+1}{2}B}(\bar{\mu})}{K_{\frac{2m+1}{2}B}(\bar{\mu}_0)}\right]\cos\frac{2m+1}{2}B\zeta + C_0\ln\frac{\mu}{\mu_0} \quad (25)$$

In the case of a zero hub radius, the coefficients, b_m, are identically zero since the $K_{\frac{2m+1}{2}B}(\bar{\mu})$ functions are infinite for zero argument. In the general case of a finite hub however, these terms are retained.

The a_m, b_m, and C_0 in the above equation and the C_n in Eq. (10) are to be determined by the three conditions:

(1) ϕ continuous at $r = R$
(2) grad ϕ continuous at $r = R$
(3) $\partial\phi/\partial\mu = 0$ at $r = r_h$

Evaluation of Undetermined Constants

In order to evaluate the coefficients a_m, b_m, C_0, and C_n it is first necessary to express ϕ for $r < R$ in terms of the sine of multiples of ζ. This is accomplished by expanding $\cos[(2m+1)/2]B\zeta$ in a half-range sine series. If this is done then it will be found that in order to satisfy the condition that ϕ be continuous at $r = R$ for all ζ, the following must hold.

$$\frac{8}{\pi}\sum_{m=0}^{\infty}\left[\frac{8}{\pi B}\frac{T_{1,\frac{2m+1}{2}B}(\bar{\mu}_0)}{(2m+1)^2} + \frac{2a_m}{B} + \frac{2b_m}{B}\right]\times\frac{n}{(2n)^2-(2m+1)^2} = \frac{2C_n}{B} \quad (26)$$

Similarly, to satisfy the condition that grad ϕ be continuous at $r = R$ a second relationship is obtained between the coefficients.

$$\sum_{m=0}^{\infty}\frac{4(2m+1)}{4n^2-(2m+1)^2}\left[\frac{8}{\pi B}\frac{T_{1,\frac{2m+1}{2}B}'(\bar{\mu}_0)}{(2m+1)^2} + \frac{2a_m}{B}\frac{I_{\frac{2m+1}{2}B}'(\bar{\mu}_0)}{I_{\frac{2m+1}{2}B}(\bar{\mu}_0)} + \frac{2b_m}{B}\frac{K_{\frac{2m+1}{2}B}'(\bar{\mu}_0)}{K_{\frac{2m+1}{2}B}(\bar{\mu}_0)}\right] = 2\pi\frac{C_n}{B}\frac{K_{Bn}'(\bar{\mu}_0)}{K_{Bn}(\bar{\mu}_0)} \quad (27)$$

and

$$C_0 = 0 \tag{28}$$

A prime in Eq. (27) denotes the derivative of the function with respect to the argument $\bar{\mu}$ and not the independent variable μ.

Finally the condition that $\partial\phi/\partial\mu = 0$ at the surface of the hub results in the following relationship between a_m and b_m.

$$b_m = -\frac{K_{\frac{2m+1}{2}B}(\bar{\mu}_0)}{K_{\frac{2m+1}{2}B}'(\bar{\mu}_h)}\left[a_m\frac{I_{\frac{2m+1}{2}B}'(\bar{\mu}_h)}{I_{\frac{2m+1}{2}B}(\bar{\mu}_0)} + \frac{4}{\pi}\frac{T_{1,\frac{2m+1}{2}B}'(\bar{\mu}_h)}{(2m+1)^2}\right] \tag{29}$$

Eliminating b_m and C_n between Eqs. (26), (27), and (29) results in an infinite number of equations ($n = 1, 2, 3 \ldots$) for the infinite number of unknowns a_m ($m = 0, 1, 2 \ldots$).

$$\frac{\pi}{4}\sum_{m=0}^{\infty}\frac{a_m}{(2n)^2-(2m+1)^2}\left\{(2m+1)\frac{I_{\frac{2m+1}{2}B}'(\bar{\mu}_0)}{I_{\frac{2m+1}{2}B}(\bar{\mu}_0)}\left[1-\frac{K_{\frac{2m+1}{2}B}'(\bar{\mu}_0)}{K_{\frac{2m+1}{2}B}'(\bar{\mu}_h)}\frac{I_{\frac{2m+1}{2}B}'(\bar{\mu}_h)}{I_{\frac{2m+1}{2}B}'(\bar{\mu}_0)}\right]-\right.$$
$$\left.2n\frac{K_{Bn}'(\bar{\mu}_0)}{K_{Bn}(\bar{\mu}_0)}\left[1-\frac{K_{\frac{2m+1}{2}B}(\bar{\mu}_0)}{K_{\frac{2m+1}{2}B}'(\bar{\mu}_h)}\frac{I_{\frac{2m+1}{2}B}'(\bar{\mu}_h)}{I_{\frac{2m+1}{2}B}(\bar{\mu}_0)}\right]\right\} = 2n\frac{K_{Bn}'(\bar{\mu}_0)}{K_{Bn}(\bar{\mu}_0)}\sum_{m=0}^{\infty}\frac{T_{1,\frac{2m+1}{2}B}(\bar{\mu}_0)}{(2m+1)^2[(2n)^2-(2m+1)^2]}\times$$
$$\left[1-\frac{K_{\frac{2m+1}{2}B}(\bar{\mu}_0)}{K_{\frac{2m+1}{2}B}'(\bar{\mu}_h)}\frac{T_{1,\frac{2m+1}{2}B}'(\bar{\mu}_h)}{T_{1,\frac{2m+1}{2}B}(\bar{\mu}_0)}\right]-\sum_{m=0}^{\infty}\frac{T_{1,\frac{2m+1}{2}B}'(\bar{\mu}_0)}{(2m+1)\left[(2n)^2-(2m+1)^2\right]}\times$$
$$\left[1-\frac{K_{\frac{2m+1}{2}B}'(\bar{\mu}_0)}{K_{\frac{2m+1}{2}B}'(\bar{\mu}_h)}\frac{T_{1,\frac{2m+1}{2}B}'(\bar{\mu}_h)}{T_{1,\frac{2m+1}{2}B}'(\bar{\mu}_0)}\right] \tag{30}$$

The effect of the finite hub is evident in the above system of equations. The terms in the square brackets represent the difference between the general case and the zero hub case. Each of these brackets will be close to unity. This will be especially true, the larger the number of blades and the smaller the value of μ_h relative to μ_0.

Calculation of the Bound Circulation

The bound circulation is given by the jump in the velocity potential at the trailing vortex sheets. Remembering that w/ω was taken to be unity, the expression for the bound circulation per blade becomes

$$\frac{B\omega\Gamma}{2\pi w} = \frac{8}{\pi^2}\sum_{m=0}^{\infty}\frac{T_{1,\frac{2m+1}{2}B}(\bar{\mu})}{(2m+1)^2} +$$
$$\frac{2}{\pi}\sum_{m=0}^{\infty}\left[a_m\frac{I_{\frac{2m+1}{2}B}(\bar{\mu})}{I_{\frac{2m+1}{2}B}(\bar{\mu}_0)} + b_m\frac{K_{\frac{2m+1}{2}B}(\bar{\mu})}{K_{\frac{2m+1}{2}B}(\bar{\mu}_0)}\right] \tag{31}$$

Calculation Procedure

Although the values of a_m can be obtained by the standard method of successive approximations, the labor involved was not considered justified for this investigation. Except as a check on the two-bladed case an approximate method which will be described was used to calculate the circulation distributions presented in the figures.

For the approximate calculation of the change in the circulation distribution due to the hub, it is assumed that, compared to the contribution from the b_m terms, the change in the a_m terms can be neglected. With this assumption, the bound circulation for the finite hub case will be given simply by the sum of the b_m terms and the circulation of the zero hub case. If Δ denotes the difference between the circulation with and without a hub, then

$$\Delta\frac{B\omega\Gamma}{2\pi w} = \frac{2}{\pi}\sum_{m=0}^{\infty}b_m\frac{K_{\frac{2m+1}{2}B}(\bar{\mu})}{K_{\frac{2m+1}{2}B}(\bar{\mu}_0)} \tag{32}$$

In order to calculate the b_m's, consider Eq. (29). b_m is composed of two terms, one involving a_m and the other involving $T_{1,\frac{2m+1}{2}B}'(\bar{\mu}_h)$. For $m = 0$, the magnitude of the $T_{1,(B/2)}'(\bar{\mu}_h)$ term is about twice to ten times as large as the magnitude of the a_m term while for larger m, the ratio is even higher. Thus a small error in the value of a_m will not affect the value of b_m to any extent. With this in mind, the approximation is made in the calculation of the b_m's that the a_m values remain unchanged with the addition of a hub. For convenience, these values of a_m given in Goldstein are repeated here.

$$a_m = -[\mu_0^2/(1+\mu_0^2)]A_m + \epsilon_m \tag{33}$$

where $A_0 = 1$, $3A_1 = 1/2$, $5A_2 = (1\cdot3)/(2\cdot4)$, $7A_3 =$

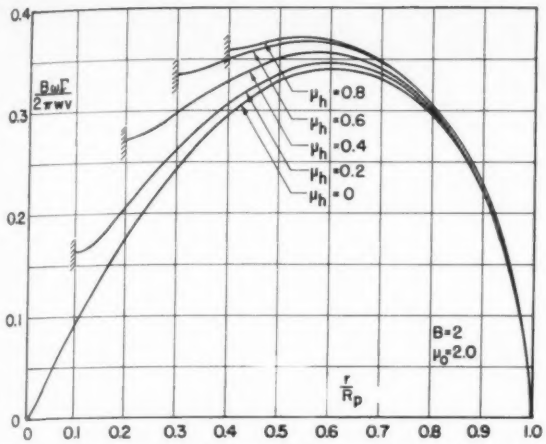

FIG. 1. The effect of different hub sizes on the circulation distribution of a two-bladed propeller.

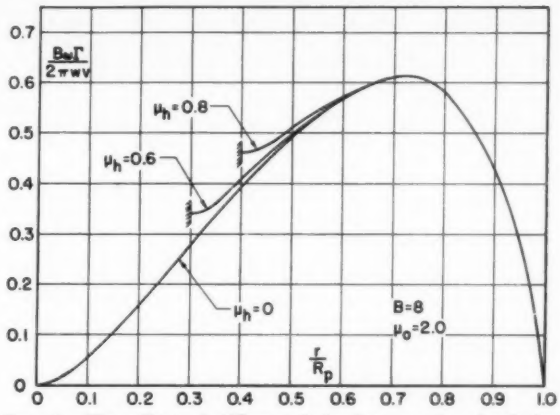

FIG. 2. The effect of different hub sizes on the circulation distribution of an eight-bladed propeller.

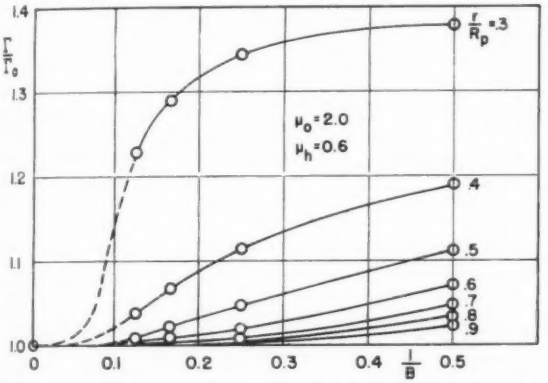

FIG. 3. Ratio of circulation with to without a hub as a function of the number of blades for different values of relative radii.

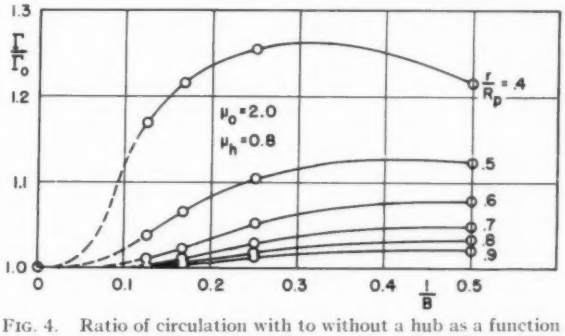

FIG. 4. Ratio of circulation with to without a hub as a function of the number of blades for different values of relative radii.

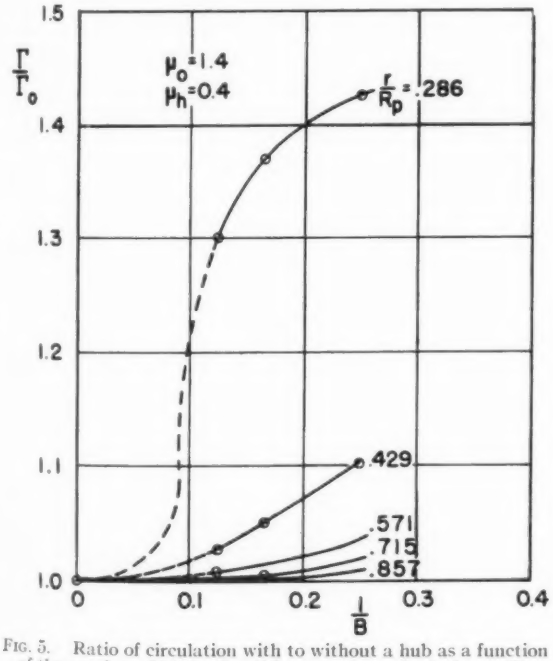

FIG. 5. Ratio of circulation with to without a hub as a function of the number of blades for different values of relative radii.

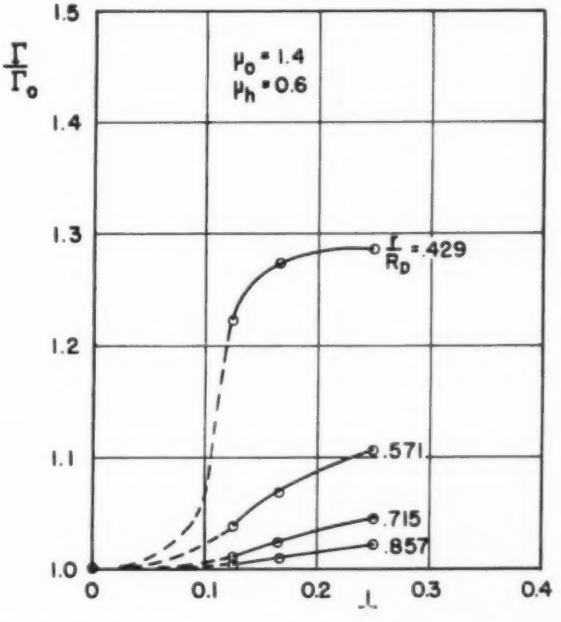

FIG. 6. Ratio of circulation with to without a hub as a function of the number of blades for different values of relative radii.

$(1\cdot3\cdot5)/(2\cdot4\cdot6)$, and for $B = 2$

$$\mu_0 = 2; \quad \epsilon_0 = -0.061, \quad \epsilon_1 = 0.013, \quad \epsilon_2 = \epsilon_3 = \ldots = 0$$

$$\mu_0 = 3; \quad \epsilon_0 = -0.047, \quad \epsilon_1 = 0.007, \quad \epsilon_2 = \epsilon_3 = \ldots = 0$$

$$\mu_0 = 5; \quad \epsilon_0 = -0.033, \quad \epsilon_1 = 0.004, \quad \epsilon_2 = \epsilon_3 = \ldots = 0$$

and for $B > 2$ $\epsilon_m \cong 0$.

These assumptions considerably simplify the calculations. Whether or not they are justified is best answered by considering actual calculations which have been performed. Circulation distributions have been calculated for two-, four-, six-, and eight-bladed propellers with hub radii of 0.3 and 0.4 of the propeller radius for different values of μ_0. In addition, for the two-bladed propeller, hub radii of 0.1 and 0.2 of the propeller radius have also been considered.

Some idea of the errors involved in the assumptions can be obtained from the magnitude of the terms in the square brackets of Eq. (30). It is evident that the larger the number of blades, the larger μ_0, the smaller μ_h, or the larger the index m, the closer these terms will be to unity. For example, for $B = 2$, $\mu_0 = 2$, and $\mu_h = 0.8$ the worst variation from unity for any of the four bracketed terms for $m = 0$ is 5 per cent. For $m = 1$ this difference is even smaller amounting to only 2 per cent. For four blades with the same μ_0 and μ_h, the worst difference for $m = 0$ is reduced to 0.7 per cent and for $m = 1$ amounts to 0.2 per cent. Thus comparable differences in the a_m values would be expected between the zero hub case and the finite hub case.

Another indication of the effect of the approximations is the value of the circulation calculated at μ_0. It was found in the case of two blades, that to the accuracy of the calculations, the circulation did not go to zero at the tip. This, of course, is due to the fact that the a_m's were assumed unchanged by the addition of a hub. However, in none of the cases considered did the calculated circulation at the tip exceed approximately 3 per cent of the maximum circulation. In such cases a first-order correction was made to a_0 to insure that the circulation vanished at the tip.

The system of Eq. (30) for a_m was solved for a_0 for the case of $B = 2$, $\mu_0 = 2$, $\mu_h = 0.6$ by assuming first that $a_1 = a_2 = a_3 = \ldots = 0$ and solving one equation for a_0; then assuming $a_2 = a_3 = a_4 = \ldots 0$ and solving two equations for a_0 and so on up to five equations. The resulting a_0's were expressed as a power series in inverse powers of the number of equations used and the limiting a_0 obtained as the number of equations become infinite. In this case a value of $a_0 = -0.863$ was obtained as compared to a value of -0.861 quoted by Goldstein for the zero hub case.

It is rather difficult to say where the approximate calculations hold or for what conditions they are insufficient. However, in general the approximate method appears satisfactory for more than two blades for not too extreme ranges of μ_0 or μ_h. This means that μ_h should not be much greater than four-tenths of μ_0 and μ_0 no smaller than one. For the two-bladed propeller it appears necessary to solve system (30) for the a_m's for μ_0 less than 2.0.

Results of Calculations

The effect of a finite hub is clearly evident in Fig. 1. In this figure circulation distributions are presented for a two-bladed propeller operating at $\mu_0 = 2$ having relative hub radii of one-, two-, three-, and four-tenths of the propeller radius. The insertion of a hub is seen to have an appreciable influence on the inboard circulation; particularly at the surface of the hub. For example, in the case of Fig. 1, the insertion of a hub having a radius of 0.2 the propeller radius increases the circulation at the 0.2 radius by a factor of 1.56.

Comparison of Fig. 2 with Fig. 1 shows that the effect of a hub is not as pronounced for a larger number of blades. Fig. 2 presents the calculated circulation distributions for an eight-bladed propeller with relative hub radii of 0.3 and 0.4 operating at a μ_0 of 2.0. In addition to Figs. 1 and 2 results which have been calculated to date for two-, four-, six-, and eight-bladed propellers are summarized in Figs. 3, 4, 5, and 6. In these figures which are for specific values of μ_0 and μ_h, the ratio of the bound circulation with a hub to the circulation without a hub is presented as a function of the reciprocal of the number of blades for various values of relative radii.

References

[1] Goldstein, S., *On the Vortex Theory of Screw Propellers*, Proc. Royal Soc. *A123*, 440, 1929.

[2] Watson, G. N., *A Treatise on the Theory of Bessel Functions*, 2nd Ed., 10.71, p. 347, University Press, Cambridge, 1945.

[3] Acharya, Y. V. G., and Janakiram, G., *Circulation Distribution for Six- and Eight-Bladed Propellers*, Appl. Sci. Res., *A3*, 410, 1953.

Readers' Forum

BRIEF REPORTS of investigations in the aeronautical sciences and discussions of papers published in the JOURNAL are presented in this special department. Publication is completed as soon as possible after receipt of the material. The Editorial Committee does not hold itself responsible for the opinions expressed by the correspondents.

Simple Shear Flow Past a Flat Plate in an Incompressible Fluid of Small Viscosity

Ting-Yi Li
Department of Aeronautical Engineering, Rensselaer Polytechnic Institute, Troy, N.Y.
March 28, 1955

IN THE STUDY OF high-speed viscous flow past a two-dimensional body it is usually necessary to consider a curved shock wave emitting from the nose or leading edge of the body. Consequently, there exists an inviscid rotational flow region between the shock wave and the boundary layer. Such a situation arises, for instance, in the study of the hypersonic viscous flow past a flat plate. The situation is somewhat different from Prandtl's classical boundary-layer problem. In Prandtl's original problem the inviscid free stream outside the boundary layer is irrotational while in a hypersonic boundary-layer problem the inviscid free stream must be considered as rotational. The possible effects of vorticity have been recently discussed by Ferri and Libby.[1] In the present paper, the simple shear flow past a flat plate in a fluid of small viscosity is investigated. It can be shown that this problem can again be treated by the boundary-layer approximation, the only novel feature being that the free stream has a constant vorticity. The discussion here is restricted to two-dimensional incompressible steady flow. The basic equations and boundary conditions are expressed in the usual notations as follows:

$$u(\partial u/\partial x) + v(\partial u/\partial y) = \nu(\partial^2 u/\partial y^2) \tag{1}$$

$$(\partial u/\partial x) + (\partial v/\partial y) = 0 \tag{2}$$

$$y = 0, \qquad u = v = 0 \tag{3}$$

$$y \to \infty, \qquad u = u_0 \qquad \partial u/\partial y = \pm\omega_0 \tag{4}$$

where

$$u_\infty = u_0 \pm \omega_0 y \tag{5}$$

Eq. (5) defines a simple shear flow in the undisturbed free stream, u_0 and ω_0 being constants. The vorticity in the free stream is equal to ω_0. Eq. (2) is satisfied if a stream function $\psi(x, y)$ is introduced as follows:

$$u = \partial\psi/\partial y \qquad -v = \partial\psi/\partial x \tag{6}$$

Then the boundary-layer equation and its boundary conditions become

$$(\partial\psi/\partial y)(\partial^2\psi/\partial x\partial y) - (\partial\psi/\partial x)(\partial^2\psi/\partial y^2) = \nu(\partial^3\psi/\partial y^3) \tag{7}$$

$$y = 0 \qquad \partial\psi/\partial x = \partial\psi/\partial y = 0 \tag{8}$$

$$y \to \infty \qquad \partial\psi/\partial y = u_0 \qquad \partial^2\psi/\partial y^2 = \pm\omega_0 \tag{9}$$

Now rewrite the free-stream velocity distribution as follows:

$$u_\infty = u_0[1 \pm (\omega_0 u_0/\sqrt{\nu x/u_0})(y/\sqrt{\nu x/u_0})] \tag{5a}$$

There appear two nondimensional parameters in Eq. (5a)

$$\eta = (y\sqrt{u_0})/\sqrt{\nu x} \qquad \text{Blasius variable} \tag{10}$$

$$\xi = \omega_0 u_0/\sqrt{\nu x/u_0} \qquad \text{"vorticity" number} \tag{11}$$

While η is a familiar variable in boundary-layer studies, ξ is a new parameter in the present problem. Since as $y \to \infty$, the present boundary-layer flow must join smoothly the free stream as given in Eq. (5a), it seems natural to assume that the solution must depend on the "vorticity" number in some manner. Indeed, $u_0/\sqrt{\nu x/u_0} \sim u_0/\delta$, where δ denotes a boundary-layer thickness, represents essentially the average vorticity strength inside the boundary layer. Therefore ξ can be interpreted as a ratio of the free-stream vorticity and the average vorticity in the boundary layer. The boundary-layer approximation implies that a thin layer of *strong* vorticity exists adjacent to the plate surface. Hence the "vorticity" number must be small—i. e., $\xi < 1$. The stream function $\psi(\xi, \eta)$ can therefore be expanded as the following series:

$$\psi = \nu\sqrt{u_0 x/\nu}\,[f_0(\eta) \pm \xi f_1(\eta) + \dots] \tag{12}$$

Substitution of Eq. (12) into Eq. (7) yields

$$u_0^2/x[-(1/2)f_0 f_0'' \pm (1/2)\xi(f_0'f_1' - 2f_0''f_1 - f_0 f_1'') + \dots] = (u_0^2/x)\,[f_0''' \pm \xi f_1''' + \dots] \tag{13}$$

where $d/d\eta$ is denoted by the prime and terms of $0(\xi^2)$ and higher order terms are indicated by the dots. Equating like power terms in ξ from Eq. (13) yields

$$f_0 f_0'' + 2f_0''' = 0 \tag{14}$$

$$2f_1''' + f_0 f_1'' - f_0' f_1' + 2f_0'' f_1 = 0 \tag{15}$$

The boundary conditions become

$$\eta = 0 \qquad f_0 = f_0' = 0 \qquad f_1 = f_1' = 0 \tag{16}$$

$$\eta \to \infty \qquad f_0' = 1 \qquad f_1'' = 1 \tag{17}$$

It is noted that f_0 is the Blasius function and that Eq. (15) is linear in f_1. The solution for f_1 can be obtained by the usual technique. First, taking $f_0 \simeq (1/2)\alpha\eta^2$ for $0 \le \eta \le \eta_1$, one finds the solution f_1 satisfying the conditions of Eq. (16) as follows:

$$f_1 = (2/3)Af_0' \int_0^{\sqrt{\alpha\eta^3/3}} I_{2/3}(\zeta)\,d\zeta/\zeta \qquad \alpha = 0.332 \tag{18}$$

where $I_{2/3}(\zeta)$ is the modified Bessel function of the first kind of the order 2/3. On the other hand, for $\eta_1 \le \eta \le \infty$, taking $f_0 \simeq \eta - \beta$, one finds the solution f_1 satisfying the conditions of Eq. (17) as follows:

$$f_1 = C + 2B\int_\eta^\infty e^{-[(\eta-\beta)^2/4]}\,{}_1F_1\left(1, \frac{1}{2}, \frac{(\eta-\beta)^2}{4}\right) d\eta - \int_\eta^\infty (\eta - \beta)\,d\eta, \qquad \beta = 1.73 \tag{19}$$

where ${}_1F_1(a, c, x)$ denotes the confluent hypergeometric function. The integration constants A, B, and C can be determined uniquely by requiring that f_1, f_1', and f_1'' evaluated at $\eta = \eta_1$ from both Eq. (18) and Eq. (19) are equal. The skin friction τ can be expressed as follows:

$$\tau = \mu(\partial u/\partial y)_{y=0} = (\mu u_0^{3/2}/\sqrt{\nu x})\,[f_0''(0) \pm \xi f_1''(0)] \tag{20}$$

It follows that the local skin-friction coefficient can be given as

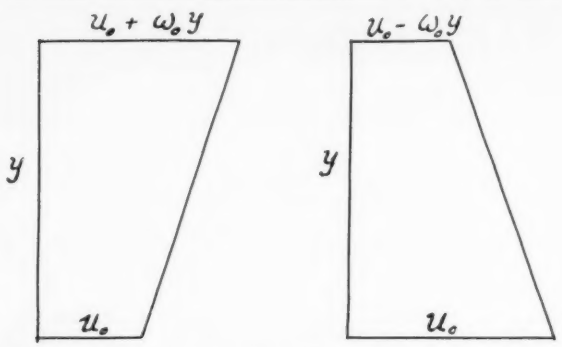

FIG. 1. The undisturbed velocity in the free stream (*left*, type I; *right*, type II).

$$C_f = \frac{\tau}{(1/2)\rho u_0^2} = 2\sqrt{\nu/u_0 x}\,[f_0''(0) \pm \xi f_1''(0)] \qquad (21)$$

In this last formula, $f_0''(0) = \alpha = 0.332$, $f_1''(0)$ can be found from Eq. (18) as

$$f_1''(0) = \frac{3\alpha^{4/3}}{4(3)^{1/3}\Gamma(2/3)} A \qquad (22)$$

Taking $\eta_1 = 3.0$ and using the results of Eqs. (18) and (19), one finds that $A = 3.28$. Thus Eq. (22) yields $f_1''(0) = 0.278$. Hence, C_f becomes

$$C_f = (0.332 \pm 0.278\xi)2\sqrt{\nu/u_0 x} \qquad (21a)$$

Therefore a shear flow of the types I or II (Fig. 1) will tend respectively to cause an increase or decrease of the skin friction on a flat plate. Suppose that in a certain region on the plate surface the average vorticity inside the boundary layer is, say, ten times stronger than the free-stream vorticity—i.e., $\xi = 0.1$—then the local C_f will be affected by the free stream vorticity about ± 8.4 per cent. The displacement thickness can also be calculated as usual. The vorticity effects are again a contribution of a term of the order of ξ. If the present computations are to be carried to ξ^2 terms, it is necessary to consider the pressure change induced by the displacement effect of the boundary layer. Such a refinement, however, has not been carried out at the present. It remains to say a few words of the limitations of the present approach, viz., the series expansion method will be inaccurate for $\xi \simeq 1$. However, it is doubtful whether the boundary-layer approximation is still applicable when the average vorticity in the boundary layer and the free-stream vorticity are of comparable order of magnitude.

REFERENCE

[1] Ferri, A., and Libby, P. A., *Note on an Interaction Between the Boundary Layer and the Inviscid Flow*, Journal of the Aeronautical Sciences, Vol. 21 No. 2, p. 130, February, 1954.

Relative Size of Turbojet Engine Components

D. Willens*
Aerodynamic Engineer, Propulsion Research Corporation, Santa Monica, Calif.
March 31, 1955

ONE OF THE IMPORTANT FACTORS to be considered in turbojet engine design is the engine frontal area. As flight speeds are pushed farther into the supersonic regime, the effect of engine frontal area increases in importance. Thus, it becomes necessary to determine which components are most likely to fix the engine outer diameter. In addition, it is necessary to determine the effect of engine design flight Mach Number upon the component relative sizes.

A brief analysis of this problem was presented in reference 1 for nonafterburning engines. In this note the analysis has been based upon a different set of initial assumptions and extended to include the afterburner and discharge area of the exhaust nozzle.

From the continuity equation, the flow area at any station in the engine can be determined in terms of the area at some reference station from the ratio of the densities and flow velocities at the two stations. The reference area used in this paper is the compressor inlet frontal area (see Fig. 1).

The density at each station in the engine can be determined from the thermodynamic cycle as a function of altitude, flight Mach Number, compressor pressure ratio, turbine inlet temperature and the exhaust nozzle temperature after reheat. The flow velocities, and in some cases the radius ratio, must be stipulated in order to obtain the frontal area of each component.

Although the results presented here are for the engine design point, consideration must be given to the off design operation in order to draw generalized curves which will be applicable over a wide Mach Number range. It has been assumed that the engines resulting from the design point analysis would be operated with constant mechanical r.p.m. at off design flight conditions. Therefore, it was necessary to allow the assumed value for the per cent of sonic flow at Station 1 to vary with flight Mach Number in order to prevent a compressor inlet choked condition at an off design operating point. The curve used for the variation in compressor inlet per cent of sonic flow with flight Mach Number is shown in Fig. 2 and is based on a value of 60 per cent at sea level static. The remainder of the assumptions used to determine the frontal area of the combustor, turbine, afterburner, and exhaust nozzle discharge are listed in Table 1.

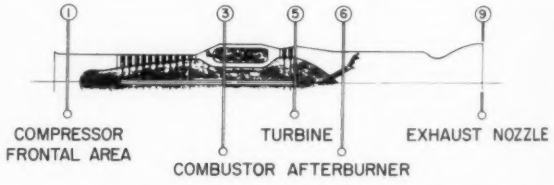

FIG. 1. Schematic engine diagram showing location of component areas.

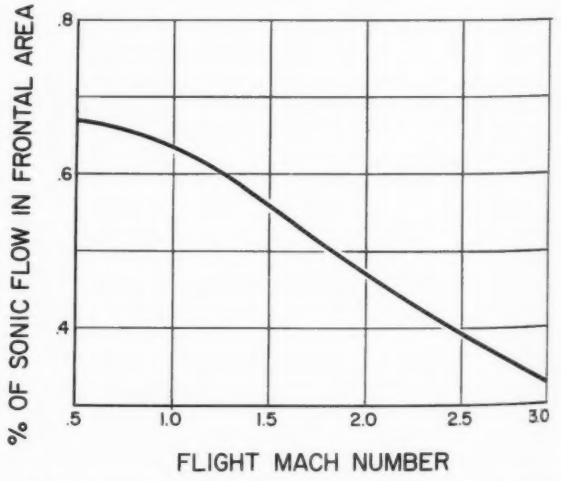

FIG. 2. Assumed variation for per cent of sonic flow in compressor frontal area (Station 1).

* Now, Head, Aero-Thermodynamics Group, Turbo Research Corporation, Santa Monica, Calif.

TABLE 1

(A) Compressor	
(1) per cent sonic flow in frontal area	Fig. 2
(B) Combustion Section	
(1) full annular combustor	
(2) average inlet velocity, ft. per sec.	100
(3) inner-to-outer radius ratio	0.4
(C) Turbine	
(1) average total temperature at first stage nozzle	2,060°R.
(2) first stage nozzle hub ratio	0.8
(3) first stage nozzle discharge angle	25°
(4) first stage nozzle choked	
(5) last stage discharge axial Mach Number	0.5
(6) constant hub diameter	
(D) Afterburner	
(1) average inlet velocity, ft. per sec.	450
(E) Exhaust Nozzle	
(1) average total temperature	3,500°R.
(2) complete expansion to ambient pressure	

In actual practice these quantities may be varied somewhat in order to obtain an optimum design for a given flight application. However, in order to show the important trends due to flight Mach Number and compressor pressure ratio, the values in Table 1 have been held constant.

Figs. 3, 4, 5, and 6 show the effect of compressor pressure ratio (PR_c) and design flight Mach Number on the ratio of frontal area of the various engine components to the frontal area of the compressor. It should be noted that the compressor pressure ratios shown are the values which exist at the various flight Mach Numbers.

Consider first the subsonic flight condition of $M = 0.9$. For a $PR_c = 6$, the turbine is the largest component. Increasing compressor pressure ratio decreases the size of all components relative to the compressor except the exhaust nozzle. At $PR_c = 12$ the compressor is slightly larger than the remaining components.

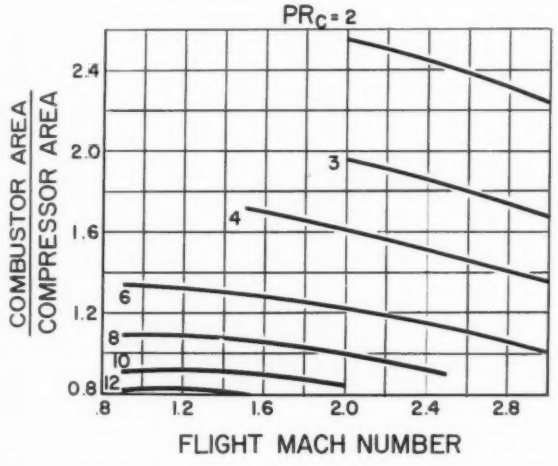

FIG. 3. The ratio of combustor frontal area (Station 3) to compressor frontal area.

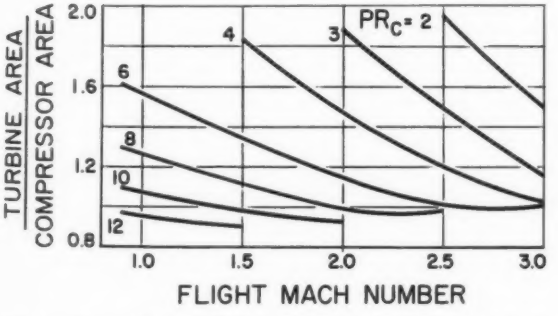

FIG. 4. The ratio of turbine frontal area (Station 5) to compressor frontal area.

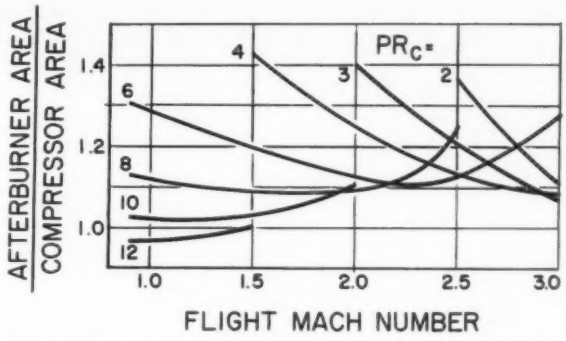

FIG. 5. The ratio of afterburner area (Station 6) to compressor frontal area.

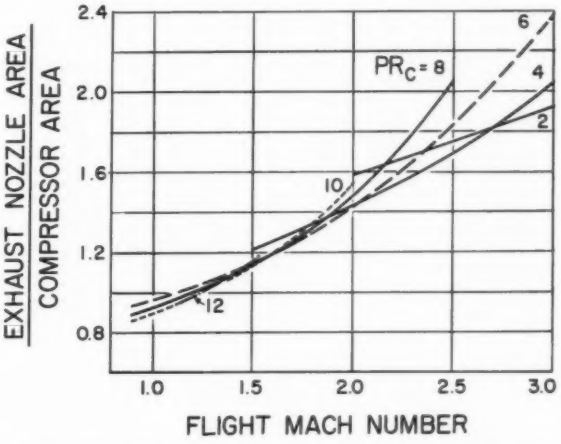

FIG. 6. The ratio of exhaust nozzle area (Station 9) to compressor frontal area.

Consider secondly a flight Mach Number of 2.0. At $PR_c = 4$ the largest component is the completely expanded exhaust nozzle. Increasing compressor pressure ratio to 8 decreases all component sizes except the exhaust nozzle discharge area.

Consider finally a flight Mach Number of 3.0. At $PR_c = 2$ the combustor is the largest component, being 2.24 times the compressor frontal area. This component can be reduced in size by designing the combustor for an inlet velocity greater than the initially assumed value of 100 ft. per sec. Using a higher combustor velocity, it is seen that the exhaust nozzle is now the largest component at 1.92 times the compressor area. At $PR_c = 4$, the largest component is the exhaust nozzle discharge.

To summarize the above results, the frontal area of high pressure ratio turbojet engines designed for an altitude flight Mach Number of 0.9 will be determined by the compressor. For afterburning engines designed for flight Mach Numbers from 2.0 to 3.0 and using an exhaust nozzle with complete expansion to ambient pressure, the maximum frontal area will be at the nozzle discharge.

REFERENCE

[1] Hensley, R. V., Sanders, N. D., and Krebs, R. P., *Performance Potentialities of the Turbojet Engine*, Institute of the Aeronautical Sciences, Preprint No. 148.

Application of Kelly's Theory to Cone-Cylinder-Frustum Bodies of Revolution*

Robert E. Lavender†
Redstone Arsenal, Huntsville, Ala.
March 9, 1955

AN IMPROVEMENT IN THE THEORY of viscous crossflow over bodies of revolution has recently been made by Kelly.[1] Excellent correlation of the normal force and pitching moment variation with angle of attack was obtained between experiment and theory for a series of bodies in both subsonic and supersonic flow. The theory assumes that the axial distribution of the cross-flow drag for an inclined body is similar to the drag for a circular cylinder moving crosswise in a fluid when started impulsively from rest. In addition, the proper cross-flow drag coefficient is assumed to depend upon whether or not the axial flow is laminar or turbulent.

Kelly has applied the theory to cone-cylinders and ogive-cylinders for cases of essentially all laminar or all turbulent axial flow. The application of Kelly's theory to cone-cylinder-frustum bodies (see Fig. 1) is presented in this note and may be used when the axial flow is all laminar, all turbulent, in transition near the cone-cylinder juncture, or in transition near the cylinder-frustum juncture.

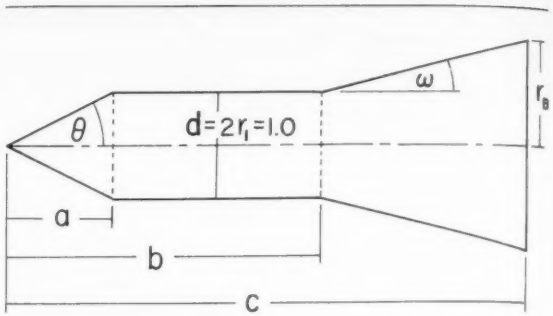

FIG. 1. Cone-cylinder-frustum body of revolution.

The expressions for the additional normal force and pitching moment due to crossflow may be written

$$\frac{S\Delta C_N}{2} = \sin^2\alpha\left[\int_0^a rC_D\,dx + \int_a^b rC_D\,dx + \int_b^c rC_D\,dx\right] \tag{1}$$

and

$$-\frac{Sd\Delta C_M}{2} = \sin^2\alpha\left[\int_0^a rC_D x\,dx + \int_a^b rC_D x\,dx + \int_b^c rC_D x\,dx\right] \tag{2}$$

where

ΔC_N = additional normal force coefficient
ΔC_M = additional pitching moment coefficient about nose
S = reference area
d = reference length

The cross-flow drag coefficient C_D as presented by Kelly is

$$C_D = C_{D_S}\left[A\frac{x}{r}\tan\alpha + B\frac{x^3}{r^3}\tan^3\alpha + D\frac{x^5}{r^5}\tan^5\alpha\right] \tag{3}$$

The steady state value C_{D_S} is considered to be 1.20 for axial laminar flow or 0.35 for axial turbulent flow.

(1) For $0 \le x \le a$; $r = x\tan\theta$, $r_1 \equiv 0.5$

$$\sin^2\alpha\int_0^a rC_D\,dx = C_{D_S}\left[\frac{1}{2}Aa^2\alpha^3 + 2Ba^4\alpha^5 + \left(\frac{Aa^2}{30} + \frac{4Ba^4}{3} + 8Da^6\right)\alpha^7\right] \tag{1A}$$

(2) For $a \le x \le b$, $r = r_1 \equiv 0.5$

$$\sin^2\alpha\int_a^b rC_D\,dx = C_{D_S}\left\{\frac{1}{2}A(b^2-a^2)\alpha^3 + B(b^4-a^4)\alpha^5 + \left[\frac{A(b^2-a^2)}{30} + \frac{2B(b^4-a^4)}{3} + \frac{8D(b^6-a^6)}{3}\right]\alpha^7\right\} \tag{1B}$$

(3) For $b \le x \le c$; $r = r_1 + (x-b)\tan\omega$, $r_1 \equiv 0.5$

$$\sin^2\alpha\int_b^c rC_D\,dx = C_{D_S}\left\{\frac{1}{2}A(c^2-b^2)\alpha^3 + BI_1\alpha^5 + \left[\frac{A(c^2-b^2)}{30} + \frac{2}{3}BI_1 + DI_2\right]\alpha^7\right\} \tag{1C}$$

where

$$I_1 = \int_b^c \frac{x^3\,dx}{[r_1 + (x-b)\tan w]^2} = \cot^4 w\left[\frac{1}{2}(r_B^2 - r_1^2) - 3(r_1 - b\tan w)(r_B - r_1) + 3(r_1 - b\tan w)^2\ln\left(\frac{r_B}{r_1}\right) - (r_1 - b\tan w)^3\left(\frac{1}{r_1} - \frac{1}{r_B}\right)\right]$$

and

$$I_2 = \int_b^c \frac{x^5\,dx}{[r_1 + (x-b)\tan w]^4} = \cot^6 w\left[\frac{1}{2}(r_B^2 - r_1^2) - 5(r_1 - b\tan w)(r_B - r_1) + 10(r_1 - b\tan w)^2\ln\left(\frac{r_B}{r_1}\right) - 10(r_1 - b\tan w)^3\left(\frac{1}{r_1} - \frac{1}{r_B}\right) + \frac{5}{2}(r_1 - b\tan w)^4\left(\frac{1}{r_1^2} - \frac{1}{r_B^2}\right) - \frac{1}{3}(r_1 - b\tan w)^5\left(\frac{1}{r_1^3} - \frac{1}{r_B^3}\right)\right]$$

* Statements and opinions advanced in this note are those of the author and not those of Redstone Arsenal.

† Acting Chief, Aerodynamics Branch, Technical Feasibility Studies Office, Ordnance Missile Laboratories.

Eqs. (1A), (1B), and (1C) are evaluated separately so that the properly C_{D_S} can be used in each region. Then, for any given body, the three equations may be combined in Eq. (1) to obtain a single equation for the addtional normal force. In obtaining the expressions as a function of angle of attack (radians), use was made of the expansions

$$\sin^2\alpha \tan\alpha = \alpha^3 + (\alpha^7/15) + \ldots$$
$$\sin^2\alpha \tan^3\alpha = \alpha^5 + (2\alpha^7/3) + \ldots$$
$$\sin^2\alpha \tan^5\alpha = \alpha^7 + \ldots$$

The evaluation of Eq. (2) is made in a similar manner.

(4) For $0 \leq x \leq a$; $r = x \tan\theta$, $r_1 \equiv 0.5$

$$\sin^2\alpha \int_0^a rC_{D}x\,dx = C_{D_S}\left[\frac{1}{3}Aa^3\alpha^3 + \frac{4}{3}Ba^5\alpha^5 + \left(\frac{Aa^3}{45} + \frac{8Ba^5}{9} + \frac{16Da^7}{3}\right)\alpha^7\right] \tag{2A}$$

(5) For $a \leq x \leq b$; $r = r_1 \equiv 0.5$.

$$\sin^2\alpha \int_a^b rC_{D}x\,dx = C_{D_S}\left\{\frac{1}{3}A(b^3 - a^3)\alpha^3 + \frac{4}{5}B(b^5 - a^5)\alpha^5 + \left[\frac{A(b^3 - a^3)}{45} + \frac{8B(b^5 - a^5)}{15} + \frac{16D(b^7 - a^7)}{7}\right]\alpha^7\right\} \tag{2B}$$

(6) For $b \leq x \leq c$; $r = r_1 + (x - b)\tan w$, $r_1 \equiv 0.5$

$$\sin^2\alpha \int_b^c rC_{D}x\,dx = C_{D_S}\left\{\frac{1}{3}A(c^3 - b^3)\alpha^3 + BI_3\alpha^5 + \left[\frac{A(c^3 - b^3)}{45} + \frac{2}{3}BI_3 + DI_4\right]\alpha^7\right\} \tag{2C}$$

where

$$I_3 = \int_b^c \frac{x^4\,dx}{[r_1 + (x - b)\tan w]^2} = \cot^5 w\left[\frac{1}{3}(r_B^3 - r_1^3) - 2(r_1 - b\tan w)(r_B^2 - r_1^2) + 6(r_1 - b\tan w)^2(r_B - r_1) - 4(r_1 - b\tan w)^3 \ln\left(\frac{r_B}{r_1}\right) + (r_1 - b\tan w)^4\left(\frac{1}{r_1} - \frac{1}{r_B}\right)\right]$$

and

$$I_4 = \int_b^c \frac{x^6\,dx}{[r_1 + (x - b)\tan w]^4} = \cot^7 w\left[\frac{1}{3}(r_B^3 - r_1^3) - 3(r_1 - b\tan w)(r_B^2 - r_1^2) + 15(r_1 - b\tan w)^2(r_B - r_1) - 20(r_1 - b\tan w)^3 \ln\left(\frac{r_B}{r_1}\right) + 15(r_1 - b\tan w)^4\left(\frac{1}{r_1} - \frac{1}{r_B}\right) - 3(r_1 - b\tan w)^5\left(\frac{1}{r_1^2} - \frac{1}{r_B^2}\right) + \frac{1}{3}(r_1 - b\tan w)^6\left(\frac{1}{r_1^3} - \frac{1}{r_B^3}\right)\right]$$

The coefficients of α^3, α^5, and α^7 in Eqs. (2A), (2B), and (2C) are also evaluated using the proper C_{D_S} for each region. The equations may then be substituted into Eq. (2) so that a single equation is obtained for the additional moment coefficient.

Use of the above equations enable one to correlate experimental data with the theory at low Reynolds Numbers and then to extend the calculations to higher Reynolds Numbers.

Reference

[1] Kelly, Howard, R., *The Estimation of Normal Force and Pitching Moment Coefficients for Blunt-Based Bodies of Revolution at Large Angles of Attack*, NOTS Tech. Memo 998, May, 1953.

Estimation of the Lift and Moment Parameters of Leading-Edge Flaps

Malcolm J. Abzug
Design Specialist, Aerodynamics, Douglas Aircraft Company, Inc., El Segundo, Calif.
April 11, 1955

THE AERODYNAMIC LIFT and moment parameters of leading-edge flaps may be obtained from trailing-edge flap theory[1] or from tests of wings with trailing-edge flaps by means of a simple geometrical transformation. This transformation is illustrated in Fig. 1, where two flapped airfoils presenting identical profiles to the relative wind are shown. Letting primed values refer to the leading-edge flap case:

$$\alpha' = \alpha + \delta \tag{1}$$
$$\delta' = -\delta \tag{2}$$
$$c_f'/c = 1 - c_f/c \tag{3}$$

Also, $c_l' = c_l$ and $c_m' = c_m$.

Using conventional NACA shorthand notation,[2] the lifting effectiveness of a leading-edge flap may be expressed in terms of linearized trailing-edge flap parameters as follows:

$$c_l = c_{l_\alpha}(\alpha - \alpha_\delta\delta)$$
$$= c_{l_\alpha}[\alpha' + \delta'(1 + \alpha_\delta)]$$

Differentiating with respect to δ' at constant section lift:

$$(\partial\alpha'/\partial\delta')_{c_l} = \alpha_\delta' = -1 - \alpha_\delta \tag{4}$$

Differentiating with respect to δ' at constant α':

$$c_{l_\delta}' = -\alpha_\delta' c_{l_\alpha} \tag{5}$$

In a like manner, it can be shown that at constant section lift:

$$c_{m_\delta}' = -c_{m_\delta} \tag{6}$$

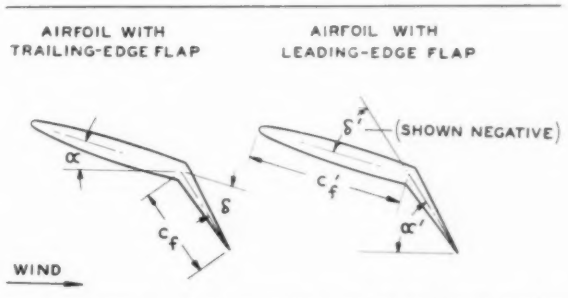

FIG. 1. Flapped airfoils presenting identical profiles to relative wind.

Using Eqs. (3) and (4), the leading-edge flap lifting effectiveness parameter α_δ' is compared with the theoretical trailing-edge flap value for incompressible flow[3] in Fig. 2. This figure shows that the lifting or control effectiveness of narrow-chord leading-edge flaps at subsonic speeds is many times less than that of narrow-chord trailing-edge flaps.

Comparisons of theoretical and experimental section lift and moment coefficients for two leading-edge flaps[4, 5] are presented in Fig. 3. Reasonably good agreement is indicated.

References

[1] Glauert, H., *Theoretical Relationships for an Aerofoil with Hinged Flap*, R&M 1095, 1927.

[2] Dods, Jules B., Jr., *Estimation of Low-Speed Lift and Hinge-Moment Parameters for Full-Span Trailing-Edge Flaps on Lifting Surfaces With and Without Sweepback*, NACA TN 2288, February, 1951.

[3] Ames, Milton B., Jr., and Sears, Richard I., *Determination of Control-Surface Characteristics from NACA Plain-Flap and Tab Data*, NACA Report No. 721, 1941.

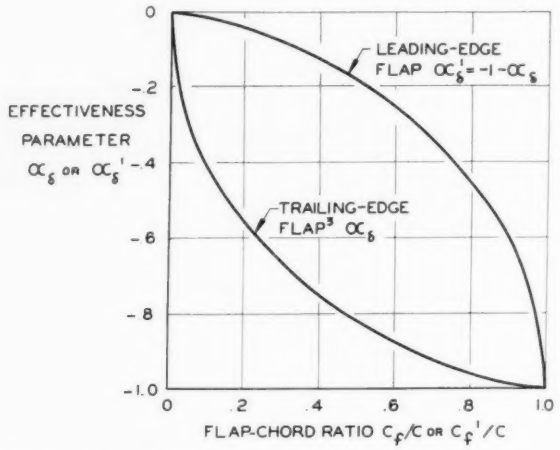

FIG. 2. Theoretical incompressible leading- and trailing-edge flap effectiveness parameters.

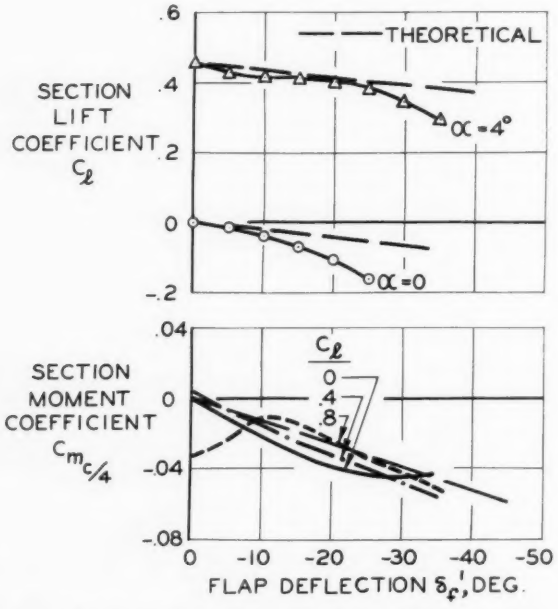

FIG. 3A. Comparisons of theoretical and experimental section lift and moment coefficients for leading-edge flaps, double wedge airfoil,[4] $c_f'/c = 0.12$.

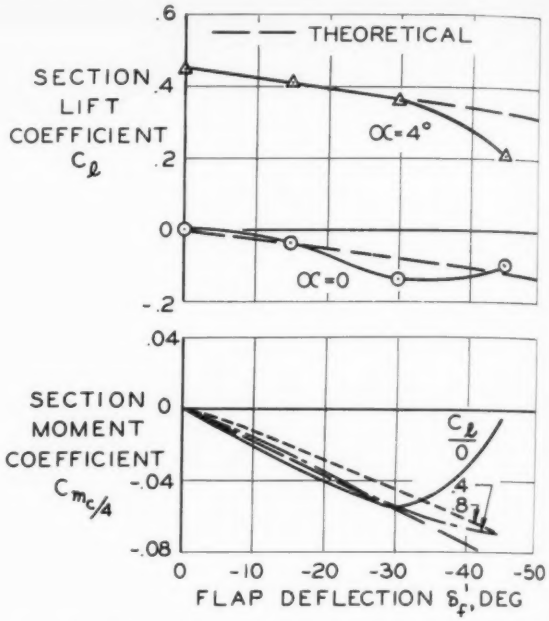

FIG. 3B. Comparisons of theoretical and experimental section lift and moment coefficients for leading-edge flaps, NACA 64A010 Airfoil,[5] $c_f'/c = 0.15$.

[4] Rose, Leonard M., and Altman, John M., *Low-Speed Investigation of a Thin, Faired, Double-Wedge Airfoil Section with Nose Flaps of Various Chords*, NACA TN 2018, February, 1950.

[5] Kelly, John A., and Hayter, Nora-Lee F., *Lift and Pitching Moment at Low Speeds of the NACA 64A010 Airfoil Section Equipped with Various Combinations of a Leading-Edge Slat, Leading-Edge Flap, Split Flap, and Double-Slotted Flap*, NACA TN 3007, September, 1953.

Remarks on "An Exact Solution for Two-Dimensional Linear Panel Flutter at Supersonic Speeds"

S. F. Shen

Associate Professor, Department of Aeronautical Engineering, University of Maryland, College Park, Md.

April 25, 1955

IN A RECENT NOTE,[1] Goland and Luke gave an "exact solution" of the panel flutter problem at supersonic speeds, based upon the integro-differential equation of motion employing the linearized aerodynamic pressure without other assumptions. The solution in Laplace transform was neatly formulated, although numerical results were not given. However, certain conclusions were drawn near the end of reference 1. Because of the "exact" nature of the treatment, these conclusions are likely to receive wide attention. For this reason, it is felt that some clarifying remarks are in order. We shall show that their conclusions are open to question by means of a simplified example. A more careful attitude toward assessing flutter instability will also be emphasized.

In reference 1, Goland and Luke defined a parameter γ which is roughly proportional to the ratio of the dynamic pressure to the inertia running load at the fundamental natural frequency. For $\gamma >> 1$, the important conclusion was that *flutter of both plate and membrane cannot occur*. "It can also be shown without difficulty that flutter cannot occur for the membrane if the Mach Number M is sufficiently large."* It should be noted here that they were

* Quotations in this note are all taken from reference 1.

really seeking the mode shape in which the panel is capable of a self-excited simple harmonic motion. By "flutter" was meant the existence of such a mode.

In this light, then, the nonexistence of a mode shape capable of self-excited simple harmonic motion, or at least an almost simple harmonic motion, at any γ, is indeed physically difficult to visualize. By going to higher and higher modes, hence frequencies, the inertia loading seems always able to attain such a magnitude as to be of the same order as the elastic and aerodynamic loadings. And, for the very highest modes, the inertia loading can always so completely dominate the aerodynamic loading that the normal modes and frequencies at the high end of the spectrum would not be seriously affected by the presence of air. More precisely, we mean here that the asymptotic behavior for the higher modes at given γ should be $[\omega(\gamma)]/\omega(0)] \sim 1 + o(1)$, where $\omega(\gamma)$ is the frequency for the given γ. The term $o(1)$ may of course be complex, indicating some amplification or decay with time. But a mode would still exist. The conclusion of reference 1 is apparently contradictory to this reasoning.

Analytically, the explanation probably lies in the limiting process which led to Eq. (19) of reference 1. While not stated in detail, the derivation of Eq. (19) must have been made by formally letting $\gamma \to \infty$ in Eq. (14) but keeping all other parameters (including the frequency as the eigenvalue) constant. Such a procedure clearly rules out the possibility that the frequency parameter may grow without limit, given a fixed γ, however large it may be.

To illustrate the inadequacy of such a limiting process, we consider the following elementary problem:

$$\left.\begin{aligned} z'' - \gamma z' + \alpha^2 k^2 z = 0 \\ z(0) = 0, \quad z(2) = 0 \end{aligned}\right\} \tag{1}$$

where symbols in reference 1 are used. This corresponds to essentially a certain membrane problem with quasi-steady aerodynamic forces. Applying the Laplace transform,

$$(p^2 - \gamma p + \alpha^2 k^2)\bar{z} = z_{x0} \tag{2}$$

or

$$\bar{z}(p)/z_{x0} = (p^2 - \gamma p + \alpha^2 k^2)^{-1} \tag{3}$$

Letting formally $\gamma \to \infty$,

$$\bar{z}(p)/z_{x0} \cong p^{-1}(p - \gamma)^{-1} \tag{4}$$

or, finding the inverse transform,

$$z(x)/z_{x0} \cong -(1 - e^{\gamma x})/\gamma \tag{5}$$

Comparing against Eq. (19) of reference 1, we see that again here the dominant term is $e^{\gamma x}/\gamma$. One would have to conclude likewise that "for large γ a physically feasible flutter mode is nonexistent."

Actually, this elementary problem can be solved explicitly to yield

$$z(x)/z_{x0} = (2/n\pi)e^{\gamma x/2} \sin(n\pi x/2) \qquad n = 1, 2, 3, \ldots, \tag{6}$$

with $2\alpha k = \sqrt{n^2\pi^2 + \gamma^2}$, to satisfy both end conditions. The fact that k increases with γ reveals itself. It may be noted that our elementary problem belongs to the classical Sturm-Liouville problem, for which the behaviors of eigenvalues and functions are well-known. The direct calculation above is merely to bring out the result in a transparent manner.

At the risk of causing a controversy, we take this opportunity to emphasize that, even if a possible mode should exist for the assumed simple-harmonic motion, without other clues it may not be correct to conclude that there is flutter instability. Obviously here only the condition for marginal stability is fulfilled. Our elementary problem defined by Eq. (1) and solved by Eq. (6) is an example. In this example, regardless of the value of γ, its effect, provided real, is simply to modify the mode shape and the frequency which goes with the mode. There is a continuous change of the mode shape and frequency with a continuous change of the parameter γ from zero upward. The motion is always neutrally stable. It corresponds to nothing more than the natural vibrations with $\gamma \neq 0$.

To confirm flutter instability, our belief is that divergent motion must be shown to exist on one side of the "flutter boundary." The job is admittedly not trivial, but probably essential in panel flutter since our example suggests that wrong interpretation may result otherwise. We have made certain investigations along this line, proposing to treat panel flutter as a complex eigenvalue problem.[2] It is hoped that the results will be summarized in a forthcoming report.

References

[1] Goland, M., and Luke, Y. L., *An Exact Solution for Two-Dimensional Linear Panel Flutter at Supersonic Speeds*, Journal of the Aeronautical Sciences, Vol. 21, No. 4, pp. 275–276, April, 1954.

[2] Shen, S. F., *Supersonic Flutter of Two-Dimensional Panels*, Presented at the Supersonic Conference, Co-sponsored by the University of Maryland and the Institute of the Aeronautical Sciences, University of Maryland, College Park, Md., May 19–20, 1954.

On the Flow Behind an Attached Curved Shock

S. I. Pai

Associate Research Professor, Institute for Fluid Dynamics and Applied Mathematics, University of Maryland, College Park, Md.

April 28, 1955

In a recent paper,[1] Eggers, Savin, and Syverston mention that in my analysis[2] of the flow behind an attached curved shock, the entropy gradient is neglected. This statement is definitely untrue. In my final results, [Eqs. (59) and (60) of reference 2] the effect of entropy variation is included.

The essential feature of this problem is shown in Fig. 1. The disturbance at any point, say "3", may be roughly decomposed into two parts: One is the basic disturbance which depends mainly on the local slope at 3—i.e., 3–4 in Fig. 1—and the other is the reflected disturbance—i.e., 2–3 in Fig. 1—which depends on the so-called "reflection factor" at the shock (point 2) as well as the basic disturbance from 1—i.e., 1–2 in Fig. 1. Eggins, Savin, and Syvertson try to show that the reflection factor is small so that the reflected disturbance 2–3 is negligible in comparison to basic disturbance 3–4. But they forget that the reflected disturbance depends not only on the reflection factor but also on the disturbance 1–2. If the disturbance 1–2 is much larger than 3–4, the reflected disturbance 2–3 may not be small in comparison with 3–4 even though the reflection factor is small.

In my analysis, I did not separate the disturbance locally in the manner shown in Fig. 1, but considered simultaneously the *whole* shape of the body and the entropy variation. In Eq. (59), the reflected disturbance includes both the effect of the so-called "reflection factor" of Eggins, etc., and also the incident disturb-

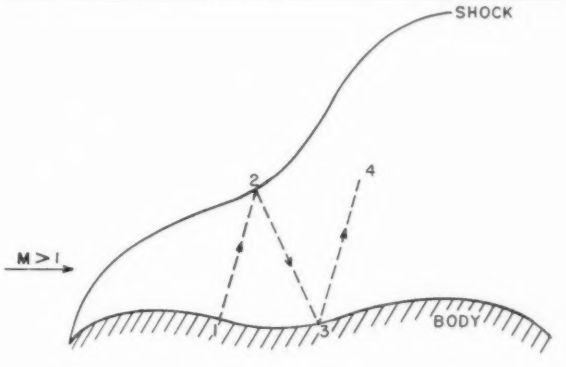

Fig. 1: FLOW BEHIND AN ATTACHED CURVED SHOCK.

ances. In this manner, we can not and should not use a single reflection factor to determine the magnitude of the reflected disturbance.

I had discussed this point with Mr. Syvertson in several communications. My "reflection factor" is not the same thing as his "reflection factor." My reflection factor is so defined that it is convenient to use in my analysis. I do not believe that any single reflection factor could be used to determine the total reflected disturbance. One should also consider the effect of incident disturbance simultaneously—i.e., the shape of the body in front of the point considered. Eggins, Savin, and Syvertson's analysis can at most apply to bodies whose slopes at every point are almost the same—i.e., disturbance 1–2 is almost the same as 3–4. In my analysis, there is no such restriction and I did not "partially neglect" the entropy gradient. In some numerical examples,[3] I found that the resultant disturbance differs considerably from the basic disturbance which shows that in those cases, the reflected disturbances are not negligible.

References

[1] Eggers, A. J., Jr., Savin, R. C., and Syvertson, C. A., *The Generalized Shock Expansion Method and its Application to Bodies Traveling at High Supersonic Air Speeds*, Journal of the Aeronautical Sciences, Vol. 22, No. 4, pp. 231–238, April, 1955.

[2] Pai, S. I., *On the Flow Behind an Attached Curved Shock*, Journal of the Aeronautical Sciences, Vol. 19, No. 11, pp. 734–742, November, 1952.

[3] Pai, S. I., *Supersonic Rotational Flow over Two-Dimensional Ogives*, Proceedings, 3rd Midwestern Conference on Fluid Mechanics, University of Minnesota, pp. 303–317, 1953.

Free Streamline Analysis for Slotted Two-Dimensional Supersonic Minimum-Length Nozzles

Robert Wesley Truitt
Professor of Aeronautical Engineering, Virginia Polytechnic Institute, Blacksburg, Virginia

May 10, 1955

The attainment of a given supersonic Mach Number in a constant cross-section two-dimensional slotted test section would require, under *minimum-length* conditions, a certain ratio of slot width to working section width. The condition for the absolute minimum-length symmetric nozzle is shown schematically in Fig. 1. The angle ν is the Prandtl-Meyer deflection such that

$$\nu = \nu'/2 \qquad (1)$$

ν' being the deflection of a sonic stream necessary to produce a given working section Mach Number M'. The solid lines show the conditions of the solid-wall supersonic nozzle; the broken line represents the transonic-type constant cross section with fixed-width slot. The length, d, is the minimum possible for M'. It is clear from Fig. 1 that, if the nozzle section is kept constant, a Mach Number, $M' > 1$, would require a certain mass rate of flow through the slotted wall. The fluid mass will have the velocity, v_2, normal to the slotted wall.

Single or Multislot

A cross section of the ideal flow conditions for a multislotted wall in region 2 may be depicted as shown in Fig. 2a. Due to symmetry, the flow may be simplified to that in Fig. 2b, where w is taken as the tunnel width; L is the actual slot width; $L'/L = \eta$, the contraction coefficient.

The analysis will be made assuming the flow through the slot (s) is the same type as the compressible *free streamline* flow through a two-dimensional orifice treated by Busemann.[1]

In a transonic-type working section, the pressure, p', and density, ρ', in the pressure chamber are the same as in the test

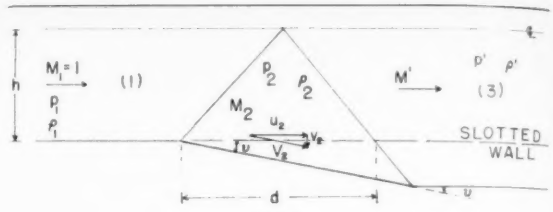

FIG 1

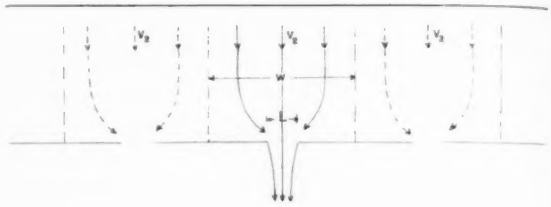

FIG 2a

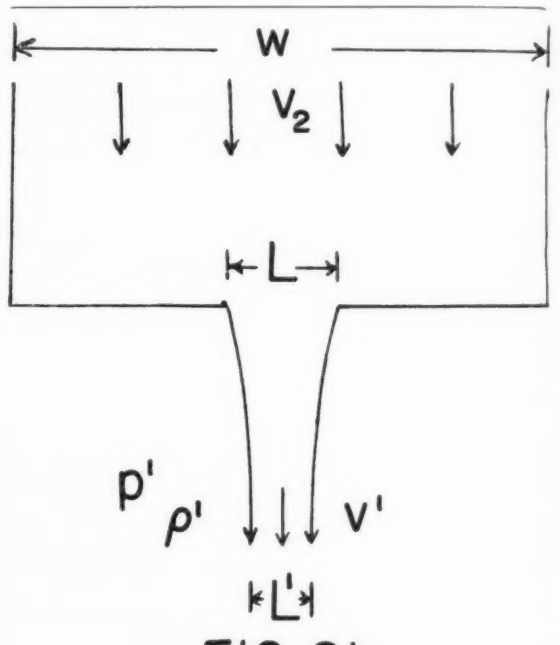

FIG. 2b

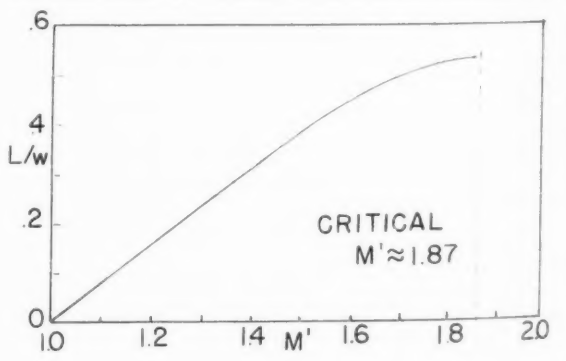

FIG. 3

section. Therefore, for any cross section of the slotted wall in the length, d, we may apply the continuity equation as (see Fig. 2b):

$$\rho_2 v_2 \bar{w} = \rho' v' L'$$

$$\text{or} \quad \rho_2 v_2 w = \rho' v' \eta L \tag{2}$$

where ρ_2 and v_2 are the mass density and normal velocity component, respectively, in region 2.

The required ratio of tunnel width to slot width is then

$$w/L = \eta(\rho'/\rho_2)(v'/v_2) \tag{3}$$

Along the centerline stream line, between region 2 and the pressure chamber, Bernoulli's compressible equation may be applied to get

$$v' = \sqrt{v_2^2 + [2\gamma/\gamma - 1]\{(p_2/\rho_2) - (p'/\rho')\}} \tag{4}$$

Eq. (4) assumes isentropic flow between region 2 and the pressure chamber so that

$$\frac{p_2}{p'} = \left\{\frac{1 + [(\gamma - 1)/2]M'^2}{1 + [(\gamma - 1)/2]M_2^2}\right\}^{\gamma/\gamma - 1} \tag{5}$$

and

$$p_2/p' = (\rho_2/\rho')^\gamma \tag{6}$$

Using Eqs. (4), (5), and (6), Eq. (3) becomes

$$\frac{w}{L} = \eta \left\{\frac{1 + [(\gamma - 1)/2]M_2^2}{1 + [(\gamma - 1)/2]M'^2}\right\}^{1/\gamma - 1} \sqrt{1 + \frac{2\gamma p'}{(\gamma - 1)v_2^2 \rho'} \left\{\frac{1 + [(\gamma - 1)/2]M'^2}{1 + [(\gamma - 1)/2]M_2^2} - 1\right\}} \tag{7}$$

Busemann's solution for the compressible contraction coefficient for the two-dimensional orifice may be written for the present case as [1]

$$\eta = \frac{\pi}{\pi + 2\sqrt{1 - (v'/c')^2}} \tag{8}$$

From Eqs. (4), (5), and (6) we may write

$$\left(\frac{v'}{c'}\right)^2 = \left(\frac{v_2}{c'}\right)^2 + \frac{2}{\gamma - 1}\left\{\frac{1 + [(\gamma - 1)/2]M'^2}{1 + [(\gamma - 1)/2]M_2^2} - 1\right\} \tag{9}$$

Using Eqs (8) and (9) and the relation for the speed of sound at L' as

$$c'^2 = \frac{\gamma p'}{\rho'} \tag{10}$$

Eq. (7) becomes

$$\frac{w}{L} = \frac{\pi \left\{\frac{1 + [(\gamma - 1)/2]M_2^2}{1 + [(\gamma - 1)/2]M'^2}\right\}^{1/\gamma - 1}}{\pi + 2\sqrt{1 - \left(\frac{v_2}{c'}\right)^2 - \frac{2}{\gamma - 1}\left\{\frac{1 + [(\gamma - 1)/2]M'^2}{1 + [(\gamma - 1)/2]M_2^2} - 1\right\}}} \sqrt{1 + \frac{2}{\gamma - 1}\left(\frac{c'}{v_2}\right)^2 \left\{\frac{1 + [(\gamma - 1)/2]M'^2}{1 + [(\gamma - 1)/2]M_2^2} - 1\right\}} \tag{11}$$

From Fig. 1

$$v_2 = V_2 \sin \nu = M_2\sqrt{\gamma p_2/\rho_2} \sin \nu \tag{12}$$

and from Eq. (10)

$$v_2/c' = M_2\sqrt{(p_2/p')(\rho'/\rho_2)} \sin \nu \tag{13}$$

Using Eqs. (5) and (6), Eq. (13) may be written as

$$\frac{v_2}{c'} = M_2(\sin \nu)\sqrt{\frac{1 + [(\gamma - 1)/2]M'^2}{1 + [(\gamma - 1)/2]M_2^2}} \tag{14}$$

Substituting Eq. (14) into Eq. (11) gives the required relation

$$\frac{w}{L} = \frac{\left\{\frac{1 + [(\gamma - 1)/2]M_2^2}{1 + [(\gamma - 1)/2]M'^2}\right\}^{1/\gamma - 1} \sqrt{1 + \frac{2}{\gamma - 1}\left(\frac{1}{\sin^2 \nu}\right)\frac{1}{M_2^2}\left\{1 - \frac{1 + [(\gamma - 1)/2]M_2^2}{1 + [(\gamma - 1)/2]M'^2}\right\}}}{1 + \frac{2}{\pi}\sqrt{1 - (\sin^2 \nu)M_2^2 \left\{\frac{1 + [(\gamma - 1)/2]M'^2}{1 + [(\gamma - 1)/2]M_2^2}\right\}} - \frac{2}{\gamma - 1}\left\{\frac{1 + [(\gamma - 1)/2]M'^2}{1 + [(\gamma - 1)/2]M_2^2} - 1\right\}} \tag{15}$$

Eq. (15) is the ratio of the working section width to the slot width as a function of M', M_2, and ν. The Mach Number, M_2, in Eq. (15), is the Mach Number the sonic stream will attain in region 2 by a Prandtl-Meyer expansion of $\nu = \nu'/2$. A plot of Eq. (15) is shown in Fig. 3. It is interesting to note that Eq. (15) has a limiting value at $M' \approx 1.87$ (see Fig. 3). This critical value is due to the fact that the Mach Number (v'/c') in Eq. (8) has reached the sonic value.

Reference

[1] Busemann, A., *Hodographenmethode der Gasdynamik*, ZAMM, Vol. 17, p. 73, 1937.

Buckling Efficiencies of Plate Materials at Elevated Temperatures

J. W. Clark

Research Engineer, Engineering Design Division, Aluminum Research Laboratories, Aluminum Company of America, New Kensington, Pa.

April 30, 1955

RECENTLY, IN THE JOURNAL, Gerard[1] compared the structural efficiencies of plate materials at various temperatures. He developed two "structural efficiency parameters," one that applied to plates that fail because of elastic buckling and the

other to plates that buckle at the compressive yield stress. The purpose of this note is to show that the latter parameter does not give a true comparison of structural efficiency.

In comparing the weights of two plate structures of different materials which fail by plastic buckling, Gerard assumes that the load and the dimensions of the plate panels are the same for the two cases. The thicknesses of the two plates are adjusted so that each buckles at the compressive yield strength of the material. The weight is then proportional to the parameter $\rho/E_s^{1/3}$, in which ρ is density and E_s is the secant modulus at the compressive yield strength.

The error in the above reasoning lies in the assumption that one variable, the thickness, can be adjusted to achieve two simultaneous results: (1) both plates buckle under the same load, and (2) both plates buckle at the compressive yield strength. In general, if both plates buckle at the same load, the buckling stress may coincide with the compressive yield stress for one material, but it will not for the other.

If two plates were designed so each would fail at the compressive yield strength, the relative weights of the two plates would be directly proportional to the density ρ and inversely proportional to the compressive yield strength. Thus the weight-strength efficiency for plates which fail at the compressive yield stress can be measured by the parameter, ρ/σ_{cy}.

However, the parameter ρ/σ_{cy} cannot serve as a measure of compressive buckling efficiency for the same reason that the parameter used by Gerard is not valid. That is, one cannot design plates of two different materials to buckle at the compressive yield strength under the same load without varying the panel dimensions as well as the thickness.

It may be that no single parameter gives an adequate picture of the relative efficiency of various materials in resisting buckling in the plastic stress range, since the comparison will depend to a large extent on the conditions encountered in an individual design problem.

Reference

[1] Gerard, George, *Buckling Efficiencies of Plate Materials at Elevated Temperatures*, Journal of the Aeronautical Sciences, Vol. 22, No. 3, pp. 194–196, March, 1955.

Errata—Nonlinear Lift and Vortex Separation

H. K. Cheng
Aerodynamicist, Bell Aircraft Corporation, Buffalo, N.Y.
June 30, 1955

Reference 1

Page 213, Eq. (3): Change the symbol "ϵ" on the left-hand side to "ϵ^*" (the conjugate of ϵ). First line after Eq. (5): The phrase "By virtue of the symmetry in the flow pattern" is inappropriate; omit. Eq. (6): Change the variable $(2\alpha t/a)^{2/3}$ to $(2\alpha Ut/a)^{2/3}$.

Page 214, second line in the first paragraph of Section (3): The word "infinity" should be replaced by the phrase "in the streamwise component." Eq. (9): Change the symbol "P" on the left-hand side to "Γ" (the circulation). Eq. (10): Change all symbols "α" on the right-hand side to "αx."

Reference 2

Page 222, Eq. (4.4): The equation should be written as

$$\rho U_\infty \zeta_0 \frac{dP}{dx} = \rho P \left[\overline{V_m}' - \frac{d\zeta_0}{dx} \right]$$

Page 223, Eq. (5.1): A superscript minus "$-$" should be added to the symbol "φ" to denote the value of the perturbation potential on the compression side of the wing. Eq. (5.2): A bracket sign "]" should be added at the end of the equation.

Page 224, Fig. 5: The exponential power 5/3 appeared in the formula of C_L^* should be written as 2/3.

Page 225, the sixth line from the beginning of Section (7): The numbers designating the equations are not correct. The correction reads, "Eqs. (4.8), (4.9), (6.2), and (6.3)."

All symbols "ϵ" appearing after Eq. (2.11), page 220, are misprints of "ε"; refer Figure 2, page 219, for clarification.

References

[1] Cheng, H. K., *Remarks on Non-linear Lift and Vortex Separation*, Readers' Forum, Journal of the Aeronautical Sciences, Vol. 21, No. 3, pp. 212–214, March, 1954.

[2] Cheng, H. K., *Aerodynamics of a Rectangular Plate with Vortex Separation in Supersonic Flow*, Journal of the Aeronautical Sciences, Vol. 22, No. 4, pp. 217–226, April, 1955.

A Note on "A Study of Surge in Compressors and Jet Engines"[1]

W. C. Randels
Military Operations Research Division, Lockheed Aircraft Corp., Burbank, Calif.
April 2, 1955

In reference 1, a mathematical analysis of compressor surge is presented. This analysis is probably as complete as is practical, but the resulting criteria are so complicated that it is difficult to see the physical meaning. A more drastic simplification which still applies to most actual cases of surge is presented in reference 2. This simplification also applies to other oscillator problems. The reasoning of reference 2 was presented earlier in reference 3 but this is a little difficult to get hold of.

References

[1] Pearson, Carl E., Journal of the Aeronautical Sciences, Vol. 22, No. 1, p. 10, January, 1955.

[2] Pearce, R. B., *Causes and Control of Power Plant Surge*, Aviation Week, January 16, 1950.
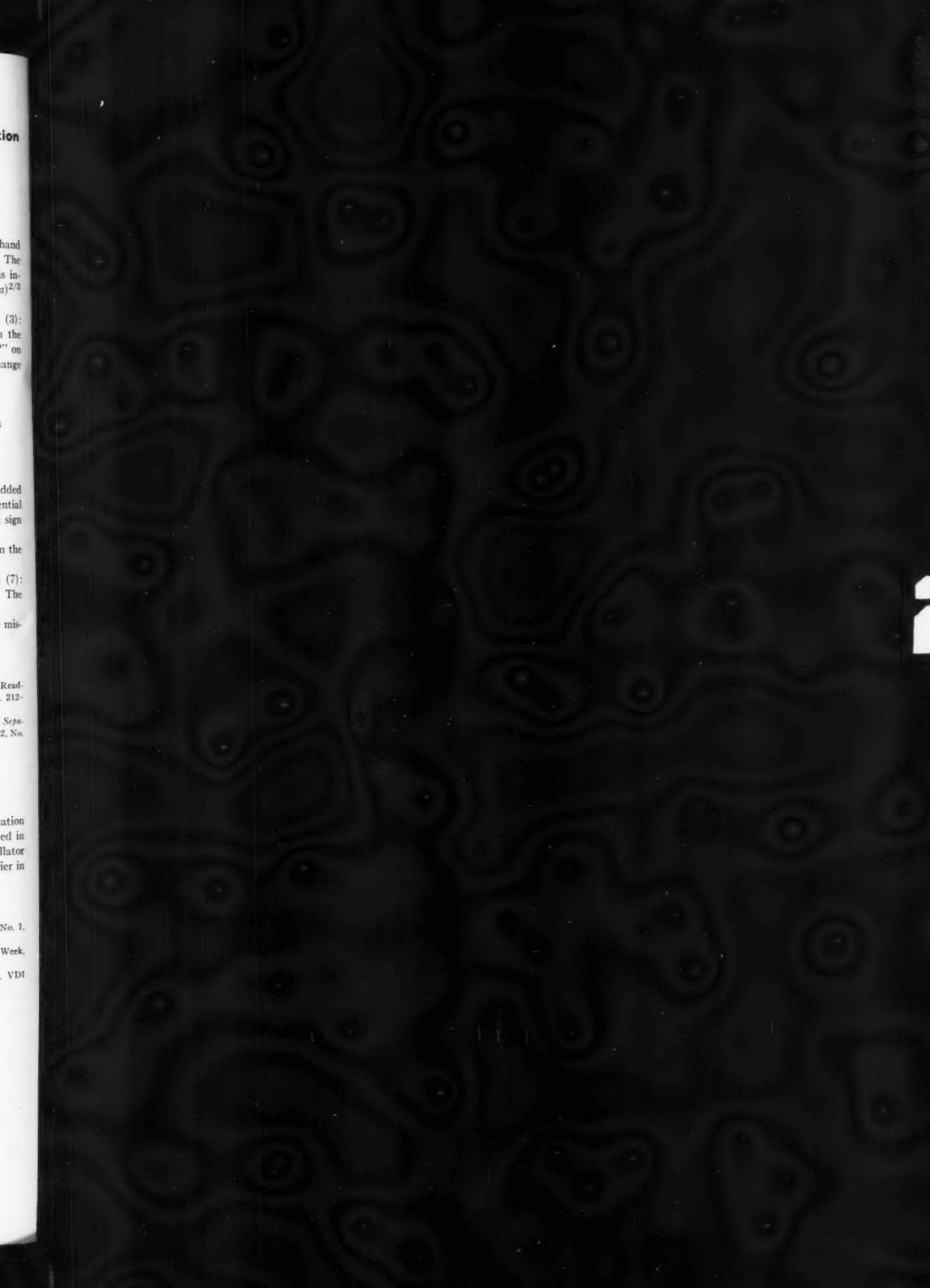
[3] Senger, *The Operating Characteristics of Multistage Compressors*, VDI Lecture, 1940, BUSHIPS (338) May, 1946.